General aspects of the nucleon-nucleon interaction and nuclear matter properties

Dissertation

Zur Erlangung des Grades eines Doktors
der Naturwissenschaften

der Fakultät für Mathematik und Physik
der Eberhard-Karls-Universität zu Tübingen

vorgelegt von

Oliver Plohl
aus Ostfildern

2008

Tag der mündlichen Prüfung:	25. Juli 2008
Dekan:	Prof. Dr. Nils Schopohl
1. Berichterstatter:	Prof. Dr. Christian Fuchs
2. Berichterstatter:	Prof. Dr. Dr. h.c. mult. Amand Fäßler

Zusammenfassung

Das Thema dieser Doktorarbeit ist, zunächst grundlegende modelunabhängige Eigenschaften der Nukleon-Nukleon (NN) Wechselwirkung im Vakuum hinsichtlich ihrer relativistischen Struktur und die Konsequenzen daraus für Eigenschaften von Kernmaterie zu untersuchen.

Hierfür werden relativistische und nicht-relativistische Meson-Austausch Potentiale, phänomenologische Potentiale und auf effektiver Feldtheorie (EFT) beruhende Potentiale auf eine relativistische Operator Basis der Clifford-Algebra abgebildet. Der Vergleich der unterschiedlichen Potentiale auf der Ebene von kovarianten Amplituden zeigt eine bemerkenswerte Übereinstimmung.

Weiterhin wird die relativistische Selbstenergie in der Hartree-Fock (HF) Näherung bestimmt. Das Auftreten eines skalaren und vektoriellen Feldes in der Größenordnung von mehreren hundert MeV ist eine universelle Eigenschaft von relativistischen Beschreibungen von Kernmaterie. Im Rahmen von QCD Summen Regeln sind diese Felder eng mit der Dichteabhängigkeit chiraler Kondensate verknüpft. Es zeigt sich, dass unabhängig von der Wahl der NN Wechselwirkung große skalare und vektorielle Felder auftreten, sobald die Symmetrien der Lorentz Gruppe wiederhergestellt sind. Im Rahmen der chiralen EFT (chEFT) wird gezeigt, dass kurzreichweitige Kontakt-Terme in nächst zu führender Ordnung, die mit der Spin-Bahn Wechselwirkung verknüpft sind, diese Felder erzeugen.

Um Auswirkungen von NN Korrelationen abzuschätzen, wird die Zustandsgleichung mit dem chiralen EFT Potential für Kern- bzw. Neutronenmaterie in der Bruckner-HF (BHF) Näherung bestimmt. Während erwartungsgemäß eine deutliche Überbindung eintritt (in nächst zu führender Ordnung wird Sättigungsverhalten beobachtet), zeigt die Symmetrieenergie im Vergleich mit phänomenologischen Potentialen (in der gleichen Näherung) bzw. anderen Zugängen ein realistisches Verhalten. Bei der Untersuchung der Pionmassenabhängigkeit im Rahmen der chEFT in nächst zu führender Ordnung zeigt sich, dass die Größenordnung der skalaren und vektoriellen Felder im chiralen Limes bestehen bleibt und nukleare Materie gebunden ist. Im Gegensatz zum Fall einer größeren Pionmasse als die physikalische verringern sich im chiralen Limes sowohl die Bindungsenergie als auch die Sättigungsdichte.

Der vorliegende Formalismus erlaubt nun im Rahmen der chEFT einen konsistenten Vergleich der In-Medium Nukleonmasse und der Dichteabhängigkeit des skalaren Kondensates, welches unter Anwendung des Hellmann-Feynman Theorems (in HF und BHF Näherung) bestimmt wird. Es zeigt sich, dass die In-Medium Nukleonmasse und das skalare Kondensat entkoppeln. Im Gegensatz zu QCD Summen Regeln bestimmen kurzreichweitige Kontakt-Terme die In-Medium Nukleonmasse, wohingegen virtuelle Pionen niedriger Impulse hauptsächlich zur Reduzierung des chiralen In-Medium Kondensates beitragen.

Abstract

The subject of the present thesis is at first the investigation of model independent properties of the nucleon-nucleon (NN) interaction in the vacuum concerning the relativistic structure and the implications for nuclear matter properties.

Relativistic and non-relativistic meson-exchange potentials, phenomenological potentials s well as potentials based on effective field theory (EFT) are therefore mapped on a relativistic operator basis given by the Clifford Algebra. This allows to compare the various approaches at the level of covariant amplitudes where a remarkable agreement is found.

Furthermore, the relativistic self-energy is determined in the Hartree-Fock (HF) approximation. The appearance of a scalar and vector field of several hundred MeV magnitude is a general feature of relativistic descriptions of nuclear matter. Within QCD sum rules these fields arise due to the density dependence of chiral condensates. We find that independent of the applied NN interaction large scalar and vector fields are generated when the symmetries of the Lorentz group are restored. In the framework of chiral EFT (chEFT) it is shown, that these fields are generated by short-range next-to-leading order (NLO) contact terms, which are connected to the spin-orbit interaction.

To estimate the effect arising from NN correlations the equation of state of nuclear and neutron matter is calculated in the Brueckner-HF (BHF) approximation applying chEFT. Although, as expected, a clear over-binding is found (at NLO a saturating behavior is observed), the symmetry energy shows realistic properties when compared to phenomenological potentials (within the same approximation) and other approaches. The investigation of the pion mass dependence within chEFT at NLO shows that the magnitude of the scalar and vector fields persists in the chiral limit – nuclear matter is still bound. In contrast to the case of a pion mass larger than the physical one the binding energy and saturation density are decreased in the chiral limit.

The present formalism allows within chEFT to perform a consistent comparison of the in-medium nucleon mass and the density dependence of the scalar condensate derived from the Hellmann-Feynman theorem (in HF and BHF approximation). A decoupling of the in-medium nucleon mass and the scalar condensate is observed. It turns out that in contrast to QCD sum rules the effective nucleon mass in matter is mainly determined by short-range contact terms while virtual low-momentum pions provide the essential contributions responsible for the reduction of the in-medium scalar condensate.

Contents

1. Introduction

The field of nuclear physics was born with the discovery of the neutron by Chadwick in 1932 [1]. Since then the nuclear force, i.e., the interaction between two nucleons, had been the heart of nuclear physics and has been investigated all over the world for the past 75 years. The reason for that outstanding importance of the nuclear force is that traditionally the main intention in nuclear physics is to determine the properties of nuclei and nuclear matter in terms of a bare nucleon-nucleon interaction.

Going back in history, the idea of meson exchange is based on Yukawa's fundamental hypothesis from 1935, namely, that the nuclear force is mediated by the exchange of massive particles [2]. Yukawa's original concept of a scalar field which interacts with the nucleons was modified consequently soon after to vector [3] and then to pseudo-scalar and pseudo-vector fields [4] and also concepts of mixed meson exchange theories came up [5]. The empirically found sign of the quadrupole moment of the deuteron could be explained correctly by the inclusion of a pseudo-scalar field. Therefore an isovector, pseudo-scalar boson has been predicted by Pauli [6] long before a massive particle with this properties was found experimentally in 1947/48.

After the experimental finding of the pion Taketani, Nakamura and Sasaki [7] proposed a subdivision of the nuclear force, an attractive long-range part for a relative distance of the two nucleons larger than 2 fm dominated by one-pion exchange (OPE), an intermediate range (1 fm $\geq r \leq$ 2 fm) and a short-range ($r \leq 1$ fm) or core region. The short-range part is is the mathematically most complicated part. From a nowadays perspective it is clear that besides multi-pion exchange (or the exchange of heavy mesons) quark-gluon exchange plays also a crucial role. It therefore becomes evident that the main difference among all theories of the nuclear force arise due to the different description of the interaction at high momenta in the short-range region.

In order to derive the nucleon-nucleon (NN) interaction the first field-theoretic attempts were based on pion exchange. OPE was well established describing the long-range part of the nuclear interaction since it proved to be suitable to describe NN scattering data and the properties of the deuteron. However, it turned out that it was not possible to get a sufficiently strong spin-orbit force by incorporating two-pion exchange (TPE). Moreover serious ambiguities arose from multi-pion exchange which led to the conclusion that the "pion theories" developed at that time were not feasible in order to describe the NN interaction.

The situation changed when heavy mesons were discovered experimentally in the early 1960s (due to the experimental investigation of a strong short-ranged spin-orbit force and from the electromagnetic structure of the nucleon the existence of vector mesons had been already suggested before [8, 9, 10, 11]). Now with the inclusion of vector bosons one-boson-exchange (OBE) models were developed which described NN scattering data fairly well. These models are based on the assumption that multi-pion exchange can be represented by the exchange of adequate multi-pion resonances. However, a main problem is the inclusion of the scalar-isoscalar sigma meson since its experimental evidence is still controversial. The sigma boson describing the intermediate range attraction is connected to correlated TPE. Therefore a lot of effort was spent in order to derive the contribution from TPE to the NN interaction. One approach of deriving the OBE potentials was based on dispersion relations which led, e.g., to a model of the nuclear force constructed from using one-pion exchange, dispersion-theoretical TPE and ω meson exchange and additionally a phenomenological short-range part.

Another promising way was to construct relativistic meson-theoretical nucleon-nucleon potentials in the framework of field theory. The advantage of a field-theoretical approach is that it can account for a well-defined off-shell behavior and medium effects when applied to the many-body problem. These properties are natural consequences of meson exchange. In summary, the field-theoretical approach led to more and more complex meson exchange potentials, which go far beyond the traditional OBE models. They are constructed from OPE, TPE including also virtual isobar excitation and finally all relevant diagrams of 3π- and 4π-exchange. Modern one-boson-exchange potentials (OBEP) as e.g. the Bonn potentials [12] are based on the exchange of these mesons and provide high precision fits to nucleon-nucleon scattering data. Meson-nucleon coupling constants and form factors are empirically fixed from the data. Thus OBEPs are the result of relativistic phenomenology at the level of the elementary NN interaction.

With the onset of quantum chromo-dynamics (QCD) which is the fundamental theory of strong interactions it became obvious that the nucleon-nucleon interaction is not fundamental. Although it is a well known fact that the nucleon-nucleon interaction is entirely determined by the underlying quark-gluon dynamics a quantitative understanding of the NN interaction in the language of QCD is far from being realized due to the non-perturbative character of QCD in the low-energy regime leading to formidable mathematical problems. Even lattice-gauge theory which is a promising tool for the treatment of low-energy QCD nowadays, fails to be appropriate concerning the NN force due to computational restrictions which appear to persist even in the near future.

Since a direct solution of QCD in the low-energy regime is not possible quark cluster models were developed inspired by QCD. Some of these models were able

to describe most of the properties of the nuclear force qualitatively but failed to reproduce them quantitatively [13, 14].

A big step was made when the methods of effective field theory (EFT) were applied to low-energy QCD by Weinberg [15].

In order to introduce this concept first a short survey of chiral symmetry in nuclear physics is presented. The QCD Lagrangian exhibits exact chiral symmetry in the limit of massless up and down quarks. In other words the massless QCD Lagrangian is invariant under global flavor $SU(2)_L \times SU(2)_R$ or alternatively $SU(2)_V \times SU(2)_A$ transformations (where the subscripts stands for vector and axial). Since the up and down current quark masses are small, i.e. of the order of 5-10 MeV, this symmetry is still approximately fulfilled. However, in nature no parity doublets are observed in the low-mass hadron spectrum. This implies that the ground state of QCD can not have the same symmetry as the Hamiltonian due to Goldstone's theorem. The axial symmetry is spontaneously broken by the non-vanishing – and large – ground state expectation value of the scalar quark density, the quark condensate $\langle \bar{q}q \rangle_0$ of the QCD vacuum. The quark condensate also plays an important role as an order parameter of spontaneously broken chiral symmetry. The spontaneous symmetry breaking, similar to the spontaneous magnetization of a ferromagnet which breaks the symmetry of the underlying Hamiltonian, implies the existence of three massless Goldstone bosons which are than the three pions $(\pi^{\pm}, \pi^0)$. Explicit symmetry breaking due to the non-vanishing current quark masses generates the mass scale for the pion mass, where spontaneous symmetry breaking generates the scale $\Lambda_\chi \sim 4\pi f_\pi$ which is then identified with the observed gap $\Delta \sim M_N$ in the spectrum of low-mass hadrons. Due to Goldstone's theorem these pions interact weakly at low energy and momenta. Moreover in the chiral limit, i.e. for vanishing pion masses and zero energy and momentum the interaction vanishes which gives the theoretical foundation for chiral perturbation theory. The small pion mass of 140 MeV ensures that the concept of chiral symmetry persists as a fundamental feature of low energy hadron physics. Thus, in the low-energy regime of QCD one ends up with pions and nucleons where spontaneously broken approximate chiral symmetry rules the interaction. One important reason for the failure of the "pion theories" based on Yukawa's meson theory is understood nowadays: (broken) chiral symmetry generates and constrains pion dynamics which was not known in the 1950s.

The main idea of an effective field theory is now that at low-energies the dynamics should be governed by the lightest particles, i.e. the pions which are the effective degrees of freedom and the symmetries of QCD. The heavy particles, i.e. the nucleons are treated as almost static sources. The scale Λ_χ governs naturally the separation between light and heavy degrees of freedom. In order to describe this one has to write down the most general Lagrangian which is consistent with the assumed symmetry principles (Lorentz covariance, parity

conservation, time-reversal and charge-conjugation invariance, (approximate) isospin symmetry and particularly spontaneously broken chiral symmetry of QCD as stated by Weinberg [15]. Since this chiral effective Lagrangian is given by an infinite series of terms an infinite number of Feynman diagrams is generated when applied to NN scattering. Weinberg showed, that a systematic expansion of the NN interaction in terms of chiral power counting exists [16]. The expansion is performed in powers of $(Q/\Lambda_\chi)^\nu$ where Q is the generic low momentum scale given by the nucleon three-momentum, or the four-momenta of virtual pions or a pion mass. $\Lambda_\chi \sim 4\pi f_\pi \sim 1$ GeV is the chiral symmetry breaking scale. In such an expansion the low-energy constants (LECs) related to pion-nucleon vertices can be fixed from pion-nucleon scattering data [17]. To the extent of terms (which are dictated by the symmetries) included in the effective Lagrangian, such an effective theory is considered as the exact mapping of QCD on effective hadronic degrees of freedom in the non-perturbative regime.

Up to now the two-nucleon system has been considered at next-to-next-to-next-to-leading order ($\mathrm{N^3LO}$) in chiral perturbation theory [18, 19, 17]. In chiral EFT the NN potential consists of one-, two- and three-pion exchanges and contact interactions which account for the short-range contributions.

Moreover, chiral EFT has a well defined quark mass dependence. For the NN interaction the chiral limit of vanishing current quark and pion masses has been evaluated up to next-to-leading order (NLO) [20, 21] and applied to the deuteron problem [22].

The most general two-nucleon interaction in the non-relativistic approximation was written down by Okubo and Marshak in 1958 [23] based on certain symmetries required by a two-body potential. The mathematical form is given by a certain set of operators (central, spin-orbit, tensor, quadratic spin-orbit,..) and corresponding potential forms. In the case of chiral EFT these potential forms are derived systematically.

There exist, however, a large number of phenomenological models, e.g. the Argonne v_{14} potential [24] or v_{18} potential [25] where the general potential form from [23] has been taken and the NN interaction has been parameterized by means of general functions (local Woods-Saxon functions).

Reducing the relativistic field-theoretic OBE exchange Feynman amplitudes to a non-relativistic representation one obtains also a potential which is thereby based on an equivalent set of spin and isospin operators as the very general two-nucleon interaction from Ref. [23].

In summary, the common spin-isospin operator structure of the potentials is enforced by NN scattering data as well as imposed by symmetry requirements [23]. However, except for covariantly formulated OBE models most modern potentials are not restricted by the requirement of covariance. Therefore the question arises whether besides chiral symmetry that establishes the connection to QCD the NN interaction is also governed by the symmetries of the Lorentz

group.

A better understanding of the common features and the differences of the various approaches is essential in order to arrive at a more model independent understanding of the NN interaction, in particular since all the well established interactions fit NN scattering data with approximately the same precision. A direct comparison of relativistic phenomenology based on meson exchange with EFT and non-relativistic phenomenology is, however, difficult since the latter two approaches lack of a clear Lorentz structure. At low momentum scales the different potentials can be mapped on each other using renormalization group (RG) methods [26]. This led recently to the construction of a "model independent" low momentum potential $V_{\mathrm{low\ k}}$ by integrating out the dynamics for momenta above a cut-off scale of about $\Lambda \simeq 2$ fm^{-1} [26]. It has been argued that beyond this scale the short-range part of the interaction, mediated by vector meson exchange or point-like counter terms, becomes dominant and leads to the deviations of the various approaches.

Although a breakthrough in some sense, the renormalization group approach does not help to clarify the relativistic structure of the potentials which is essential e.g. in order to generate (or not to generate) large scalar/vector mean fields in nuclear matter as will be discussed later on.

The present work tries to answer the question whether all NN potentials contain a "hidden" relativistic structure imposed by the symmetries of the Lorentz group in a model-independent way.

This is done by reconstructing the symmetries of the Lorentz group by applying projection techniques to map the various NN potential models which are usually represented in an angular-momentum basis on Dirac phenomenology given by the Clifford algebra in Dirac space. This finally allows to identify the different Lorentz components of the interaction. Such a transformation is well defined in the positive energy sector for on-shell amplitudes and allows to compare the NN potentials on the basis of Lorentz invariant amplitudes.

One could argue that the information which pieces of the interaction are of scalar, vector, etc type is not of relevance at low energies.

It is, however, a fundamental question which role relativity plays in nuclear systems. Inside nuclei nucleons move with maximally about 1/4 of the velocity of light considering the ratio of the Fermi momentum over the nucleon mass $k_{\mathrm{F}}/M \simeq 0.25$. This fact implies only moderate corrections from relativistic kinematics in finite nuclei. Non-relativistic density functionals such as Skyrme or Gogny forces are widely used in structure calculations. In such approaches there exists only one relevant scale for the mean field which is the depth of the single particle potential of about -50 MeV. The same is true for *ab initio* calculations like Brueckner-Hartree-Fock (BHF) or variational calculations.

However, there exists a fundamental difference between relativistic and non-relativistic dynamics for nuclear systems such as finite nuclei or infinite nuclear

matter. A genuine feature of relativistic nuclear dynamics is the appearance of large scalar and vector mean fields, each of a magnitude of several hundred MeV. The scalar field Σ_s is attractive and the vector field Σ_μ is repulsive. In relativistic mean field (RMF) theory, both, the sign and the size of the large scalar and vector fields are enforced by the nuclear saturation mechanism [27]. At nuclear saturation density $\rho_0 \simeq 0.16$ fm^{-3} the empirical fields deduced from RMF fits to finite nuclei are of the order of $\Sigma_s \simeq -350$ MeV and $\Sigma_0 \simeq +300$ MeV [28].

The single particle potential in which the nucleons move originates from the cancellation of these scalar and vector fields $U_{\rm cent} \simeq \Sigma_0 + \Sigma_s$ and is of the order of -50 MeV. Therefore one has no direct experimental access to the interpolating scalar and vector fields. There exist, however, several features in nuclear structure which can be explained naturally within Dirac phenomenology while models based on non-relativistic dynamics have difficulties or, at least, one has to introduce additional model parameters. The most well known feature is the large *spin-orbit splitting* in finite nuclei. In a relativistic framework the strong spin-orbit force appears naturally from the coupling to the lower components of the Dirac equation where the scalar-vector mean fields add up in the spin-orbit potential $U_{\rm S.O.} \propto (\Sigma_0 - \Sigma_s) \simeq 750$ MeV. Due to this fact RMF theory is able to reproduce the strong spin-orbit splitting in spherical nuclei quantitatively without the introduction of additional parameters [28]. A second symmetry, observed more than thirty years ago in single-particle levels of spherical nuclei is the so called *pseudo-spin symmetry* [29]. While all attempts to understand this symmetry within non-relativistic approaches failed, it can naturally be understood within RMF theory as has been shown by Ginocchio [30] a few years ago. This symmetry, again a consequence of the coupling to the lower components, is exact in the limit $\Sigma_0 = -\Sigma_s$ and is broken in nature by the amount $(\Sigma_0 + \Sigma_s)/(\Sigma_0 - \Sigma_s)$ which is less than 10%. A third example are the *moments of inertia in rotating nuclei*. Relativistic dynamics implies that in the rotating system a Coriolis term occurs due to the spatial vector currents, however, with all couplings already fixed through the time-like components [31].

The relativistic phenomenology has been extremely successful for the description of nuclear systems, i.e. finite nuclei and nuclear matter and is in the meantime widely used. Relativistic mean field theory enforces the existence of large scalar and vector mean fields in nuclear matter and a variety of strong arguments support this scenario. However, RMF cannot prove the existence of these fields since they are introduced by hand into the theory, i.e. a direct link to the bare nuclear force and NN scattering is missing. The coupling strength of the effective σ and ω exchange in RMF models adjusted to nuclear matter bulk properties differs essentially from their counterparts in OBE type potentials adjusted to NN scattering data.

An alternative approach for nuclear matter are *ab initio* many-body calcu-

lations. Based on high precision NN interactions one treats short-range and many-body correlations explicitly. A typical example for a successful many-body approach is Brueckner theory [32]. In the relativistic Dirac-Brueckner-Hartree-Fock (DBHF) approach the nucleon inside the medium is dressed by the self-energy Σ. The in-medium T-matrix is obtained from the relativistic Bethe-Salpeter (BS) equation and plays the role of an effective two-body interaction which contains all short-range and many-body correlations of the ladder approximation. Solving the BS equation the Pauli principle is respected and intermediate scattering states are projected out of the Fermi sea. The summation of the T-matrix over the occupied states inside the Fermi sea yields finally the self-energy Σ in Hartree-Fock approximation [33, 34, 35, 36, 37, 38, 39]. The scalar and vector self-energy components $\Sigma_{\rm s}$ and Σ_0 are found to be of similar magnitude as in RMF theory.

In summary, the scalar field $\Sigma_{\rm s}$ and the time-like component of the vector field Σ_0 are key quantities of each relativistic hadronic theory since they determine the spin-orbit potential $U_{\rm S.O.}$, the nuclear equation of state (EOS), the single-particle potential as well as the effective nucleon mass[1] $M^* = M + \Sigma_{\rm s}$.

However, in relativistic approaches the nuclear interaction is always described in some sort of a relativistic field-theoretical meson exchange picture. The mesons represent effective bosonic degrees of freedom which are either directly adjusted to the properties of nuclear matter and finite nuclei, as in the case of RMF theory, or to vacuum NN scattering. Hence it is a fundamental question to decide whether the large scalar and vector fields enforced by Dirac phenomenology of nuclear systems are an artefact of the meson exchange picture or whether they reflect a deeper characteristics of nature.

An alternative approach to address this question from the phenomenology of non-perturbative QCD is provided by QCD sum rules [43, 44, 45]. As already mentioned the QCD ground state is populated by strong condensates of quark-antiquark pairs and gluons. Hadrons represent excitations on this condensed ground state. When baryonic matter is added to the vacuum a change of the scalar condensate $\langle \bar{q}q \rangle$ is induced what is believed to give a substantial contribution to the strengths of the scalar mean field $\Sigma_{\rm s}$ what nucleons and other hadrons feel in matter. In this interpretation the density dependence of the scalar condensate[2] $\langle \bar{q}q \rangle_{\rho_B}$ determines directly the shift of the effective nucleon mass $M^* = M + \Sigma_{\rm s}$. The breaking of Lorentz invariance due to the presence of the medium introduces the vector quark condensate $\langle q^\dagger q \rangle_{\rho_B}$ giving rise to a repulsive vector mean field Σ_0 which is of the same magnitude as the scalar field [43]. These fields are astonishingly close to the empirical values derived

[1] It is well established that the effective nucleon mass in the nuclear medium deviates substantially from its vacuum value [40, 41, 42].

[2] The subscript denotes that the expectation value of the quark condensate is taken with respect to the nuclear ground state at finite baryon density ρ_B.

from RMF fits to the nuclear chart.

It is remarkable that relativistic many-body calculations yield again scalar and vector fields which are of the same sign and magnitude as obtained from RMF theory or, alternatively, from QCD sum rules. Such a coincidence could not have been expected a priori. Moreover, DBHF calculations [36] agree even on a quantitative level surprisingly well with the QCD based approach of Ref. [46, 47] where chiral fluctuations from the long and intermediate range pion-nucleon dynamics were considered on top of the chiral condensates.

These facts suggest that preconditions for the existence of large fields in matter or, alternatively, the density dependence of the QCD condensates, must already be inherent in the vacuum NN interaction. The connection of the nucleon-nucleon force to QCD is given by the fact that the interaction is described by the exchange of the low lying mesonic degrees of freedom

The present work will demonstrate for the first time, explicitly and quantitatively, that the appearance of large scalar and vector fields in matter is a direct - and model independent - consequence of the vacuum NN interaction when the symmetries of the Lorentz group are respected. For this purpose we calculate the self-energy components using a variety of modern relativistic and non-relativistic high precision NN potentials based on different theoretical approaches in infinite nuclear matter in Hartree-Fock approximation at tree-level.

The main result of this investigation is, that whenever modern NN interactions are mapped on a Lorentz covariant operator basis large scalar and vector self-energy components of comparable size and sign are found where the magnitude is set already at tree-level. This is found to be true for OBE type potentials, purely phenomenological potentials as well as for EFT potentials.

It has been known for decades from Dirac phenomenology that the generation of the large scalar and vector fields is induced by the short-range vector (ω) and scalar (σ) meson exchange which are connected intimately to the large spin-orbit interaction.

Since chiral EFT nucleon-nucleon potentials stem from a systematic expansion of an effective Lagrangian which respects the basic symmetries of QCD, chiral EFT is considered to be equivalent to QCD. The procedure of subjecting the chiral N^{3}LO Idaho potential [19] to the projection scheme onto a covariant operator basis allows to identify the contributions to the self-energy components from pion dynamics and short-range contact terms at the given chiral order up to N^{3}LO. Hence a systematic investigation of the connection between the appearance of large scalar and vector fields in nuclear matter and chiral dynamics can be performed.

This has been done elaborately in the present work in order to explore the structure of the self-energy from chiral EFT, its generation mechanism, and the connection to meson-exchange phenomenology.

It is well known that a realistic description of nuclear matter requires NN short-range correlations beyond Hartree-Fock. The latter are known to be essential for nuclear binding when realistic NN potentials are used. In lowest order of the Brueckner hole-line expansion this leads to the ladder approximation of the Bethe-Goldstone equation for the in-medium G-matrix [32], or the BS equation in the relativistic case [33]. Despite the long history of improving BHF theory the latter fails to describe nuclear saturation quantitatively. Strong over-binding at too large densities is observed particularly when modern OBE potentials are used. Relativistic DBHF theory on the other hand turned out to be very successful in describing nuclear saturation properties [35, 36] due to higher order density dependences introduced by a dressing of the two-body interaction by in-medium spinors. When the low momentum interactions V_{lowk} is applied isospin symmetric nuclear matter turns out to collapse already at Hartree-Fock level due to the strong suppression of the hard core by high momentum cut-offs. A full summation of the Brueckner ladder does not improve on the situation [48].

In the present work the chiral EFT low-momentum interaction [19] is explored in the context of the nuclear matter problem. To estimate the effect of short range NN correlations this has been done both in Hartree-Fock approximation (tree level) and in the non-relativistic BHF approach[3] calculating the EOS for symmetric nuclear matter as well as for neutron matter for all orders, i.e. from leading-order (LO) up to N^{3}LO. Though the results for the EOSs obtained from chiral EFT are not expected to be realistic even in BHF approximation they are required in order to determine the symmetry energy at the different chiral orders. Moreover these results are instructive particularly with regard to the investigation of the pion mass dependence of nuclear matter within chiral EFT.

The expansion of the nuclear force in the context of chiral perturbation theory is well defined for small quark masses and should still be valid in the limit $m_q \to 0$ which is equivalent to $m_\pi \to 0$. Therefore hadronic properties at low energies are not expected to change dramatically in the chiral limit. This is also the case in the context of the analysis of QCD sum rules where qualitative changes of the properties of nuclei are not expected in the chiral limit. This can be seen from the assumption that the nuclear properties can be described by vacuum condensates which can be determined in the chiral limit. Then, however, the qualitative properties of the nuclear EOS as well as the magnitude of the scalar and vector self-energy components should naturally persist even in the chiral limit since hadronic properties are not expected to change dramatically in the case of massless quarks or pions.

[3] It is not possible to apply chiral EFT in the relativistic DBHF approach since is not a covariantly formulated NN interaction.

Therefore the question arises how do the properties of nuclei and nuclear matter change in the chiral limit or if the physics of nuclei in a world with $m_\pi = 0$ is qualitatively similar to what in fact is observed, e.g. if bound nuclei can exist in the scenario of massless light quarks.

Within chiral EFT the explicit and implicit pion mass dependence of the nuclear force is known derived up to the chiral order NLO [20, 22]. Thus the behaviour of nuclear matter in the chiral limit can be explored.

This has been done in the present work. The pion mass dependence of the scalar and vector self-energies is investigated by restoring the symmetries of the Lorentz group with the help of projection techniques onto a covariant operator basis. Moreover possible changes of the properties of the EOS in Hartree-Fock and Brueckner-Hartree-Fock approximation are explored in particular in the chiral limit, i.e. for vanishing pion masses but also for pion masses much larger than the physical one.

As already mentioned, such an investigation is not only of academic interest, in particular with regard to the interpolation of lattice gauge calculations which are usually performed at pion masses much larger than the physical one.

QCD sum rules connect the nucleon mass in the chiral limit to the chiral condensate $\langle \bar{q}q \rangle_0$. Hence, according to Ioffes's formula [49] the (leading order) vacuum nucleon mass is directly proportional to the chiral condensate $\langle \bar{q}q \rangle_0$. This gives an important hint since it implies that a change of the scalar condensate with increasing baryon density leads to a sizeable decrease of the nucleon mass in matter [50]. As already mentioned, this is found to be true within the approach of in-medium QCD sum rules where the change of the scalar condensate at finite baryon density determines the deviation of the effective nucleon mass from its vacuum value. This, however, requires the knowledge of the density dependence of the scalar condensate $\langle \bar{q}q \rangle_{\rho_B}$. The latter can be estimated with the help of the Hellmann-Feynman theorem which relates the in-medium scalar condensate with the quark mass derivative of the total energy density [43, 51]. To leading order in density one finds that the in-medium scalar condensate drops linearly with the nuclear density (with the proportionality given by the pion-nucleon sigma term σ_N). In order to estimate the corrections to this leading density dependence a lot of different models have been used: the Nambu-Jona-Lasinio (NJL) model [43, 52, 53, 54], various versions of the linear sigma model [55, 56], the Quark Meson Coupling model (QMC) [57] or recently the Polyakov-NJL model [58], hadron effective field theory [43, 59, 60] such as $\sigma\omega$ type models [27] and the relativistic DBHF theory [34, 35, 36]. While DBHF allows a quite reliable determination of the nuclear EOS up to at least two times nuclear density as a conservative estimate - recent DBHF calculations [38, 39] have been shown to be consistent with astrophysical and accelerator based constraints concerning their high density behavior [61] - the unknown quark mass

dependence of the mesonic couplings and masses introduces large uncertainties in the determination of the in-medium quark condensate [59, 60].

Our investigations [62] show that at moderate nuclear densities the chiral N^3LO scalar and vector fields at Hartree-Fock almost agree with the prediction from leading order QCD sum rules. This coincidence of the nucleon mass shifts obtained from QCD sum rules and relativistic nuclear phenomenology has been stressed in many works.

However, there are still open questions left. Regarding the modification of the quark condensate in matter one has to distinguish between contributions coming from the pion cloud and those of non-pionic origin [63, 64]. As pointed out in [63] a dependence of the nucleon mass in any simple way on the quark condensate alone is ruled out by chiral symmetry. A considerable contribution to the change of the scalar condensate in the medium comes from low momentum virtual pions, i.e. from the pion cloud. Such contributions are, however, found to play only a minor role for the reduction of the nucleon mass and therefore cannot as easily be related to a partial restoration of chiral symmetry as the QCD in-medium sum rule for the scalar mean field implies.

We are in the situation to calculate both quantities, the scalar quark condensate $\langle \bar{q}q \rangle_{\rho_B}$ in matter and the effective nucleon mass M^* from the same chiral effective interaction in the present work. The condensate is determined making use of the Hellmann-Feynman theorem and the fact that, at least up to NLO, the quark mass dependence of the potential is known from its analytic formulation in the chiral limit. The effective mass, on the other hand, can be determined in Hartree-Fock approximation making use of projection techniques on a relativistic operator basis. Doing so, we observe a *decoupling of the effective nucleon mass and the scalar condensate*. Furthermore our investigation of the structure of the self-energy from chiral EFT shows that *contributions coming from pion dynamics only play a minor role for the reduction of the nucleon mass* [62]. This supports the conclusions of Refs. [63, 64]. The quark condensate is reduced to large extent by the pion cloud surrounding the nucleons while the nucleon mass is not.

The present thesis is organized as follows:

In Chapter 2 the appearance of large attractive scalar and repulsive vector mean fields as a consequence of a relativistic formulation of the nuclear matter problem is discussed. Therefore the $\sigma\omega$ model, a phenomenological relativistic mean field (RMF) theory as the simplest realization of Quantum Hadron Dynamics is presented followed by a short description of the adjustment of its model parameters to the saturation properties of nuclear matter and consequently the natural appearance of large mean fields in matter.

The formalism of the microscopic DBHF approach is presented in the second

part with the introduction of the T-matrix approximation acting as an effective two-body potential as well as the self-energy operator in T-matrix approximation. Moreover the determination of the self-energy is discussed briefly where the scalar and time-like components of the self-energy operator are found to be of the same magnitude as those obtained from RMF theory.

Finally QCD in-medium sum rules are introduced and discussed. This approach builds the bridge between QCD and the appearance of large scalar and vector self-energy fields felt by a nucleon in nuclear matter.

In Chapter 3 an overview over modern high-precision NN potentials is given. These are the Bonn A and CD Bonn potentials as examples of covariantly formulated OBE type interactions. The Nijm93 [65] interaction as an example of a non-relativistic meson-theoretical potential is introduced followed by the phenomenological Nijm I, Nijm II, Reid93 potentials [65] and the Argonne v_{18} potential [25]. Finally low-momentum EFT interactions are introduced. These are the chiral Idaho N^{3}LO potential [19] and the 'universal' effective low-momentum potential $V_{\text{low k}}$ [26] based on RG methods. Additionally the chiral EFT NN interaction is presented where the implicit and explicit pion mass dependence of the nuclear force has been derived up to the chiral order NLO [20].

The general connection between the operator structure of covariantly formulated potentials as well as non-relativistic potentials is discussed.

In Chapter 4 the projection formalism for the restoration of the symmetries of the Lorentz group is outlined. This procedure allows to map any NN potential amplitudes usually represented in an angular-momentum basis onto a covariant operator basis given by the Clifford algebra in Dirac space. This allows to study the Lorentz structure of the various NN potentials and to compare the latter by identifying the Lorentz components of the interactions. The results of this model independent study are presented and discussed.

Nuclear bulk properties are investigated in Chapter 5. In the first part the formalism for the determination of the self-energy components is outlined in detail followed by a discussion of the results for the relativistic self-energy fields obtained from the various interactions from Chapter 3. Furthermore the density dependence of the fields as well as the implications for the nuclear EOS are discussed. In order to test the reliability of the obtained tree level Hartree-Fock results a comparison with a fully self-consistent DBHF calculation [36] is performed. In order to check the applicability and accuracy of the projection scheme outlined in Chapter 4 the single particle potential is calculated from the self-energy components for the various potentials and compared to a non-relativistic calculation.

The structure of the relativistic self-energy fields as well as its generation

mechanism from chiral EFT is explored. The conclusion drawn on the generation mechanism are then compared to other potentials as well as to studies which connect the structure of chiral EFT to the structure extracted from other realistic nuclear forces.

The effects of higher order corrections in the density are investigated in a self-consistent Hartree-Fock calculation. The results for the density dependence of the self-energy fields as well as the EOS calculated with three different potentials (Bonn A, Nijm93 and Nijm I) are discussed and compared to tree level results.

The results for the EOS of symmetric nuclear matter and pure neutron matter from chiral EFT in Hartree-Fock and in Brueckner-Hartree-Fock approximation for all orders in the chiral expansion up to N^3LO as well as the symmetry energy are shown and compared to calculations based on different interactions as well as on in-medium chiral perturbation theory. The investigation of the pion-mass dependence of the self-energy fields in matter as well as the nuclear EOS in Hartree-Fock and Brueckner-Hartree-Fock approximation is shown in the last part of this chapter.

In Chapter 6 the connection between chiral EFT and QCD sum rules is investigated. The density dependence of the chiral condensate is determined with the help of the Hellmann-Feynman theorem applying chiral EFT at NLO in Hartree-Fock and Brueckner-Hartree-Fock approximation. The Hartree-Fock result is compared to a determination of the effective in-medium nucleon mass based on the same chiral EFT interaction where the scalar self-energy is calculated using the projection scheme outlined in Chapter 4.

2. Mean fields in nuclear matter

Considering the ratio of the Fermi momentum over the nucleon mass which is $k_F/M \simeq 0.25$ at saturation density $\rho_0 \simeq 0.16$ fm^{-3} kinematic corrections due to special relativity do not seem to play a significant role in the description of finite nuclei as well as infinite nuclear matter. Moreover, non-relativistic approaches as, e.g., Skyrme-Hartree-Fock, describe finite nuclei quantitatively well and therefore a relativistic description seems not to be appropriate.

Nevertheless, the understanding of nuclear dynamics has been improved fairly by relativistic field theories where nuclear interactions are described by the coupling of the nucleon to meson fields.

This becomes evident in the case of the description of the saturation properties of nuclear matter. Although non-relativistic many-body calculations are able to describe the saturation properties of nuclear matter qualitatively, they fail quantitatively. In the framework of relativistic approaches the quantitative description of the saturation properties is improved and moreover a different understanding of the underlying saturation mechanism is obtained. Furthermore there exist several features, e.g., the large spin-orbit force in nuclear structure which can be described quantitatively well and naturally within a relativistic field theory.

This indicates that there are large relativistic effects in nuclei and nuclear matter under normal conditions and therefore relativistic approaches are the appropriate approach in describing nuclear matter and finite nuclei.

The reason for that are not corrections due to relativistic kinematics but due to an implicit feature of relativistic field theories namely the appearance of large scalar and vector fields, each of a magnitude of several hundred MeV. This is an unique property of the Clifford algebra where the Dirac equation is based on.

But besides relativistic fields theories on the mean field level or effective field theories of the nuclear many-body problem, e.g., the DBHF theory based on vacuum nucleon-nucleon interactions which are both referred to as Quantum Hadron Dynamics (QHD) there is evidence from QCD sum rule analysis that these scalar and vector fields are a direct consequence of the dynamics of the underlying quantum chromodynamics (QCD).

In this chapter first the basic concepts of density functional theory (DFT) will be reviewed since it builds the basis of any mean field theory. Then the simplest relativistic mean field model for nuclear matter, the $\sigma\omega$-model, will be presented. The DBHF theory a more elaborate and also more fundamental

many-body approach will be discussed later. Finally the appearance of the scalar and vector fields in the framework of QCD sum rule analysis is discussed.

2.1. Density functional approach to QHD

The basic idea of density functional theory is that the exact energy E given by the expectation value of the exact Hamiltonian $\hat{H}$ in the exact ground state $|\Psi\rangle$ is approximated by the expectation value of an effective Hamiltonian $\hat{H}_{eff}$ for a simple product wave function $|\Phi\rangle$ the Slater determinant (where the formalism is taken from [66])

$$E = \langle\Psi|\hat{H}|\Psi\rangle \approx \langle\Phi|\hat{H}_{eff}|\Phi\rangle = E[\hat{\rho}]\,. \tag{2.1}$$

The product wave function

$$|\Phi\rangle := \mathcal{A}(\phi_1(\mathbf{r}_1)\ldots\phi_A(\mathbf{r}_A)) \tag{2.2}$$

is directly connected to the single particle density matrix

$$\hat{\rho} := \sum_{i=1}^{A} |\phi_i\rangle\langle\phi_i|\,. \tag{2.3}$$

Therefore the exact energy can be expressed as a functional of the single particle density matrix $\hat{\rho}$. Now with the energy density functional $E[\hat{\rho}]$ one is able to determine the average field $\hat{h}$

$$\hat{h} = \frac{\delta E}{\delta\hat{\rho}} \tag{2.4}$$

and the effective interaction

$$\hat{V} = \frac{\delta^2 E}{\delta\hat{\rho}^2} \tag{2.5}$$

where the single particle wave functions are eigenfunctions of the mean field $\hat{h}$

$$\hat{h}|\phi_i\rangle = \epsilon_i|\phi_i\rangle\,. \tag{2.6}$$

This non-linear problem requires a self-consistent solution due to the fact that the single particle field $\hat{h}$ depends on the density. That means that self-consistent changes of the mean field $\hat{h}$ and the wave functions corresponding to the field are allowed.

The task is now to find the correct density functional $E[\rho]$ which minimizes the many-body Hamiltonian. That such a density functional exists can be proven within density functional theory (Kohn-Sham Theory [67, 68]), how it looks like depends on the problem. To find a functional which comes as close as possible to

the - in principle existing - exact solution is the task to be solved. An additional caveat for nuclear systems is thereby that the existence theorem, the Hohenberg-Kohn theorem [69] has been proven for particles in an external field, e.g. atoms in the electromagnetic field. That this theorem holds as well for self-bound systems, such as nuclei, is assumed but has not been proven explicitly.

As already explained in the introduction the nuclear system is a relativistic one and therefore a Lorentz invariant formulation of DFT is required. The relevance of a Lorentz invariant formulation can be understood if one start from the Dirac equation for the relativistic single particle

$$h_D = \boldsymbol{\alpha}\,\mathbf{p} + \beta\,\Sigma \tag{2.7}$$

where the structure of Σ the relativistic mass operator is given by

$$\Sigma = M - S + \gamma_\mu V^\mu\,. \tag{2.8}$$

M denotes the nucleon mass. The field S is a Lorentz scalar and the fields $V^\mu = (V, \boldsymbol{V})$ give a Lorentz vector. Therefore one can write down the static Dirac equation

$$\begin{pmatrix} V - S & \boldsymbol{\sigma}(\mathbf{p} - \boldsymbol{V}) \\ \boldsymbol{\sigma}(\mathbf{p} - \boldsymbol{V}) & V + S - 2M \end{pmatrix} \begin{pmatrix} f_i \\ g_i \end{pmatrix} = \epsilon_i \begin{pmatrix} f_i \\ g_i \end{pmatrix} \tag{2.9}$$

where $-S < 0$ is an attractive field and $V > 0$ a repulsive field, respectively. The vector potential $\boldsymbol{V}$ vanishes in time reversal invariant systems. The two-dimensional spinor f_i is the large component of the Dirac spinor and g_i is the corresponding small component, respectively. The single particle energy is denoted by ϵ_i. As mentioned before there exist strong indications that in nuclear dynamics the scale of the fields S and V has to be very large and why it is important to account for Lorentz invariance.

Due to the coupling to the negative energy states or in other words to the lower components of the positive energy Dirac spinors an additional density dependence is introduced by the scalar field S in relativistic mean-field (RMF) theories. This genuine relativistic density dependence is one reason explaining, e.g., the great success in describing the nuclear saturation properties. The fields are not accessible directly since the large scalar (~ -350 MeV) and vector ($\sim +300$ MeV) fields cancel each other to a large extent giving the single-particle potential which is of the order of $\simeq -50$ MeV.

There exist also several features in nuclear structure which can be explained naturally within Dirac phenomenology while models based on non-relativistic dynamics have difficulties or, at least, one has to introduce additional model parameters.

The most well known feature is the large *spin-orbit splitting* in finite nuclei. In a relativistic framework the strong spin-orbit force appears naturally from the

coupling to the lower components of the Dirac equation where the scalar-vector mean fields add up in the spin-orbit potential $U_{\text{S.O.}} \propto (V - S) \simeq 750$ MeV. Due to this fact RMF theory is able to reproduce the strong spin-orbit splitting in spherical nuclei quantitatively throughout the Periodic Table without the introduction of additional parameters [28].

The next important feature in nuclear matter is the so-called *pseudo-spin symmetry* which has been found more than 30 years ago [29]. While all attempts to understand this symmetry within non-relativistic approaches failed, it can naturally be understood within RMF theory as has been shown by Ginocchio [30] a few years ago. This symmetry, again a consequence of the coupling to the lower components, is exact in the limit $V = -S$ and is broken in nature by the amount $(V + S)/(V - S)$ which is less than 10%.

The next example are the *moments of inertia in rotating nuclei*. Relativistic dynamics implies that in the rotating system a Coriolis term occurs due to the spatial vector currents, however, with all couplings already fixed through the time-like components [31].

2.1.1. The $\sigma\omega$-model

Although one can derive the relativistic equations of motion from an energy density functional they are usually derived by variation of a covariant Lagrangian density as will be shown in the following for the $\sigma\omega$-model.

The $\sigma\omega$-model is an effective, also renormalizable quantum field theory, which is often referred to as the Walecka model, who developed the first version of QHD in 1974 [70]. However, the original idea of an effective scalar and vector exchange goes even back to the year of 1956 (Dürr 1956 [71]).

The $\sigma\omega$-model is the simplest possible version of QHD, since the nucleon-nucleon interaction is described by the exchange of only two mesons. The repulsive short-range part of the nuclear force is described by isoscalar ω meson and the attractive intermediate part by the isoscalar σ meson. Although it is about a hadron-meson theory these two meson are regarded as effective, since they describe the complete nuclear force including all mesonic degrees of freedom. Pionic degrees of freedom are not included explicitly in this model because pion exchange does not contribute to the potential at the mean field level but only by exchange terms (Fock-diagrams). Moreover nuclear matter is a spin and isospin saturated system and therefore spin- and isospin-dependent forces are averaged out. Also the spin- and isospin-dependent contributions from two-pion exchange are omitted. The scalar part of the two-pion exchange is effectively included in the σ meson. This is the philosophy of an effective model, i.e., to treat contributions which are beyond the approximation scheme of the model not explicitly but to absorb them into the free model parameters. which then have to be adjusted to the properties of nuclear matter, in particular to the

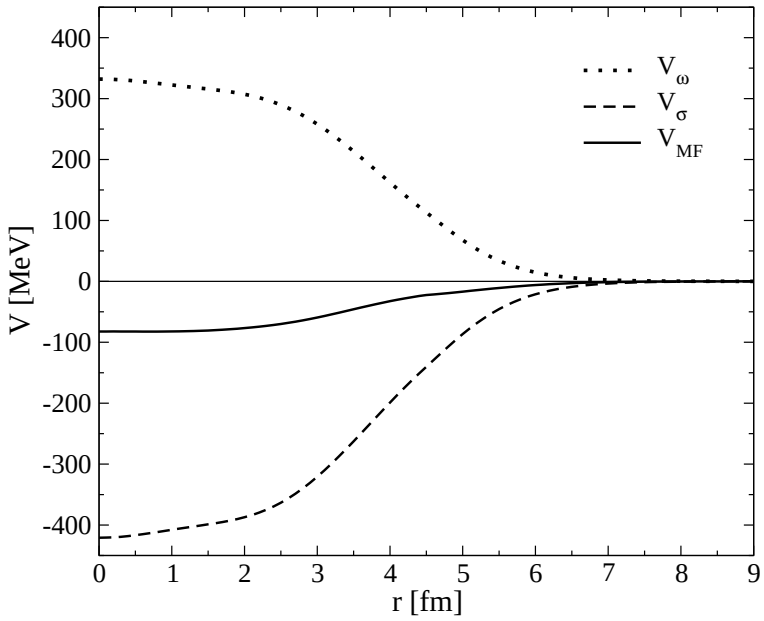

Figure 2.1: *The different mesonic potentials in the nucleus ^{40}Ca from QHD-I as a function of the radius r. V_{MF} is the total potential arising from the near compensation of the σ and ω contributions.*

nuclear saturation point.

Nevertheless the Walecka model exhibits already at that level the relevant aspects of relativistic nuclear dynamics. This becomes evident in Fig. 2.1 where the meson fields for ^{40}Ca are plotted. The attractive scalar field generated by the σ meson is approximately -420 MeV large whereas the repulsive vector field from the ω meson exchange is approximately 340 MeV large. These potentials almost cancel resulting in the standard nuclear potential V_{MF} which is of the order of $\simeq 80$ MeV.

The ρ-meson is neglected in the following since it its inclusion is of importance for a very accurate description of finite nuclei properties (single particle spectra, neutron skins etc.) but does not contribute in infinite nuclear matter.

2.1.2. Lagrange density and field equations

The starting point of relativistic models with nucleonic and mesonic degrees of freedom is given by the Lagrangian density where Dirac spinors describe the nucleons which interact via meson exchange (σ and ω) [70, 27, 28]. It consists of three parts: a baryonic part $\mathcal{L}_B$, a mesonic part $\mathcal{L}_M$, and a part describing the interactions $\mathcal{L}_{int}$

$$\begin{aligned}
\mathcal{L} &= \mathcal{L}_B + \mathcal{L}_M + \mathcal{L}_{int} \\
\mathcal{L}_B &= \bar{\psi}(i\gamma_\mu \partial^\mu - M)\psi \\
\mathcal{L}_M &= \frac{1}{2}\left\{(\partial_\mu \sigma)^2 - m_\sigma^2 \sigma^2\right\} - \frac{1}{4}F_{\mu\nu}F^{\mu\nu} + \frac{1}{2}m_\omega^2 \omega_\mu \omega^\mu \\
\mathcal{L}_{int} &= g_\sigma \bar{\psi}\psi\sigma - g_\omega \bar{\psi}\gamma_\mu \psi \omega^\mu \,. \qquad (2.10)
\end{aligned}$$

The spinorfield operator of the baryonic field is denoted by ψ where the nucleon mass is $M = 939$ MeV. σ is the fieldoperator of the scalar σ meson and ω^μ is the fieldoperator of the vector ω meson, where m_σ and m_ω and the masses of the mesons. The interaction part $\mathcal{L}_{int}$ is given by the minimal coupling of the bosonic fields to the fermionic field. g_σ and g_ω are the corresponding coupling constants. The antisymmetric field-strength-tensor is defined by

$$F^{\mu\nu} = \partial^\mu \omega^\nu - \partial^\nu \omega^\mu \,. \qquad (2.11)$$

The field equations are obtained applying the Euler-Lagrange equations

$$\begin{aligned}
\left[\gamma_\mu(i\partial^\mu - g_\omega \omega^\mu) - (M - g_\sigma \sigma)\right]\psi &= 0 \qquad (2.12) \\
\left[\partial_\mu \partial^\mu + m_\sigma^2\right]\sigma &= g_\sigma \bar{\psi}\psi \qquad (2.13) \\
\left[\partial_\nu F^{\mu\nu} + m_\omega^2\right]\omega^\mu &= g_\omega \bar{\psi}\gamma^\nu \psi \,. \qquad (2.14)
\end{aligned}$$

Eq. (2.12) is a Dirac equation of the nucleon field with minimally coupled scalar- and vectorfields of the mesons. Eq. (2.13) is a Klein-Gordon equation of a massive scalar field where the source term is given by the scalar density $\bar{\psi}\psi = \hat{\rho}_S$. The vector field is described by an inhomogeneous Proca equation where the source term is given by the four-vector baryon current $\hat{j}^\mu = \bar{\psi}\gamma^\mu\psi = (\hat{\rho_B}, \hat{\boldsymbol{j}})$. Here, $\hat{\rho}_B$ is the baryon density, whereas $\hat{\boldsymbol{j}}$ represents the vector current.

The energy-momentum-tensor is given by

$$T^{\mu\nu} = \mathcal{L}\delta_{\mu\nu} - \frac{\partial \mathcal{L}}{\partial(\partial_\mu \Phi)}\partial_\nu \Phi \,. \qquad (2.15)$$

For isotropic and homogeneous systems, $T^{\mu\nu}$ takes the form

$$T^{\mu\nu} = (\epsilon + P)u^\mu u^\nu - P g^{\mu\nu} \qquad (2.16)$$

with the four-velocity $u_\mu = (\gamma,\ \gamma\boldsymbol{v})$, which becomes $(1,\ \vec{0})$ in the local rest frame of the matter. ϵ stands for the energy density and P for the pressure.

This coupled, non-linear system for the field operators is not solvable in the form as represented by the Eqs.(2.12-2.14). Nevertheless when applying mean field approximation the problem becomes well treatable.

2.1.3. Mean field theory

In mean-field theory the meson fields and the corresponding source terms are substituted by their classical expectation values, i.e., only the nucleon fields $\bar{\psi}$ and ψ are quantized while the meson fields are treated as classical fields. More precisely,

$$\begin{aligned} \hat{\sigma} &\rightarrow \langle\hat{\sigma}\rangle = \Phi \\ \hat{\omega}^{\mu} &\rightarrow \langle\hat{\omega}^{\mu}\rangle = V^{\mu} \end{aligned}$$

With increasing baryon density the classical approximation of the fields becomes evidently better since quantum fluctuations are small when compared to the source terms in Eq. 2.13 and 2.14. Therefore also the source terms are replaced by their expectation values

$$\begin{aligned} \bar{\psi}\psi &= \hat{\rho}_s \rightarrow \left\langle\bar{\psi}\psi\right\rangle = \rho_s \\ \bar{\psi}\gamma^{\mu}\psi &= \hat{j}^{\mu} \rightarrow \left\langle\bar{\psi}\gamma^{\mu}\psi\right\rangle = j^{\mu} \end{aligned}$$

Due to spacial homogeneity and isotropy of infinite nuclear matter the meson field equations (2.13) and (2.14), respectively, are reduced to the determination of their source densities

$$m_{\sigma}^2\Phi = g_{\sigma}\rho_S \tag{2.17}$$

and

$$m_{\omega}^2 V^{\mu} = g_{\omega} j^{\mu} \ . \tag{2.18}$$

Besides the classical mesonic fields the baryon fields are quantized. Expanding the field operator in one-particle states one has also to sum over negative energy states, i.e., the Dirac sea. If one calculates expectation values of observables which can be represented as multi linear combinations of the field operators $\hat{\psi}$, ψ this produces divergences. This again requires a renormalization of the theory. To avoid this contributions from negative energy nucleons from the Dirac sea are neglected. This can be done by a normal ordering of the field operators before a determination of the expectation values.

The solutions of the Dirac equation in nuclear matter (2.12) are given by plane waves

$$\psi_{k,\lambda}(x) = u_{\lambda}(k)e^{-ik_{\mu}x^{\mu}} \ . \tag{2.19}$$

The four-component spinors $u_{\lambda}(k)$ with the helicity index λ fulfil the Dirac equation in momentum space. Introducing the momentum $k^{*\mu}$ and an effective mass m^*

$$k^{*\mu} = k^{\mu} - g_{\omega}V^{\mu} \tag{2.20}$$

$$M^* = M - g_{\sigma}\Phi \tag{2.21}$$

the effective Dirac equation (2.12) can be written as the free Dirac equation

$$(\gamma_\mu k^{*\mu} - M^*)\ u_\lambda(k^*) = 0\ . \tag{2.22}$$

The next step is to introduce the nuclear self-energy Σ now. Then the Dirac equation can be written as

$$(\gamma_\mu k^\mu - M - \Sigma)\ u_\lambda(k^*) = 0\ . \tag{2.23}$$

The self-energy has a scalar and a vector contribution

$$\Sigma = \Sigma_\mathrm{s} - \gamma_\mu \Sigma^\mu\ . \tag{2.24}$$

The scalar and vector parts of the nuclear self-energy are then proportional to the meson fields

$$\Sigma_\mathrm{s} = -\frac{g_\sigma^2}{m_\sigma^2}\rho_S \tag{2.25}$$

$$\Sigma_\mu = -\frac{g_\omega^2}{m_\omega^2} j^\mu\ . \tag{2.26}$$

The kinetic momentum k^* is on-shell in nuclear matter, i.e.

$$E^*(\mathbf{k}) = p_0^* = \sqrt{\mathbf{k}^{*2} + M^{*2}}\ . \tag{2.27}$$

Due to the normal ordering the expectation values are determined over the Fermi-sea where one then obtains the scalar- and vector density

$$\rho_S = \int_F \frac{d^3k}{(2\pi)^3}\frac{M^*}{E^*(\mathbf{k})}\sum_\lambda \langle \bar{u}_\lambda(k)|u_\lambda(k)\rangle = \frac{\kappa}{(2\pi)^3}\int_F d^3k \frac{M^*}{E^*(\mathbf{k})} \tag{2.28}$$

$$j^\mu = \int_F \frac{d^3k}{(2\pi)^3}\frac{M^*}{E^*(\mathbf{k})}\sum_\lambda \langle \bar{u}_\lambda(k)|\gamma^\mu|u_\lambda(k)\rangle = \frac{\kappa}{(2\pi)^3}\int_F d^3k \frac{k^{*\mu}}{E^*(\mathbf{k})} \tag{2.29}$$

The sum over the helicity index λ is the spin-isospin degeneracy factor since the normalization of the basis spinors is chosen such that $\bar{u}_\lambda u_\lambda = 1$. Therefore κ is 4 for symmetric nuclear matter and 2 in the case of pure neutron matter.

Considering nuclear matter in the rest frame the spacial components of the baryon current and the vector field, respectively, vanish due to spacial isotropy

$$j^\mu = \delta_0^\mu \rho_B \tag{2.30}$$

$$V^\mu = \delta_0^\mu V_0 \tag{2.31}$$

what then leads to the final expressions for the densities

$$\rho_S = \frac{\kappa}{4\pi^2}M^*\left[k_F E_F^* - M^{*2} ln(\frac{k_F + E_F^*}{M^*})\right] \tag{2.32}$$

$$\rho_B = \frac{\kappa}{6\pi^2}k_F^3 \tag{2.33}$$

where the Fermi momentum is denoted by k_F and the corresponding Fermi energy

$$E_F^* = \sqrt{k_F^2 + M^{*2}} \ . \tag{2.34}$$

Finally one is left with a non-linear system of equations consisting of Eq. (2.32) for the scalar density, Eq. (2.21) for the effective mass and Eq. (2.17) describing the classically approximated σ meson field. Therefore this problem requires a self-consistent solution.

Determination of the model parameters

In its minimal version of QHD-I the $\sigma\omega$-model has two free parameters, namely the coupling constants g_σ and g_ω of the two mesons. The meson masses are constants with $m_\sigma = 550$ MeV and $m_\omega = 783$ MeV. The meson-nucleon coupling constants g_σ and g_ω are now fixed to the saturation properties of nuclear matter. Therefore the model has to fulfil the following requirements:

1. The energy density has to be negative for a certain density range:
   $\frac{\epsilon}{\rho_B} - M < 0$ in order to permit a bound state.
   This condition can be realized, because the model contains two fields, the attractive scalar field $\Phi = \frac{g_\sigma}{m_\sigma^2}\rho_S$ and the repulsive vector field $V_0 = \frac{g_\omega^2}{m_\omega^2}\rho_B$.

2. To ensure a stable ground state, the binding energy E_B must have a minimum, i.e., $\frac{d}{dk_F}E_B = 0$ at saturation density and the condition

   $$\frac{g_\sigma^2}{m_\sigma^2} > \frac{g_\omega^2}{m_\omega^2}$$

   must be fulfilled.

   This requirement can be satisfied since the scalar density ρ_S, Eq. (2.32), to which the scalar field is directly proportional, saturates with increasing density ρ_B (or increasing k_F). The saturation behavior of the scalar density ρ_S is based on a pure relativistic effect and leads to an additional repulsion at large densities. This can be seen directly from an expansion of the scalar density in the Fermi momentum k_F

   $$\rho_S = \rho_B \left[1 - \frac{3k_F^2}{10M^2} + O\left(\frac{k_F^4}{M^4}\right)\right] \ . \tag{2.35}$$

   The leading term is proportional to ρ_B but with increasing k_F the higher order negative correction terms come into play. This correction appear in the same way in the resulting expression for the binding energy

   $$E_B = \frac{3k_F^2}{10M} + \frac{1}{2}\left(\frac{g_\omega^2}{m_\omega^2} - \frac{g_\sigma^2}{m_\sigma^2}\right)\rho_B + \frac{g_\sigma^2}{m_\sigma^2}\frac{\rho_B}{M}\frac{3k_F^3}{10M} \ . \tag{2.36}$$

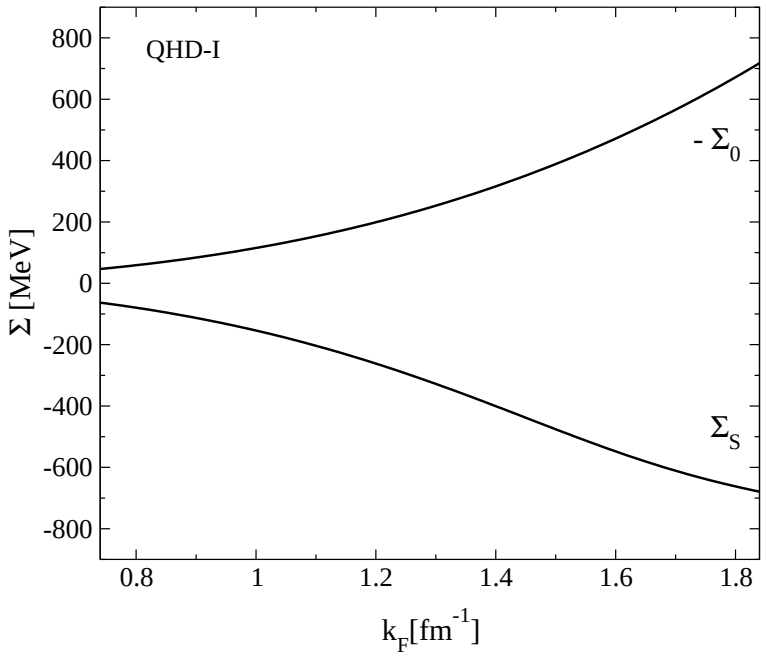

Figure 2.2: *The scalar- and vector fields* Σ_s *and* Σ_0 *from QHD-I as a function of the Fermi momentum* k_F*.*

The first term comes from the kinetic energy of the Fermi-motion. The second term proportional to the baryon density ρ_B describes the first order potential. The last term is a purely relativistic effect which introduces an additional repulsion which finally is responsible for the fact that with increasing density the repulsive vector field V_0 wins over the attractive scalar field Φ.

3. An adaption of the minimum $\frac{d}{dk_F}E_B = 0$ to empirical data

$$(\rho_0 = 0.17 \pm 1) \quad \frac{\text{nucleons}}{\text{fm}^3} \quad \text{and} \quad E_B = -16 \text{ MeV}$$

yields the final values for the coupling constants (in dimensionless units)

$$C_\sigma^2 = g_\sigma^2(\frac{M^2}{m_\sigma^2}) = 267.1, \qquad C_\omega^2 = g_\omega^2(\frac{M^2}{m_\omega^2}) = 195.9$$

with a nucleon mass of $M = 939$ MeV.

The optimal fit leads to $k_{F0} = 1.42$ fm^{-1} for QHD-I. This value is still slightly too large and can be improved by extensions of the QHD-I model.

At the saturation point the kinetic energy is approximately 20 MeV which leads to the following condition

$$20 \text{ MeV} + \frac{1}{2}\left(\frac{g_\omega^2}{m_\omega^2} - \frac{g_\sigma^2}{m_\sigma^2}\right)\rho_0 = -16 \text{ MeV}$$

This forces the scalar coupling constant g_σ to be large. Due to subtle cancellation effects between attractive scalar and repulsive vector fields also the vector coupling g_ω must be large.

The resulting self-energy fields Σ_s and Σ_0 as a function of the Fermi momentum are shown in Fig. 2.2. As one can see the fields are of opposite sign and of the same magnitude. At the saturation density predicted by the model $k_{F0} = 1.42$ fm^{-1} the scalar field $\Sigma_\text{s} \approx -410$ MeV and the vector field $\Sigma_0 \approx 330$ MeV. The appearance of these large fields exhibits a feature which is typical for all relativistic nuclear models namely large vector- and scalar fields with opposite sign which nearly compensate each other.

Nevertheless the $\sigma\omega$ model is an effective one since the model parameters are adjusted directly to the properties of nuclear matter. An alternative approach for nuclear matter are many-body calculations based on high precision nucleon-nucleon interactions where one treats short-range and many-body correlations explicitly. The Dirac-Brueckner theory which will be introduced in the next section is a very successful example for such an approach. It is in principle also based on the Lagrange density of QHD but goes far beyond the Hartree approximation. The free parameters are adjusted to free NN scattering data and one tries to reproduce the properties of nuclear matter on parameter free microscopic many-body physics.

2.2. The Dirac-Brueckner theory

Besides the very successful relativistic mean-field theories there have been been also attempts to describe nuclear matter on a microscopic level. The basic input for a microscopic approach is thereby the vacuum NN interaction where the potential model parameters are adjusted to empirical NN scattering data. The quantum mechanical many-body problem is then parameter free. Since the NN interaction is based on the strong interaction, i.e., on QCD, a solution within perturbation theory is not possible. Therefore another approach is more reliable namely to sum up certain classes of perturbative diagrams completely. In the Brueckner approximation or so-called hole-line expansion the problem is treated by summing up the so-called ladder diagrams [32]. The central equation of the BHF approximation is the Bethe-Goldstone equation which describes the scattering of two nucleons in matter. The resulting G-Matrix serves then as an effective two-particle potential containing the higher order correlations in

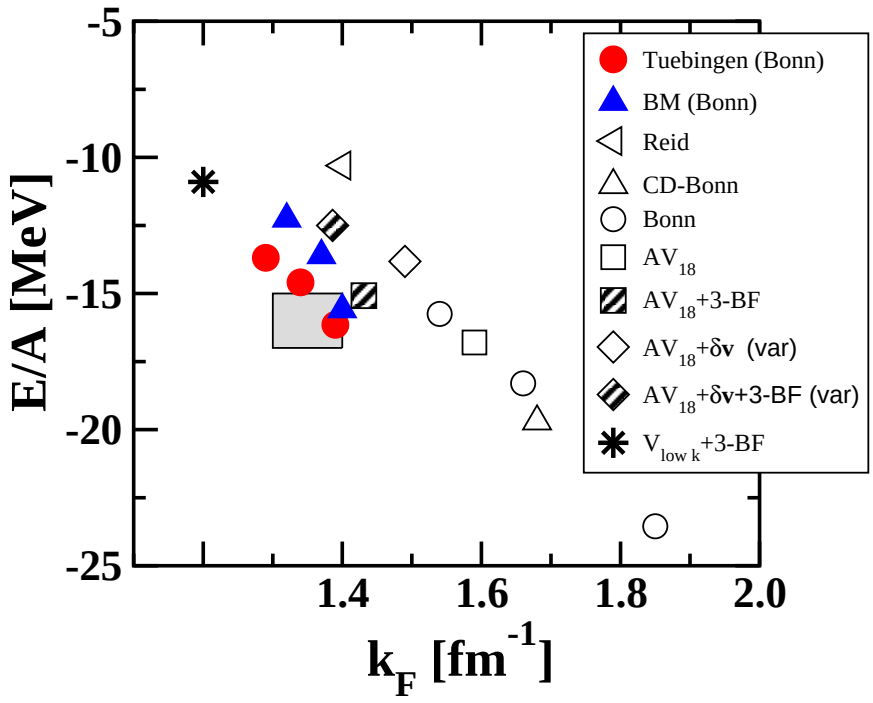

Figure 2.3: *Nuclear saturation points obtained with different nucleon-nucleon potentials. Full symbols correspond to relativistic and open symbols to non-relativistic Brueckner-Hartree-Fock calculations. The diamonds denote variational calculations and shaded symbols show calculations including 3-body forces. The star denotes a non-relativistic calculation up to second-order in many-body perturbation theory + 3-body forces for the low-momentum potential V_{lowk}. The empirical region of saturation is represented by the shaded area. (The figure was taken from [73]).*

ladder approximation. Nevertheless even very extensive non-relativistic many-body calculations do not reproduce quantitatively well the saturation properties of nuclear matter ($\rho_{sat} = 0.17 \pm 1$ fm^{-3}, $E_B = 16$ MeV) for all different choices of nucleon-nucleon interactions. This becomes apparent in Fig. 2.3 where the saturation points of isospin saturated matter are shown based on different nucleon-nucleon potentials calculated within different approaches. In fact the saturation points obtained in non-relativistic Brueckner calculations (open symbols) do not meet the empirical region of saturation. In contrast the saturation points obtained for various types of nucleon-nucleon potentials are located on the so-called Coester line [72].

In the early 1980s it became possible to treat the nuclear matter problem within a relativistic Brueckner approximation, the Dirac-Brueckner-Hartree-Fock (DBHF) approximation [74, 75]. In this approach a coupled set of equa-

tions has to be solved self-consistently: a Dyson equation for the in-medium baryon propagator, a Bethe-Salpeter equation for the in-medium T-matrix (the relativistic counterpart to the non-relativistic Bethe-Goldstone equation) and an equation for the self-energy of the nucleons in the nuclear medium.

The relativistic DBHF approach leads to rather reasonable saturation properties [34, 35, 36, 73]. The Coester line is shifted much closer to the empirical area of saturation as one can see from Fig. 2.3 for the relativistic calculations performed by Brockmann and Machleidt (BM) [35] or later by Fuchs et al. [73] (Tuebingen).

The nucleon-nucleon interaction is described in a meson-theoretical framework where the covariantly formulated one-boson-exchange potentials which will be described in detail in the next chapter are fitted to empirical NN vacuum scattering data. From this it follows that the full relativistic quantum mechanical many-body approach is parameter free. Nuclear matter calculations with the DBHF approach show that within a relativistic theory the saturation properties as well as the momentum dependence of the optical potential are reproduced better than in a non-relativistic approach.

2.2.1. T-matrix approximation

The Martin-Schwinger hierarchy of equations of motion for N-particle Green's functions allows to describe the quantum-mechanical many-body problem [76, 77]. The one particle Green's function is defined as

$$G(1,1') = (-i)\left\langle T(\psi(1)\bar{\psi}(1'))\right\rangle \tag{2.37}$$

and the corresponding two-particle Green's function

$$G(12,1',2') = (-i)^2\left\langle T(\psi(1)\psi(2)\bar{\psi}(2')\psi(1'))\right\rangle \tag{2.38}$$

where $\langle\rangle$ denotes the expectation value of the bilinear forms of the baryon field operators in the Heisenberg picture. T represents the usual chronological time ordering operator. The notation is $1 = (t_1, \boldsymbol{x_1}, \alpha)$ with the spin- and isospin index α. The expectation value is taken with respect to the ground state of cold, homogeneous and isotropic nuclear matter in rest.

The equation of motion for the one-particle Green's function is given as

$$(i\gamma_\mu\partial^\mu_{x_1} - M)G(1,1') = \delta(1-1') - i\int d2d3d4\,\langle 12|V|34\rangle\, G(34,1'2)\ . \tag{2.39}$$

It contains the two-particle potential V and the two-particle Green's function. Corresponding the N-particle Green's function then contains the $(N+1)$-particle Green's function. From this it follows that Eq. (2.39) describing the one-particle density already contains the full information of all N-particle correlations of the

system. That comes from the fact that in Eq. (2.39) the two-particle Green's function appears which is coupled to all higher Green's functions through the Martin-Schwinger hierarchy. The usual way to deal with the one-particle Green's function is to cut the hierarchy on the level of the two-particle Green's function. Therefore one needs a suitable approximation for the two-particle Green's function in Eq. (2.39). A convenient way is to use the Hartree or Hartree-Fock approximation for the two-particle Green's function which is then replaced by a uncorrelated product of two one-particle Green's functions.

To include two-particle correlations a better approximation is given by the introduction of the T-matrix which then acts as an effective two-particle potential. The T-matrix is defined

$$\langle 12|V|34\rangle\, G(34,1'2') = \int d3d4\, \langle 12|T|\bar{3}4\rangle\, G(3,1')G(4,2') \ . \tag{2.40}$$

Eq. (2.40) has to satisfies a Bethe-Salpeter equation [78]

$$\begin{aligned} \langle 12|T|1'2'\rangle &= \langle 12|V|1'2'\rangle \\ &+ i\int d3d4d3'd4'\, \langle 12|V|34\rangle\, G(3,3')G(4,4')\, \langle 3'4'|T|1'2'\rangle \ . \end{aligned} \tag{2.41}$$

Iterating Eq. (2.41) yields the so-called ladder approximation of the T-matrix.

The next step is to introduce the self-energy operator Σ (also called mass operator). Now the equation of motion for the baryon propagator (2.39) can formally be rewritten as a Dyson equation [77]

$$G(1,1') = G^0(1,1') + \int d2d3\, G^0(1,2)\Sigma(2,3)G(3,1') \ . \tag{2.42}$$

G^0 is the free Green's function, i.e. satisfying the free Dirac equation

$$(i\gamma_\mu \partial^\mu_{x_1} - M)G^0(1,1') = \delta(1-1') \ . \tag{2.43}$$

Consequently one obtains the expression for the self-energy in T-matrix approximation

$$\Sigma(1,1') = -i\int d2d2'\, [\langle 12|T|1'2'\rangle - \langle 12|T|2'1'\rangle\, G(2',2)] \ . \tag{2.44}$$

The system of coupled integral equations what has to be solved is given by the Eqs. (2.41), (2.42) and (2.44). Usually these equations on which the DBHF approach is based on are written in a more compact form as

$$T = V + i\int VGGT \tag{2.45}$$

$$\Sigma = -i\int (tr[GT] - GT) \tag{2.46}$$

$$G = G^0 + G^0\Sigma G \tag{2.47}$$

Nevertheless this system of coupled equations even for infinite nuclear matter is only solvable by applying further approximations [34]. The results obtained with the DBHF approach depend naturally not only on the approximations used but also on the choice of the theory describing the NN interaction. Since the DBHF theory is a relativistic one relativistic meson exchange potential are used where the two-particle potential V is given by one-boson-exchange potentials

$$\langle 12|V|1'2'\rangle \rightarrow \delta(1-1')\delta(2-2')V_{OBE}(1-2) \ . \tag{2.48}$$

These potentials are non-local in time and depend only on one four-momentum after a Fourier transformation. These covariantly formulated one-boson-exchange potentials will be described in greater detail in the subsequent chapter.

2.2.2. Self-energy in nuclear matter

In this section a brief discussion about the determination of the self-energy is shown where detailed information can be found in [35, 34].

The properties of dressed nucleons in nuclear matter are expressed by the self-energy entering the in-medium nucleon propagator which can be defined formally as the solution of the Dyson equation (2.42)

$$G(k) = \frac{1}{\gamma_\mu k^\mu - M - \Sigma(k)} \ . \tag{2.49}$$

The general form of the self-energy Σ is given by

$$\Sigma(k) = \Sigma_{\rm s}(k) - \gamma_\mu \Sigma^\mu(k) \ . \tag{2.50}$$

This form is determined by Lorentz invariance where the pseudo-scalar, pseudo-vector, and tensor contributions vanish due to the requirement of hermiticity, parity conservation, and time reversal invariance. In the nuclear matter rest frame the full self-energy reads [34, 79]

$$\Sigma(k) = \Sigma_{\rm s}(k) - \gamma_0 \, \Sigma_0(k) + \boldsymbol{\gamma} \cdot \mathbf{k} \, \Sigma_{\rm v}(k) \ . \tag{2.51}$$

The self-energy components are Lorentz scalar functions depending on the Lorentz invariants k^2, $k \cdot j$ and j^2, where k_μ is the nucleon four-momentum and j_μ denotes the four-vector baryon current. The streaming velocity is defined as $u^\mu = j_\mu/\sqrt{j^2}$. In nuclear matter at rest the time-like component is just the baryon density and spatial components of the current vanish, i.e., $j_\mu = (\rho_B, \mathbf{0})$. Hence, the Lorentz invariants can be expressed in terms of k_0, $|\mathbf{k}|$ and k_F, where k_F denotes the Fermi momentum.

The components of the self-energy are computed by taking the respective traces in the Dirac space [79, 80]

$$\Sigma_{\rm s} = \frac{1}{4} tr\left[\Sigma\right], \tag{2.52}$$

$$\Sigma_{0} = \frac{-1}{4} tr\left[\gamma_0\,\Sigma\right], \tag{2.53}$$

$$\Sigma_{\rm v} = \frac{-1}{4|\mathbf{k}|^2} tr\left[\boldsymbol{\gamma}\cdot\mathbf{k}\,\Sigma\right]. \tag{2.54}$$

The Dirac equation for the in-medium spinor basis can be deduced from the Green's function (2.49). The presence of the medium leads to effective masses and effective momenta of the nucleons

$$M^* = M + Re\,\Sigma_{\rm s} \tag{2.55}$$

$$k^*_\mu = k_\mu + Re\,\Sigma_\mu \tag{2.56}$$

and the Dirac equation is then given by

$$[\gamma_\mu k^\mu - M - Re\,\Sigma] u^*_\lambda(k) = 0 \quad . \tag{2.57}$$

The solution of this Dirac equation provides the in-medium nucleon spinors

$$u^*_\lambda(k) = \sqrt{\frac{E^* + M^*}{2M^*}} \begin{pmatrix} 1 \\ \frac{\boldsymbol{\sigma}\cdot\mathbf{k}^*}{E^*+M^*} \end{pmatrix} \chi_\lambda \tag{2.58}$$

where χ_λ denotes a two-component spinor.

Another important approximation in the DBHF approach is the no sea approximation where the subspace of negative energy states is omitted. This procedure avoids the problem of infinities which generally appear due to contributions from negative energy nucleons in the Dirac sea [27, 79]. Therefore the full propagator Eq. (2.49) is replaced by its Dirac part G_D [79]

$$G^D(k) = 2\pi i(\gamma_\mu k^{*\mu} + M^*)\delta(k^{*2} - M^{*2})\Theta(k^*_0)\Theta(k_F - |\mathbf{k}|) \tag{2.59}$$

for the determination of the self-energy (2.44). Here k denotes the momentum of a nucleon inside the Fermi sea. Due to the Θ functions in the propagator only positive energy nucleons are allowed in the intermediate scattering states.

In general the self-energy is complex but the philosophy of the DBHF approach is to treat the nucleons as quasiparticles in the medium which obtain their physical masses and momenta by the interaction with the nuclear medium. Therefore only the real part of the self-energy is taken into account. Thus the

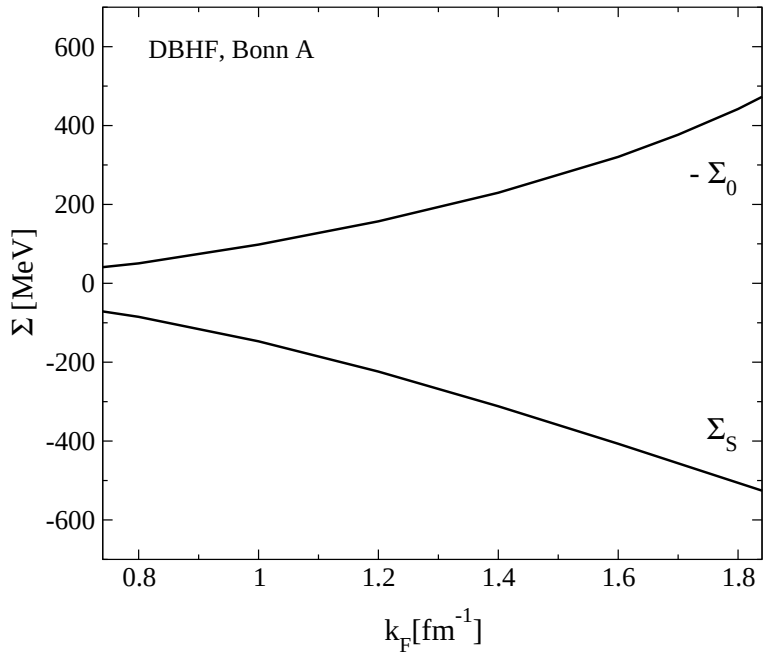

Figure 2.4: The scalar- and vector fields Σ_s and Σ_0 derived within the DBHF approach as a function of the Fermi momentum k_F. The Bonn A nucleon-nucleon interaction is used.

effective nucleon momentum is on mass shell even above the Fermi surface, i.e. $k^*_\mu k^{*\mu} = M^{*2}$. The four momentum follows from Eq. (2.56)

$$\mathbf{k}^* = \mathbf{k}(1+\Sigma_v), \qquad k^*_0 = E^* = \sqrt{\mathbf{k}^2(1+\Sigma_v)^2 + M^{*2}} \tag{2.60}$$

which allows one to rewrite the Dirac equation

$$[\gamma_\mu \tilde{k}^{*\mu} - \tilde{M}^*] u^*_\lambda(k) = 0 \tag{2.61}$$

by introducing the reduced effective mass and kinetic momentum

$$\tilde{M}^* = \frac{M^*}{1+\Sigma_v}, \tag{2.62}$$

$$\tilde{k}^*_\mu = \frac{k^*_\mu}{1+\Sigma_v} \ . \tag{2.63}$$

It is known from consistent Hartree-Fock calculations that the self-energy components in Eq. (2.51) depend weakly on the momentum inside the Fermi sphere. Therefore the momentum dependence of Σ_s, Σ_0, and Σ_v is neglected and the fields are approximated by their values at the Fermi momentum

$$Re\,\Sigma(k) = Re\,\Sigma(k_F) \ , \qquad |\mathbf{k}| \le k_F \ . \tag{2.64}$$

This so-called *reference spectrum approximation* is used to simplify the calculation. Finally one has to verify the consistency of the assumption $Re\,\Sigma(k) \approx Re\,\Sigma(k_F)$ at the end of the calculation.

Furthermore for the determination of the self-energy (2.44) the in-medium two-body T-matrix derived from the free NN interaction has to be represented Lorentz invariantly. This is done by projecting the two-body amplitudes on a set of linearly independent covariant operators. Since the Dirac sea, i.e., the coupling to anti-nucleons, is neglected the choice of the covariant operators is in principle ambiguous. In a full DBHF calculation the final results like e.g. the shape the equation of state as well as the value for the saturation point depend to some extent on this choice. The formalism for the projection scheme as well as the choice of the set of covariant operators is presented in Chapter 4.

In Fig. 2.4 the self-energy fields Σ_s and Σ_0 are shown as a function of the Fermi momentum derived within the DBHF approach. The fields have opposite signs and are of the same magnitude. When compared to the results from the phenomenological QHD-1 model shown in Fig. 2.2 one sees that the fields from the DBHF approach are reduced. The reason for that lies in the fact that in the full microscopic DBHF calculation short range ladder correlations are included.

As already mentioned in the introduction again an implicit feature of relativistic models is shown namely the appearance of large vector- and scalar fields with opposite sign. Nevertheless since in the DBHF approach relativistic meson exchange NN potentials are used it not clear if theses large fields are an artefact of the meson exchange picture or in other words if these large fields also appear when non-relativistic NN interactions are applied.

2.3. In-medium QCD sum rules

As described in the previous sections in the Dirac phenomenology nucleon propagation is described by a Dirac equation with an optical potential exhibiting large Lorentz scalar and vector components. The relativistic phenomenology provides an accurate model to describe spin observables as well as saturation properties of nuclei.

A connection to QCD the fundamental theory of strong interactions is established by QCD sum rules [43, 44, 45]. Within this approach the self-energy of an intermediate energy nucleon in nuclear matter is determined. One finds that QCD in-medium sum rules predict an attractive scalar and repulsive vector self-energy which are astonishingly close to the empirical values derived from RMF fits to the nuclear chart. These QCD in-medium sum rules depend to leading order directly on the scalar and vector condensates $\langle\bar{q}q\rangle, \langle q^\dagger q\rangle$ at finite density.

QCD sum rules were introduced first by Shifman et al. [81, 82] in the late 1970's. They applied QCD sum rules to describe mesonic properties in vacuum.

Later the method was expanded for the description of the characteristics of nucleons in vacuum by Ioffe [49] and others [83].

The sum rule approach is based on a Fourier transformed correlation function of an interpolating field $\eta(x)$ which is constructed from quark fields in such a way that it carries the quantum numbers of the nucleon (see Eq. 2.68):

$$\Pi(q) \equiv i \int d^4x e^{iq\cdot x} \langle T[\eta(x)\bar{\eta}(0)]\rangle_0 \ . \tag{2.65}$$

The short notation $\langle\Omega\rangle_0 = \langle 0|\Omega|0\rangle$ is introduced, where Ω is an arbitrary operator. T is the time-ordering operator and the state $|0\rangle$ denotes the physical non-perturbative vacuum. This function is equivalent to a nucleon propagator in a hadronic theory.

The correlator function $\Pi(q)$ can also be written in terms of the operator product expansion. It is then given by a sum of coefficient functions, the so-called Wilson coefficients which can be calculated in QCD perturbation theory, multiplied with matrix elements of composite operators constructed from quark and gluon fields and organized according to their mass dimensions. The operators of lowest non-trivial dimension are given by $\bar{q}q$ and $G^a_{\mu\nu}G^{a\mu\nu}$ where q denotes an up or down quark and $G^a_{\mu\nu}$ $(a = 1-8)$ is the gluonic field-strength tensor. In vacuum these matrix elements are just the non-perturbative quark and gluon condensates. The next step is a spectral decomposition of the correlator showing that the correlator describes the propagation of a (virtual) nucleon as well as higher mass states with nucleon quantum numbers. A sum rule is obtained by equating the operator product expansion correlator and the spectral expansion. Then a phenomenological ansatz for the spectral density has to be assumed, which is chosen to be the in-medium nucleon propagator of a dressed quasi-particle in the finite density case .

A differential operation, the so-called Borel transformation is applied to both sides, the theoretical and the phenomenological one, which improves convergence properties of the operator product expansion because it suppresses contributions coming from higher-dimensional operators. Moreover it stresses the contribution from the nucleon pole on the phenomenological side [81, 82]. Finally the identification of the correlation function with the phenomenological ansatz leads then to scalar and vector self-energies $\Sigma_{\rm s}$ and Σ_0 [43].

In the zero-density limit of the nucleon sum rule [49] the phenomenological ansatz for the spectral density is chosen to be a nucleon pole plus a smooth continuum which accounts for all higher-mass excitations. Due to Ioffe the contributions from higher-dimensional condensates and the continuum are small and one obtains the well known expression for the nucleon mass in vacuum [83]

$$M \simeq -\frac{8\pi^2}{\Lambda_B^2}\langle\bar{q}q\rangle_0 \ . \tag{2.66}$$

The vacuum value of the lowest-dimensional quark condensate is about [84] $\langle\bar{q}q\rangle_0 \simeq -(225\pm25\,\mathrm{MeV})^3$. The formula has to be evaluated for $\Lambda_B^2 \simeq M^2$ where Λ_B is the mass parameter of the Borel transform. It is the generic low energy scale of QCD which separates the non-perturbative from the perturbative regime and coincides with the chiral symmetry breaking scale Λ_χ of chiral perturbation theory.

It appears natural to apply QCD sum rule methods to determine the scalar and vector self-energies of a nucleon quasi particle in nuclear matter, i.e., to generalize the Ioffe formula to finite density [45, 43, 44]. Changes of the quark condensate due to finite baryon density should lead to changes in the nucleon spectrum. This can be concluded from the fact that a basic assumption of the QCD sum rule approach is that the low-lying structure of the spectrum is strongly influenced by the quark interactions with the vacuum condensates. Therefore the quark condensates should set the scale for the nucleon self-energy in nuclear matter.

In a finite density approach one has to consider the correlation function $\Pi(q)$ of the same interpolating field $\eta(x)$ but now evaluated in the ground state of finite nuclear matter [43]

$$\Pi(q) \equiv i \int d^4x e^{iq\cdot x} \langle T[\eta(x)\bar{\eta}(0)]\rangle_{\rho_B} \ . \tag{2.67}$$

The interpolating field $\eta(x)$ for the proton is given in terms of up- and down-quark fields as proposed by Ioffe [49]

$$\eta(x) = \epsilon_{abc}[u^{aT}(x)C\gamma_\mu u^b(x)]\gamma_5\gamma^\mu d^c(x) \tag{2.68}$$

where a,b, and c are color indices, T means transpose, and C is the charge-conjugation matrix [78]. The interpolating field for the neutron is obtained by interchanging the up and down quarks.

Since the correlation function is a 4×4 matrix in Dirac space it can be expanded in a set of Dirac matrices. Due to Lorentz covariance, parity and time reversal invariance $\Pi(q)$ then reads

$$\Pi(q) \equiv \Pi_s(q^2, q\cdot u) + \Pi_q(q^2, q\cdot u)\ \not{q} + \Pi_u(q^2, q\cdot u)\ \not{u} \ . \tag{2.69}$$

The four-velocity of the nuclear medium is denoted by u^μ and therefore $u^\mu = (1, \mathbf{0})$ in the rest frame. Thus there are three invariant functions. An expansion of the coordinate space quark propagator in the presence of the non-perturbative medium gives [43]

$$\begin{aligned} \langle T[q_i^a(x)\bar{q}_j^b(0)]\rangle_{\rho_B} &= \frac{i}{2\pi^2}\delta^{ab}\frac{x^\mu}{x^4}[\gamma_\mu]_{ij} \\ &- \frac{1}{4N_c}\delta^{ab}[\gamma_\mu]_{ij}\langle\bar{q}\gamma^\mu q\rangle_{\rho_B} \\ &- \frac{1}{4N_c}\delta^{ab}\delta_{ij}\langle\bar{q}q\rangle_{\rho_B} + \ldots \end{aligned} \tag{2.70}$$

where i and j are Dirac indices and N_c denotes the number of colors. For each invariant function now only the leading term in the operator product expansion is kept. In contrast to the vacuum case a new vector condensate $\langle\bar{q}\gamma^\mu q\rangle_{\rho_B}$ shows up at finite density. It is the rest-frame quark density times u^μ. Current quark masses as well as gluon condensates are neglected since their contribution is small. By applying Wick's theorem to Eq. (2.67) where Eq. (2.70) is used for each contraction the correlator is evaluated. After a projection of the leading contributions to each invariant function one obtains the following expressions for the invariant functions in Eq. (2.69) in the nuclear matter rest frame, where $q \cdot u \to q_0$

$$\begin{aligned}
\Pi_s(q^2, q_0) &= \frac{1}{4\pi^2} q^2 \ln(-q^2)\langle\bar{d}d\rangle_{\rho_B} + \dots \,, && (2.71)\\
\Pi_q(q^2, q_0) &= -\frac{1}{64\pi^4}(q^2)^2 \ln(-q^2) \\
&\quad + \frac{1}{6\pi^2} q_0 \ln(-q^2)[\langle u^\dagger u\rangle_{\rho_B} + \langle d^\dagger d\rangle_{\rho_B}] + \dots \,, && (2.72)\\
\Pi_u(q^2, q_0) &= \frac{1}{12\pi^2} q^2 \ln(-q^2)[7\langle u^\dagger u\rangle_{\rho_B} + \langle d^\dagger d\rangle_{\rho_B}] \dots \,. && (2.73)
\end{aligned}$$

Interchanging the fields u and d one obtains the corresponding expressions for the neutron.

Now on the phenomenological side of the sum rule a quasiparticle pole for the nucleon with real self-energies is taken to formulate the QCD sum rule ansatz. The propagator is given by Eq. (2.49)

$$G(q) = -\Lambda_N^2 \frac{1}{(q - \Sigma^\mu)\gamma_\mu - (M - \Sigma_\mathrm{s})} + \dots \,. \tag{2.74}$$

where the self-energies are assumed to be independent of energy and momentum. In general one can write $\Sigma^\mu = \Sigma_0 u^\mu + \Sigma_\mathrm{v} q^\mu$ where Σ_v is neglected and it is assumed that Σ_0 and Σ_s are constants. These are the on-shell self-energies of a quasinucleon with three momentum $\mathbf{q}$ in the language of hadronic theories as discussed in the previous sections. Λ_N is the coupling strength of the current $\eta(x)$ to the nucleon quasiparticle. The phenomenological representations of the invariant functions in the nuclear matter rest frame are then [43]

$$\begin{aligned}
\Pi_s(q^2, q_0) &= -\Lambda_N^2 \frac{M^*}{(q^2 - \mu^2)} + \dots \,, && (2.75)\\
\Pi_q(q^2, q_0) &= -\Lambda_N^2 \frac{1}{(q^2 - \mu^2)} + \dots \,, && (2.76)\\
\Pi_u(q^2, q_0) &= \Lambda_N^2 \frac{\Sigma_0}{(q^2 - \mu^2)} + \dots \,, && (2.77)
\end{aligned}$$

with $M^* = M + \Sigma_s$ and $\mu^2 = M^{*2} - \Sigma_0^2 + 2q_0\Sigma_0$. The Eqs. (2.75)-(2.77) follow from dispersion relations in q^2 with $q \cdot u$ fixed effectively at the quasinucleon energy what suppresses antinucleon contributions [43, 44]. To improve the overlap of the theoretical and phenomenological descriptions of the correlator a Borel transform is applied to both sides. Equating the Borel transforms one obtains [43]

$$\Lambda_N^2 M^* e^{-\mu^2/\Lambda_B^2} = -\frac{1}{4\pi^2}\Lambda_B^4 \langle\bar{q}q\rangle_{\rho_B} \ , \tag{2.78}$$

$$\Lambda_N^2 e^{-\mu^2/\Lambda_B^2} = \frac{1}{32\pi^4}\Lambda_B^6 - \frac{1}{3\pi^2} q_0 \Lambda_B^2 \langle q^\dagger q\rangle_{\rho_B} \ , \tag{2.79}$$

$$\Lambda_N^2 \Sigma_0 e^{-\mu^2/\Lambda_B^2} = \frac{2}{3\pi^2}\Lambda_B^4 \langle q^\dagger q\rangle_{\rho_B} \ . \tag{2.80}$$

The sum rules depend on two parameters, namely the Borel mass Λ_B and q_0. q_0 is taken to be the energy of the quasiparticle which is studied. The on-shell four-momentum squared of the quasiparticle is equal to μ^2. As one can see from Eqs. (2.78)-(2.80) one also needs to know the scalar and vector condensates $\langle\bar{q}q\rangle_{\rho_B}$ already present in vacuum, and the vector condensate $\langle q^\dagger q\rangle_{\rho_B}$ which is introduced by the breaking of Lorentz invariance due to the presence of the medium. Due to the fact that isoscalar quantities are considered one sets

$$\langle\bar{u}u\rangle_{\rho_B} \simeq \langle\bar{d}d\rangle_{\rho_B} \equiv \langle\bar{q}q\rangle_{\rho_B} \ , \tag{2.81}$$

$$\langle u^\dagger u\rangle_{\rho_B} = \langle d^\dagger d\rangle_{\rho_B} \equiv \langle q^\dagger q\rangle_{\rho_B} = \frac{3}{2}\rho_B \ , \tag{2.82}$$

where $\langle q^\dagger q\rangle_{\rho_B}$ denotes the quark density for one flavor in the nuclear matter rest-frame and since the baryon current is conserved it is trivially proportional to the nucleon density. A model independent estimation of the density dependence of the scalar condensate to lowest order can be found with the help of the Hellman-Feynman theorem as explained in Section 6.2 in greater detail. The change of the scalar condensate to lowest order in a density expansion is related to the pion-nucleon σ_N term [51, 45]

$$\langle\bar{q}q\rangle_{\rho_B} = \langle\bar{q}q\rangle_0 + \frac{\rho_B \sigma_N}{m_u + m_d} + \ldots \tag{2.83}$$

where m_u and m_d denote the current quark masses and σ_N the pion-nucleon sigma term (Section 6.2). It is determined by the u and d-quark content of the nucleon and represents the contribution from explicit chiral symmetry breaking to the nucleon mass through the small, but non-vanishing current quark masses.

Taking ratios of Eqs. (2.78)-(2.80) yields the following expressions for the scalar and vector self-energies

$$\Sigma_{\rm s} = -\frac{8\pi^2}{\Lambda_B^2}[\langle\bar{q}q\rangle_{\rho_B} - \langle\bar{q}q\rangle_0] = -\frac{8\pi^2}{\Lambda_B^2}\frac{\sigma_N\rho_B}{m_u+m_d} \tag{2.84}$$

$$\Sigma_0 = \frac{64\pi^2}{3\Lambda_B^2}\langle q^\dagger q\rangle_{\rho_B} = \frac{32\pi^2}{\Lambda_B^2}\rho_B \quad . \tag{2.85}$$

which are assumed to be valid up to nuclear saturation density. The second term in Eq. (2.79) which is of higher order in the operator product expansion is neglected and the vacuum result Eq. (2.66) for the nucleon mass has to be subtracted in order to obtain Eq. (2.84).

The ratio of Eqs. (2.84) and (2.85) gives

$$\frac{\Sigma_{\rm s}}{\Sigma_0} = -\frac{\sigma_N}{4(m_u+m_d)} \tag{2.86}$$

where the Borel mass Λ_B drops out. With typical values for $m_{u,d}$ of about $m_u + m_d = 14 \pm 4$ MeV and $\sigma_N = 45 \pm 7$ MeV [85] for the pion-nucleon sigma term the ratio is close to -1 (-0.8 ± 0.3) which indicates a considerable cancellation. This is in qualitative agreement with Dirac phenomenology where the scalar and vector self-energies cancel approximately. The scalar and vector self-energies derived within the QCD sum rule approach at the most simple level depend on the Borel mass as one can see from Eqs. (2.84) and (2.85). Assuming that the scales on both the phenomenological and theoretical sides of the sum rules are comparable to the vacuum case, then the Borel mass will be close to the best working value in the vacuum sum rule case, i.e., $\Lambda^2 \approx 1$ GeV^2 [43]. This gives values for the scalar and vector self-energies of ≈ 400 MeV at nuclear saturation density. This is again in qualitative agreement with Dirac phenomenology where the magnitude of the cancelling scalar and vector self-energies is similar as depicted in Section 2.1.3 for the simple mean-field case and in Section 2.2.2 where self-energies derived within the microscopic DBHF approach are shown.

Nevertheless one has to keep in mind that the derivation of Eqs. (2.84) and (2.85) is based on certain assumptions and approximations. In the operator product expansion of the correlator higher-dimensional condensate contributions are neglected e.g. four-quark condensates [44]. These corrections can contribute significantly. For example including the second term in Eq. (2.79) leads to a reduction of $\Sigma_{\rm s}$ by $\approx 50\%$.

Moreover the sum rule for the scalar field Eq. (2.84) corresponds to a Fermi gas of non-interacting nucleons. Therefore important corrections from higher orders in the density expansion can occur. An estimate of the density dependence of the scalar condensate is shown in Section 6.2. It is derived with the help of the

Hellmann-Feynman theorem in Hartree-Fock approximation and in Brueckner-Hartree-Fock approximation based on a chiral nucleon-nucleon interaction.

In the framework of in-medium QCD sum-rules the effective nucleon mass $M^* = M + \Sigma_s$ at finite density depends directly on the scalar condensate (2.84) which is assumed to be valid at least below nuclear saturation density. The validity of this assumption is discussed in Chapter 6.

3. The NN interaction

As already mentioned in the introduction, a quantitative description of the nuclear force in the framework of QCD is not be possible due to the non-perturbative nature of QCD at the relevant low energy scales. Nevertheless besides the formidable mathematical problems in describing the nuclear force another argument justifies the choice of the relevant degrees of freedom to be nucleons (and their excited states) and massive bosons, e.g., pions mediating the nuclear force. In order to resolve the substructure of the nucleon in deep inelastic scattering experiments at least a momentum transfer of $q^2 > 1$ GeV^2 is needed. However, the nucleon-nucleon interaction in nuclei or neutron stars takes place on an energy scale of about $q^2 \sim 0.1$ GeV^2. Since the nuclear substructure is not resolved anymore quantitative descriptions of nuclear many-body systems can be based on models which describe the NN interaction via effective degrees of freedom.

The nucleon-nucleon potential has a Van-der-Waals like structure schematically displayed in Fig. 3.1. As already mentioned in the introduction the nuclear force can be subdivided into three regions: an attractive long-range part for $r \geq 2$ fm (r is the relative distance of the two nucleons) dominated by one-pion exchange (OPE), an intermediate range attractive part (1 fm $\geq r \leq 2$ fm) and a short-range repulsive part ($r \leq 1$ fm), the so-called *hard core*. This short-range part is is the mathematically most complicated part, since multi-pion exchange and various heavy mesons play a role.

In this chapter first an example of a covariantly formulated meson exchange potential constructed in the framework of field theory is presented. Then non-relativistic meson-exchange potentials as well as phenomenological potentials will be discussed and finally two types of low-momentum interactions will be introduced.

The goal to investigate the Dirac structure of the nucleon-nucleon interaction in a model independent way does not require a complete description of the studied potentials. Therefore the conceptual and theoretical differences of the models are rather of importance.

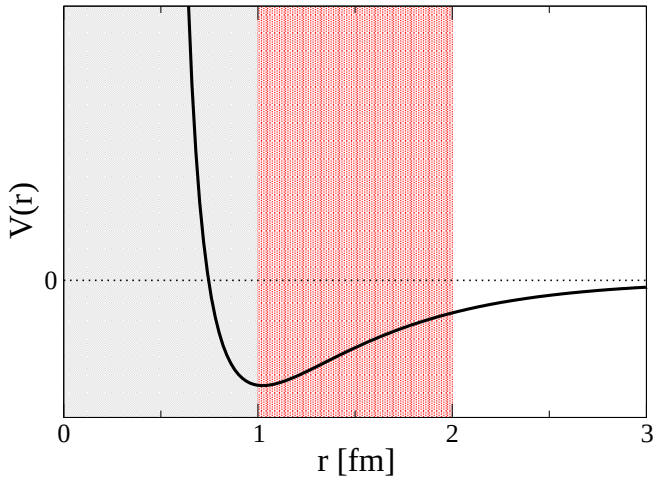

Figure 3.1: Schematic picture of the nucleon-nucleon potential generated by the exchange of various mesons. The relative distance of the two nucleons is denoted by r.

3.1. Boson exchange potentials

As typical examples for modern high precision one-boson-exchange (OBE) potentials we consider the Bonn A [12, 86] and the high-precision, charge-dependent Bonn (CD-Bonn) potential [87]. The Bonn potentials are based on the exchange of the six non-strange bosons $(\pi, \eta, \rho, \omega, \delta, \sigma)$ with masses below the nucleon mass. These are the two scalar mesons σ (isoscalar) and δ (isovector), the two pseudo-scalar mesons π (isovector) and η (isoscalar), and the two vector mesons ω (isoscalar) and ρ (isovector). The potentials are derived in the *no sea* approximation which neglects the coupling to anti-particles.

The following Lagrangians describe the coupling of the included mesons to the nucleons

$$\mathcal{L}_{\mathrm{NNps}} = -g_{ps}\,\bar{\psi}\,i\gamma_5\,\psi\,\varphi_{\mathrm{ps}} \tag{3.1}$$

$$\mathcal{L}_{\mathrm{NNs}} = -g_s\,\bar{\psi}\psi\varphi_{\mathrm{s}} \tag{3.2}$$

$$\mathcal{L}_{\mathrm{NNv}} = -g_v\,\bar{\psi}\,\gamma_\mu\,\psi\,\varphi_{\mathrm{v}}^{\mu} - \frac{f_{\mathrm{v}}}{4M_p}\bar{\psi}\,\sigma_{\mu\nu}\,\psi\cdot(\partial^\mu\,\varphi_{\mathrm{v}}^{\nu} - \partial^\nu\,\varphi_{\mathrm{v}}^{\mu}) \tag{3.3}$$

where ψ represents the nucleon and φ_α meson field operators. M_p is the nucleon mass. For isospin $I = 1$ mesons the corresponding φ_α has to be replaced by $\boldsymbol{\tau}\cdot\boldsymbol{\varphi_\alpha}$. The lowest order contribution to the nuclear force in the centre-of-mass frame is then given by the amplitude $\mathcal{A}$ describing the Feynman diagram depicted in Fig.3.2

$$-i\mathcal{A}_\alpha(q',q) = \bar{u}_1(\mathbf{q}')\kappa_\alpha^{(1)}u_1(\mathbf{q})\;D_\alpha(q'-q)\;\bar{u}_2(-\mathbf{q}')\kappa_\alpha^{(2)}u_2(-\mathbf{q}). \tag{3.4}$$

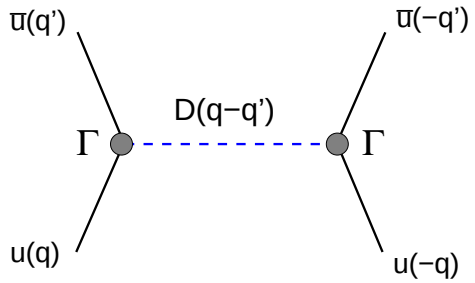

Figure 3.2: Schematic representation of one-boson-exchange diagram.

The Dirac structure of the potential is contained in the meson-nucleon vertices $\kappa_\alpha^{(i)}$ $(i = 1, 2)$ derived from the above Lagrangians

$$\kappa_{\rm s} = g_{\rm s}\mathbf{1}, \quad \kappa_{\rm ps} = g_{\rm ps}\frac{\not{q}' - \not{q}}{2M} i\gamma^5, \quad \kappa_{\rm v} = g_{\rm v}\gamma^\mu + \frac{f_{\rm v}}{2M} i\sigma^{\mu\nu} \quad . \tag{3.5}$$

For the pseudo-scalar mesons π and η a pseudo-vector coupling is used in order to fulfil soft pion theorems. The ω meson has no tensor coupling, i.e., $f_{\rm v}^{(\omega)} = 0$. The meson propagators $D_\alpha(q' - q)$ read

$$D_{\rm s,ps}(q' - q) = i\frac{1}{(q' - q)^2 - m_{\rm s,ps}^2} \tag{3.6}$$

$$D_{\rm v}^{\mu\nu}(q' - q) = i\frac{-g^{\mu\nu} + (q' - q)^\mu (q' - q)^\nu / m_{\rm v}^2}{(q' - q)^2 - m_{\rm v}^2} \tag{3.7}$$

for scalar and pseudo-scalar mesons s,ps and vector mesons v. In case of on-shell scattering the $(q' - q)^\mu (q' - q)^\nu$ vanishes for vector bosons. The meson-exchange potential is then obtained by (i times) the sum over the several OBE exchange Feynman amplitudes describing the exchange of a single meson α

$$V(\mathbf{q}', \mathbf{q}) = \sum_{\alpha={\rm s,ps,v}} \mathcal{A}_\alpha(\mathbf{q}', \mathbf{q})\ \mathcal{F}_\alpha^2(\mathbf{q}', \mathbf{q})\ . \tag{3.8}$$

In the two-nucleon centre-of-mass frame (c.m.) the four-momenta of the incoming nucleons are $q_\mu^{(1/2)} = (E(\mathbf{q}), \pm\mathbf{q})$ and correspondingly, the four-momenta of the outgoing nucleons are $q_\mu'^{(1/2)} = (E(\mathbf{q}'), \pm\mathbf{q}')$. The initial and final relative c.m. momenta are $q_\mu = \frac{1}{2}(q_\mu^{(1)} - q_\mu^{(2)})$ and $q'_\mu = \frac{1}{2}(q_\mu'^{(1)} - q_\mu'^{(2)})$, respectively. For on-shell scattering $|\mathbf{q}| = |\mathbf{q}'|$ with $E(\mathbf{q}) = E(\mathbf{q}') = \sqrt{M^2 + \mathbf{q}^2}$ the energy-transfer is zero, i.e., $q'_\mu - q_\mu = (0, \mathbf{q}' - \mathbf{q})$. In the standard Bonn potentials [86] phenomenological form factors are applied to the meson-nucleon vertices to regularize the amplitudes. They have the following form

$$\mathcal{F}_\alpha(q', q) = \left(\frac{\Lambda_\alpha^2 - m_\alpha^2}{\Lambda_\alpha^2 + (\mathbf{q}' - \mathbf{q})^2}\right)^{n_\alpha} \tag{3.9}$$

Table 3.1: *Basic parameters and constants included in the Bonn A potential*

Particle	Mass(MeV)	$g^2/4\pi$	f/g	$\Lambda(GeV)$
π	138.03	14.9		1.05
σ	550	8.3141		2.0
δ	983	0.7709		2.0
η	548.8	7		1.5
ω	782.6	20		1.5
ρ	769	0.99	6.1	1.3

where m_α is the corresponding meson mass and Λ_α is a cut-off in order to avoid divergences at short distances.

In helicity representation the Dirac spinor basis used in Eqs. (3.4) and (3.8) is given by

$$u_\lambda(\mathbf{q}) = \sqrt{\frac{E+M}{2M}} \begin{pmatrix} 1 \\ \frac{2\lambda|\mathbf{q}|}{E+M} \end{pmatrix} \chi_\lambda \quad , \tag{3.10}$$

where χ_λ denotes a two-component Pauli spinor with $\lambda = \pm\frac{1}{2}$. The normalization of the Dirac spinor is chosen such that $\bar{u}_\lambda u_\lambda = 1$.

To summarize: The general structure of the Born scattering matrix is given by the sum over the corresponding scalar, pseudo-scalar and vector mesons

$$\hat{V}(q',q) = \sum_{\alpha=\mathrm{s,ps,v}} \mathcal{F}_\alpha^2(q',q)\ \kappa_\alpha^{(2)}\ D_\alpha(q'-q)\ \kappa_\alpha^{(1)} \quad , \tag{3.11}$$

where the matrices (3.11) factorize for each meson α into the form factors $\mathcal{F}_\alpha$ at each meson-nucleon vertex, the meson propagator D_α and the meson-nucleon vertices κ_α themselves. The relativistic operator structure is thus completely determined by the matrix elements of the vertices κ_α.

The standard Bonn (A,B,C) potentials [86] also includes the lowest lying Δ-resonance with a mass of 1232 MeV and therefore besides the nucleon-nucleon-meson vertices also nucleon-isobar-meson vertices are included. The Bonn potentials contain 13 free parameters for coupling constants and cut-off masses and two additional parameters if one considers the masses of the scalar mesons as effective parameters (see Table 3.1).

In contrast to the standard Bonn potentials [86] the OPE part of the CD-Bonn potential [87] accounts for charge symmetry breaking in nn, pp and np

scattering due to the different pion masses m_{π^0} and $m_{\pi^\pm}$. In the CD-Bonn potential the mesons π, $\rho(770)$, and $\omega(782)$ are included (η is dropped since a vanishing coupling is assumed) and moreover two scalar-isoscalar σ mesons are introduced to describe more complicated multi-meson exchanges. Since the parameters of the σ mesons are readjusted in each partial wave the CD-Bonn potential is often referred to as a phenomenological NN potential. This fine-tuning of the partial wave fits minimizes χ^2 per datum to 1.02 and results in a total of 43 free parameters.

A consequence of the Feynman amplitudes (3.4) is the general non-local structure of the boson exchange which distinguishes the field theoretical relativistic OBE approach from local non-relativistic potentials. This is even true for the relativistic OPE compared to the local, non-relativistic OPE (see e.g. the discussion in [88]). However, for on-shell scattering the relativistic amplitudes acquire a local structure in the sense that they are functions of $\mathbf{q}^2$ and $\mathbf{q}' - \mathbf{q}$. In particular for forward and backward scattering, i.e., $\theta = 0, \pi$, the amplitudes are "local" functions of $\mathbf{q}^2$ and $\mathbf{q}$. The non-local structure of the relativistic amplitudes becomes evident when going off-shell, e.g. in the intermediate states in the Bethe-Salpeter equation [89, 88].

The matrix elements are calculated with the OBNNS code of R. Machleidt [90] when Bonn A is used and the corresponding CDBONN package of R. Machleidt when CD-Bonn is used.

3.2. Non-relativistic potentials

3.2.1. Non-relativistic reduction

The OBE potentials as e.g. the Bonn potentials can be reduced to a non-relativistic representation by expanding the full field-theoretical OBE Feynman amplitudes into a set of spin and isospin operators

$$V = \sum_i [V_i + V_i' \, \boldsymbol{\tau}_1 \cdot \boldsymbol{\tau}_2] \; O_i. \tag{3.12}$$

The operators O_i obtained in this low energy expansion, assuming identical particle scattering and charge independence, are defined as

$$\begin{aligned} O_1 &= \mathbf{1}, \\ O_2 &= \boldsymbol{\sigma}_1 \cdot \boldsymbol{\sigma}_2, \\ O_3 &= (\boldsymbol{\sigma}_1 \cdot \mathbf{k})(\boldsymbol{\sigma}_2 \cdot \mathbf{k}) \\ O_4 &= \tfrac{i}{2}(\boldsymbol{\sigma}_1 + \boldsymbol{\sigma}_2) \cdot \mathbf{n}, \\ O_5 &= (\boldsymbol{\sigma}_1 \cdot \mathbf{n})(\boldsymbol{\sigma}_2 \cdot \mathbf{n}), \end{aligned} \tag{3.13}$$

where $\mathbf{k} = \mathbf{q}' - \mathbf{q}$, $\mathbf{n} = \mathbf{q} \times \mathbf{q}' \equiv \mathbf{P} \times \mathbf{k}$ and $\mathbf{P} = \frac{1}{2}(\mathbf{q} + \mathbf{q}')$ is the average momentum. The potential forms V_i are then functions of $\mathbf{k}$, $\mathbf{P}$, $\mathbf{n}$ and the energy. In order to perform a non-relativistic reduction, the energy E is expanded in $\mathbf{k}^2$ and $\mathbf{P}^2$

$$E(\mathbf{q}) = \left(\frac{\mathbf{k}^2}{4} + \mathbf{P}^2 + M^2 \right)^{\frac{1}{2}} \simeq M + \frac{\mathbf{k}^2}{8M} + \frac{\mathbf{P}^2}{2M}. \tag{3.14}$$

and terms to leading order in $\mathbf{k}^2/M^2$ and $\mathbf{P}^2/M^2$ are taken into account. The meson propagators $D_\alpha(k^2)$ given in Eqs. (3.6, 3.7) are approximated by their static form $(-1)/(\mathbf{k}^2 + m^2)$. The explicit expressions in momentum space are given in appendix B.

The equivalent to Eq. (3.12) in configuration space is given by

$$\begin{aligned} O_1 &= \mathbf{1}, \\ O_2 &= \boldsymbol{\sigma}_1 \cdot \boldsymbol{\sigma}_2, \\ O_3 &= S_{12} = 3(\boldsymbol{\sigma}_1 \cdot \hat{\mathbf{r}})(\boldsymbol{\sigma}_2 \cdot \hat{\mathbf{r}}) - \boldsymbol{\sigma}_1 \cdot \boldsymbol{\sigma}_2, \\ O_4 &= \mathbf{L} \cdot \mathbf{S}, \\ O_5 &= Q_{12} = \tfrac{1}{2}[(\boldsymbol{\sigma}_1 \cdot \mathbf{L})(\boldsymbol{\sigma}_2 \cdot \mathbf{L}) + (\boldsymbol{\sigma}_2 \cdot \mathbf{L})(\boldsymbol{\sigma}_1 \cdot \mathbf{L})]. \end{aligned} \tag{3.15}$$

These operators are the well known central, spin-spin, tensor, spin-orbit and quadratic spin-orbit operators, respectively. The total angular momentum is denoted by $\mathbf{L} = \mathbf{r} \times \mathbf{P}$ and the total spin $\mathbf{S} = \frac{1}{2}(\boldsymbol{\sigma}_1 + \boldsymbol{\sigma}_2)$.

3.2.2. Meson-theoretical potentials

We consider the modern Nijmegen soft-core potential Nijm93 [65] as the first example of a non-relativistic meson-theoretical potential. It is an updated version of the Nijm78 [91] potential, where the low energy NN interaction is based on Regge-pole theory leading to the well known OBE forces. The contributions considered in this model are the pseudo-scalar mesons π, η, η', the vector mesons ρ, ϕ, ω and the scalar mesons δ, S^*, ϵ and the Pomeron P and the $J = 0$ tensor contributions, leading all in all to a number of 13 free parameters. Since it is constructed from approximate OBE amplitudes it is based on the operator structure given in Eq. (3.13) plus an additional operator $O_6 = \frac{1}{2}(\boldsymbol{\sigma}_1 - \boldsymbol{\sigma}_2) \cdot \mathbf{L}$ accounting for charge independence breaking which is new compared to the older version Nijm78. Exponential form factors reguralize the interaction at very short distances. This potential gives a χ^2 per datum of 1.87, which is comparable to similar OBE potentials like the standard Bonn potentials.

3.2.3. Phenomenological potentials

Another class of non-relativistic NN potentials are the so called high quality potentials where $\chi^2/N_{data} \approx 1.0$. Here we study the Nijmegen potentials Nijm I, Nijm II and Reid93 [65]. The Nijm I and Nijm II potentials are both based on the Nijm78 potential. In the Nijm I potential some nonlocal terms in the central force are kept whereas in the Nijm II potential all nonlocal terms are removed. Although based on the meson-theoretical Nijm78 potential these potentials are often referred to as purely phenomenological models, since the parameters are adjusted separately in each partial wave leading to a total of 41 parameters. At very short distances, both potentials are regularized by an exponential form factor.

The Nijmegen soft-core Reid93 [65] potential is a phenomenological potential and is therefore based on a completely different approach. In the meson-theoretical Nijmegen potential Nijm93 the potential forms V_i are the same for all partial waves, whereas in the Reid93 potentials every partial wave is parameterized separately by a convenient choice of combinations of central, tensor and spin-orbit functions (local Yukawas of multiples of the pion mass) and the related operators, i.e., the operators O_1 to O_4 from Eq. (3.15). It is regularized by a dipole form factor and has 50 phenomenological parameters giving all in all a $\chi^2/N_{data} = 1.03$. All the Nijmegen potentials contain the proper charge dependent OPE accounting for charge symmetry breaking in nn, pp and np scattering due to different pion masses $m_{\pi^0}, m_{\pi^\pm}$.

The same holds for the Argonne potential v_{18} [25], also an example for a widely used modern high precision phenomenological NN potential. It is given by the sum of an electromagnetic (EM) part, the proper OPE, and a phenomenological intermediate- and short-range part unrestricted by a meson-theoretical picture:

$$V = V^{EM} + V^{\pi} + V^{R}\,. \tag{3.16}$$

The EM interaction is the same as that used in the Nijmegen partial-wave analysis. Short-range terms and finite-size effects are taken into account as well [25].

The strong interaction part $V^{\pi} + V^{R}$ can be written in a form like given in Eq. (3.12) in configuration space, where the Argonne v_{18} potential is not constructed by approximating the field-theoretical OBE amplitudes (except for the OPE), but by assuming a very general two-body potential constrained by certain symmetries. The potential forms V_i parameterizing the intermediate and short-range part are mostly local Woods-Saxon functions.

The local two-body operators are the same charge independent ones used in the Argonne v_{14} potential

$$O_i \;=\; \mathbf{1}, \boldsymbol{\sigma}_1\cdot\boldsymbol{\sigma}_2, S_{12}, \mathbf{L}\cdot\mathbf{S}, L^2, L^2(\boldsymbol{\sigma}_1\cdot\boldsymbol{\sigma}_2), (\mathbf{L}\cdot\mathbf{S})^2. \tag{3.17}$$

Due to isovector exchange these operators have to be multiplied by the isospin matrices $\boldsymbol{\tau}_1 \cdot \boldsymbol{\tau}_2$ which than adds up to 14 operators. Additionally, four operators accounting for charge independence breaking are introduced

$$O_{i=15,18} = T_{12},\ (\boldsymbol{\sigma}_1 \cdot \boldsymbol{\sigma}_2) T_{12},\ S_{12} T_{12},\ (\tau_{z1} + \tau_{z2})\ , \tag{3.18}$$

where $T_{12} = 3\tau_{z1}\tau_{z2} - \tau_1 \cdot \tau_2$, is the isotensor operator, defined analogously to the spin tensor S_{12} operator.

Thus the operator structure is more general than that imposed by a non-relativistic, local OBE picture, in particular for the intermediate and short distance part. In total, Argonne v_{18} contains 40 adjustable parameters and gives a χ^2 per datum of 1.09 for 4301 pp and np data in the range 0–350 MeV [25]. The code used to calculate the potential matrix elements of the Argonne v_{18} model in momentum space was provided by H. Muether and T. Frick.

3.3. EFT interactions

3.3.1. Chiral EFT potentials

There has been substantial progress in recent time in order to derive quantitative NN potentials from chiral effective field theory (EFT) applied to low-energy QCD. In chiral EFT the effective Lagrangian is made up of an infinite number of terms (which have to be consistent with the assumed symmetry principles of QCD, like chiral symmetry) where the number of derivatives and/or nucleon fields increases. Calculating matrix elements, like NN scattering amplitudes, generates a delicate problem, namely one is left with an infinite number of Feynman diagrams. However, Weinberg proposed [16] that a systematic expansion of the nuclear amplitude can be performed in powers of $(Q/\Lambda_\chi)^\nu$ were Q is the generic low momentum scale given by the nucleon three-momentum, or the four-momenta of virtual pions or a pion mass. $\Lambda_\chi \sim 4\pi f_\pi \sim 1$ GeV is the chiral symmetry breaking scale which coincides roughly with the Borel mass Λ_B (see Section 2.3). This scheme is called chiral perturbation theory. $\nu = 0$ corresponds to leading order (LO), $\nu = 2$ to next-to-leading order (NLO), $\nu = 3$ to next-to-next-to-leading ($\mathrm{N^2LO}$) and finally $\nu = 4$ to next-to-next-to-next-to-leading order ($\mathrm{N^3LO}$). In this power counting scheme the number of contributing terms which are uniquely defined is finite at a given order ν. Depending on the accuracy required in the calculation of the amplitude one has to include higher orders in the expansion. Unfortunately the number of constants which appear in such an expansion increases when going to higher orders. Some can be fixed from pion-nucleon scattering data [17] whereas the remaining free parameters are adjusted to NN scattering.

The effective chiral Lagrangian describing the nuclear force is given as

$$\mathcal{L} = \mathcal{L}_{\pi\pi} + \mathcal{L}_{\pi N} + \mathcal{L}_{NN} \quad , \tag{3.19}$$

where

$$\begin{aligned} \mathcal{L}_{\pi\pi} &= \mathcal{L}^{(2)}_{\pi\pi} + \mathcal{L}^{(4)}_{\pi\pi} + \dots \quad , & (3.20)\\ \mathcal{L}_{\pi N} &= \mathcal{L}^{(1)}_{\pi N} + \mathcal{L}^{(2)}_{\pi N} + \mathcal{L}^{(3)}_{\pi N} + \dots \quad , & (3.21)\\ \mathcal{L}_{NN} &= \mathcal{L}^{(0)}_{NN} + \mathcal{L}^{(2)}_{NN} + \mathcal{L}^{(4)}_{NN} + \dots \quad . & (3.22) \end{aligned}$$

The superscript refers to the number of derivatives or pion mass insertions (chiral dimension) and the ellipsis stands for terms of higher chiral order. In the framework of chiral perturbation theory the NN scattering amplitude is then given by pion-exchange diagrams and contact terms.

Contact terms

Contacts terms describe the short range part of the NN interaction that remains unresolved in chiral EFT. The diagrammatic expansion of the NN interaction is shown in Fig. 3.3. At LO there are two contact terms which are represented by the four-nucleon diagram with a vertex (small-dot) with zero derivatives shown in the first row of Fig. 3.3. At NLO there are seven contact terms where the corresponding diagram is shown in the second row. The solid square represents a vertex with two derivatives. At N^{3}LO there are already 15 contact contributions which are represented by the four-nucleon diagram. The vertex of chiral dimension four is represented by the solid diamond. The strength of each contact term is given by a free parameter. Hence, at N^{3}LO there are 2+7+15 = 24 free parameters which are used to adjust the chiral EFT potential to NN scattering data. The corresponding expressions for the contact terms up to N^{3}LO are [17]

$$\begin{aligned} V^{(0)}_{\rm cont} &= C_S + C_T(\boldsymbol{\sigma}_1\cdot\boldsymbol{\sigma}_2)\,,\\ V^{(2)}_{\rm cont} &= C_1\mathbf{k}^2 + C_2\mathbf{P}^2 + (C_3\mathbf{k}^2 + C_4\mathbf{P}^2)(\boldsymbol{\sigma}_1\cdot\boldsymbol{\sigma}_2) + iC_5\frac{\boldsymbol{\sigma}_1+\boldsymbol{\sigma}_2}{2}\cdot(\mathbf{P}\times\mathbf{k})\\ &\quad + C_6(\boldsymbol{\sigma}_1\cdot\mathbf{k})(\boldsymbol{\sigma}_2\cdot\mathbf{k}) + C_7(\boldsymbol{\sigma}_1\cdot\mathbf{P})(\boldsymbol{\sigma}_2\cdot\mathbf{P})\,,\\ V^{(4)}_{\rm cont} &= D_1\mathbf{k}^4 + D_2\mathbf{P}^4 + D_3\mathbf{k}^2\mathbf{P}^2 + D_4(\mathbf{k}\times\mathbf{P})^2\\ &\quad + \left(D_5\mathbf{k}^4 + D_6\mathbf{P}^4 + D_7\mathbf{k}^2\mathbf{P}^2 + D_8(\mathbf{k}\times\mathbf{P})^2\right)(\boldsymbol{\sigma}_1\cdot\boldsymbol{\sigma}_2)\\ &\quad + i\left(D_9\mathbf{k}^2 + D_{10}\mathbf{P}^2\right)\frac{\boldsymbol{\sigma}_1+\boldsymbol{\sigma}_2}{2}\cdot(\mathbf{P}\times\mathbf{k}\,)\\ &\quad + \left(D_{11}\mathbf{k}^2 + D_{12}\mathbf{P}^2\right)(\boldsymbol{\sigma}_1\cdot\mathbf{k})(\boldsymbol{\sigma}_2\cdot\mathbf{k})\\ &\quad + \left(D_{13}\mathbf{k}^2 + D_{14}\mathbf{P}^2\right)(\boldsymbol{\sigma}_1\cdot\mathbf{P})(\boldsymbol{\sigma}_2\cdot\mathbf{P})\\ &\quad + D_{15}\left(\boldsymbol{\sigma}_1\cdot(\mathbf{k}\times\mathbf{P})\boldsymbol{\sigma}_2\cdot(\mathbf{k}\times\mathbf{P})\right) \end{aligned} \tag{3.23}$$

where $\mathbf{q}$ and $\mathbf{q}'$ denote again the initial and final nucleon momenta in the center-of-mass frame and $\mathbf{k} = \mathbf{q}' - \mathbf{q}$ and $\mathbf{P} = \frac{1}{2}(\mathbf{q} + \mathbf{q}')$ are the transferred and the average momentum. Isospin breaking correction to the short-range part of the potential are not included.

In the case of OBE potentials short-range physics is described by the exchange of heavy mesons. The connection between chiral EFT and boson-exchange potentials can be understood by expanding the heavy boson propagators

$$\frac{g^2}{\mathbf{k}^2 + m_b^2} \approx \frac{g^2}{m_b^2} - \frac{g^2}{m_b^2}\left(\frac{\mathbf{k}^2}{m_b^2}\right) + \frac{g^2}{m_b^2}\left(\frac{\mathbf{k}^4}{m_b^2}\right) - \dots \quad . \tag{3.24}$$

where m_b denotes the mass and g the meson-nucleon coupling constant of a heavy boson (ω, ρ or σ meson). The first term in the expansion on the right hand side corresponds to the LO contact diagram in Fig. 3.3 with zero derivatives in the first row, the second term to the NLO contact diagram with two derivatives represented by the solid square vertex and so forth. Thus short-range physics described by heavy meson exchange in the OBE picture is encoded in the coefficients of the contact terms. This was investigated by Epelbaum et. al [92] who compared the LECs from chiral EFT and those extracted from various NN potentials by performing such an expansion (3.24). The results of this investigation are shown in Fig. 5.7. The left-most brown bar corresponds to the LECs at NLO whereas the middle black bar to NNLO. The length of the bars indicates the range for the value of each LEC which stems from the fact that the cut-off Λ (3.26) has been varied in the range of 500 MeV to 600 MeV [92]. As one can see in Fig. 5.7 there is a good agreement between the LECs obtained from the phenomenological OBE potentials Bonn B and Nijm93, the high-precision potentials CD Bonn, Nijmegen I/ II and Argonne v_{18} and the LECs from chiral EFT. However, it is not yet clear whether this reflects the fact that reasonable models for the short-range part of the NN interaction are encoded in the various potentials. It could also be the case that the agreement just originates from the fact that all potentials fit the same data.

Pion exchange and many-body forces

The one-, two- and three-pion exchange diagrams which occur in the chiral expansion up to the considered order are also shown in Fig. 3.3. At LO ($\nu = 0$) only the well known static OPE contributes represented by the second diagram in the first row. TPE starts at NLO in the chiral expansion and all leading order TPE diagrams are shown. The sub-leading TPE occurs at N^{2}LO and N^{3}LO where only two and three diagrams, respectively, are depicted. In Ref. [18] all TPE contributions up to N^{3}LO are summarized. At this order 3π exchange occurs for the first time where one representative diagram is shown in Fig. 3.3. Nevertheless in Ref. [94, 95] it was shown by Kaiser that 3π exchange at this

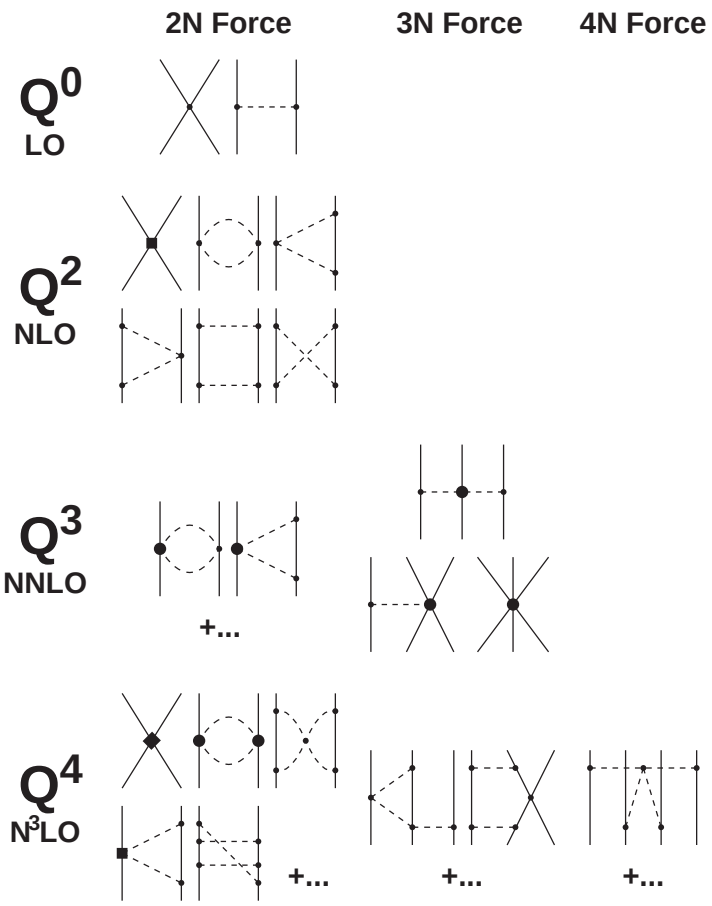

Figure 3.3: *Expansion of the nuclear force in chiral perturbation theory. Dashed lines represent pions and solid lines nucleons. The figure is taken from [93].*

order is negligible. It turned out that for a quantitative description of NN scattering data one has to go up to N^{3}LO [18, 19, 17] in the chiral expansion for the two-nucleon problem. N^{2}LO contributions were still found to be very large compared to NLO. This implies that TPE contributions have to be included up to order four. The TPE contributions to the NN interaction at order four have been derived by Kaiser [96, 97, 98]. Recently, quantitative NN potentials including contact terms at N^{3}LO were derived by Entem and Machleidt, the so-called Idaho potential [18, 19], and by Epelbaum, Glöckle and Meissner [17].

Since chiral perturbation theory provides an systematic expansion of the NN interaction besides the 2N force also 3N forces (and higher many-nucleon forces) appear on an equal footing as can be seen from Fig. 3.3. 3N forces are generated for the first time at N^{2}LO and therefore are weak. This naturally also holds for 4N forces occurring at N^{3}LO which are even weaker.

The Idaho N^{3}LO potential

The corresponding chiral NN potential is defined by

$$V(\mathbf{q}\,',\mathbf{q}) \equiv \left\{ \begin{array}{c} \text{sum of irreducible} \\ \boldsymbol{\pi + 2\pi} \text{ contributions} \end{array} \right\} + \text{ contacts} \tag{3.25}$$

and then applied in a scattering equation (Lippmann-Schwinger equation) to obtain the NN amplitude.

Since chiral perturbation theory is a low-momentum expansion it is valid only for momenta $Q \ll \Lambda_\chi \approx 1$ GeV. Therefore the chiral EFT potential has to be regularized, i.e. all expressions, i.e. irreducible pion exchanges and contacts, are multiplied with a regulator function

$$V(\mathbf{q}',\mathbf{q}) \longmapsto V(\mathbf{q}',\mathbf{q})\; \boldsymbol{e}^{-(|\mathbf{q}'|/\Lambda)^{2n}}\; \boldsymbol{e}^{-(|\mathbf{q}|/\Lambda)^{2n}}\,. \tag{3.26}$$

The exponent is chosen such that it does not affect the chiral order of the potential, but introduces contributions beyond that order.

For the present investigations we apply the Idaho potential [19]. The operator structure of the momentum-space NN amplitude has the general form given in Eq. (3.12) and the operators O_i from Eq. (3.13). The potential forms V_i ($i = C, S, T, LS, \sigma L$) can be expressed as functions of $|(\mathbf{q}' - \mathbf{q})|$ and $|\mathbf{k}|$. $\Lambda = 0.5$ GeV in all partial waves throughout the present work. The total number of free model parameters in the Idaho N^{3}LO potential is 29 [19].

For the evaluation of the matrix elements we applied the N^{3}LO program package provided by D. R. Entem and R. Machleidt.

3.3.2. Quark mass dependence of the chiral EFT interaction

Deriving the NN interaction in the framework of chiral effective field theory allows to account for the current quark mass or, equivalently, the pion mass dependence of the nuclear force [20]. This is of outstanding importance for the investigations of the structure of the nuclear self-energy components and the nuclear equation of state when going away from the physical value of m_π to the chiral limit in Section 5.5 and moreover when the chiral condensate is calculated in Section 6.2. Therefore the explicit form of the chiral NN interaction is presented here. In Ref. [20] the light quark mass of the nuclear force has been derived up to NLO in the framework of a modified Weinberg power counting, i.e., additionally to the one-pion exchange potential and contact terms the leading two-pion exchange has been considered. In this work [20] corrections have been considered from contact terms with two derivatives or one m_π^2-insertions, renormalization of OPE and contact terms and two-pion exchange to account for the

explicit and implicit quark mass dependence. The explicit form of the chiral effective NN potential $V_{\rm NLO}$ is given by

$$V_{\rm NLO} = V^{\rm OPE} + V^{\rm TPE} + V^{\rm cont}\,, \tag{3.27}$$

where

$$V^{\rm OPE} = -\frac{1}{4}\frac{g_A^2}{f_\pi^2}\left(1+2\Delta-\frac{4\tilde{m}_\pi^2}{g_A}\bar{d}_{18}\right)\boldsymbol{\tau}_1\cdot\boldsymbol{\tau}_2\,\frac{(\boldsymbol{\sigma}_1\cdot\mathbf{k})(\boldsymbol{\sigma}_2\cdot\mathbf{k})}{\mathbf{k}^2+\tilde{m}_\pi^2}, \tag{3.28}$$

$$\begin{aligned} V^{\rm TPE} = {} & -\frac{\boldsymbol{\tau}_1\cdot\boldsymbol{\tau}_2}{384\pi^2 f_\pi^4}\Big\{L(|\mathbf{k}|)\Big[4\tilde{m}_\pi^2(5g_A^4-4g_A^2-1) \\ & \qquad + \mathbf{k}^2(23g_A^4-10g_A^2-1)+\frac{48g_A^4\tilde{m}_\pi^4}{4\tilde{m}_\pi^2+\mathbf{k}^2}\Big] \\ & \qquad + \mathbf{k}^2\,\ln\frac{\tilde{m}_\pi}{m_\pi}\,(23g_A^4-10g_A^2-1)\Big\} \\ & -\frac{3g_A^4}{64\pi^2 f_\pi^4}\left(L(|\mathbf{k}|)+\ln\frac{\tilde{m}_\pi}{m_\pi}\right)\Big\{\boldsymbol{\sigma}_1\cdot\mathbf{k}\,\boldsymbol{\sigma}_2\cdot\mathbf{k}-\mathbf{k}^2\,\boldsymbol{\sigma}_1\cdot\boldsymbol{\sigma}_2\Big\}\,, \end{aligned} \tag{3.29}$$

$$\begin{aligned} V^{\rm cont} = {} & \bar{C}_S+\bar{C}_T(\boldsymbol{\sigma}_1\cdot\boldsymbol{\sigma}_2) \\ & +\tilde{m}_\pi^2\left(\bar{D}_S-\frac{3g_A^2}{32\pi^2 f_\pi^4}(8f_\pi^2C_T-5g_A^2+2)\ln\frac{\tilde{m}_\pi}{m_\pi}\right) \\ & +\tilde{m}_\pi^2\left(\bar{D}_T-\frac{3g_A^2}{64\pi^2 f_\pi^4}(16f_\pi^2C_T-5g_A^2+2)\ln\frac{\tilde{m}_\pi}{m_\pi}\right)(\boldsymbol{\sigma}_1\cdot\boldsymbol{\sigma}_2) \\ & +C_1\mathbf{k}^2+C_2\mathbf{P}^2+(C_3\mathbf{k}^2+C_4\mathbf{P}^2)(\boldsymbol{\sigma}_1\cdot\boldsymbol{\sigma}_2) \\ & +iC_5\frac{\boldsymbol{\sigma}_1+\boldsymbol{\sigma}_2}{2}\cdot(\mathbf{P}\times\mathbf{k})+C_6(\boldsymbol{\sigma}_1\cdot\mathbf{k})(\boldsymbol{\sigma}_2\cdot\mathbf{k}) \\ & +C_7(\boldsymbol{\sigma}_1\cdot\mathbf{P})(\boldsymbol{\sigma}_2\cdot\mathbf{P})\,, \end{aligned} \tag{3.30}$$

with g_A and f_π the physical values of the nucleon axial coupling and pion decay constant, respectively. Because at NLO any shift in g_A and f_π for a different value of m_π in the TPE is a N^{4}LO effect the physical values are used where $g_A = 1.26$ and $f_\pi = 92.4$ MeV. The value of the pion mass is indicated by $\tilde{m}_\pi$ compared to the physical one denoted by m_π. $L(|\mathbf{k}|)$ is given by

$$L(|\mathbf{k}|) = \frac{\sqrt{4\tilde{m}_\pi^2+\mathbf{k}^2}}{|\mathbf{k}|}\,\ln\frac{\sqrt{4\tilde{m}_\pi^2+\mathbf{k}^2}+|\mathbf{k}|}{2\tilde{m}_\pi}\,. \tag{3.31}$$

Δ represents the relative shift in the ratio g_A/f_π compared to its physical value since they show an implicit dependence on the pion mass

$$\begin{aligned} \Delta \equiv {} & \frac{(g_A/f_\pi)_{\tilde{m}_\pi}-(g_A/f_\pi)_{m_\pi}}{(g_A/f_\pi)_{m_\pi}} \\ = {} & \left(\frac{g_A^2}{16\pi^2 f_\pi^2}-\frac{4}{g_A}\bar{d}_{16}+\frac{1}{16\pi^2 f_\pi^2}\bar{l}_4\right)(m_\pi^2-\tilde{m}_\pi^2)-\frac{g_A^2\tilde{m}_\pi^2}{4\pi^2 f_\pi^2}\ln\frac{\tilde{m}_\pi}{m_\pi}\,. \end{aligned} \tag{3.32}$$

The low-energy constants (LECs) $\bar{C}_{S,T}$ and $\bar{D}_{S,T}$ are related to the $C_{S,T}$ from [17] via

$$C_{S,T} = \bar{C}_{S,T} + m_\pi^2 \bar{D}_{S,T} \,. \tag{3.33}$$

The LECs $\bar{D}_{S,T}$ have not been fixed by experiment till now. In Ref. [20] natural values have been assumed for these constants

$$\bar{D}_{S,T} = \frac{\alpha_{S,T}}{f_\pi^2 \Lambda_\chi^2} \,, \quad \text{where} \quad \alpha_{S,T} \sim 1 \quad \text{and} \quad \Lambda_\chi \simeq 1 \,. \tag{3.34}$$

The LECs $\bar{d}_{16}$,$\bar{d}_{18}$ and $\bar{l}_4$ are related to pion-nucleon interactions. We take $\bar{l}_4 = 4.3$ which is fixed with relatively small error bars. The LECs $\bar{d}_{16}$,$\bar{d}_{18}$ are not yet uniquely fixed, i.e. there exists a certain range of possible values fixed from different observables. The implications on the results induced by these uncertainties of the LECs will be discussed later in greater detail.

3.3.3. Renormalization Group approach to the NN interaction

All potentials discussed up to now in this chapter have been adjusted to elastic NN scattering data for lab. energies $E_{lab} \leq 350$ MeV which corresponds to the pion threshold. Hence for relative c.m. momenta $\mathbf{k} > 400$ MeV or distances $r < 0.5$ fm the details of the nuclear force are not constrained by experimental data and the potentials differ essentially in the treatment of the intermediate and short-range parts of the NN interaction. Due to these strong high-momentum components which are included in the NN potentials model dependences arise in many-body calculations like in DBHF. This can be seen from Fig. 2.3 where different nuclear saturation points are obtained using various interactions within the same many-body approach. The differences become also obvious in Fig. 3.4 where the 'bare' diagonal matrix elements in the $^1S_0$ partial wave are shown for various potentials. Again the strong deviations are due to the different treatment of the hard core. Nevertheless one has to keep in mind that matrix elements for the bare potentials are shown, i.e., when iterated in a Lippmann-Schwinger equation all potentials lead to about the same T-matrices and therefore agree much better.

Another example is shown in Chapter 5.1.3 where in Fig. 5.5 the tree level calculations of the single particle potential $U_{s.p.}$ in symmetric nuclear matter are presented for all the different potentials. Again, since at tree level the model dependent hard core contributes completely one observes strong deviations.

To circumvent this model dependent parameterization of the short range part another approach has been proposed where an 'universal' effective low-momentum potential $V_{\text{low k}}$ is derived from any given realistic NN potential [99, 26, 100].

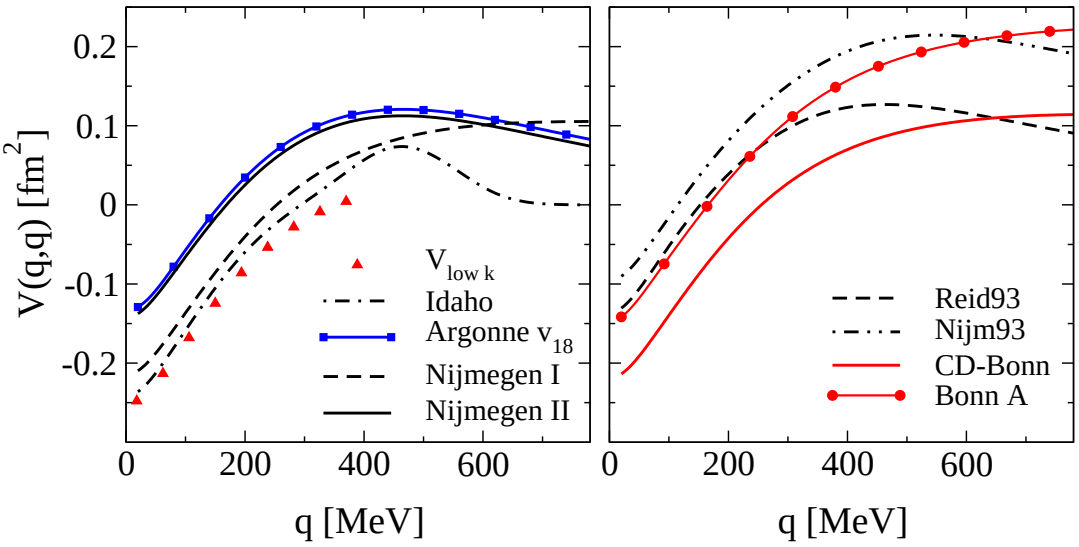

Figure 3.4: Diagonal matrix elements $V(\mathbf{q},\mathbf{q})$ in the $^1S_0$ partial wave for different high precision NN potential models.

Here the method is shortly sketched. Starting from a given potential model V the low-momentum part is separated by integrating out the high-momentum modes above a cut-off Λ. The resulting low-momentum interaction $V_{\mathrm{low\,k}}$ has momentum components only below Λ, i.e. one evolves the NN potential models from the full Hilbert space to the low momentum subspace [99, 26].

Moreover, $V_{\mathrm{low\,k}}$ has to evolve with Λ in such a way that the low-momentum scattering amplitude $T(k',k;k^2)$ is reproduced, i.e. the same results for the phase shifts and the deuteron pole as the models which serve as input have to be obtained. This leads (in every scattering channel) to

$$T(k',k;k^2) = V(k',k) + \frac{2}{\pi}\,\mathcal{P}\int_0^\infty \frac{V(k',p)\,T(p,k;k^2)}{k^2-p^2}\,p^2dp, \tag{3.35}$$

$$T(k',k;k^2) = V^\Lambda_{\mathrm{low\,k}}(k',k) + \frac{2}{\pi}\,\mathcal{P}\int_0^\Lambda \frac{V^\Lambda_{\mathrm{low\,k}}(k',p)\,T(p,k;k^2)}{k^2-p^2}\,p^2dp \tag{3.36}$$

where k',k and p are the relative momenta of the outgoing, incoming and intermediate nucleons. The changes of the effective interaction with the cut-off Λ are then described by the renormalization group (RG) equation [99]

$$\frac{d}{d\lambda}V^\Lambda_{\mathrm{low\,k}}(k',k) = \frac{2}{\pi}\frac{V^\Lambda_{\mathrm{low\,k}}(k',\Lambda)\,T^\Lambda(\Lambda,k;\Lambda^2)}{1-(k/\Lambda)^2}\,. \tag{3.37}$$

For every cut-off $V_{\mathrm{low\,k}}$ defines a new NN potential. Since the low-momentum T matrix for a given cut-off has to be reproduced, $V_{\mathrm{low\,k}}$ is renormalized for

scattering to intermediate states with $p > \Lambda$. This is done by a resummation of the high-momentum ladders in an energy-dependent effective interaction, which is the solution to the two-body Bloch-Horowitz equation in momentum space. By using the equations of motion the energy dependence can then be converted to a momentum dependence. Both steps are technically equivalent to the Lee-Suzuki basis transformation in momentum space. At a cut-off of $\Lambda = 2.1$ fm^{-1} all the various NN potential models are then found to collapse to a model-independent effective interaction $V_{\mathrm{low\,k}}$ which is shown in Fig. 3.4 denoted by red triangles. In summary, the philosophy behind the RG approach is to replace the unresolved short distance structure by something simpler, e.g. contact terms, without distorting low-energy observables.

The difference to the chiral EFT approach presented in the previous section is that the NN interaction is not expanded in powers of local operators. In chiral EFT power counting is used to calculate observables to a given order. In contrast in the $V_{\mathrm{low\,k}}$ approach one starts from a Hamiltonian in a large space which reproduces the low-energy observables. The large space is then truncated to a smaller low-momentum space where still the observables are reproduced.

4. Dirac structure of the NN interaction

As shown in the first chapter of this work relativistic many-body calculations (based on meson theoretical covariantly formulated NN interactions) yield scalar and vector fields which are of the same sign and magnitude as obtained from relativistic mean field theory (RMF) theory. Properties arising in nuclear structure like, e.g., the large spin-orbit splitting in finite nuclei can naturally be explained within Dirac phenomenology with these fields as shown in Chapter 2.1 Moreover in Chapter 2.3 a completely different approach has been discussed, QCD in-medium sum rules. There it was shown that the density dependence of the chiral condensates gives rise to large scalar and vector fields comparable to those obtained in relativistic phenomenology.

Considering the differences in these theoretical approaches such a coincidence could not have been expected a priori. Moreover it implies that the occurrence of large fields in nuclear matter or, alternatively, the density dependence of the QCD condensates, must already be inherent in the vacuum NN interaction.

The connection of the nucleon-nucleon force to QCD is given by the fact that the interaction is described by the exchange of the low lying mesonic degrees of freedom. In the previous chapter different approaches to the nucleon-nucleon interaction have been discussed. Though all these well established interactions fit NN scattering data with approximately the same precision the various NN interactions are based on quite different theoretical approaches.

Whereas one knows that in relativistic many-body approaches (e.g. DBHF) the appearance of large fields is due to the meson exchange picture of the relativistic OBE interactions (σ and ω meson exchange) it is not clear whether these fields would be generated if non-relativistic interactions (chiral EFT, phenomenological interactions) were applied in relativistic many-body theory.

A direct comparison of relativistic phenomenology based on the meson exchange with chiral EFT and non-relativistic phenomenology is, however, difficult since the latter two approaches lack of a clear Lorentz structure which is essential in order to generate large scalar and vector mean fields in nuclear matter like it is known for the relativistic OBE potentials.

Therefore in this chapter a model independent investigation of the NN interaction in terms of the Lorentz structure is presented. This is done by applying projection techniques to map the various potentials on an operator basis of Dirac

phenomenology which is given by the Clifford algebra in Dirac space [101, 79]. This transformation leads to a restoration of the symmetries of the Lorentz group. Such a transformation is well defined in the positive energy sector for on-shell amplitudes and allows to compare the various NN potentials by identifying the different Lorentz components of the interaction.

The philosophy behind this approach is based on the fact, that any NN interaction, independent whether relativistic or non-relativistic, is essentially based on an equivalent operator basis – in the non-relativistic limit covariant operators are linear combinations of the operators in which non-relativistic potentials are usually expanded (see Section 3.2.1)– and therefore data fitting enforces coefficients of comparable strength or in other words one ends up with a reorganization of the original contributions (central part, spin-orbit, tensor interaction etc.). It is clear that in the case of already manifestly covariantly formulated OBE interactions the procedure is trivial.

In this model independent study of the NN interaction a remarkable agreement at the level of Lorentz invariant amplitudes between relativistic and non-relativistic OBE potentials, non-relativistic phenomenological potentials and EFT potentials, respectively, is observed.

4.1. Covariant operators in Dirac space

Any two-body amplitude can be represented covariantly by Dirac operators and Lorentz invariant amplitudes. A detailed discussion of the general structure of relativistic two-body amplitudes can be found in Refs. [101, 102].

The inclusion of negative energy excitations with 4 states for each spinor yields altogether $4^4 = 256$ types of two-body matrix elements with respect to their spinor structure. Symmetry arguments reduce these to 44 for on-shell particles [102].

Naturally a fully relativistic treatment invokes the excitation of anti-nucleons. However, standard NN potentials (even OBE type potentials such Bonn, CD-Bonn or Nijmegen) are restricted to the positive energy sector and neglect the explicit coupling to anti-nucleons. As a consequence one has to work in a subspace of the full Dirac space. This shortcoming can be avoided using fully covariant potentials which explicitly include anti-nucleon states [103, 104]. The present investigations have, however, been restricted to "standard" potentials based on the no sea approximation. Similarly, the EFT potentials [18, 19] applied here do not explicitly include anti-nucleons, in contrast to covariant approaches which require renormalization procedures to restore chiral power counting [105].

Therefore taking only the subspace of positive energy solutions into account this leads to $2^4 = 16$ two-body matrix elements. Considering in addition only on-shell matrix elements the number of independent matrix elements can be further

reduced by symmetry arguments (parity and spin conservation, time-reversal invariance) down to 5. Thus, all on-shell two-body matrix elements can be expanded in terms of five Lorentz invariant amplitudes and a set of five covariant operators. These five invariants are not unique since the Dirac matrices involve always also negative energy states. Therefore a decomposition of the one-body NN potential into a Lorentz scalar and a Lorentz vector contribution depends to some part on the choice of the set of Dirac covariants.

A natural choice of a set of five linearly independent covariant operators to represent a 4×4 Dirac matrix are the scalar, vector, tensor, pseudo-scalar and axial-vector Fermi covariants

$$\mathrm{S} = 1 \otimes 1 \ , \quad \mathrm{V} = \gamma^\mu \otimes \gamma_\mu \ , \quad \mathrm{T} = \sigma^{\mu\nu} \otimes \sigma_{\mu\nu} \ , \tag{4.1}$$

$$\mathrm{P} = \gamma_5 \otimes \gamma_5 \ , \quad \mathrm{A} = \gamma_5\gamma^\mu \otimes \gamma_5\gamma_\mu \ . \tag{4.2}$$

Since one works with physical, i.e., antisymmetrized matrix elements, one has to realize that the Fierz transformation $\mathcal{F}$ [101] couples direct and exchange covariants which mixes the different Lorentz structures

$$\begin{pmatrix} \tilde{\mathrm{S}} \\ \tilde{\mathrm{V}} \\ \tilde{\mathrm{T}} \\ \tilde{\mathrm{A}} \\ \tilde{\mathrm{P}} \end{pmatrix} = \frac{1}{4} \begin{pmatrix} 1 & 1 & \frac{1}{2} & -1 & 1 \\ 4 & -2 & 0 & -2 & -4 \\ 12 & 0 & -2 & 0 & 12 \\ -4 & -2 & 0 & -2 & 4 \\ 1 & -1 & \frac{1}{2} & 1 & 1 \end{pmatrix} \begin{pmatrix} \mathrm{S} \\ \mathrm{V} \\ \mathrm{T} \\ \mathrm{A} \\ \mathrm{P} \end{pmatrix} \ . \tag{4.3}$$

The covariants on the left hand side of Eq. (4.3) are the interchanged Fermi covariants defined in Ref. [101] as

$$\tilde{\mathrm{S}} = \tilde{\mathrm{S}}\mathrm{S} \ , \quad \tilde{\mathrm{V}} = \tilde{\mathrm{S}}\mathrm{V} \ , \quad \tilde{\mathrm{T}} = \tilde{\mathrm{S}}\mathrm{T} \ , \quad \tilde{\mathrm{A}} = \tilde{\mathrm{S}}\mathrm{A} \ , \quad \tilde{\mathrm{P}} = \tilde{\mathrm{S}}\mathrm{P} \ , \tag{4.4}$$

where the operator $\tilde{\mathrm{S}}$ exchanges the Dirac indices of particles 1 and 2, i.e., $\tilde{\mathrm{S}} u(1)_\sigma u(2)_\tau = u(1)_\tau u(2)_\sigma$.

Therefore the direct covariants Γ_m with $m = \{\mathrm{S}, \mathrm{V}, \mathrm{T}, \mathrm{P}, \mathrm{A}\}$ can be expressed in terms of the exchange covariants $\tilde{\Gamma}_m$ with $m = \{\tilde{\mathrm{S}}, \tilde{\mathrm{V}}, \tilde{\mathrm{T}}, \tilde{\mathrm{P}}, \tilde{\mathrm{A}}\}$.

In contrast to the NN potentials where the pion-nucleon coupling is given by a pseudo-vector vertex, the set (4.2,4.4) contains the pseudo-scalar covariant P. This suggests to replace P in Eqs. (4.2,4.4) by the corresponding pseudo-vector covariant

$$\mathrm{PV} = \frac{\not{q}' - \not{q}}{2M}\gamma_5 \otimes \frac{\not{q}' - \not{q}}{2M}\gamma_5 \ . \tag{4.5}$$

This leads to an on-shell equivalence since the matrix elements of the pseudo-vector and the pseudo-scalar matrix operators are identical in the case of on-shell scattering between positive energy states:

$$\bar{u}(\mathbf{q}')\frac{\not{q}' - \not{q}}{2M}\gamma_5 u(\mathbf{q}) = \bar{u}(\mathbf{q}')\gamma_5 u(\mathbf{q}) \ . \tag{4.6}$$

On the other hand the PV vertex suppresses the coupling to antiparticles since the overlap matrix elements vanish for on-shell scattering

$$\bar{v}(\mathbf{q}')\frac{\not{q}' - \not{q}}{2M}\gamma_5 u(\mathbf{q}) = 0 \tag{4.7}$$

where $v(\mathbf{q})$ is a negative energy spinor. In order to identify the PV contributions clearly in the antisymmetrized amplitudes - note that due to the Fierz transformation (4.3) all operators are coupled - one can switch to a set of covariants originally proposed by Tjon and Wallace [102]. Based on the following operator identities

$$\frac{1}{2}(\mathrm{T} + \tilde{\mathrm{T}}) = \mathrm{S} + \tilde{\mathrm{S}} + \mathrm{P} + \tilde{\mathrm{P}} \tag{4.8}$$

$$\mathrm{V} + \tilde{\mathrm{V}} = \mathrm{S} + \tilde{\mathrm{S}} - \mathrm{P} - \tilde{\mathrm{P}} \tag{4.9}$$

one finds that the following set of covariants

$$\Gamma_m = \{\mathrm{S}, \tilde{\mathrm{S}}, (\mathrm{A} - \tilde{\mathrm{A}}), \mathrm{PV}, \widetilde{\mathrm{PV}}\} \tag{4.10}$$

provides a set of Dirac operators for the positive energy sector [102] which completely separates the direct and exchange PV contributions from the remaining operator structure. This has the advantage that the OPE exchange which is dominant at low energies is decoupled from the remaining amplitudes and gives only a contribution to the $\widetilde{\mathrm{PV}}$ operator. In the following we will refer to the set of covariants in Eq. (4.10) as the $pseudo-vector$ representation and that of Eq. (4.2) as the $pseudo-scalar$ representation. Note that on-shell matrix elements of $\mathrm{PV}, \widetilde{\mathrm{PV}}$ in (4.10) are equivalent to those where the pseudo-vector covariants are replaced by $\mathrm{P}, \tilde{\mathrm{P}}$.

The on-shell equivalence does not affect physical observables which are built on complete matrix elements as e.g. the single particle potential U

$$U(\mathbf{k})_{\text{s.p.}} \propto \sum_{\mathbf{q}} \langle \bar{u}(\mathbf{k})\bar{u}(\mathbf{q})|\hat{V}(\mathbf{k},\mathbf{q})|u(\mathbf{k})u(\mathbf{q}) - u(\mathbf{q})u(\mathbf{k})\rangle \tag{4.11}$$

but it leads to uncertainties in operators which are, like the self-energy Σ, based on traces over only one particle. As discussed in [106, 36], a pseudo-vector πN coupling leads to the $pseudo-vector$ representation (4.10) as the most natural choice of the relativistic operator basis. Therefore for the calculation of the self-energy components in nuclear matter shown in Chapter 5 the pseudo-vector representation has been used.

4.2. Projection onto covariant operators

The technique is described which is necessary to project the amplitudes from an angular-momentum basis onto a covariant basis, given by Eqs. (4.2) or (4.10).

The procedure is standard and runs over the following steps

$$\begin{aligned} |LSJ\rangle &\rightarrow \text{partial wave helicity states} \rightarrow \text{plane wave helicity states} \\ &\rightarrow \text{covariant basis .} \end{aligned}$$

The first two transformation can be found in Refs. [107, 86]. The last step depends on the choice of the covariant operator basis, see e.g. [79, 36]. Here the essential steps are briefly sketched.

Independent of the various models, the two-body amplitudes are determined normally in the angular-momentum $|LSJM\rangle$-representation and can be denoted as $V^{JS}_{L',L}(\mathbf{q}', \mathbf{q})$. As already explained in the case of on-shell scattering ($|\mathbf{q}| = |\mathbf{q}'|$) due to symmetry arguments five of sixteen possible matrix elements –taking only the subspace of positive energy states– are linearly independent for a fixed total angular momentum J (spin singlet and triplet states). By inversion of Eq. (3.32) in [107] these five partial wave amplitudes are transformed from the $|LSJM\rangle$-representation into the partial wave helicity representation $|JM\lambda_1\lambda_2\rangle$ and are then decoupled via inversion of Eq. (3.28) from Ref. [107]. Since we deal with two-nucleon states, i.e. two-fermion states, we have to evaluate the fully antisymmetrized matrix elements by restoring the total isospin $\mathrm{I} = 0, 1$ via the standard selection rule

$$(-1)^{L+S+\mathrm{I}} = -1 \ . \tag{4.12}$$

The five plane wave helicity matrix elements are then obtained by a summation over the total angular momentum J

$$\langle \lambda_1' \lambda_2' \, \mathbf{q}' \left| V^{\mathrm{I}} \right| \lambda_1 \lambda_2 \, \mathbf{q} \rangle = \sum_J \left(\frac{2J+1}{4\pi} \right) d^J_{\lambda\,\lambda'}(\theta) \langle \lambda_1' \lambda_2' | V^{J,\mathrm{I}}(\mathbf{q}', \mathbf{q}) | \lambda_1 \lambda_2 \rangle \ . \tag{4.13}$$

Here θ denotes the scattering angle between $\mathbf{q}'$ and $\mathbf{q}$ while $\lambda = \lambda_1 - \lambda_2$ and $\lambda' = \lambda_1' - \lambda_2'$ denote the in- and outgoing helicity states. The reduced rotation matrices $d^J_{\lambda\,\lambda'}(\theta)$ are those defined by Rose [108].

These plane wave helicity matrix elements can now be projected onto a set of five covariant amplitudes in Dirac space. A set of five linearly independent covariants is sufficient for such a representation since on-shell we deal with five matrix elements independent of the chosen representation. Using the covariants of Eq. (4.2) (the 'pseudo-scalar choice') the on-shell potential matrix elements for definite isospin I can be represented covariantly as [79]

$$\begin{aligned} \hat{V}^{\mathrm{I}}(|\mathbf{q}|, \theta) \ &= \ F^{\mathrm{I}}_{\mathrm{S}}(|\mathbf{q}|, \theta)\, \mathrm{S} + F^{\mathrm{I}}_{\mathrm{V}}(|\mathbf{q}|, \theta)\, \mathrm{V} + F^{\mathrm{I}}_{\mathrm{T}}(|\mathbf{q}|, \theta)\, \mathrm{T} \\ &\quad + F^{\mathrm{I}}_{\mathrm{P}}(|\mathbf{q}|, \theta)\, \mathrm{P} + F^{\mathrm{I}}_{\mathrm{A}}(|\mathbf{q}|, \theta)\, \mathrm{A} \ . \end{aligned} \tag{4.14}$$

The Lorentz invariant amplitudes $F^{\mathrm{I}}_m(|\mathbf{q}|, \theta)$ with $m = \{\mathrm{S}, \mathrm{V}, \mathrm{T}, \mathrm{P}, \mathrm{A}\}$ from Eq. (4.14) depend only on the relative c.m. momentum $|\mathbf{q}|$ and the scattering

angle θ and are related to the plane wave helicity states defined in Eq. (4.13) by

$$\langle \lambda_1' \lambda_2' \, \mathbf{q}' | V^{\mathrm{I}} | \lambda_1 \lambda_2 \, \mathbf{q} \rangle = \sum_m \langle \lambda_1' \lambda_2' \, \mathbf{q}' | \Gamma_m | \lambda_1 \lambda_2 \, \mathbf{q} \rangle F_m^{\mathrm{I}}(|\mathbf{q}|, \theta) \ . \tag{4.15}$$

The indices (1) and (2) refer to particle one and two. Eq. (4.15) is a matrix relation between the five independent plane wave helicity amplitudes V_i^{I} (where $i = \{\lambda_1', \lambda_2', \lambda_1, \lambda_2\} = 1, ..., 5$ denotes five of sixteen possible amplitudes) and the five unknown covariant amplitudes $F_m^{\mathrm{I}}(|\mathbf{q}|, \theta)$. For fixed values of the variables ($|\mathbf{q}| = |\mathbf{q}'|, \theta$) this equation can be written in a more compact form

$$V_i^{\mathrm{I}} = \frac{1}{M^2} \sum_m C_{im} F_m^{\mathrm{I}} \ . \tag{4.16}$$

The covariant amplitudes F_m^{I} are obtained by matrix inversion of Eq. (4.16) which corresponds to Eq. (3.23) of Ref. [79].

Eq. (4.16) has to be inverted for two scattering angles, i.e., for $\theta = 0$ for the direct and $\theta = \pi$ for the exchange part of the interaction. These two scattering angles are required for the Hartree-Fock potential. Details of the inversion of Eq. (4.16) as well as the treatment of kinematical singularities of the matrix C_{im} occurring at $\theta = 0$ and $\theta = \pi$ are shown in appendix C of Ref. [79] where Eq. (4.16) is explicitly given for $\theta = 0$ and $\theta = \pi$ (Eqs. (C10,11)). Following Ref. [79] we calculate the real part of the five Lorentz invariant amplitudes $F_m^{\mathrm{I}=0,1}(|\mathbf{q}|, \theta = 0, \pi)$ for the direct and exchange case in both, the isospin singlet and triplet channels. When derived from physical partial wave amplitudes which are already antisymmetrized according to the selection rule (4.12), the exchange amplitudes $F_m(|\mathbf{q}|, \pi)$ contain redundant information.

Due to the restriction to the subspace of positive energy states, the choice of a set of five linearly independent covariants suffers from on-shell ambiguities, as discussed above. Thus the set of covariants (4.10) is a more appropriate choice [36, 106]. In this representation the scattering matrix reads [102, 36]

$$\begin{aligned} \hat{V}^{\mathrm{I}}(|\mathbf{q}|, \theta) \ &= \ g_{\mathrm{S}}^{\mathrm{I}}(|\mathbf{q}|, \theta) \, \mathrm{S} - g_{\tilde{\mathrm{S}}}^{\mathrm{I}}(|\mathbf{q}|, \theta) \, \tilde{\mathrm{S}} + g_{\mathrm{A}}^{\mathrm{I}}(|\mathbf{q}|, \theta) \, (\mathrm{A} - \tilde{\mathrm{A}}) \\ &\quad + g_{\mathrm{PV}}^{\mathrm{I}}(|\mathbf{q}|, \theta) \, \mathrm{PV} - g_{\widetilde{\mathrm{PV}}}^{\mathrm{I}}(|\mathbf{q}|, \theta) \, \widetilde{\mathrm{PV}} \ . \end{aligned} \tag{4.17}$$

The new amplitudes g_m^{I} are related to the Lorentz invariant amplitudes F_m^{I} from Eq. (4.14) by the linear transformation

$$\begin{pmatrix} g_{\mathrm{S}}^{\mathrm{I}} \\ g_{\tilde{\mathrm{S}}}^{\mathrm{I}} \\ g_{\mathrm{A}}^{\mathrm{I}} \\ g_{\mathrm{PV}}^{\mathrm{I}} \\ g_{\widetilde{\mathrm{PV}}}^{\mathrm{I}} \end{pmatrix} = \frac{1}{4} \begin{pmatrix} 4 & -2 & -8 & 0 & -2 \\ 0 & -6 & -16 & 0 & 2 \\ 0 & -2 & 0 & 0 & -2 \\ 0 & 2 & -8 & 4 & 2 \\ 0 & 6 & -16 & 0 & -2 \end{pmatrix} \begin{pmatrix} F_{\mathrm{S}}^{\mathrm{I}} \\ F_{\mathrm{V}}^{\mathrm{I}} \\ F_{\mathrm{T}}^{\mathrm{I}} \\ F_{\mathrm{P}}^{\mathrm{I}} \\ F_{\mathrm{A}}^{\mathrm{I}} \end{pmatrix} \ . \tag{4.18}$$

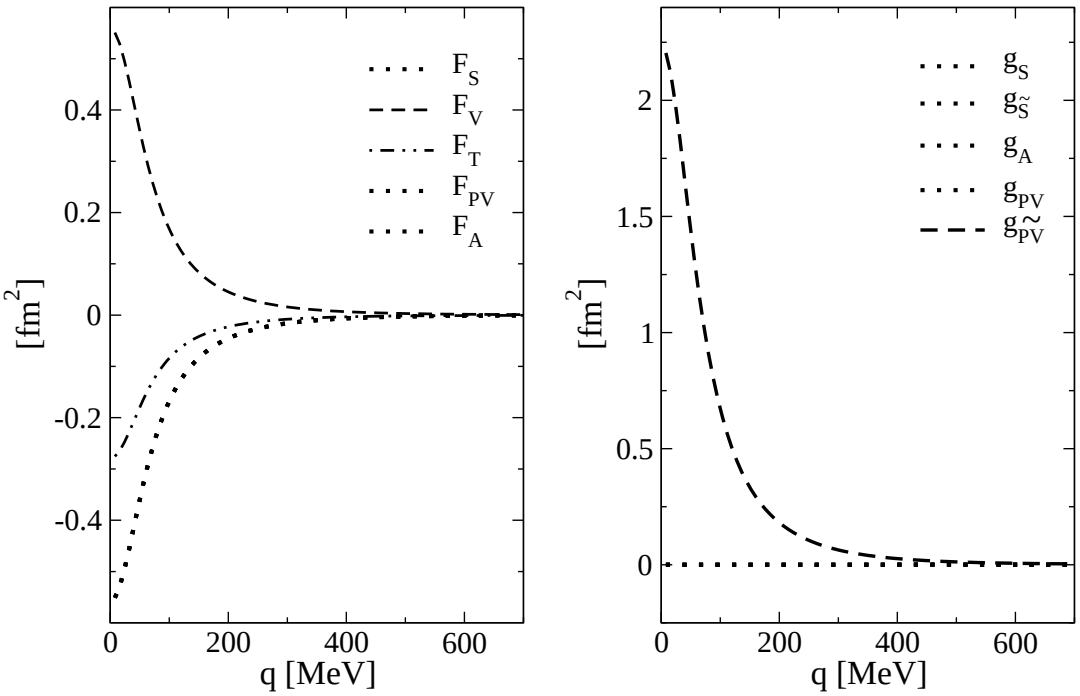

Figure 4.1: *Covariant amplitudes for the OPE in different choices of the relativistic operator basis, i.e., the pseudo-scalar representation* $F_m(|\mathbf{q}|, \theta = 0)$ *(left) and the pseudo-vector representation* $g_m(|\mathbf{q}|, \theta = 0)$ *(right).*

As mentioned before, the representation of the potential given in Eq. (4.17) has the advantage that the OPE contribution to the amplitudes is completely decoupled from the rest of the interaction. The OPE contributes only in the pseudo-vector exchange amplitude $g^{\rm OPE}_{\widetilde{\rm PV}}$ and vanishes in all other amplitudes $g^{\rm OPE}_{\rm S} = g^{\rm OPE}_{\tilde{\rm S}} = g^{\rm OPE}_{\rm A} = g^{\rm OPE}_{\rm PV} = 0$. Thus one avoids that the low momentum behavior of these four amplitudes is to large extent dominated by OPE exchange contributions which are present in all five amplitudes $F^{\rm I}_m$ from Eq. (4.14) due to the Fierz transformation. In order to compare the various potentials at the level of covariant amplitudes the pseudo-vector representation is therefore the most efficient and transparent one.

4.3. Results

In order to demonstrate the dependence of the relativistic amplitudes on the choice of the operator basis we consider in Fig. 4.1 first the single OPE. The figure shows the corresponding amplitudes F_m of the pseudo-scalar representation (4.2) and the g_m amplitudes of pseudo-vector representation (4.10), both for the

OPE part of the Bonn A potential. Since one is dealing with antisymmetrized amplitudes it is sufficient to consider the direct Lorentz invariants $F_m(|\mathbf{q}|, \theta = 0)$ and $g_m(|\mathbf{q}|, \theta = 0)$ at scattering angle $\theta = 0$. As the starting point the OPE is given in the $|LSJ\rangle$ basis and antisymmetrization is ensured by the selection rule (4.12). The figure shows the isospin averaged amplitudes defined as

$$F_m(|\mathbf{q}|, 0) := \frac{1}{2}\left[F_m^{\mathrm{I}=0}(|\mathbf{q}|, 0) + 3F_m^{\mathrm{I}=1}(|\mathbf{q}|, 0)\right] \tag{4.19}$$

and correspondingly for g_m. In the case of pure neutron matter the isospin dependence is given by

$$F_m(|\mathbf{q}|, 0) := \left[2F_m^{\mathrm{I}=1}(|\mathbf{q}|, 0)\right] \ . \tag{4.20}$$

It is evident that in the pseudo-scalar representation all amplitudes F_m have large non-vanishing contributions from OPE due to the mixing of direct and exchange contributions described by the Fierz transformation (4.3). Moreover, as discussed above the on-shell equivalence for the pseudo-scalar covariant P and the pseudo-vector covariant $\widetilde{\mathrm{PV}}$ in (4.14) leads to identical Lorentz invariant amplitudes $F_{\mathrm{PS}} = F_{\mathrm{PV}} \equiv F_{\mathrm{P}}$ [36]. The pseudo-vector representation (4.10), on the other hand, has the advantage that it decouples the OPE contribution from the remaining amplitudes, i.e., the OPE gives a non-zero contribution only in the $g_{\widetilde{\mathrm{PV}}}$ amplitude while the others are zero. For the single pion exchange $g_{\widetilde{\mathrm{PV}}}$ is now easy to interpret: it is just the pion propagator (3.6) times the pion-nucleon form factor (3.9).

When the various NN potentials are compared, this is done most efficiently in the pseudo-vector representation. All potentials contain an OPE of similar strength which dominates at small momenta. The pseudo-vector representation decouples the OPE contribution from the remaining amplitudes $g_m \neq g_{\widetilde{\mathrm{PV}}}$ and allows thus a more transparent investigation of the short and intermediate range parts of the potentials which are actually the interesting ones. Fig. 4.2 shows the isospin-averaged amplitudes $g_m^D(|\mathbf{p}|, \theta = 0)$ for Bonn A, CD-Bonn, Argonne v_{18}, Nijm93, Nijmegen I and II, Reid93, the effective low momentum interaction $V_{\mathrm{low\ k}}$ and the chiral Idaho potential. The amplitudes are obtained going through the transformation scheme discussed above. Partial waves are taken into account up to $J = 90$ (Bonn A, CD-Bonn, Idaho), $J = 9$ (Argonne v_{18}, Nijmegen I/II, Nijm93, Reid93) and $J = 6$ ($V_{\mathrm{low\ k}}$).

The amplitudes determined from the complete NN potentials are no more as easy to interpret as for a single meson exchange where they represent essentially the propagators times the form factors. This is also true for the full OBE since the contributions from the various mesons are coupled through their exchange parts. Since these amplitudes are not very transparent quantities, Fig. 4.2 includes as a reference in addition the contributions from only OPE and from only σ and ω exchange, both taken from Bonn A.

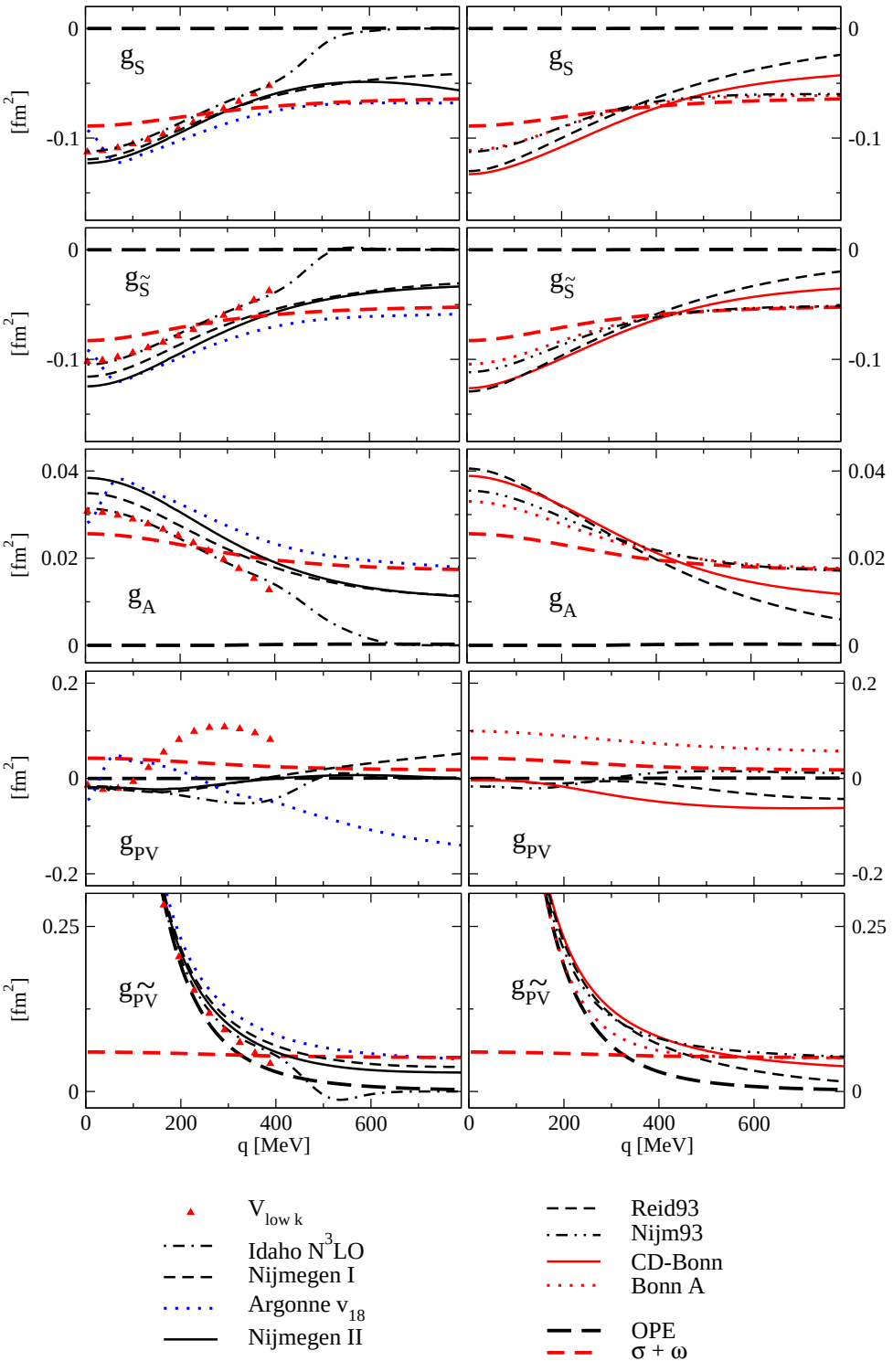

Figure 4.2: *Isospin-averaged Lorentz invariant amplitudes* $g_m^D(|\mathbf{q}|, \theta = 0)$ *for the different NN potentials in the pseudo-vector representation. As a reference the amplitudes from solely OPE and from* $\sigma + \omega$ *exchange, both with Bonn A parameters, are shown.*

Several features can now be seen from Fig. 4.2: First of all the four amplitudes $g_{\rm S},\ g_{\tilde{\rm S}},\ g_{\rm A}$ and $g_{\widetilde{\rm PV}}$ are very close for the OBE potentials Bonn A, CD-Bonn and Nijm93 and the phenomenological non-relativistic Argonne v_{18} and Nijmegen I/II potentials. Only at very small $|\mathbf{q}|$ Argonne v_{18} shows a deviating structure. The direct pseudo-vector amplitude $g_{\rm PV}$ falls somewhat out of systematics. This amplitude is, however, of minor importance since it does not contribute to the Hartree-Fock self-energy (5.5-5.7) and to the single particle potential.

The dominance of the OPE at low $|\mathbf{q}|$ is reflected in the pseudo-vector exchange amplitude $g_{\widetilde{\rm PV}}$ which is at small $|\mathbf{q}|$ almost two orders of magnitude larger than the other amplitudes. In the OBE potentials the high momentum part of the interaction, on the other hand, is dominated by heavy meson exchange and the corresponding amplitudes $g_{\rm S},\ g_{\tilde{\rm S}},\ g_{\rm A}$ approach the $\sigma+\omega$ exchange result. Deviations from the $\sigma+\omega$ amplitudes, e.g. due to exchange of isovector mesons ρ and δ in the OBE potentials are moderate at large $|\mathbf{q}|$. These deviations are more pronounced at small $|\mathbf{q}|$.

The remarkable agreement between the OBE amplitudes and those derived from the non-relativistic Argonne v_{18} potential demonstrates two things: first of all, it means that for on-shell scattering the Argonne v_{18} can be mapped on the relativistic operator structure where the local phenomenological functions V_i, Eq. (3.12), play the same role as the meson propagators plus corresponding form factors in the meson exchange picture. Secondly, the effective treatment of the short-distance physics in Argonne v_{18} is very similar to that in the OBE potentials Bonn A, CD-Bonn and Nijm93. This fact can be estimated from Fig. 3.4 where the $^1S_0$ partial wave amplitudes are close as well. On the other hand the softer character of the Reid93 and also the Nijmegen I and II potentials is reflected clearly in the stronger deviation from the $\sigma+\omega$ amplitudes at large $|\mathbf{q}|$.

4.3.1. Effective low momentum potentials

In order to have a better representation in Fig. 4.3 the isospin-averaged Lorentz invariant amplitudes from the effective low momentum potentials $V_{\rm low\ k}$ and the chiral Idaho N^{3}LO potential are shown separately. The amplitudes derived from the OBE potentials Bonn A and CD-Bonn, respectively, are serving as a reference. The amplitudes from the $V_{\rm low\ k}$ potential are only plotted up to the intrinsic cut-off of 400 MeV. In this momentum range the amplitudes fall practically on top of those from the Idaho N^{3}LO potential. This is not the case for the direct pseudo-vector amplitude $g_{\rm PV}$ as already mentioned before. At low $|\mathbf{q}|$ the amplitudes derived from Idaho N^{3}LO and $V_{\rm low\ k}$ behave qualitatively and quantitatively like those from the OBE potentials Bonn A or CD-Bonn. The conclusion is therefore that also the effective low momentum potentials can be mapped on a relativistic operator structure. For the Idaho N^{3}LO potential

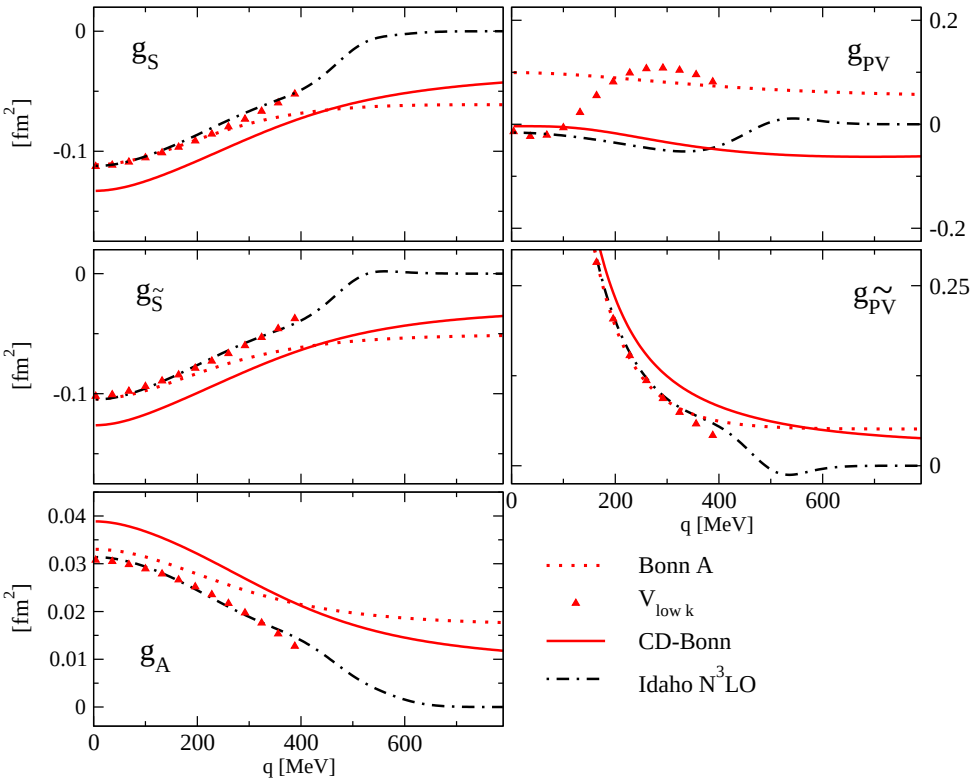

Figure 4.3: *Isospin-averaged Lorentz invariant amplitudes* $g_m^D(|\mathbf{q}|, \theta = 0)$ *for the effective low momentum NN potentials after projection on the Dirac operator structure (pseudo-vector representation). Additionally the Bonn A and the CD-Bonn potentials are shown as a reference.*

which is also based on the operator structure given in Eq. (3.13), the functions V_i and V_i' in combination with the corresponding operators, derived from fourth order two-pion exchange plus contact terms, lead to a structure which is similar to that imposed by the OBE picture up to a certain cut-off scale. However, clear deviations appear in the cut-off region between 400 and 500 MeV. Since chiral perturbation theory is a low-momentum expansion, it applies for momenta $Q \ll \Lambda_\chi \approx 1$ GeV and therefore the short-range interactions are strongly suppressed by the exponential regulator function Eq. (3.26). As a consequence the amplitudes derived from the Idaho potential drop rapidly to zero for momenta above 400 MeV. The question which arises in this context is now:

- How reliable is the extrapolation of standard OBE type potentials to higher momenta above the pion threshold?
- Can low momentum potentials be used around and above the momentum cut-off region?

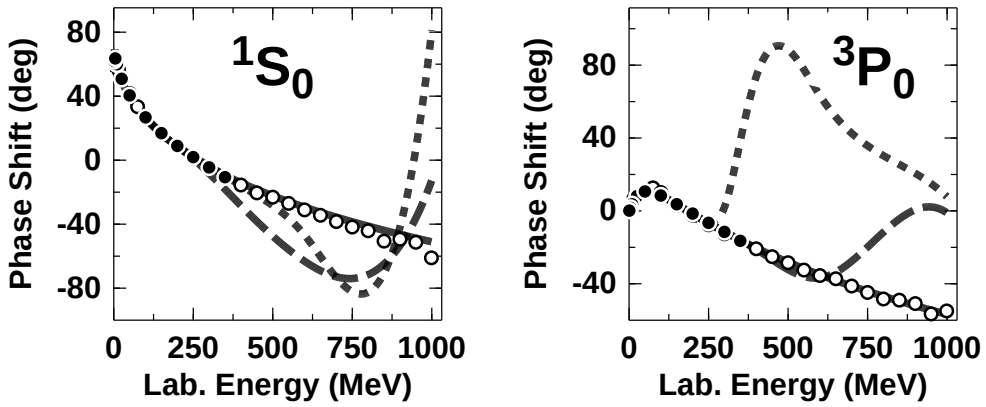

Figure 4.4: *np phase shifts. Solid dots indicate the Nijmegen multienergy np phase shift analysis [109] and open circles the GWU/VPI single-energy np analysis SM99 [110]. The solid line represents the prediction by the CD-Bonn potential [87] which is almost completely hidden by the symbols indicating the data. Also the N^{3}LO chiral potential developed by the Idaho group [19] is shown (dashed line) as well as by the Bochum/Juelich group [17] (dotted line). The figure was taken from [111].*

These two questions are addressed by the next figure. In Fig. 4.4 phase shift predictions by various potentials are shown up to 1000 MeV lab. energy for the incident nucleon. As discussed in [111] the high-precision CD-Bonn potential predicts the data correctly up to about 1 GeV, although it is adjusted to the data only up to an energy of 350 MeV. This is not the case for the chiral NN potentials indicated by the dashed line [19] and dotted line [17] which are able to describe the data up to about 300 MeV lab. energy correctly. For higher momenta chiral NN potentials do not yield any reasonable predictions which can be seen from the deviating behavior [111]. This deviating behavior is naturally also reflected in the Lorentz invariant amplitudes in Fig. 4.3, e.g., in the $g_{\widetilde{PV}}$ channel, for relative c.m. momenta beyond 400 MeV which corresponds roughly to 300 MeV lab. energy.

From this figure one can conclude that OBE type potentials provide a realistic momentum dependence also above the pion threshold and can be extrapolated safely to higher energies. The covariant amplitudes shown in Fig. 4.3 could in future serve as a guideline to construct an effective potential based on effective field theory at low energies and then follows the OBE momentum dependence at higher energies above the cut-off region.

5. Nuclear matter properties

In Chapter 2 it has been shown that the appearance of large scalar and vector mean fields of several hundred MeV in nuclear matter is a crucial feature of relativistic approaches to the nuclear structure problem. This is also true for the microscopic DBHF theory (see Section 2.2). In the case of DBHF relativistic meson exchange interactions have to be used like the Bonn potentials described in Section 3.1. As already mentioned in the introduction it has often been argued that the large scalar and vector fields enforced by Dirac phenomenology might be an artefact of the relativistic meson exchange picture. Since only covariantly formulated nucleon-nucleon interactions can be applied in such relativistic self-consistent calculations it has not been understood yet whether the generation of the large scalar and vector mean fields displays an implicit property of the nucleon-nucleon interaction.

Nevertheless in Chapter 4 relativistic and non-relativistic modern nucleon-nucleon potentials described in Chapter. 3 are mapped on a relativistic operator basis using projection techniques. This is possible since any two-body amplitude can be decomposed into a set of Dirac operators and Lorentz invariants. The comparison of the various potentials shows a remarkable agreement of the relativistic structure of the potentials at the level of covariant amplitudes.

Consequently the next step in this work is to determine the relativistic self-energy Σ in Hartree-Fock approximation in nuclear matter with its scalar and vector components with the various potentials. To project out the self-energy components the interaction nucleon-nucleon interaction matrix has to be decomposed into Lorentz invariants where the projection formalism is explained in the previous Chapter 4. The calculation of the self-energy components is done at tree level since a self-consistent treatment requires to evaluate in-medium scattering amplitudes which is not possible with most of the potentials. The results are presented in the first part of this chapter. The main finding is that the generation of the large scalar and vector components in nuclear matter is a model independent property of the nucleon-nucleon interaction.

A comparison of the self-energy components obtained at tree level to those obtained within a full self-consistent DBHF calculation (both with the Bonn A potential) shows that the corrections due to higher order density dependences are small and that the magnitude of the self-energy components is already set at tree level.

To check the applicability and accuracy of the method, i.e. of the projection

scheme the single particle potential is calculated with the help of the self-energy components. The results for the various potentials are then compared to a non-relativistic calculation where an almost perfect agreement is found.

Moreover, with the projection formalism at hand one is able to investigate the connection between the appearance of the matter fields and chiral dynamics in more detail. It allows in particular a straightforward and transparent discussion of the contributions which arise at different orders in the chiral expansion of the NN interaction, see Eqs. (3.19) and (3.25). Throughout this work the chiral Idaho potential [18, 19] is applied[1].

The main outcome of this investigation is that the generation of the large scalar and vector fields is intimately connected to the short-range spin-orbit force from NLO contact terms in the chiral expansion.

All investigations up to here have been performed at tree level. It is clear that a realistic description of nuclear matter requires to go beyond the Hartree-Fock approximation as it is done in the DBHF approach. In this approach one has to solve the set of equations self-consistently as explained in Section 2.2. Such a procedure is restricted to covariantly formulated nucleon-nucleon potentials like Bonn A [12, 86]. There it is possible to evaluate in-medium amplitudes since higher order corrections in the density are taken into account through a dressing of the nucleon-nucleon interaction with an effective nucleon mass M^*. Therefore in the present work the aim was not to perform a fully self-consistent DBHF calculation. In fact the influence of the dressing of the interaction on the Hartree-Fock level on the self-energy and the implications for the equation of state (EOS) can be studied with OBE-like potentials: Bonn A [12, 86], Nijm93, and Nijm I [65].

To account for higher order corrections in density at Hartree-Fock the bare nucleon mass has to be dressed by the self-energy, Eq. (2.55), i.e. the bare nucleon spinor is replaced by the in-medium one (2.58). This leads to a self-consistency problem when the self-energy is calculated. Since the higher order density dependences introduced by the dressing of the bare interaction lead mainly to a reduction of the attractive scalar field significantly more repulsion at the level of the EOS is observed.

In the last part of this chapter isospin symmetric nuclear and pure neutron matter are investigated within chiral effective field theory (EFT). Therefore the Idaho N^{3}LO potential derived in chiral EFT is applied.

The EOS is investigated at tree level in Hartree-Fock approximation. It is a well known fact that at Hartree-Fock level saturation of nuclear matter is not observed. Therefore we apply chiral EFT in a second step within the

[1] All investigations are based on a version of the chiral N^{3}LO Idaho potential which allows to separate the contributions from different orders. The code was provided by R. Machleidt (private communication).

non-relativistic Brueckner-Hartree-Fock approach. In the present work a non-relativistic approach is applied since it is not possible to use the chiral NN potential in a relativistic BHF calculation (DHBF) where one accounts in addition for the dressing of the potential matrix elements $V \mapsto V^*$ as explained in Section 2.2. The latter requires, however, a definite relativistic structure of the NN interaction, like for covariantly formulated OBE type potentials (see Section 5.3). Nevertheless Brueckner-Hartree-Fock theory is known to be able to produce saturation due to Pauli blocking and short-range correlations with realistic NN potentials like the phenomenological Argonne v_{18} [25] potential or the OBE Bonn A [12, 86] although it fails to reproduce quantitatively the empirical saturation properties.

Since chiral EFT allows to investigate nuclear matter and neutron matter at the different orders of the chiral expansion the EOS is determined for all orders up to N^{3}LO in order to obtain a qualitative understanding of the properties of chiral EFT applied in many-body calculations. Moreover the symmetry energy obtained from chiral EFT is explored and compared to the result from other realistic interactions.

Though it is also a well known fact that Hartree-Fock calculations for nuclear matter are not realistic the study of the latter serves as a basis for the subsequent investigation of the pion mass dependence of the self-energy fields and the EOS of nuclear matter (especially in the chiral limit) where the same chiral EFT interaction is applied at NLO.

Naturally one assumes that the magnitude of the self-energy fields and the qualitative behavior of the nuclear EOS should persist even in the chiral limit since hadronic properties are not expected to change dramatically in the case of massless quarks or pions. The reason for this is that the expansion of the nuclear force in the context of chiral perturbation theory is well defined for small quark masses and should still be valid in the limit $m_q \to 0$ which is equivalent to $m_\pi \to 0$. In order to estimate the implications for the self-energy components and the EOS when going to the chiral limit one needs a nucleon-nucleon interaction where the quark mass dependence is known. Therefore the chiral EFT interaction derived by Epelbaum et al. [20] (see also Section 3.3.2) up to NLO is applied in a tree-level Hartree-Fock calculation and moreover in a non-relativistic Brueckner-Hartree-Fock calculation. Furthermore the properties of nuclear matter are tested with a considerably higher pion mass. This might be of interest when corresponding QCD Lattice results are compared since due to technical difficulties these calculations have to be performed with a pion mass much larger than the physical one.

5.1. Self-energy in Hartree-Fock approximation

The self-energy in Hartree-Fock approximation at tree level is given by

$$\Sigma_{\alpha\beta}(k) = -i \int \frac{d^4q}{(2\pi)^4} \left[\langle kq|V|kq\rangle_{\alpha\gamma;\beta\delta} - \langle kq|V|qk\rangle_{\alpha\gamma;\delta\beta}\right] G^D_{\gamma\delta}(q) \tag{5.1}$$

where in contrast to a full self-consistent calculation the T-matrix in Eq. (2.44) is replaced by the bare interaction matrix V. Eq. (5.1) describes the summation of the interaction of a nucleon with four-momentum k with all nucleons inside the Fermi sea in Hartree-Fock approximation. Since

Since fully antisymmetrized matrix elements are applied which contain already the direct (Hartree) and exchange (Fock) contributions, it is sufficient to evaluate the Hartree integral for the self-energy

$$\Sigma_{\alpha\beta}(k) = -i \int \frac{d^4q}{(2\pi)^4} \left[\langle kq|V|kq\rangle_{\alpha\gamma;\beta\delta}\right] G^D_{\gamma\delta}(q) \ . \tag{5.2}$$

$G^D(q)$ is the Dirac propagator as given by Eq. (2.59)

$$G^D(q) = 2\pi i(\gamma_\mu k^\mu + M)\delta(k^2 - M^2)\Theta(q_0)\Theta(k_F - |\mathbf{q}|) \ , \tag{5.3}$$

without effective nucleon masses and momenta. Here, $\mathbf{k}$, taken along the z-axis, is the single particle momentum of the incoming nucleon in the nuclear matter rest frame. The relative momentum in the two-nucleon c.m. frame where the matrix elements V are evaluated, is given by $|\mathbf{p}| = \sqrt{s/4 - M^2}$, where $s = (E(\mathbf{k}) + E(\mathbf{q}))^2 - (\mathbf{k} + \mathbf{q})^2$ is the total energy of the two nucleons.

Using the pseudo-vector representation for the on-shell matrix elements V, Eq. (4.17), the self-energy operator reads

$$\begin{aligned}
\Sigma_{\alpha\beta}(k, k_F) \ = \ & \int \frac{d^3\mathbf{q}}{(2\pi)^3} \frac{\Theta(k_F - |\mathbf{q}|)}{4E(\mathbf{q})} \Bigg\{ (\not{k}_{\alpha\beta} - \not{q}_{\alpha\beta}) \frac{2q_\mu(k^\mu - q^\mu)}{4M^2} g_{\widetilde{\mathrm{PV}}} \\
& + m 1_{\alpha\beta} \left[4g_{\mathrm{S}} - g_{\tilde{\mathrm{S}}} + 4g_{\mathrm{A}} - \frac{(k^\mu - q^\mu)^2}{4M^2} g_{\widetilde{\mathrm{PV}}} \right] \\
& + \not{q}_{\alpha\beta} \left[-g_{\tilde{\mathrm{S}}} + 2g_{\mathrm{A}} - \frac{(k^\mu - q^\mu)^2}{4M^2} g_{\widetilde{\mathrm{PV}}} \right] \Bigg\} \ .
\end{aligned} \tag{5.4}$$

Note that the sign convention for the vector field $\Sigma = \Sigma_{\mathrm{s}} - \gamma_\mu \Sigma^\mu$ with $\Sigma_\mu = (\Sigma_0, \mathbf{k}\Sigma_{\mathrm{v}})$ in Eq. (2.51) is that used standardly in DBHF [34, 36, 112]. It differs from that used standardly in QHD ($\Sigma = \Sigma_{\mathrm{s}} + \gamma_\mu \Sigma^\mu$) and also that of Eqs. (2.84) and (2.85).

To project out the Lorentz components of the self-energy operator (5.4) one has to take the respective traces in Dirac space Eqs. (2.52)-(2.54)

$$\Sigma_{\rm s}(k,k_F) = \int \frac{d^3\mathbf{q}}{(2\pi)^3}\Theta(k_F-|\mathbf{q}|)\frac{M}{E(\mathbf{q})}T_{\rm s}(\mathbf{k},\mathbf{q}) \ , \tag{5.5}$$

$$\Sigma_0(k,k_F) = \int \frac{d^3\mathbf{q}}{(2\pi)^3}\Theta(k_F-|\mathbf{q}|)T_0(\mathbf{k},\mathbf{q}) \ , \tag{5.6}$$

$$\Sigma_{\rm v}(k,k_F) = \int \frac{d^3\mathbf{q}}{(2\pi)^3}\Theta(k_F-|\mathbf{q}|)\frac{\mathbf{k}\cdot\mathbf{q}}{|\mathbf{k}|^2E(\mathbf{q})}T_{\rm v}(\mathbf{k},\mathbf{q}) \ . \tag{5.7}$$

where the abbreviations are used

$$T_{\rm s}(\mathbf{k},\mathbf{q}) = \frac{1}{4}\left[4g_{\rm S}-g_{\tilde{\rm S}}+4g_{\rm A}-\frac{(k^\mu-q^\mu)^2}{4M^2}g_{\widetilde{\rm PV}}\right] \ , \tag{5.8}$$

$$T_0(\mathbf{k},\mathbf{q}) = \frac{1}{4}\left[g_{\tilde{\rm S}}-2g_{\rm A}+\frac{E(\mathbf{k})}{E(\mathbf{q})}\frac{(k^\mu-q^\mu)^2}{4M^2}g_{\widetilde{\rm PV}}\right] \ , \tag{5.9}$$

$$T_{\rm v}(\mathbf{k},\mathbf{q}) = \frac{1}{4}\left[g_{\tilde{\rm S}}-2g_{\rm A}+\frac{k_z}{q_z}\frac{(k^\mu-q^\mu)^2}{4M^2}g_{\widetilde{\rm PV}}\right] \ . \tag{5.10}$$

5.1.1. Results for various NN interactions

In Fig. 5.1 the tree level scalar and vector self-energy components in nuclear matter are shown obtained with the various NN potentials at nuclear saturation density with Fermi momentum $k_{\rm F} = 1.35$ fm^{-1} which corresponds to a density of $\rho = 0.166$ fm^{-3}. As a remarkable result, all potentials yield scalar and vector mean fields $\Sigma_{\rm s}$ and Σ_0 of comparable strength: a large and attractive scalar field $\Sigma_{\rm s} \simeq -(450\div400)$ MeV and a repulsive vector field of $-\Sigma_0 \simeq +(350\div400)$ MeV. These values are comparable to those derived from RMF phenomenologically and also from QCD sum rules. Also the explicit momentum dependence of the self-energy is similar for the various potentials. The Idaho mean fields follow the other approaches at low k but show a stronger decrease above $k \simeq 2$ fm^{-1} which reflects again the influence of the cut-off parameter. Fig. 5.2 shows the spatial component of the vector self-energy $\mathbf{k}\Sigma_{\rm v}$, Eq. (5.7). Also here the various potentials agree quite well. As known from self-consistent DBHF calculations [34, 36], the spatial vector self-energy is a moderate correction to the large scalar and time-like vector components $\Sigma_{\rm s}$ and Σ_0. This is found to be also the case at tree level where $\mathbf{k}\Sigma_{\rm v}$ is about one order of magnitude smaller than the other two components. The spatial self-energy originates exclusively from exchange contributions, i.e., the Fock term, and vanishes e.g. in the mean field approximation of RMF theory. Fig. 5.3 displays the density dependence of the fields, evaluated at momentum $k = k_{\rm F}$. At moderate densities the different

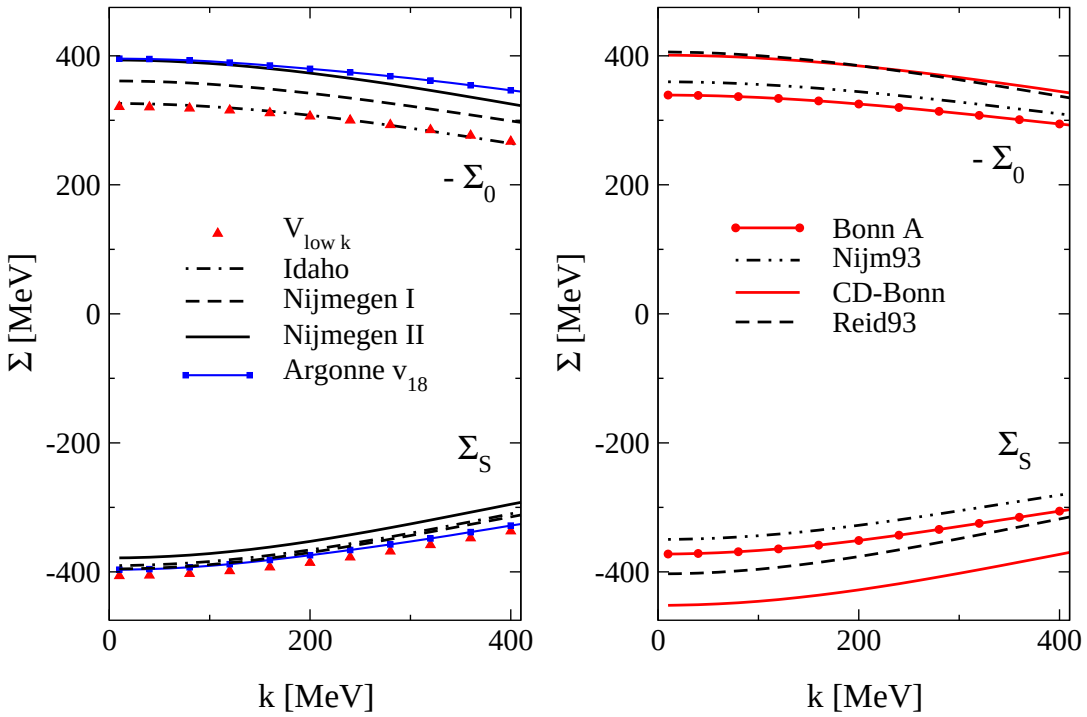

Figure 5.1: *Tree level scalar and vector self-energy components in nuclear matter at* $k_F = 1.35$ fm^{-1} *obtained with different NN interaction models.*

potentials yield scalar and vector fields which are rather close in magnitude. At higher densities the results start to split up which reflects again the different treatment of short distance physics in the various interactions. Only the two low momentum interactions Idaho N^{3}LO and $V_{\text{low k}}$ lie practically on top of each other.

5.1.2. Reliability of tree level calculations

All results presented in the previous section have been obtained at tree level, i.e., in lowest order in density. Hence, the results are only 'realistic' in the low density limit but not at higher densities since short-range correlations are missing. In order to estimate the influence of short-range NN correlations and self-consistency, which are getting substantially important at higher densities in Fig. 5.4 the scalar and vector self-energy components obtained at tree level from Fig. 5.1 for Bonn A to those obtained in a corresponding full self-consistent DBHF calculation are compared at $k_F = 1.35$ fm^{-1}. For DBHF the approach of [36] is used (subtracted T-matrix in *pv* representation). The DBHF calculation yields reasonable saturation properties with a binding energy of $E_{\text{bind}} = -15.72$ MeV and

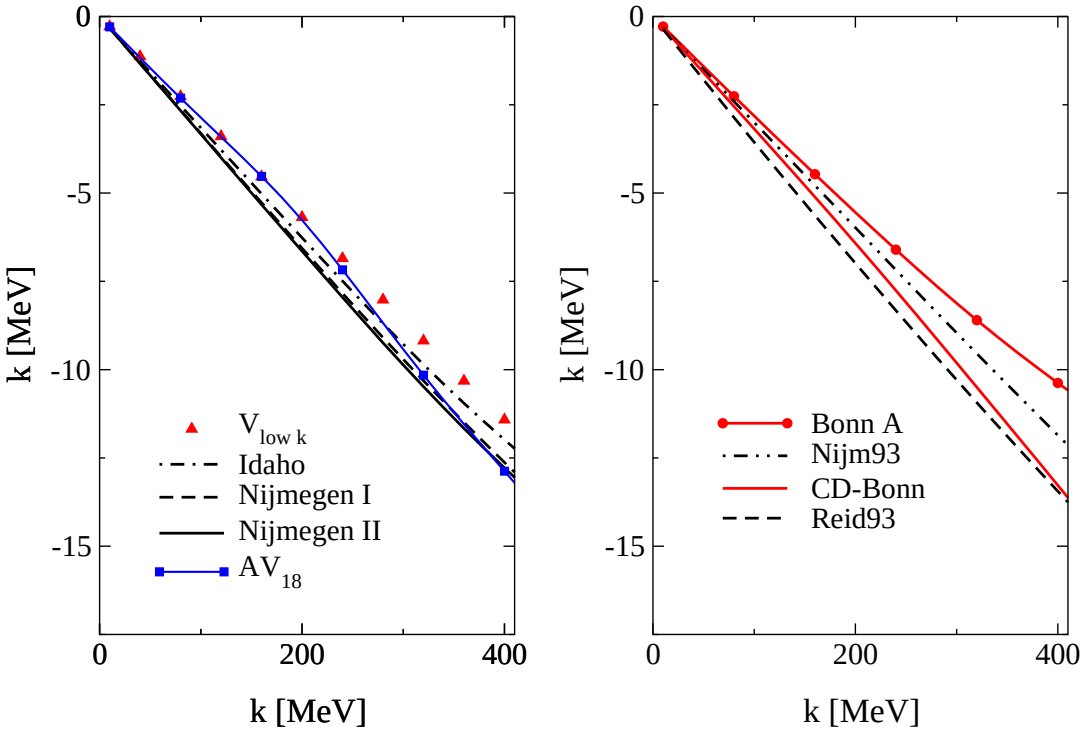

Figure 5.2: *Tree level spatial vector self-energy component* $\mathbf{k}\Sigma_{\rm v}$ *in nuclear matter at* $k_{\rm F} = 1.35$ fm^{-1} *for the various potentials.*

a saturation density of $\rho = 0.181$ fm^{-3} [36]. The correlations lead to a general reduction of the vector self-energy by a shift of about 70 MeV. Self-consistency and correlations also weakens the momentum dependence, in particular for $\Sigma_{\rm s}$. However, except of the 70 MeV shift of Σ_0, the absolute magnitude of the self-energies is not strongly modified in the realistic calculation. This means that one can expect that the large attractive scalar and repulsive vector self-energy components will also persist for the other interactions when short-range correlations are accounted for in a full relativistic many-body calculation.

5.1.3. Comparison with non-relativistic single particle potential

In Fig. 5.5 finally the single particle potential in nuclear matter at $k_{\rm F} = 1.35$ fm^{-1} is shown, determined from the relativistic self-energy components. The single particle potential is defined as the expectation value of the self-energy

$$U_{\rm s.p.}(k, k_{\rm F}) = \frac{< u(k)|\gamma^0\Sigma|u(k) >}{< u(k)|u(k) >} = \frac{M}{E(\mathbf{k})} < \bar{u}(k)|\Sigma|u(k) > \qquad (5.11)$$

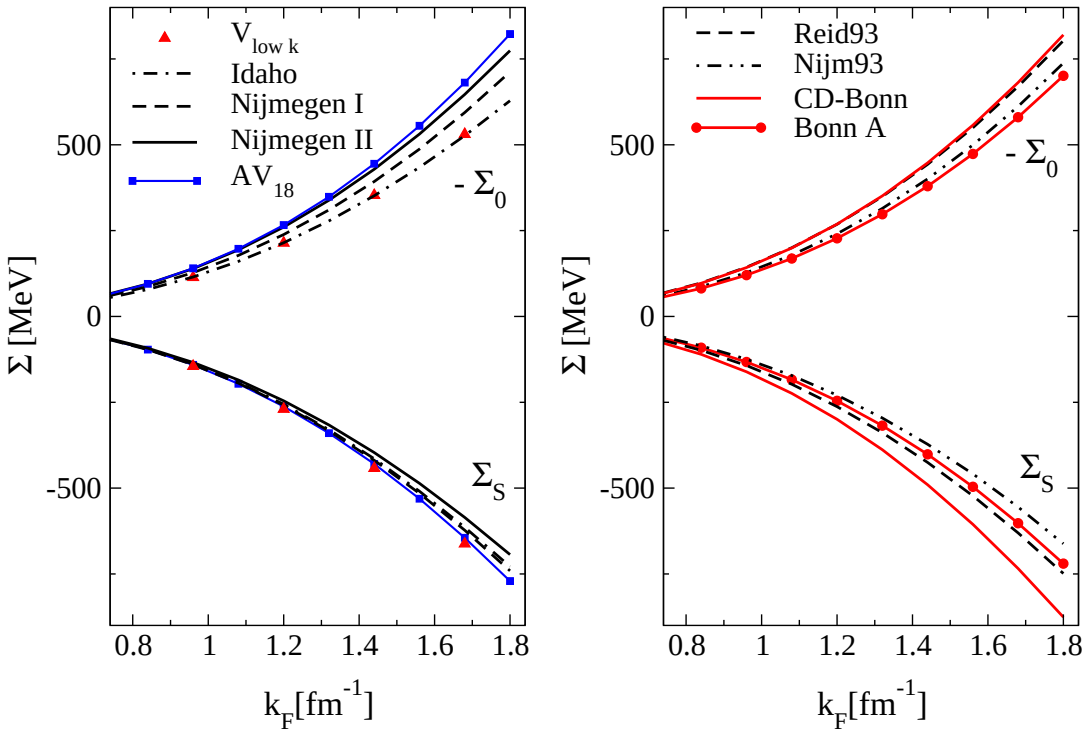

Figure 5.3: *Density dependence of the tree level scalar and vector self-energy components in nuclear matter obtained with the various potentials.*

and reads

$$U_{\text{s.p.}}(k, k_{\text{F}}) = \frac{M}{E}\Sigma_{\text{s}} - \frac{k_\mu \Sigma^\mu}{E} = \frac{M\Sigma_{\text{s}}}{\sqrt{\mathbf{k}^2 + M^2}} - \Sigma_0 + \frac{\Sigma_{\text{v}}\mathbf{k}^2}{\sqrt{\mathbf{k}^2 + M^2}} \ . \qquad (5.12)$$

Eq. (5.12) represents the single particle potential at tree level, i.e., the expectation value of Σ with the bare spinor basis without taking the effective nucleon mass Eq. (2.55) into account. The next step towards a self-consistent treatment would be to use an in-medium spinor basis which includes the scalar and vector self-energy components via effective masses and effective four-momenta as defined by Eq. (2.55) and (2.56) in Section2.2.2. This would, however, involve higher order corrections in the baryon density and is not intended in the present investigations which are restricted to leading oder.

The single particle potential reflects the well known fact that phase-shift equivalent two-body potentials which describe NN scattering data with about the same accuracy [89], can be rather different [89]. This can already be seen from Fig. 3.4 where the $^1S_0$ matrix elements of the various potentials are shown. The differences are mainly due to a different treatment of the short-range part of the nuclear interaction, i.e., the hard core which is not well constraint by scatter-

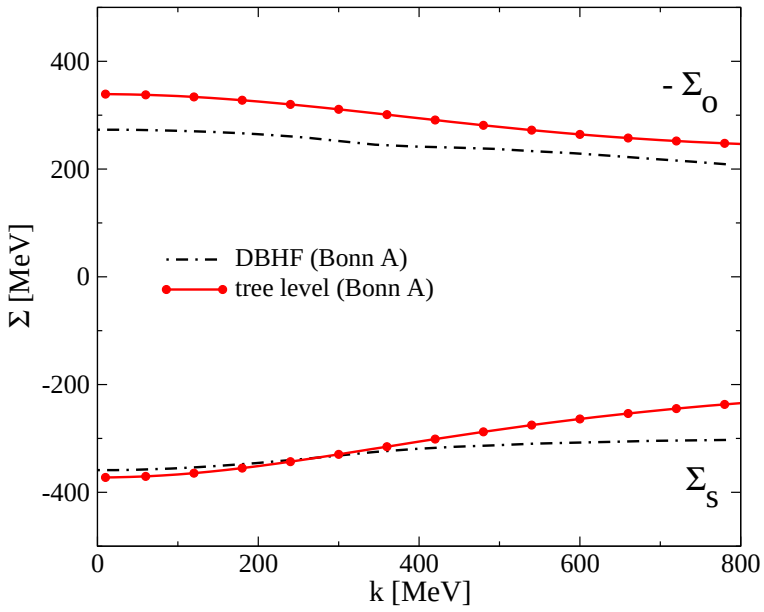

Figure 5.4: *Tree level scalar and vector self-energy components in nuclear matter at* $k_F = 1.35$ fm^{-1} *are compared to corresponding values from a full self-consistent relativistic Brueckner (DBHF) calculation. In both cases the Bonn A potential is used.*

ing data. Thus the various potentials lead to about the same T-matrices when iterated in the Lippmann-Schwinger or Bethe-Salpeter equation. However, at tree-level the hard core contributes fully to $U_{\text{s.p.}}$ which explains the shift of the various results in Fig. 5.5. Integrating out the high momentum components, e.g. by renormalization group methods, one arrives at equivalent low-momentum potentials $V_{\text{low k}}$ [26]. Since $V_{\text{low k}}$ contains no significant contributions from the hard core it gives already at tree level a realistic single-particle potential. The situation is similar for the chiral EFT N^{3}LO Idaho potential. As can be seen from Fig. 3.4 Idaho is rather close to $V_{\text{low k}}$, not only in the $^1S_0$ partial wave, and correspondingly both lead to comparable potentials. However, the slight shift of about 10 MeV between $V_{\text{low k}}$ and Idaho reflects again the subtle cancellation effects between the large scalar and vector fields, since at the scale of the fields, Fig. 5.3, both lie practically on top of each other.

In the present context the single particle potential serves as an important check of the whole applied projection procedure which is described in Chapter 4. In Fig. 5.5 the single particle potential $U_{\text{s.p.}}$ is shown, calculated from Eq. (5.12), i.e., after projecting the NN potentials from the partial wave basis onto the covariant operator basis, determining then the relativistic self-energy

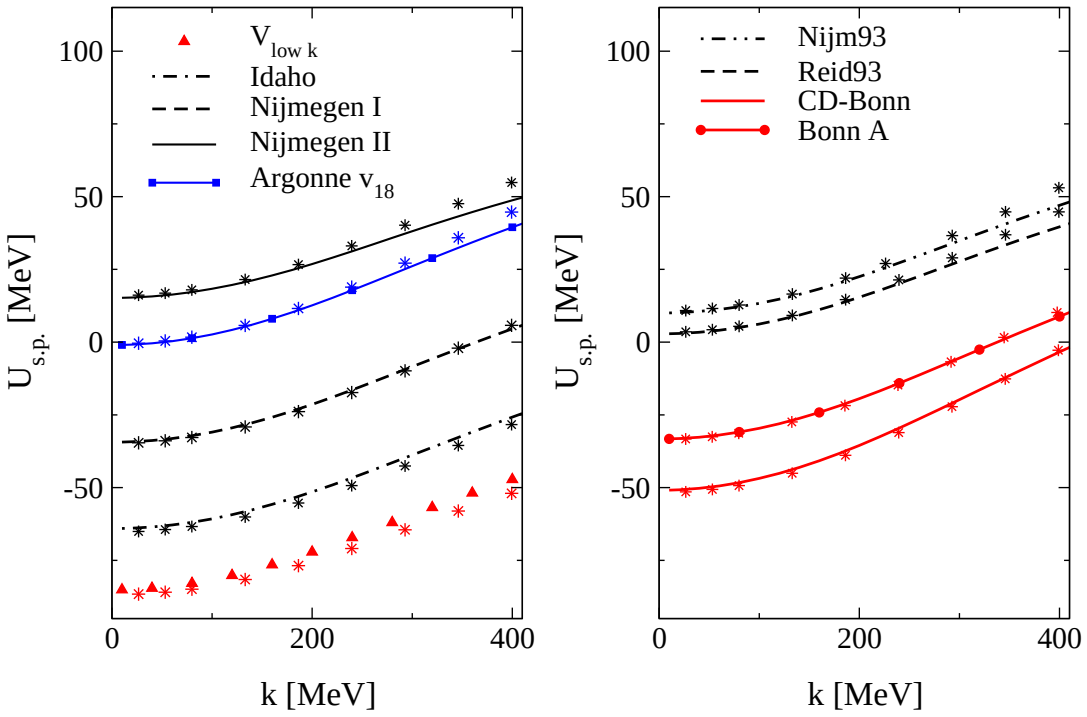

Figure 5.5: *Single particle potential in nuclear matter at* $k_{\mathrm{F}} = 1.35$ fm^{-1}*, determined from the tree level Born amplitudes of the various potentials. The single particle potential determined from the relativistic self-energy components after projection onto the covariant operator basis is compared to a non-relativistic calculation (stars) where partial wave amplitudes are summed up directly.*

components and finally $U_{\mathrm{s.p.}}$. Fig. 5.5 includes also the results from a 'non-relativistic' calculation of $U_{\mathrm{s.p.}}$ where the partial wave amplitudes are directly summed up. To do so a non-relativistic Brueckner-Hartree-Fock program[2]was used and the single particle potential in Born approximation was determined. The non-relativistic results are represented by stars in Fig. 5.5 and shown up to a momentum of 400 MeV. This avoids distortions from non-relativistic kinematics which occur at higher momenta. At moderate momenta the non-relativistic and the relativistic calculations show an excellent agreement which demonstrates the accuracy of the applied projection techniques. One has thereby to keep in mind that $U_{\mathrm{s.p.}}$ originates in the relativistic approach from the cancellation of the two scalar and vector fields which are both of the order of about 400 MeV.

[2]This code was provided by H. Müther and used in the Born option. For each potential partial waves up to $J = 9$ are taken into account.

5.2. Self-energy from chiral EFT

Chiral EFT nucleon-nucleon potentials provide a systematic expansion of the nuclear force as explained in Section 3.3.1. Therefore a connection of chiral dynamics to the appearance of the large scalar and vector fields in matter can be established. Calculating the scalar and vector self-energies components from a chiral EFT nucleon-nucleon potential order by order allows to investigate the structure of the self-energy. Moreover one is able to separate the contributions from different orders in the chiral expansion of the NN interaction and study the connection of the self-energy components to the low energy constants (LECs) appearing at different orders.

In Fig. 5.6 the tree level results for the scalar and vector self-energy components in nuclear matter at $k_\mathrm{F} = 1.35$ fm^{-1} obtained with the chiral Idaho potential [19] in leading order (LO) up to next-to-next-to-next-to-leading order (N^{3}LO) are shown. To leading order the chiral NN interaction does not generate significant mean fields. The scalar self-energy Σ_s is of the order of about -70 MeV and the vector self-energy is practically zero. At LO only the static one-pion exchange (OPE) and contact terms without derivatives appear which involve the operators O_1 and O_2 from the operator basis (3.13). Hence at LO no pieces from vector exchange occur which would involve all operators $O_i, i = 1..5$. The small scalar field means, on the other hand, that the nucleon mass $M^* = M + \Sigma_\mathrm{s}$ does not change significantly in matter to leading order in chiral EFT. The dominant contributions arise at next-to-leading order (NLO). NLO involves leading two-pion exchange (TPE) and contact terms with two derivatives (see Fig. 3.3). The NLO contact terms contain the full operator structure O_i. At this level both, scalar and vector self-energy components of about $\mp$400 MeV magnitude are generated. Also the signs, i.e., the attractive scalar and the repulsive vector mean field, are fixed at NLO. The higher orders, N^{2}LO and N^{3}LO provide corrections which tend to reduce the NLO result, are, however, moderate. As can be seen from Fig. 3.3 chiral EFT at N^{2}LO contains subleading TPE and no contact terms at all, while at N^{3}LO sub-subleading TPE, leading 3π exchange, corrections to OPE and TPE and contact terms with four derivatives occur [17].

In order to investigate the role of pion dynamics and that of contact terms in more detail, Table 5.1 shows the contributions which arise from pion dynamics $\Sigma^{(\pi)}$, i.e., OPE, TPE, 3π and corrections, and those from the contact terms $\Sigma^{(\mathrm{cont})}$ separately. The contributions to the self-energy at a particular order is given by the sum $\Sigma^{(\pi)} + \Sigma^{(\mathrm{cont})}$, the full self-energy at a certain order ν is obtained by adding the contributions from the lower orders $\Sigma^{(\nu)} = \sum_{\lambda=0}^{\nu} \Sigma^{(\lambda)}$. From Table 5.1 it becomes evident that the dominant contributions to the scalar and vector self-energy are generated by the contact terms which arise at next-to-leading order. At N^{2}LO no contact terms occur in the chiral expansion.

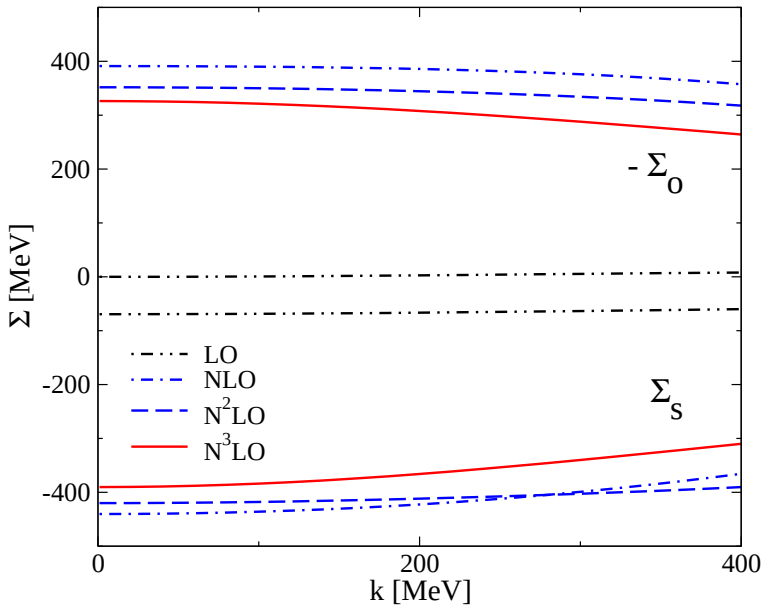

Figure 5.6: *Tree level scalar and vector self-energy components in nuclear matter at* $k_{\rm F} = 1.35$ fm^{-1} *obtained with the chiral EFT NN interaction [19]. The fields obtained in leading order (LO) up to next-to-next-to-next-to-leading order (N^{3}LO) are shown.*

The N^{3}LO contacts provide sizeable corrections to both, scalar and vector self-energy components and are of opposite sign than the NLO contributions. The contribution from pion dynamics to the self-energy components are found to be generally moderate. The largest contributions appear at N^{3}LO and are of opposite sign than those from corresponding contact terms. Hence the reduction of the nucleon mass $M^* = M + \Sigma_{\rm s}$ is driven by short-distance physics, dominantly by contact terms which occur at NLO. These are four-nucleon contacts with two derivatives. The explicit expressions are given in Section 3.3.1. From Eq. (3.23) one can see that at this order the short-range spin-orbit interaction (proportional to O_4 in (3.13))

$$iC_5(\boldsymbol{\sigma}_1 + \boldsymbol{\sigma}_2) \cdot (\mathbf{q} \times \mathbf{q}') \tag{5.13}$$

is generated. The appearance of large scalar and vector fields at NLO is therefore in perfect agreement with Dirac phenomenology where the large spin-orbit force is intimately connected to the appearance of the scalar and vector fields which are generated by short-range isoscalar scalar (σ) and vector meson (ω) exchange [36, 37]. In EFT the strength of the short-range spin-orbit interaction is determined by the C_5 parameter which is given by a linear combination of

Table 5.1: *Contributions from pion dynamics and contact terms to the scalar and vector self-energy components (in MeV) which appear at different orders in the chiral expansion. The evaluation is performed at nuclear saturation density* $k_{\rm F} = 1.35$ fm^{-1}.

	$\Sigma_{\rm s}$	$\Sigma_{\rm s}^{(\pi)}$	$\Sigma_{\rm s}^{(\rm cont)}$	$-\Sigma_0$	$-\Sigma_0^{(\pi)}$	$-\Sigma_0^{(\rm cont)}$
LO	-64.76	17.14	-81.90	4.49	19.02	-14.53
NLO	-344.22	4.40	-348.62	376.47	5.16	371.31
N^{2}LO	2.06	2.06	0.00	-41.92	-41.92	0.00
N^{3}LO	56.82	-89.34	146.16	-43.27	79.06	-122.33
sum	-350.10	-65.74	-284.36	295.77	61.32	234.45

the ^3P-wave low energy constants (LECs) [19, 17]

$$C_5 = \frac{1}{16\pi}\left[2C_{^3P_0} + 3C_{^3P_1} - 5C_{^3P_2}\right] \quad . \tag{5.14}$$

Hence the short-range spin-orbit interaction is dictated by P-wave NN scattering. As shown by Kaiser [113] the large values of the C_5 parameter is in good agreement with corresponding values extracted from high precision OBE type potentials (Bonn, CD-Bonn, Nijm93, Nijmegen I,II) and from Argonne v_{18} which are all in the range of $3C_5/8 \sim 80 \div 90$ MeV fm^5. In [113] these values were also compared to purely phenomenological Skyrme type density functionals designed for nuclear structure calculations [114, 115]. The values of the corresponding spin-orbit strength parameter W_0 in Skyrme models are also very close in magnitude, i.e. $3W_0/4 \sim 75 \div 97$ MeV fm^5. The contribution from chiral OPE to the spin-orbit terms in the density functional were found to be almost negligible (less than 1%). The lowest order irreducible TPE which occurs at NLO in the chiral expansion provides moderate corrections to the isoscalar spin-orbit strength function whereas the isovector strength is more strongly affected (TPE contributions lead to a $\sim$ 30% reduction) [113]. Thus the analysis of Kaiser is fully consistent with the small fields $\Sigma_{\rm s}^{(\pi)}$ and $\Sigma_0^{(\pi)}$ of $\sim \mp 5$ MeV generated by pion dynamics at NLO, as observed within the framework of the present analysis.

Epelbaum et al. [92] compared the spectroscopic LECs connected to the contact terms up to NLO from chiral EFT to those extracted from various NN potentials by performing a low-momentum expansion. As explained in Ref. [92]

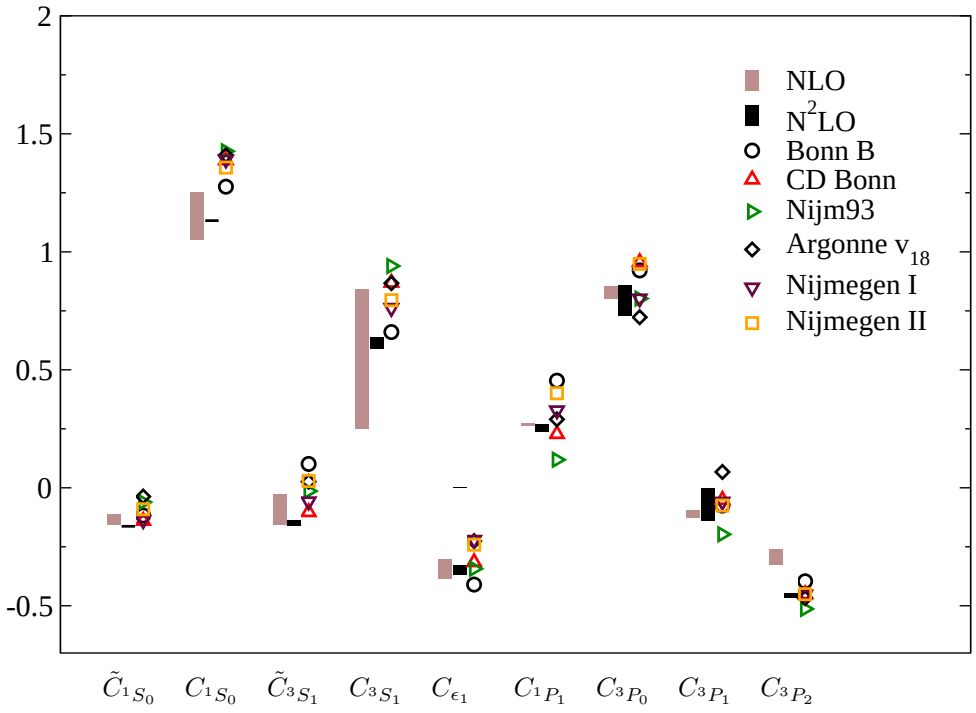

Figure 5.7: *Low energy constants from chiral EFT compared to extracted coefficients from various NN potentials. The left brown bars correspond to NLO and the middle bar is N^{2}LO. The length of the bars indicates the variation of the LECs with the cutoff Λ between 500 MeV and 600 MeV. The $\tilde{C}_i$ are in 10^4 GeV^{-2} and the C_i in 10^4 GeV^{-4}. The values for the LECs were taken from [92].*

in the limit of large meson masses and a fixed ratio of coupling constants and masses meson exchange diagrams can be interpreted as a sum of local four-nucleon operators where the number of derivatives or momentum insertions, respectively, increases in the expansion as indicated in Eq. (3.24). In Fig. 5.7 the values of the 9 spectroscopic LECs of this study [92] are shown. The left-most bar (brown) shows the fitted LECs of the NLO chiral EFT potential whereas the middle (black) bar indicates the LECs fitted at NNLO. The length of the bars reflects the range of the value of each LEC resulting from a variation of the momentum-cutoff Λ in the range of 500 MeV to 600 MeV. These spectroscopic LECs are related to the LECs appearing in the LO (C_S and C_T) and NLO ($C_1 \cdots C_7$) contact terms of the chiral EFT potential (see Eq. (3.23)). Note that to be able to compare directly the LECs from chiral EFT to OBE potentials also the contributions coming from chiral TPE to the spectroscopic LECs have been considered [92]. The extracted LECs from the various potentials are indicated

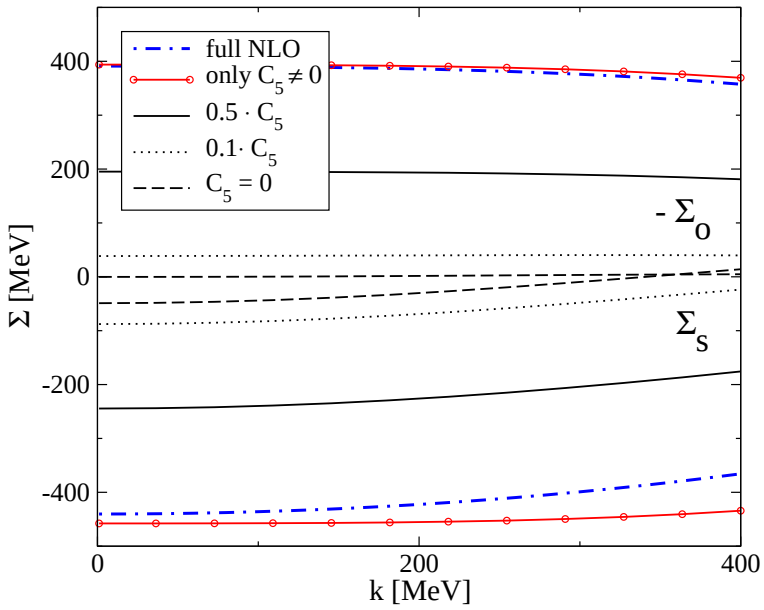

Figure 5.8: *Influence of the C_5 low energy constant. The figure compares the self-energies at NLO to those where all contacts except of C_5 are switched off and those results where the strength of the C_5 parameter is varied.*

by symbols. As one can see in Fig. 5.7 there is a qualitative agreement between the LECs obtained from the phenomenological OBE potentials Bonn B and Nijm93, the high-precision potentials CD Bonn, Nijmegen I/II and Argonne v_{18} and those from chiral EFT. Note that the last three spectroscopic LECs $C_{^3P_0}$, $C_{^3P_1}$ and $C_{^3P_2}$ in Fig. 5.7 which are connected to P-wave NN scattering determine the LEC C_5 in Eq. (5.13) which sets the strength of the spin-orbit force. The quantitative similarity of these extracted LECs to those from chiral EFT is in full agreement with the investigations of Kaiser [113] related to th LEC C_5. The striking similarity of the spectroscopic LECs shown in Fig. 5.7 allows to draw the conclusion that the contact part of the NN interaction does not depend on the type of parameterization of the short-distance physics [92]. Thus short-range physics described by heavy meson exchange in the OBE picture is encoded in the coefficients of the contact terms.

Fig. 5.8 analyzes the dependence of the fields on the value of the LEC C_5 in more detail. As already mentioned, at LO ($V_{\rm cont}^{(0)}$) two contact terms appear and at NLO ($V_{\rm cont}^{(2)}$) 7 contacts, respectively (Eq. (3.23)). The figure contains the full NLO result, including contributions from LO and NLO pion dynamics and contacts and compares this to the case where all contacts which appear up to NLO were switched off except of the C_5 contribution. It contains in addition

results with again all contributions, however, scaling the value of C_5 down to 50%, 10% and 0.1%. It becomes evident that the large scalar and vector mean fields are a direct consequence of the large value of C_5 connected to the spin-orbit force in the interaction. Chiral EFT is therefore not only in qualitative but quantitative agreement with the picture known from meson-exchange. In both cases the fields are related to short-distance physics and their strength is dictated by P-wave NN scattering data where the spin-orbit forces occur.

Now one is able to build the bridge between chiral EFT, OBE *and* phenomenological potentials. The agreement between the generation mechanism of the large fields in chiral EFT and OBE potentials (fields are related to short-range spin-orbit force connected to σ and ω meson exchange) is not accidental but reflected in the results found by Epelbaum et al. [92] and Kaiser [113]. Moreover the agreement of the LECs between chiral EFT and the various phenomenological potentials [92] shows that the appearance of large scalar and vector fields which has been proven to be a model independent fact, see Section 5.1.1, is indeed intimately connected to the structure of the short-distance physics of the NN interaction (especially to the spin-orbit force). The corresponding contributions have been found to be comparable for all potentials when represented as a sum of local four-nucleon contact operators [92].

A comparison of the Lorentz invariant amplitudes of all potentials revealed a remarkable agreement. This also holds for the Lorentz invariant amplitudes connected to the short-range physics encoded in the NN potentials and confirms moreover that the short-distance part of the NN interaction does not depend on the type of parameterization. Different approaches of describing the short-range part, e.g. contact interactions (chiral EFT), heavy boson exchange (OBE), or simple phenomenological fitting with a general operator set (Argonne v_{18}) reveal the same intrinsic relativistic structure. In terms of the expansion performed in [92] one obtains coefficients of similar strength which supports the universality of the present findings.

5.3. Self-consistency at Hartree-Fock

All calculations shown up to now have been performed in Hartree-Fock approximation at tree level. Nevertheless it is a well known fact that a realistic description of nuclear dynamics requires correlations beyond Hartree-Fock as well as higher order density dependences in relativistic approaches. Short-range correlations are known to be essential for nuclear binding whenever realistic interactions are used. This leads in lowest order of the Brueckner hole-line expansion to the ladder approximation of the Bethe-Goldstone equation for the in-medium G-matrix [32], or the Bethe-Salpeter equation (2.41) in the relativistic case [33].

In Hartree-Fock matter turns out to be unbound, in particular when high precision potentials with a relatively strong repulsive hard core are applied, e.g. OBE type potentials or Argonne v_{18}. The situation is qualitatively different for low momentum interactions ($V_{\text{low k}}$, Idaho N^{3}LO) where the hard core is strongly suppressed by the high momentum cut-offs. For these interactions isospin saturated nuclear matter collapses and Brueckner ladder correlations do not improve on this situation [48]. Here the matter has to be stabilized by the inclusion of repulsive three-body-forces [100]. Doing so, there appears a strong cut-off dependence at tree-level which can be removed when the second order term of the Brueckner perturbation series is added. $V_{\text{low k}}$ in combination with three-body-forces does not require a full resummation of the ladder diagrams but can already be treated within second-order perturbation theory [100]. The nuclear saturation point calculated in this approach is denoted by a star in Fig. 2.3. As one can see it does not meet the empirical region of saturation. The authors assume that the reason for that is that the calculations are not complete at second-order in many-body perturbation theory and the result may be improved quantitatively by the inclusion of missing contributions [100].

In the present work we do not aim for a fully realistic description of the nuclear many-body problem but restrict the investigations to the Hartree-Fock level. The tree-level results discussed up to now are of leading order in density ρ. Higher order corrections in density are taken into account when the bare potential matrix elements are replaced by in-medium matrix elements $V \mapsto V^*$. As in Chapter 2.2 described such a treatment is well defined in a relativistic BHF approach. It means to evaluate the corresponding Feynman amplitudes describing nucleon-nucleon interaction (3.8) through an in-medium spinor basis $u^*_\lambda(k)$ (see Eq. (2.58)) where the nucleons are dressed by the self-energy. Such a treatment requires, however, a definite structure of the interaction which allows to evaluate corresponding in-medium amplitudes. It is therefore at present restricted to OBE-type potentials.

The dressing of the interaction through the self-energy leads automatically to a self-consistency problem. The higher order density dependences which are introduced by such a procedure are considered to be one of the essential reasons for the improved saturation behavior of relativistic DBHF compared to non-relativistic BHF. In the following the role of self-consistency at the Hartree-Fock level is studied.

The in-medium spinors of helicity λ are given by

$$u^*_\lambda(k) = \sqrt{\frac{\tilde{E}^* + \tilde{M}^*}{2\tilde{M}^*}} \begin{pmatrix} 1 \\ \frac{2\lambda|\mathbf{k}|}{\tilde{E}^* + \tilde{M}^*} \end{pmatrix} \chi_\lambda \tag{5.15}$$

where the kinetic energy follows from Eqs. (2.62) and (2.63)

$$\tilde{k}_0^* = \tilde{E}^* = \frac{E^*}{1+\Sigma_\mathrm{v}} = \sqrt{\mathbf{k}^2 + \tilde{M}^{*2}}\ . \tag{5.16}$$

Thus the effective mass $\tilde{M}^*$ introduces a density dependence into the interaction. The effective mass is, however, in general not only density but also momentum dependent. Based on the observation that this explicit momentum dependence is moderate, it is usually neglected and $\tilde{M}^*$ is fixed at the reference point $|\mathbf{k}| = k_F$. In the so-called *reference spectrum approximation* (see Section 2.2.2) the reduced effective mass $\tilde{M}_F^* = \tilde{M}^*(|\mathbf{k}| = k_F, k_F)$ serves as an iteration parameter. $\tilde{M}^*$ is then the solution of the non-linear equation

$$\tilde{M}^* = M + \Sigma_\mathrm{s}(k_F, \tilde{M}^*) - \tilde{M}^*\Sigma_\mathrm{v}(k_F, \tilde{M}^*) \tag{5.17}$$

which follows from the definition of the reduced effective mass (2.62). Self-consistency is now achieved by determining for a given start value of $\tilde{M}^*$ the in-medium matrix elements $V^{JS}_{L',L}(\mathbf{q}', \mathbf{q})$. Therefore the Lorentz invariant amplitudes $F^\mathrm{I}_m(|\mathbf{q}|, \theta)$ and $g^\mathrm{I}_m(|\mathbf{q}|, \theta)$, Eqs. (4.14) and (4.17), as well as the transformation matrix C_{im} of Eq. (4.16) depend on $\tilde{M}^*$ and the Fermi momentum k_F since the plane-wave helicity states $|\lambda_1\lambda_2\,\mathbf{q}\rangle$ of Eq. (4.15) are now medium-dependent (5.15). The next step is to compute the self-energy components Σ_s, Σ_0 and $\mathbf{k}\Sigma_\mathrm{v}$ (Section 5.1). Since the Dirac propagator (5.3) describes dressed quasi-particles now, also in (5.5), (5.6) and (5.7) the mass M and energy E have to be replaced by the effective quantities $\tilde{M}^*$, $\tilde{E}^*$. Finally the new $\tilde{M}^*$ is determined. This iteration procedure is repeated until convergence is reached.

In Fig. 5.9 the results for the self-consistently calculated self-energy components Σ_s and Σ_0 for Bonn A, Nijm 93 and Nijmegen I are shown as a function of the Fermi momentum k_F compared to the tree level results from Fig. 5.3. For the Bonn A case the result of a full self-consistent DBHF calculation is shown as well taken from [36]. From this figure two features can be observed: the higher order density dependences which are introduced by the dressing of the potential affect mainly the scalar part of the self-energy for all three potentials. The modification of Σ_0 is moderate while Σ_s is significantly reduced. The short range ladder correlations included in the full DBHF calculation (Bonn A) influence the self-energy in an opposite way. The deviations of Σ_s from the self-consistent HF result are rather small, however, the vector component gets now strongly suppressed. This fact is understandable since the ladder correlations prevent the two-nucleon wave functions from too strong overlap with the hard core. In OBE potentials the hard core is mainly mediated by vector ω-exchange and determines thus the vector self-energy component.

The next step in this work is now to study the influence of self-consistency on the EOS which is determined with the self-consistent Hartree-Fock self-energies.

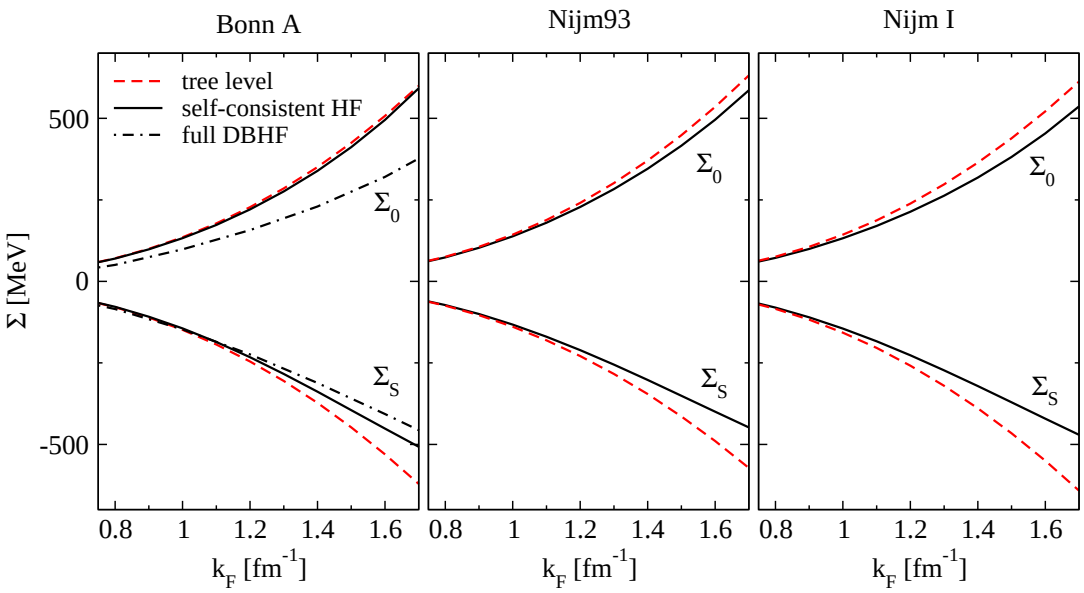

Figure 5.9: Comparison of the tree level scalar and vector self-energy components (dashed line) with self-consistent results (solid line). Additionally a full self-consistent DBHF calculation is shown in the first graph denoted by the dot-dashed line.

Like in DBHF the EOS, i.e., the energy per particle is defined as the kinetic plus half of the potential energy

$$\begin{aligned} \mathrm{E/A} &= \frac{1}{\rho}\sum_{\mathbf{k},\lambda} < \overline{u}^*_\lambda(\mathbf{k})|\boldsymbol{\gamma}\ \cdot\mathbf{k} + M + \frac{1}{2}\Sigma(k)|u^*_\lambda(\mathbf{k}) > \frac{\tilde{M}^*}{\tilde{E}^*} - M \qquad (5.18) \\ &= \frac{1}{\rho}\int_F \frac{d^3\mathbf{k}}{2\pi^3}\Big[((1+\Sigma_{\mathrm{v}}(|\mathbf{k}|))\tilde{E}^* - \Sigma^0(|\mathbf{k}|)) \\ &\qquad - \frac{1}{2\tilde{E}^*}(\Sigma_{\mathrm{s}}(|\mathbf{k}|)\tilde{M}^* - \Sigma_\mu(|\mathbf{k}|)\tilde{k}^{*\mu})\Big] - M \qquad (5.19) \end{aligned}$$

with the self-consistent spinors u^*_λ from Eq. (5.15).

In Fig. 5.10, the self-consistent Hartree-Fock results for the energy per particle in symmetric nuclear matter are shown for the Bonn A, Nijm93, Nijmegen I potentials as a function of the Fermi momentum k_F.

Also a non-self-consistent calculation is shown (dashed line) where the energy per particle is given by

$$\mathrm{E/A} = \frac{\kappa}{\rho}\int_F \frac{d^3\mathbf{k}}{(2\pi)^3}\left[\frac{k^2}{2M} + \frac{1}{2}U_{\mathrm{s.p.}}(k,k_{\mathrm{F}})\right] \qquad (5.20)$$

with $U_{\mathrm{s.p.}}(k,k_{\mathrm{F}})$ as defined in Eq. (5.12). The Fermi momentum k_F is connected

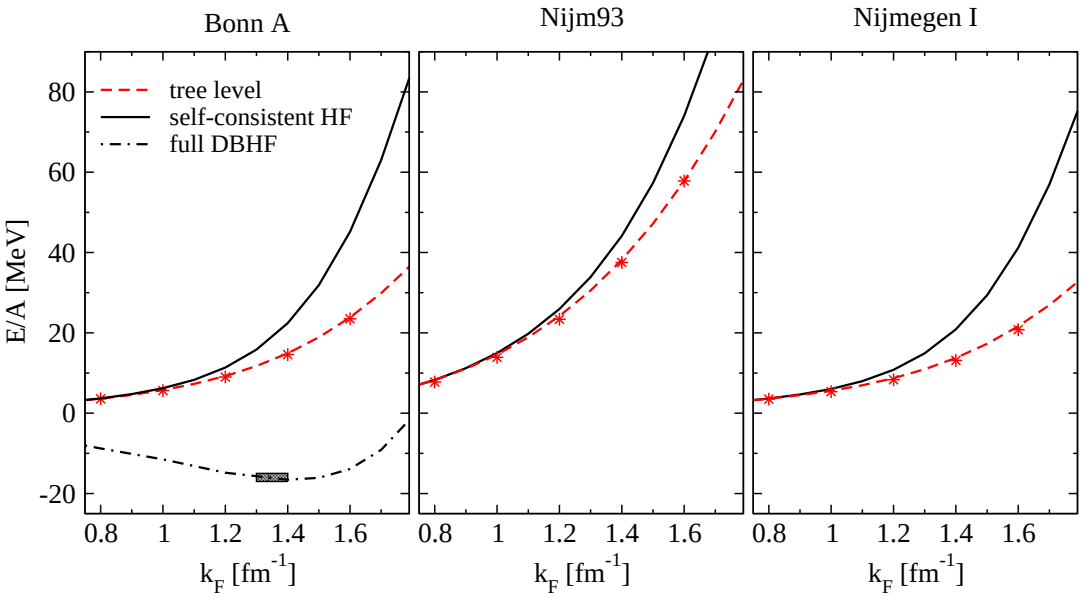

Figure 5.10: Hartree-Fock calculation of the nuclear equation of state, i.e., energy per particle E/A as a function of the Fermi momentum k_F for three different potentials. The dashed line indicates a tree level calculation and the solid line represents a self-consistent Hartree-Fock calculation, i.e., higher order corrections in density are included. A full self-consistent DBHF calculation denoted by the dot-dashed line with the Bonn A potential and the empirical region of saturation are shown in the first graph. The red stars show a non-relativistic Hartree-Fock calculation.

to the density $\rho = \kappa/(6\pi^2)k_F^3$ where κ is the isospin degeneracy, i.e. $\kappa = 4(2)$ for symmetric nuclear matter (pure neutron matter).

In this case one obtains the same result as in a non-relativistic Hartree-Fock calculation (denoted by stars in Fig. 5.10). The latter demonstrates again the numerical accuracy of the procedures.

For the Bonn A case again the EOS from the full DBHF calculations is shown as a reference [36]. It is clear that ladder correlations and other in-medium effects such as Pauli-blocking of intermediate states in the Bethe-Salpeter equation are responsible for nuclear saturation. The relatively moderate deviations from self-consistent Hartree-Fock at the scale of the self-energies in Fig. 5.9 are essential at the scale of the binding energy. Like in relativistic mean field theory of QHD subtle cancellation effects in the large scalar and vector fields are responsible for nuclear binding. The higher order density dependences introduced via the dressing of the bare interaction V lead to significantly more repulsion at the level of the EOS. This is a direct consequence of the reduced

attractive scalar field (see Fig. 5.9). Thus Fig. 5.10 serves also as a demonstration for the success of DBHF compared to BHF what concerns the quantitative description of nuclear saturation: In particular for modern high precision potentials such as Bonn, Nijmegen or Argonne v_{18} the BHF approach leads to strong over-binding and too high saturation densities. The additional repulsion introduced by higher order terms in density through the dressed potentials shifts the corresponding saturation points towards the empirical region [35, 112, 73]. It is important to note that the density dependence of the dressed potential V^* should not be mixed up with the density dependence of the G-matrix. The latter originates from the dressed two-nucleon propagator and the Pauli-operator in the Bethe-Goldstone (or Bethe-Salpeter) equations while V^* enters into the Bethe-Salpeter for iteration. In non-relativistic BHF [116] or variational calculations [117] a non-linear density dependence which improves the saturation behavior is usually introduced through net repulsive three-body-forces. In such a treatment the dependence on the third particle is integrated out such that one is left with an additional effective density dependent two-body force which acts in a similar way as a dressing of the two-body interaction. In this context one should mention that a dressing of the interaction has also more subtle consequences when iterated in the Bethe-Salpeter equation. It leads e.g. to a quenching of the second order OPE exchange [118, 119] which plays an essential role for saturation in non-relativistic approaches.

In summary, one could expect that a dressing of the interaction would allow to comply with weaker three-body forces which may in particular be of interest concerning the application of low momentum EFT potentials to the nuclear many-body problem. As the studies of Bogner et al. [100] have demonstrated, $V_{\text{low k}}$ requires rather strong three-body forces in order to stabilize nuclear matter. There the strength of the three-body contributions has already been pushed to its limits. Although a dressing of the interaction will probably not be possible for $V_{\text{low k}}$ due to the partially non-analytic structure of the potential, it may be a promising perspective for the application of other EFT potentials, e.g. the chiral N^{3}LO.

5.4. EOS in chiral EFT

In this section the properties of isospin symmetric nuclear and pure neutron matter in chiral EFT are investigated. For this purpose the Idaho N^{3}LO potential is applied where it is possible to determine the EOS order by order up to N^{3}LO. This has been done at tree level in Hartree-Fock approximation and in a second step within the non-relativistic Brueckner-Hartree-Fock approach. It is evident that Hartree-Fock calculations for nuclear matter are not very realistic. Nevertheless it is instructive to discuss the EOSs derived from chiral EFT at

the different orders in order to obtain a qualitative understanding of the properties of chiral EFT applied in many-body calculations. Moreover, the results presented in this section serve as a basis for the investigation of the pion mass dependence of the self-energy fields and the EOS of isospin symmetric nuclear matter where the same chiral EFT interaction is applied at NLO. The results are presented in the subsequent section.

For the determination of the tree-level EOS in Hartree-Fock approximation again Eq. (5.20) is applied which corresponds to a non-relativistic calculation since relativistic effects like the dressing of the NN interaction by an effective nucleon mass is still not feasible for chiral EFT. It is a well known fact and has been also shown in the previous section that at Hartree-Fock level nuclear matter is normally unbound, in particular when high precision OBE type potentials are applied. The situation turns out to be qualitatively different for low momentum interactions like the Idaho N^3LO potential where the hard core is strongly suppressed by high momentum cut-offs. This is shown on the l.h.s. of Fig. 5.11 where the EOSs for isospin symmetric nuclear matter are displayed for the different orders from LO up to N^3LO. There appear large jumps in the EOS when going from LO up to N^3LO. As discussed in Section 5.2 and [62] the contact terms which generate the large attractive scalar and repulsive vector potentials arise at NLO. Contributions from higher order provide corrections to these potentials. These are moderate on the scale of the fields of several hundred MeV magnitude. However, due to the subtle cancellation between scalar attraction and vector repulsion such corrections may be large on the scale of the binding energy, i.e. several tenth of MeV. This behavior is exactly reflected in the EOSs shown in Fig. 5.11 which jump from unbound at NLO to over-bound at LO and N^2LO to loosely bound at N^3LO which is due to the high momentum cut-off suppressing the repulsive hard core.

On the right hand side of Fig. 5.11 the EOS for pure neutron matter are shown. (Note, that in the case of neutron matter for a given Fermi momentum k_F the neutron density is given by $\rho_n = k_F^3/3\pi^2$.) It is not surprising that large deviations at the different orders are also observed in the case of pure neutron matter. Nevertheless, at Hartree-Fock level neutron matter turns out to be unbound in chiral EFT for all orders up to N^3LO. This is in agreement with all existing realistic calculations of neutron matter [120, 121, 38, 39].

The present tree level calculations are again of course not realistic microscopic nuclear matter calculations which requires to perform a self-consistent summation of the Brueckner ladder diagrams [36, 38, 39]. The difference between a tree-level and a full relativistic Brueckner calculation on the level of the nuclear self-energies has been discussed in Section 5.1.2. Moreover, a comparison of a tree-level calculation and a fully self-consistent DBHF calculation of the nuclear EOS has been shown in Section 5.3 in Fig. 5.10 using the Bonn A potential. Nuclear saturation is only obtained when short-range correlations and Pauli-

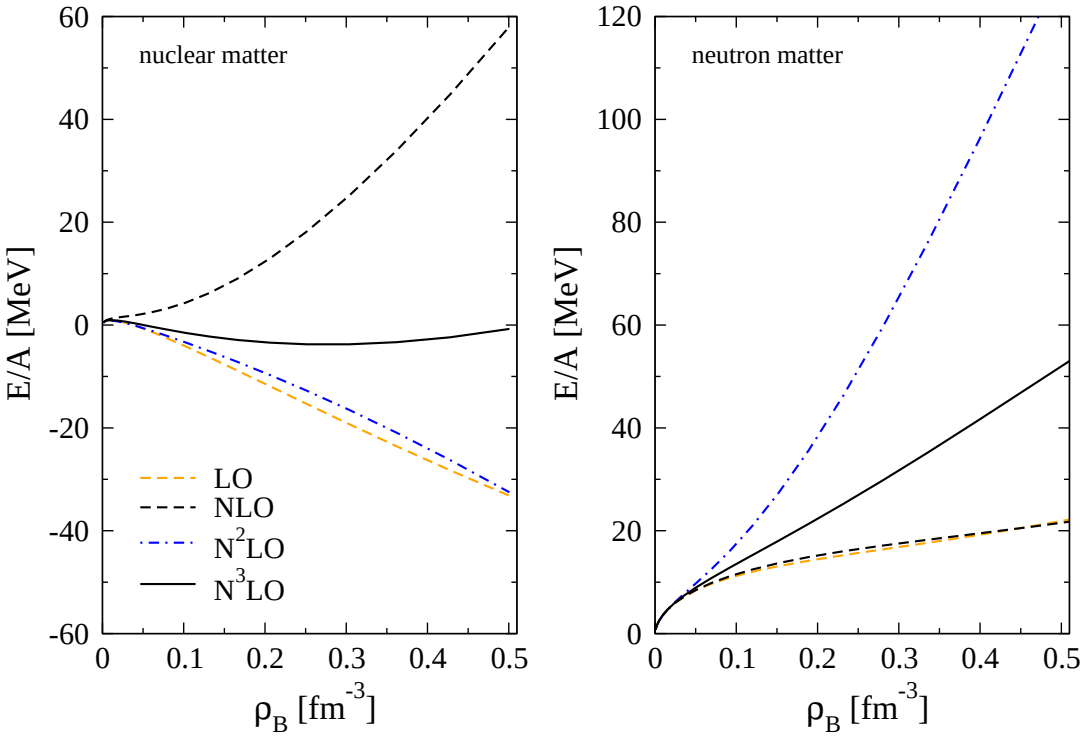

Figure 5.11: *Hartree-Fock calculation of the energy per particle E/A as a function of the baryon density ρ_B order by order up to N^{3}LO for symmetric nuclear matter (left) and for pure neutron matter (right).*

blocking are introduced. As already mentioned it is not possible to solve the full Brueckner ladder within the relativistic DBHF framework for chiral EFT since the latter is not a covariantly formulated potential. Therefore in contrast to the previous results shown in Fig. 5.10 we apply the non-relativistic BHF approach[3].

Relativistic Brueckner theory has been outlined in detail in Section 2.2. Here shortly the basic, and analogous, features of the non-relativistic approach are sketched. Corresponding to the relativistic Bethe-Salpeter equation (2.41) or (2.46) the central equation in the BHF approach is the so called Bethe-Goldstone equation

$$\langle k_1 k_2|G(\omega)|k_3 k_4\rangle = \langle k_1 k_2|V|k_3 k_4\rangle + \sum_{k_3' k_4'} \langle k_1 k_2|V|k_3' k_4'\rangle \frac{Q(k_3', k_4')}{\omega - \epsilon(k_3') - \epsilon(k_4')} \langle k_3' k_4'|G(\omega)|k_3 k_4\rangle \quad (5.21)$$

[3]For the numerical calculation again the BHF-code provided by H. Müther has been used. Partial waves up to $J = 9$ have been taken into account and for angular momenta larger than 6 the Born approximation has been used.

where ω is the starting energy and V is the bare NN interaction. The function appearing in the kernel of Eq. (5.21) is the so-called Pauli operator $Q(k,k') = (1-\Theta_F(k))\,(1-\Theta_F(k'))$ where $\Theta_F(k) = 1$ for $k < k_F$ and zero otherwise which forces the intermediate momenta to lie outside of the Fermi sphere. The single particle energies $\epsilon(k)$ are given by

$$\epsilon(k) = \frac{q^2}{2M} + U(k)\,. \tag{5.22}$$

The single particle potential is determined by the self-consistent equation

$$U(k) = \sum_{k'<k_F} \langle kk'|G(\epsilon(k)+\epsilon(k'))|kk'\rangle \tag{5.23}$$

which is coupled with the equation for the G-matrix Eq. (5.21). In the present work the standard choice is applied, i.e. the energy spectrum of the intermediate two-particle state is chosen in such a way that the self-consistency requirement Eq. (5.22) is restricted to hole states $k < k_F$ and the free spectrum is kept for particle states above the Fermi surface $k > k_F$.

The energy per particle E/A is then obtained from the G-Matrix $G(\omega)$ corresponding to the equation

$$\mathrm{E/A} = \frac{\kappa}{\rho_B}\left[\sum_{k_1<k_F}\frac{k_1^2}{2M} + \frac{1}{2}\sum_{k_1,k_2<k_F}\langle k_1k_2|\,G[\epsilon(k_1)+\epsilon(k_2)]\,|k_3k_4\rangle_A\right] \tag{5.24}$$

where the subscript A means that the G-matrix has to be antisymmetrized. The density is denoted by $\rho_B = \kappa/(6\pi^2)k_F^3$. κ is the isospin degeneracy, i.e. $\kappa = 4(2)$ for symmetric nuclear matter (pure neutron matter).

This self-consistent set of equations (5.21)-(5.23) is then solved by an iteration procedure. The G-matrix is expanded in partial waves according to the two-particle states. In order to avoid coupling between different two-particle channels the calculation is simplified by averaging the two-particle energies $\epsilon_{k_3'} - \epsilon_{k_4'}$ in the denominator in Eq. (5.21) and the Pauli operator over the angle between the relative momentum $q = (k_3' - k_4')/2$ and the total momentum $P = k_3' + k_4'$. Due to this so-called angle average approximation which has been tested in Ref. [122] the Bethe-Goldstone Eq. (5.21) can be solved separately for each partial wave.

Usually it is assumed that the single particle potential $U(k)$ or equivalently the single particle energy $\epsilon(k)$ has an approximately quadratic dependence

$$\epsilon(k) \approx \frac{k^2}{2m_{nr}^*} + U \tag{5.25}$$

which represents a parameterization in terms of an effective mass m_{nr}^* and a constant potential U. That means that one has to calculate the potential at

each iteration step in a few points only and can then interpolate these obtained values. This has been also done in the present calculation.

The non-relativistic mass m^*_{nr} parameterizes the momentum dependence of the single particle potential and it is the result from a quadratic parameterization of the single particle spectrum. Hence, it is a measure of the nonlocality of the single particle potential U which can be due to nonlocalities in space, resulting in a momentum dependence, or in time, resulting in an energy dependence.

As discussed, e.g., by Frick et al. [123] the spatial nonlocalities of U are mainly generated by exchange Fock terms. Nonlocalities in time are generated by Brueckner ladder correlations (mainly short-range correlations) due to the scattering to intermediate states which are off-shell [42, 123].

As already mentioned the introduction of an effective mass is a common concept to characterize the quasi-particle properties of a particle inside a strongly interacting medium. It is also well established that the effective nucleon mass in nuclear matter deviates substantially from its vacuum value [40, 41, 42]. However, the effective nucleon mass is defined in different ways depending on the physical approach and therefore should not be mixed up.

In contrast to the non-relativistic effective mass m^*_{nr} the relativistic counterpart is the Dirac mass M^*_D which has been already defined in the framework of relativistic mean field theory, Section 2.1.3, or in the DBHF approach described in Section 2.2, respectively. As one can see from Eq. (2.21) in combination with Eq. (2.25) or from Eq. (2.55) the relativistic effective nucleon mass is given by the real part of the scalar self-energy Σ_s in the Dirac field equation which is absorbed into the effective mass $M^*_D = M + Re\,\Sigma_s(k, k_\mathrm{F})$. Taking only the real part of the self-energy, which in general is complex, means to treat the nucleons as quasiparticles. The resulting effective nucleon mass is a smooth function of momentum and follows naturally from the presence of the medium in relativistic approaches.

Although related, one has to be careful when relativistic and non-relativistic approaches are compared on the basis of effective masses because of the different definitions. While the Dirac mass M^*_D is a genuine relativistic quantity the non-relativistic mass m^*_{NR} can be determined from both, relativistic as well as non-relativistic approaches. A detailed discussion of these two definitions of the effective mass can be found in [124]. There the momentum and isospin dependence of the effective nucleon masses in symmetric and asymmetric nuclear matter have been studied comparing the Dirac mass M^*_D and the non-relativistic mass m^*_{NR}. Both were calculated within the DBHF approach.

Fig. 5.12 shows the results for the Brueckner-Hartree-Fock binding energy as a function of the baryon density ρ_B for the orders NLO and N^{3}LO for nuclear and neutron matter[4]. The empirical saturation point of symmetric nuclear matter is

[4] A BHF calculation at the chiral order N^{2}LO turned out to be unworkably due to numerical

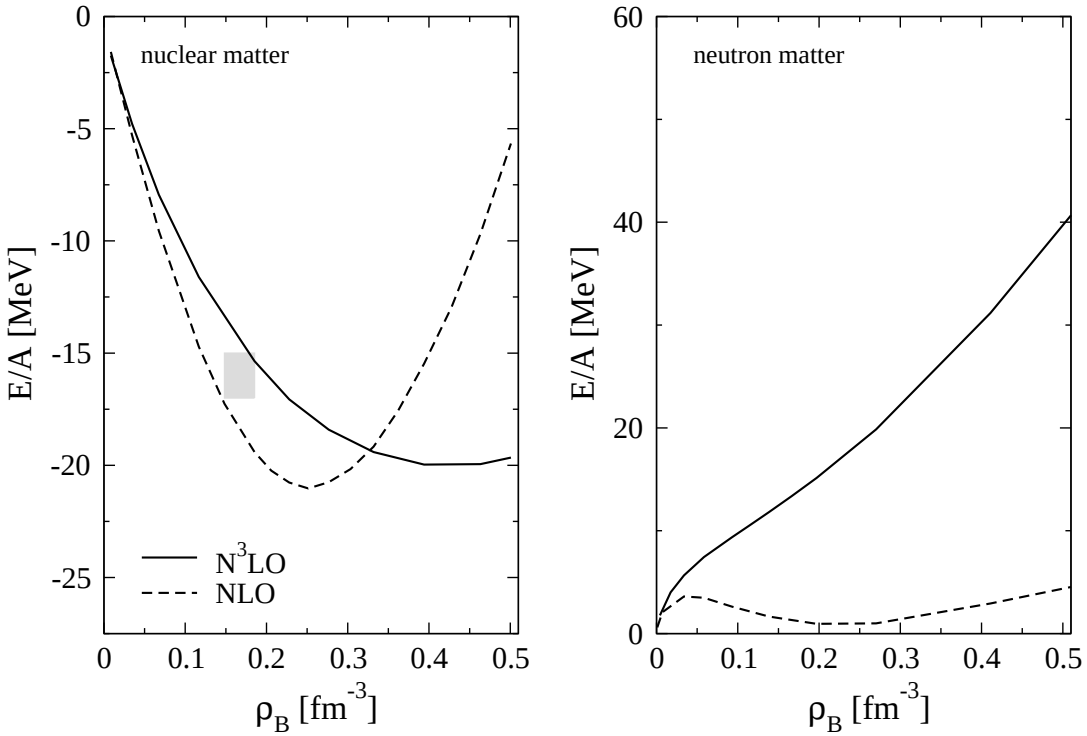

Figure 5.12: *The energy per particle E/A determined within the Brueckner-Hartree-Fock approach at the chiral orders NLO and N^{3}LO for symmetric nuclear matter (left) and for pure neutron matter (right). The empirical region of saturation is indicated by the grey area.*

indicated by the shaded area. Symmetric nuclear matter appears to be bound at NLO and N^{3}LO . At NLO one observes a clear saturating behavior of the EOS. The binding energy as well as the saturation density are overestimated when compared to the empirical values. The binding energy at the saturation point is $E/A = -21$ MeV and the corresponding equilibrium density is $\rho_0 = 0.25$ fm^{-3}.

At N^{3}LO the situation is different. In Hartree-Fock approximation symmetric nuclear matter is almost unbound at N^{3}LO indicated by the solid line in Fig. 5.11. In the Brueckner-Hartree-Fock approach short range correlations lead to a considerable over-binding and the EOS stabilizes at unrealistic high densities. Although the N^{3}LO potential reproduces the empirical phase shifts with high accuracy the suppression of the hard core by high-momentum cutoffs leads too much attraction. However, chiral EFT at NLO reproduces the empirical NN phase shifts with very poor quality [19]. This also true for the most important $^1S_0$, $^3S_0$ and $^3P_1$, $^3P_2$ phase shifts contributing to the energy

problems. Nevertheless the EOS at this order seems to be unbound.

per particle in our calculation. Therefore, in order to obtain a reliable EOS one has to apply chiral EFT at order N^{3}LO. Since the chiral NN potential is based on a low-momentum expansion high-momentum cut-offs have to be introduced. The latter suppress the repulsive short-range part of the NN interaction. It was shown that using low-momentum interactions (chiral EFT, $V_{\text{low k}}$) repulsive three-body forces have to be included since the latter are essential in order to obtain saturation in a perturbative scheme [100].

The inclusion of three-body forces is beyond the scope of the present thesis. Moreover, we work with the lowest-order Brueckner-Hartree-Fock method which does not allow to perform highly competitive calculations of the EOS:

- It is a well known fact that BHF theory is able to produce saturation due to short-range correlations but fails to reproduce the empirical region of saturation quantitatively. This is true for all realistic and high-precision NN potentials.

- Approximations like the angle-averaged Pauli operator, ambiguities in the choice of the particle state spectrum in the Bethe-Goldstone equation (5.21) introduce additional uncertainties [122]. As already mentioned the self-consistent single particle potential $\epsilon(k)$ Eq. (5.23) depends strongly on the momentum. In order to simplify the calculations the single particle energies $\epsilon(k)$ are parameterized with a parabola (see Eq. (5.25)). This parabolic approximation, which has been also used in our calculations, introduces an uncertainty of about 1-2 MeV around saturation density [125].

Nevertheless the main features known to be essential for nuclear saturation in BHF theory are included: the tensor force coming from second-order (iterated) OPE and its interplay with Pauli blocking.

Recently, the EOS has been also calculated by the Bonn group [126] by applying the NLO version of their chiral NN potential [17] to symmetric nuclear matter. This has been done by modifying the vacuum two-nucleon interaction by Pauli blocking effects. The binding energy is then obtained by summing all two-nucleon irreducible diagrams as it is done in Brueckner-Hartree-Fock theory. Also in [126] nuclear saturation is found in chiral EFT at NLO. The binding energy is larger ($E/A = -17.8$ MeV) than in the present calculation and also the corresponding saturation density $\rho_0 = 0.28$ fm^{-3} is somewhat larger than in the present case ($\rho_0 = 0.25$ fm^{-3}). In both cases ρ_0 is significantly overestimated with respect to the empirical saturation region.

As discussed in [126] the saturation curve depends crucially on the choice of the cut-off parameter $\tilde{\Lambda}$ which is introduced in the spectral function representation of the two-pion exchange diagrams [17]. The authors conclude, that saturation is entirely due to the regulators $\tilde{\Lambda}$ and Λ (see Eq. (3.26)) since no three-body forces are included in the calculation at NLO. These were found

to be essential in order to obtain saturation in a perturbative scheme [100]. The same has also been observed in the chiral approach of Kaiser et al. [127] where the inclusion of three-body effects from TPE with excitations of virtual $\Delta(1232)$-isobars has been found essential in order to obtain saturation. However, the contributions of the three-body effects are attractive in [127] whereas in Ref. [100] the contributions from three-body forces in a Hartree-Fock calculation with the low-momentum interaction $V_{\text{low k}}$ lead to additional repulsion.

In this thesis the Idaho NN potential [19] is applied where Entem and Machleidt calculated the contributions from chiral two-pion exchange for $\tilde{\Lambda} = \infty$ expressing the corresponding contributions in terms of the loop functions $L^{\infty}(q)$ and $A^{\infty}(q)$ [18]. Therefore in the chiral Idaho potential used in the present calculation only the Lippman-Schwinger regulator Λ occurs which is also likely to influence the shape of the EOS in a similar way as the spectral regulator $\tilde{\Lambda}$ in the calculations of [126].

Nuclear matter has been also investigated by the Munich group [128, 129, 130] based on a systematic chiral approach known as in-medium chiral perturbation theory. In this approach the methods of effective field theory (chiral perturbation theory) already applied successfully to describe the NN interaction in vacuum [131, 132, 133, 134] are used to describe nuclear systems at finite density.

In effective field theories a power counting scheme has to be found relying on a separation of short and long distance physics. In nuclear matter the relevant momentum scale is given by the Fermi momentum k_F. At the empirical saturation density $k_{F0} \approx 2m_\pi$, i.e., the Fermi momentum k_F and the pion mass m_π are of comparable magnitude implying that pions should be included as explicit degrees of freedom. Since both k_F and m_π are small compared to the chiral scale $4\pi f_\pi \approx 1.2$ GeV, consequently the EOS is represented as an expansion in powers of k_F where the expansion coefficients are non-trivial functions of the dimensionless ratio of the two relevant scales k_F/m_π in this problem. Another important element to perform finite density calculations is the in-medium nucleon propagator replacing the vacuum one [130].

In this chiral approach OPE, iterated OPE and irreducible TPE up to three-loop order in the energy density have been included in the calculation of the EOS [128]. The short-range physics, which cannot be resolved in an effective low-energy theory is parameterized by a momentum-space cut-off Λ. The cut-off Λ stems from the regularization of divergent parts connected with chiral two-pion exchange and the contribution to the energy per particle corresponds to that of a zero-range contact NN interaction. Therefore Λ sets the strength of it. Adjusting Λ the empirical saturation point can be reproduced in contrast to our NLO calculation where no free parameters occur. It is clear that the saturation properties strongly depend on the cut-off Λ which is the only free parameter in the approach of [128]. Again the main reason for saturation is Pauli blocking in

second-order (iterated) OPE [128, 127].

In contrast to our calculation and that of the Bonn group [126] which are based on the same chiral expansion of the NN interaction the chiral field theory in [128] is developed to be applied exclusively in nuclear matter, i.e. without a direct link to the NN interaction in vacuum. Nevertheless, since the same pion exchange diagrams are considered in [128] the approaches are comparable to some extent.

Our calculation agrees with the result of the Bonn group [126] (and that of [128]) concerning the fact that chiral EFT exhibits saturation at NLO. However, it is not clear whether at order N^{2}LO where three-body forces appear in the chiral expansion a quantitative improvement can be expected. Though it was only possible to obtain the Brueckner-Hartree-Fock EOS at order N^{2}LO at low densities due to numerical difficulties, the tendency is, however, that the EOS is unbound at N^{2}LO. This jumping behavior was already observed at the Hartree-Fock level, see Fig. 5.11.

Fig. 5.12 shows also the energy per particle for pure neutron matter for the orders NLO and N^{3}LO calculated within the BHF approach. At NLO the EOS shows unrealistic properties since it stays quite constant over the considered density range at a value of $\approx 3 - 4$ MeV. Nevertheless neutron matter at NLO appears to be unbound. This can already be seen from the Hartree-Fock calculation where the NLO EOS is considerably softer than that at the order N^{3}LO. As in the case of symmetric nuclear matter iterating the full Brueckner ladder leads to more attraction bending the Hartree-Fock EOS downwards.

An improved behavior is observed at N^{3}LO where the neutron matter EOS is also unbound with the energy per particle rising approximately monotonical which is in agreement with most of the state-of-the-art many-body calculations [38, 39, 117].

Fig. 5.13 shows an overview of the EOSs obtained in our BHF calculations with the chiral interaction [19] at the orders NLO and N^{3}LO (already shown in Fig. 5.12) and the phenomenological high precision Argonne v_{18} potential in nuclear matter and neutron matter. These are compared to the results from other approaches: DBHF [36] with the Bonn A potential and a variational calculation [117] based also on the Argonne v_{18} potential. Additionally a BHF calculation with the low-momentum interaction $V_{\mathrm{low\ k}}$ is shown.

As already mentioned in Section 4.3.1 empirical NN scattering data constrain the interaction up to about 400 MeV, corresponding to the pion threshold. Therefore NN interaction models differ in the description of the short-range part. In the framework of EFT the unresolved short-range part is replaced by contact terms. In the case of chiral EFT which is only valid at low momenta high-momentum cut-offs lead to a strong over-binding as can be seen from the EOS at N^{3}LO. This effect becomes even more drastic in the case of the $V_{\mathrm{low\ k}}$ potential. This potential is obtained from any given realistic NN potential

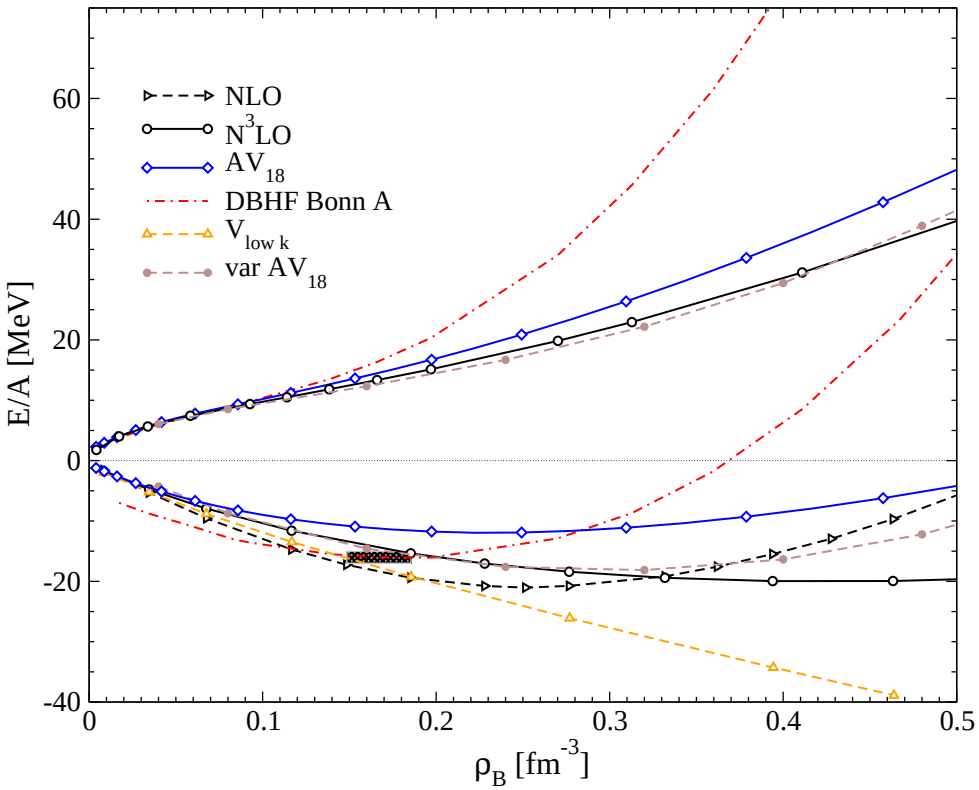

Figure 5.13: *The energy per particle E/A in nuclear matter and neutron matter. The BHF results (open symbols) obtained at NLO/N^{3}LO of the chiral interaction and from the Argonne v_{18} potential are compared to DBHF and variational calculations. The empirical region of saturation is indicated by the shaded area.*

by integrating out the high-momentum modes with the help of RG methods. At a cut-off of $\lambda \approx 2$ fm^{-1} all potentials are found to collapse to the model-independent low-momentum interaction $V_{\text{low k}}$. As one can see in Fig. 5.13 the EOS obtained with $V_{\text{low k}}$ in a BHF calculation collapses considerably faster than the N^{3}LO calculation. This is already the case at Hartree-Fock level [48, 100]. As already mentioned the repulsion generated by three-body forces which appear at N^{2}LO turned out to be essential to stabilize nuclear matter and to obtain reasonable saturation properties with the $V_{\text{low k}}$ potential [100]. However, as can be seen from Fig. 2.3, even with the inclusion of three-body forces the corresponding $V_{\text{low k}}$ saturation point is still relatively far from the empirical value. The inclusion of three-body forces is beyond the scope of the present work, in particular what concerns the pion mass dependence, but for a quantitative determination of the EFT EOS they should be included. In the case of chiral

EFT one has to keep in mind, that the latter provides a systematic expansion of the nuclear force, i.e. besides two-body forces also three-body forces are generated on an equal footing. However, due to the restricted region of validity of the chiral expansion (ensured by high-momentum cut-offs) chiral EFT is essentially applicable at moderate densities.

At moderate densities the variational calculation [117] agrees well with the N^{3}LO EOS in the case of nuclear matter. At densities above $\rho_B > 0.3$ fm^{-1} the repulsive short-range part of the Argonne v_{18} potential leads to a stiffer EOS. For neutron matter one observes a surprisingly good agreement over the displayed density range. This seems to be somewhat accidental since the EOS from our BHF calculation with Argonne v_{18} deviates in the case of symmetric nuclear matter and neutron matter, respectively. In both cases the EOS obtained from Argonne v_{18} appears to be stiffer than that from chiral EFT at N^{3}LO.

It is a well known fact that non-relativistic many-body calculations fail to reproduce nuclear matter saturation quantitatively [135]. This can be also seen from the present BHF calculations with chiral EFT at N^{3}LO and the Argonne v_{18} potential as well as from the variational calculation [117] displayed in Fig. 5.12.

Therefore the effect of three-body forces has been studied in both approaches, i.e. within non-relativistic BHF [135] and variational calculations [117]. The BHF calculation [135] as well as the variational calculation [117] are based on the Argonne v_{18} potential. It was found that the contributions from three-body forces are in total repulsive in the variational calculation [117] and in the BHF approach [135]. This leads to a stiffer EOS where the non-relativistic calculations come closer to their relativistic counterparts like the DBHF results shown in Fig. 5.13. The three-body forces applied in both cases are phenomenological, where the Tucson-Melbourne three-body force is used in [135] and the Urbana IX three-body force in [117].

It is often argued that in non-relativistic treatments three-body forces yield an equivalent effect as the dressing of the two-body interaction by in-medium spinors in Dirac phenomenology which has been described in Section 2.2. Both mechanisms lead essentially to an effective density dependent two-body interaction V which is naturally of different origin. One class of three-body forces contains virtual excitations of nucleon-antinucleon pairs which are already present in the relativistic BHF approach. These Z-graphs are in total repulsive and can be considered as a renormalization of the meson vertices and propagators. In DBHF the representation of nucleons by Dirac spinors with an effective mass M_D^* on the other hand can be interpreted as considering also virtual nucleon-antinucleon excitations effectively.

This again implies that a dressing of the chiral EFT interaction might be a promising perspective in order to create a harder EOS and finally 'realistic' EOS since three-body forces are already included in the systematic chiral expansion.

5.4.1. Symmetry energy from chiral EFT

Having the EOSs for symmetric and pure neutron matter the symmetry energy E_{sym} can be investigated which shows the isospin dependence of the chiral EFT interaction. In isospin asymmetric matter the binding energy E_B is a functional of the proton and neutron densities described by the asymmetry parameter $\beta = Y_n - Y_p$, i.e. the difference between the neutron fraction $Y_n = \rho_n/\rho_B$ and the proton fraction $Y_p = \rho_p/\rho_B$. Performing an expansion in terms of the asymmetry parameter β the isospin dependent part of the energy functional can be separated from that of symmetric matter

$$E_B(\rho_B, \beta) = E_B(\rho_B) + E_{\mathrm{sym}}\ \beta^2 + \mathcal{O}(\beta^4) + \cdots \tag{5.26}$$

where the symmetry energy is

$$E_{\mathrm{sym}} = \frac{1}{2}\left[\frac{\partial^2 E_B(\rho_B, \beta)}{\partial \beta^2}\right]_{\beta=0} \quad . \tag{5.27}$$

Since the binding energy shows an approximately quadratic dependence on the asymmetry parameter, the symmetry energy can be evaluated equivalently as the difference of the two extreme cases of neutron matter ($\beta = 1$) and symmetric nuclear matter ($\beta = 0$)

$$E_{\mathrm{sym}} = E_B(\rho_B, \beta = 1) - E_B(\rho_B, \beta = 0) \ . \tag{5.28}$$

Fig. 5.14 compares the symmetry energy E_{sym} obtained in our BHF calculation with the chiral interaction at the orders NLO and N^{3}LO and with the Argonne v_{18} potential to non-relativistic variational calculations [117] also with the Argonne v_{18} potential. The first variational calculation of the symmetry energy corresponds to the EOSs already displayed in Fig. 5.13 and the second one contains contributions due to boost corrections (δv) accounting for relativistic kinematics and the inclusion of three-body forces (3-BF) [117]. Additionally the symmetry energy obtained within the DBHF approach using the Bonn A potential is displayed [36, 73].

The symmetry energy at NLO reaches its maximum at $\rho_B \approx 0.25$ which corresponds to the density of saturation ρ_0 as one can see from Fig. 5.12.

However, a declining behavior at densities above the saturation density is observed. Nevertheless this is in agreement with the chiral approach of Ref. [128] which shows the same characteristics. As already mentioned the latter has the same pion dynamics included as in the calculation presented in this thesis. In Chapter 4.3.1 the limits of chiral NN potentials have been discussed and in Ref. [111] it was estimated that chiral NN potentials can be used up to densities of about $\approx 4\rho_0$ where ρ_0 is the empirical saturation density. Therefore the characteristics of a decreasing symmetry energy E_{sym} for densities higher than

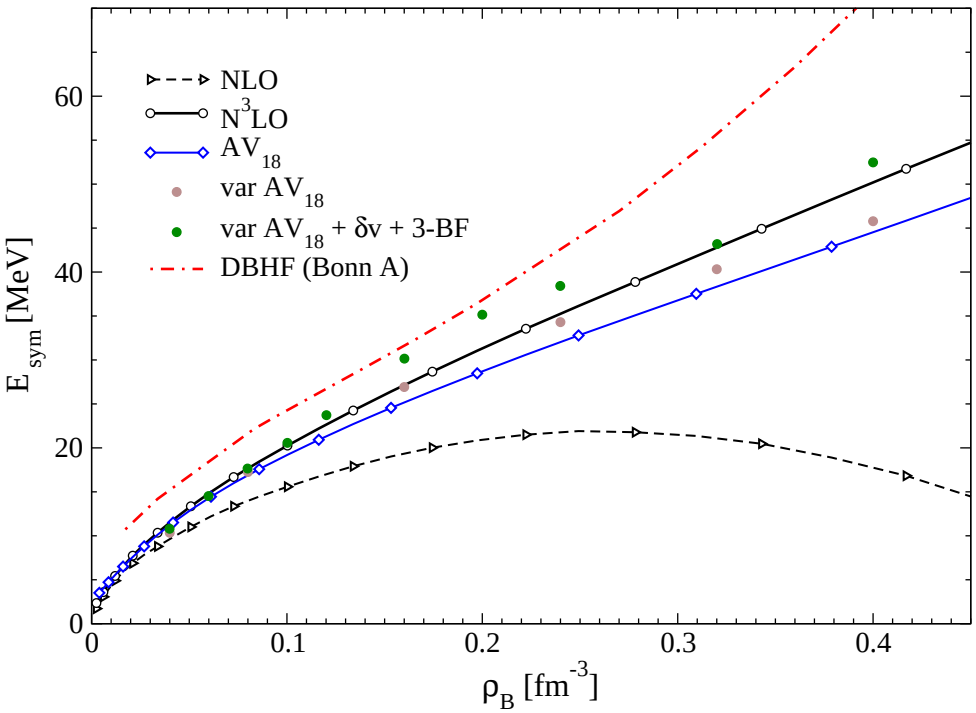

Figure 5.14: *Symmetry energy as a function of the baryon density as predicted by chiral EFT at the orders NLO and N^{3}LO in comparison with the result for the Argonne v_{18} potential obtained in the non-relativistic BHF approach (indicated by open symbols). Additionally the results from DBHF (Bonn A) and from variational calculations [117] are displayed.*

ρ_0 could be a natural behavior at order NLO even if one considers the estimation of Ref. [111] as a very optimistic one.

The N^{3}LO calculation on the other hand shows a raising symmetry energy which is in agreement with the result for the Argonne v_{18} potential, the predictions from DBHF (Bonn A) and the variational calculations [117]. The DBHF lies somewhat higher than our non-relativistic N^{3}LO calculation. The non-relativistic BHF result with the Argonne v_{18} and moreover the variational calculation [117] agree well with our N^{3}LO calculation. This shows on the one hand that the effect of the high-momentum cut-off λ drops out in the N^{3}LO calculation. On the other hand it shows that a high precision phenomenological potential as Argonne v_{18} and the QCD based chiral EFT potential lead to almost identical results for the nuclear many-body system when applied in comparable approximation schemes.

As already mentioned in the case of low-momentum NN interactions like chiral EFT or $V_{\mathrm{low\ k}}$ the inclusion of three-body forces is essential in order to stabilize

nuclear matter and to obtain reasonable saturation properties [100].

The inclusion of repulsive three-body forces in the variational calculations lead to EOSs for neutron and symmetric matter which are shifted in the same direction [117]. Since these three-body forces are only weakly isospin dependent, at least at moderate densities, the symmetry energy, i.e. the difference between these two extreme cases, is not strongly affected as can be seen from the comparison of the two variational results. This should be also true for chiral EFT.

5.5. Self-energy and EOS in the chiral limit

The purpose of the present part is to investigate the pion mass dependence of symmetric nuclear matter. Therefore the large attractive scalar and repulsive vector self-energy components as well as the nuclear EOS are analyzed in the chiral limit. This is done in Hartree-Fock approximation at tree level and in the non-relativistic BHF approach (introduced in the previous section) using the chiral EFT interaction derived by Epelbaum et al. [20]. In this NN interaction the explicit and implicit light quark mass dependence of the nuclear force is known up to NLO where additionally to the one-pion exchange potential and contact terms the leading two-pion exchange has been considered (see also Section 3.3.2). This allows consequently to investigate possible changes of the properties of symmetric nuclear matter up to this order.

The calculation of the self-energy components requires the knowledge of the pion mass dependence of the nucleon mass M since it enters the expressions for the self-energy and the EOS. Within the framework of chiral EFT the physical (vacuum) nucleon mass M can be expressed as

$$M = M_0 + \sigma_N \tag{5.29}$$

where M_0 is the value of the nucleon mass M in the chiral limit. The nucleon sigma term σ_N represents the contribution from explicit chiral symmetry breaking to the nucleon mass and determines the quark mass dependence of the nucleon mass

$$\sigma_N = \sum_{q=u,d} m_q \frac{dM}{dm_q} = m_\pi^2 \frac{dM}{dm_\pi^2} \tag{5.30}$$

which, through $m_\pi^2 \sim m_q$ translates into a dependence on the pion mass (see also Section 6.2). The chiral limit of the nucleon mass and of the sigma term, respectively, has been evaluated up to NNLO [136], where the corrections to the NLO dependence were, however, found to be small.

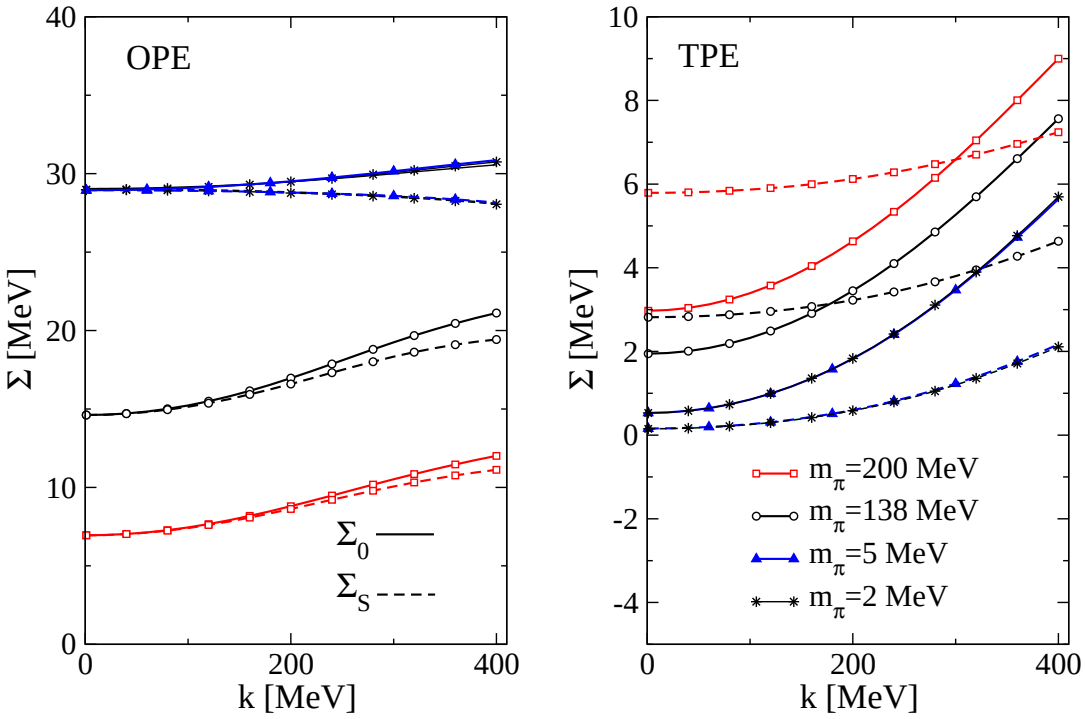

Figure 5.15: *The tree level scalar (dashed lines) and vector (full lines) self-energy components in matter at* $k_{\rm F} = 1.35$ fm^{-1} *are shown for different values of the pion mass* m_π*. The NLO one-pion exchange (left panel) and two-pion exchange (right panel) are shown. The one-pion exchange is obtained with* $\bar{d}_{16} = -1.23$ *and* $\bar{d}_{18} = -0.97$*.*

In order to be consistent with the NN interaction we account for the pion mass dependence of the nucleon mass M at NLO (expressions given in [136]) when the self-energy components and the EOS are studied in the chiral limit.

The analysis of the chiral EFT potential in Section 5.2 revealed that the large scalar and vector self-energy components are generated by contact terms which occur at NLO in the chiral expansion. These are four-nucleon contact terms with two derivatives which generate the short-range spin-orbit interaction. The strength of the corresponding low energy constants, in particular those connected to the spin-orbit force, is dictated by P-wave NN scattering data. Pion dynamics as well as LO and N^{3}LO contacts provide only corrections to the fields generated by the NLO contact terms. Thus one could expect that the quark mass dependence of the fields is mainly determined by the quark mass dependence of the contact terms which is moderate. However, before coming to the full self-energy, the contributions from one-pion exchange and two-pion exchange are discussed separately. Fig. 5.15 shows the scalar $\Sigma_{\rm s}$ and

vector Σ_0 self-energy components from the next-to-leading order OPE and TPE contributions at a Fermi momentum of $k_\mathrm{F} = 1.35$ fm^{-1} which corresponds to a nuclear density of $\rho_B = 0.166$ fm^{-3}. As a well known result, at the physical pion mass the scalar and vector self-energy components from the pseudo-vector OPE are of the same sign and of moderate strength. This is also true in the chiral limit. The self-energy components Σ_s, Σ_0 approach a constant value of about 30 MeV. For the not yet uniquely fixed LECs entering into the expression for the renormalized OPE the values $\bar{d}_{16} = -1.23$ and $\bar{d}_{18} = -0.97$ have been taken [20]. The uncertainty due to these LECs $\bar{d}_{16,18}$ does not significantly affect the scalar and vector fields. The same is true for the corresponding EOS (see below). This is, however, not the case what concerns the scalar quark condensate as discussed in detail in the following chapter.

The scalar Σ_s and vector Σ_0 self-energy components generated by the TPE are already small for the physical case ($m_\pi = 138$ MeV) and are further reduced by $\approx 2,5$ MeV in the chiral limit. At zero momentum both components almost vanish and show a slight increase with increasing momentum. As for the OPE the fields are repulsive and approach a constant value in the chiral limit.

Next the role of the contact terms will be considered. The contact terms connected to the LECs $C_{1...7}$, Eq. (3.30), do not depend on the pion mass at NLO. Since the magnitude of the scalar and vector self-energy components is mainly set by contact interactions connected to the spin-orbit force where the strength is proportional to the LEC C_5 in Eq. (3.30) the modification of the fields in the chiral limit can in total be expected to be moderate. The pion mass dependent part of the contact interactions, i.e., the first to lines in Eq. (3.30) provides only small contributions.

The uncertainties due to the not yet uniquely fixed LECs $\bar{d}_{16,18}$ entering the renormalized OPE (3.28) do not strongly affect the self-energy components. However, a second source of uncertainty appears in the the part of the contact interactions connected to the not known LECs $\bar{D}_{S,T}$ which depend on the pion mass. In Ref. [20] this range of uncertainty has been explored through an independent variation of the parameters $\alpha_{S,T}$ in Eq. (3.34) in the range of $-3.0 < \alpha_{S,T} < 3.0$. In Ref. [20] this rather wide variation of the LECs $\bar{D}_{S,T}$ was motivated by a wide range of possible parameter sets of NLO LECs fitted with different cut-off combinations. However, in the present case - using the Idaho chiral potential - one is restricted to one parameter set with a general cut-off of $\lambda = 500$ MeV. A variation of the LECs over a wide range is therefore likely to overestimate the uncertainty originating from the LECs $\bar{D}_{S,T}$. Therefore we restrict the present discussion of the self-energies to values $\alpha_{S,T} \approx 1$. Results turned out to be stable against a variation of α_S and α_T in the same direction, i.e. small deviations from combinations of $\alpha_{S,T}$ where both parameters are close to each other do practically not change the results. Nevertheless the range of the uncertainty is shown for the nuclear EOS which is presented in the last part

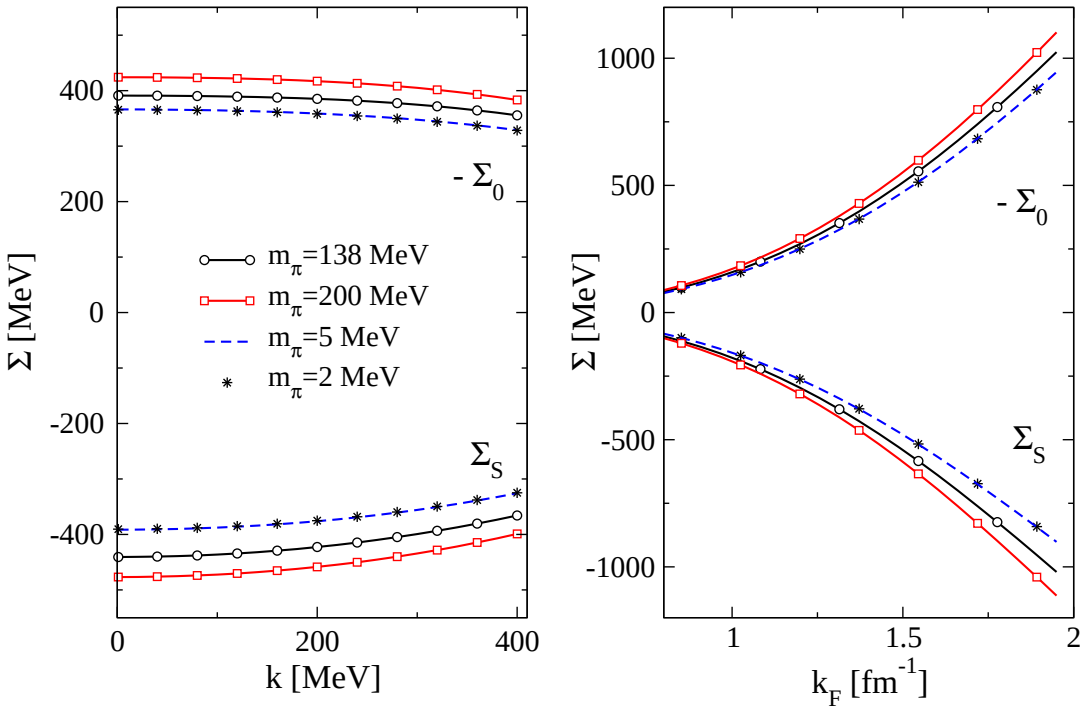

Figure 5.16: *Left: momentum dependence of the tree level scalar and vector self-energy components in nuclear matter at* $k_{\mathrm{F}} = 1.35$ fm^{-1} *evaluated for different values of the pion mass* m_π. *Right: tree level scalar and vector self-energy components in nuclear matter as a function of the Fermi momentum* k_{F} *for different values of the pion mass* m_π.

of this section.

In Fig. 5.16 the full tree-level self-energy components are now shown as a function of the momentum k. An approximately vanishing pion mass, i.e. $m_\pi = 2$ MeV and $m_\pi = 5$ MeV, leads to a small reduction of the repulsive vector field (≈ 30 MeV) and of the attractive scalar field (≈ 50 MeV), respectively. The same can be seen on the right hand side in Fig. 5.16 where the fields are shown as a function of the Fermi momentum k_{F}. An increase of the pion mass to $m_\pi = 200$ MeV leads to an opposite behavior.

In summary, a careful analysis of the chiral EFT NN interaction leads to large scalar and vector fields which essentially maintain their strength in the chiral limit, however, with the tendency of a slight decrease of absolute size.

In this context it is interesting to compare this behavior with the naive assumption of a dropping σ meson mass within the framework of Quantum-Hadron-Dynamics (QHD) [27]. In this case the scalar and vector fields are

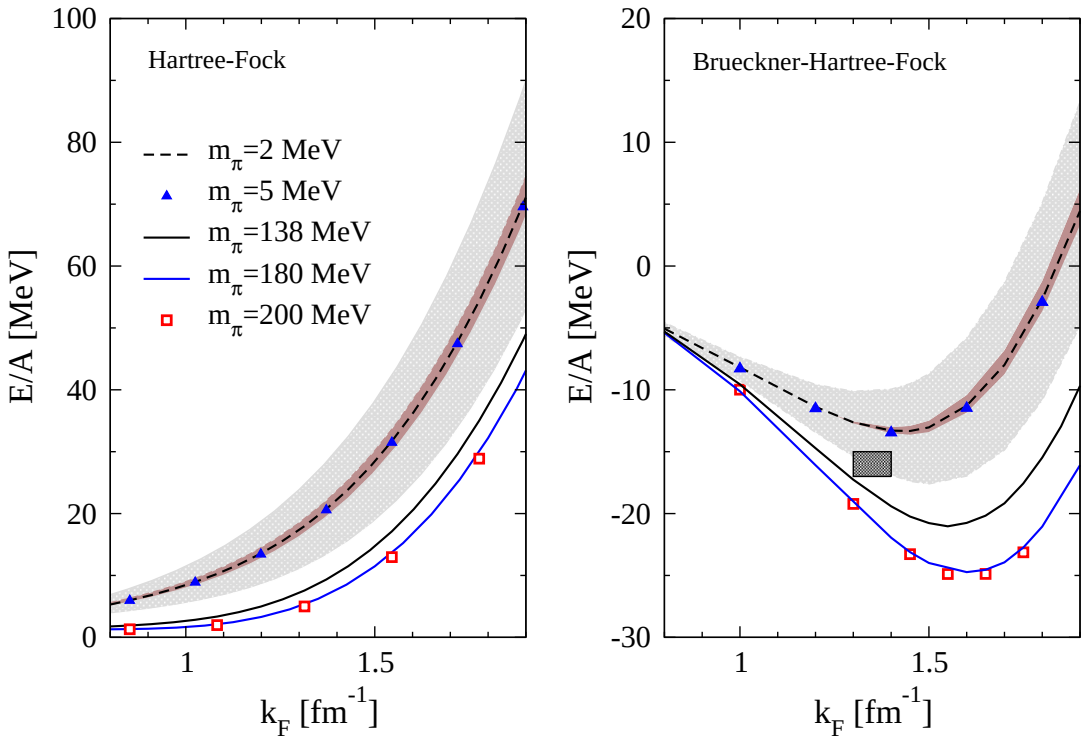

Figure 5.17: *Pion mass dependence of the nuclear equation of state E/A as a function of the Fermi momentum k_F. On the l.h.s. the Hartree-Fock calculations at NLO are shown for the physical case of $m_\pi = 138$ MeV compared to the case of $m_\pi = 2$ MeV, $m_\pi = 5$ MeV, $m_\pi = 180$ MeV and $m_\pi = 200$ MeV. On the r.h.s the Brueckner-Hartree-Fock results are shown. The brown shaded area denotes the uncertainty in the LEC $\bar{d}_{16}$ varied from $\bar{d}_{16} = -0.91$ GeV^{-2} to $\bar{d}_{16} = -1.76$ GeV^{-2}. The grey shaded area shows the overall uncertainty if one additionally takes into account the unknown LECs $\bar{D}_{S,T}$. The shaded square denotes the empirical region of nuclear saturation.*

inverse proportional to the masses of the σ and ω mesons

$$\Sigma_s = -\frac{g_\sigma^2}{m_\sigma^2}\rho_S \quad , \quad \Sigma_0 = +\frac{g_\omega^2}{m_\omega^2}\rho_B \tag{5.31}$$

where g_σ and g_ω are the corresponding meson-nucleon coupling constants and $\rho_S \sim \rho_B$ is the scalar nucleon density. The assumption of dropping σ and ω meson masses according to a naive Brown-Rho scaling [137] together with fairly constant couplings would lead to a strong increase of scalar and vector fields in size. Chiral EFT predicts the opposite behavior, namely slightly decreasing fields. Interpreting this result in terms of the simple QHD picture means that the ratio of coupling functions and meson masses in Eq. (5.31) has to stay fairly constant. Assuming dropping meson masses the coupling functions should show

the same density dependence. Such a scenario is not completely unrealistic since in the framework of density dependent relativistic mean field theory [138] where density dependent meson coupling functions $g^2_{\sigma,\omega}(\rho_B)$ are derived from the Brueckner G-matrix [139, 140] or fitted to finite nuclei [141, 142, 143], such a behavior is usually obtained.

It is clear that a rather small reduction of the scalar and vector fields has only moderate consequences for the EOS in Hartree-Fock approximation in the chiral limit. As it was shown in the previous chapter the tree-level EOSs for isospin symmetric nuclear matter calculated with the chiral EFT interaction show a wide variation depending on the chiral order. The EOSs jump from unbound at NLO to over-bound at LO and N^{2}LO to loosely bound at N^{3}LO. Therefore a NLO tree level Hartree-Fock calculation is of course not a realistic microscopic nuclear matter calculation but it allows a consistent investigation of the chiral limit at the order at which the pion mass dependence of the chiral NN potential has been derived.

How the change in the fields affects the nuclear EOS is depicted on the left hand-side in Fig. 5.17 which compares the EOS at NLO at the physical pion mass $m_\pi = 138$ MeV to that at $m_\pi = 180$ MeV, $m_\pi = 200$ MeV, $m_\pi = 2$ MeV and $m_\pi = 5$ MeV, respectively. The shaded bands show the uncertainty due to the unknown LECs for $m_\pi = 2$ MeV and $m_\pi = 5$ MeV, i.e., approximately in the chiral limit. The brown shaded band results from varying the LEC $\bar{d}_{16}$ entering into the expression for the renormalized OPE from $\bar{d}_{16} = -0.91$ GeV^{-2} to $\bar{d}_{16} = -1.76$ GeV^{-2} [20]. The mean result is obtained with $\bar{d}_{16} = -1.23$ here and in the following discussion.

The grey shaded band shows the uncertainty if in addition the unknown LECs $\bar{D}_{S,T}$ are varied. As already pointed out, the main source of uncertainty arises from these LECs entering the renormalized contact forces.

As one can see one obtains almost the same EOS for the cases of $m_\pi = 2$ MeV and $m_\pi = 5$ MeV, i.e., that any further reduction of the pion mass (which requires additional numerical effort) does not change the results for the EOS anymore and one can safely speak about having reached the chiral limit. In the chiral limit the scalar attraction is slightly stronger reduced than the vector repulsion (see Fig. 5.16) and therefore the EOS becomes more repulsive. This is still true if one takes into account the band of uncertainty.

In the case of an extrapolation to higher pion masses, i.e. $m_\pi = 180$ MeV and $m_\pi = 200$ MeV in Fig. 5.17 one observes a slight softening of the repulsive NLO EOS. Increasing the pion mass to $m_\pi = 200$ MeV does not change the EOS significantly. Nevertheless one has to take care that one does not leave the region where the chiral expansion is still valid, i.e. for $\bar{m}_\pi \leq 2m_\pi$ [20]. Calculations may not be trustable anymore when the pion mass is extrapolated to much towards this value. The uncertainties for $m_\pi = 180$ MeV due to the unknown LECs are depicted separately in Fig. 5.18 on the left hand side. In

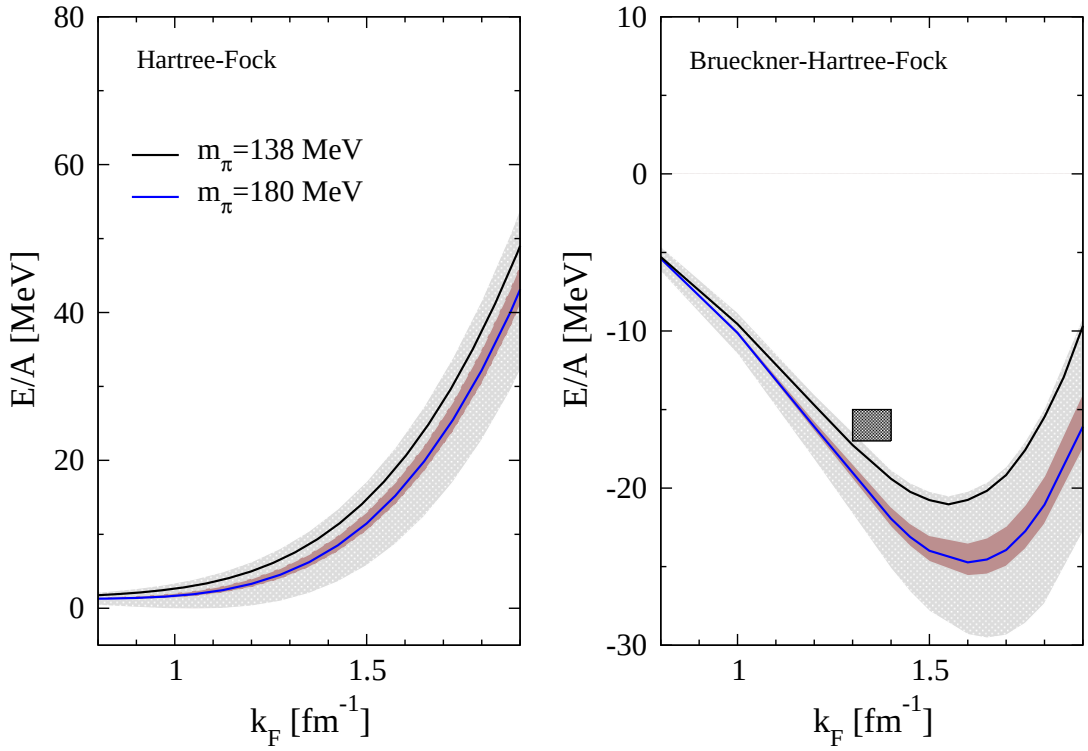

Figure 5.18: *Pion mass dependence of the nuclear equation of state E/A as a function of the Fermi momentum k_F. On the l.h.s. the Hartree-Fock calculations at NLO are shown for the physical case of $m_\pi = 138$ MeV compared to the case of $m_\pi = 180$ MeV. The Brueckner-Hartree-Fock results are shown on the right hand side. The brown shaded area denotes the uncertainty in the LECs $\bar{d}_{16}$ and $\bar{d}_{18}$, i.e., $\bar{d}_{16}$ varied from $\bar{d}_{16} = -0.91$ GeV^{-2} to $\bar{d}_{16} = -1.76$ GeV^{-2} and $\bar{d}_{18}$ is varied from $\bar{d}_{18} = -0.84$ GeV^{-2} to $\bar{d}_{18} = -1.54$ GeV^{-2}, respectively. The grey shaded area shows the overall uncertainty if one additionally takes into account the unknown LECs $\bar{D}_{S,T}$. The shaded square denotes the empirical region of nuclear saturation.*

contrast to the chiral limit where the LEC $\bar{d}_{18}$ vanishes it has to be also varied here where the mean results are obtained with $\bar{d}_{18} = -0.97$ ($\bar{d}_{16} = -1.23$ like in the chiral limit). As already mentioned a variation of $\alpha_{S,T}$ over the whole range $-3.0 < \alpha_{S,T} < 3.0$ as it is done in [20] is likely to overestimate the uncertainty when the chiral Idaho potential is used since the EOS for the physical case, i.e. $m_\pi = 138$ MeV also lies in this range of uncertainty.

NN correlations, in particular short-range and tensor correlations, have to be considered in a realistic microscopic nuclear matter calculation in order to obtain saturation properties. As already found in the previous section one observes nuclear saturation using chiral EFT at least at NLO as shown in Fig. 5.12

on the left. Nevertheless one can expect that the effects observed at Hartree-Fock level survive when a full Brueckner ladder is summed, i.e. if short-range correlations are taken into account. Therefore in Fig. 5.17 on the right hand-side the EOS obtained with the physical pion mass is compared to those obtained in the chiral limit, i.e. $m_\pi = 2$ MeV and $m_\pi = 5$ MeV as well as to those at higher pion masses, i.e. $m_\pi = 180$ MeV and $m_\pi = 200$ MeV, respectively. Again the shaded bands show the uncertainty for $m_\pi = 2$ MeV. The range of uncertainty for $m_\pi = 180$ MeV is shown separately in Fig. 5.18 on the right hand side. In the case of higher pion masses stronger attraction is observed as it was already found at tree level in Hartree-Fock approximation. The saturation point is shifted towards higher Fermi momenta and the binding energy is increased to $E/A = -25 \pm 4.5$ MeV.

In the chiral limit on the other hand the EOS becomes more repulsive in agreement with the corresponding Hartree-Fock calculation. The binding energy at the saturation point is shifted from the value in the physical case $E/A = -21$ MeV to $E/A = -13.4 \pm 3.5$. The equilibrium Fermi momentum k_F is shifted from $k_F = 1.55$ fm^{-1} to $k_F = 1.42 \pm 0.1$ fm^{-1} in the chiral limit. Therefore one can conclude that explicit chiral symmetry breaking is not an essential condition for nuclear saturation at least at NLO in the chiral expansion.

This confirms the investigations performed by Bulgac et al. [144] who analyzed the properties of nuclear matter taking basically the explicit pion mass dependence of the OPE potential into account and assuming that the short range and intermediate range part of the NN interaction is not affected. They concluded that in the chiral limit the physics of infinite nuclear matter is similar to that of a non-vanishing pion mass.

As already introduced in the previous section Kaiser et al. [128] described nuclear matter properties based on in-medium chiral perturbation theory. In this work also the nuclear EOS in the chiral limit has been investigated. OPE, iterated OPE and irreducible TPE up to three-loop order in the energy density have been included in the calculation of the EOS. The only free parameter is a momentum-space cut-off Λ due to the regularization of divergent parts connected with chiral two-pion exchange. Since the contributions coming from this regularization to the energy per particle correspond to that of a zero-range contact interaction the cut-off Λ parameterizes effectively its strength. The chiral pion exchange diagrams included in the present calculation are the same as in [128] and therefore the results can be compared. However, in contrast to the calculation presented in this thesis the pion mass dependence of g_A, M, f_π is not taken into account in [128]. The empirical saturation point is met by adjusting the free cut-off parameter Λ in contrast to our calculation where no free adjustable parameters occur. Fig.6 of Ref. [128] shows the dependence of the saturation point on the cut-off Λ for the physical pion mass as well as in the chiral limit. It has been also found that nuclear matter is bound in the chiral

limit. However, the dependence of the cut-off Λ on the pion mass is not known. Using, e.g., the same value for Λ from the physical case in the chiral limit, the binding energy and the saturation density are strongly increased. In our work where free adjustable parameters are not included the saturation density and the binding energy are decreased as shown in Fig. 5.17. In order to obtain the same result within the approach of [128] Λ has to be considerably smaller than in the case of the physical pion mass.

This section can be summarized as follows: the uncertainty due to the LECs $\bar{d}_{16,18}$ does not significantly affect the EOS. Though the parameters $\alpha_{S,T}$ setting the strength of the chiral contact force are varied in the range of $-3.0 < \alpha_{S,T} < 3.0$ (which is likely to overestimate the uncertainty) qualitative conclusions can be drawn. Concerning the tree level EOS as well as that calculated within the BHF approach, however, no tendency of a qualitative change even for large, probably unrealistic variations of the dimensionless coefficients $\alpha_{S,T}$ is found. This is also true in the case of an extrapolation to higher pion masses.

Therefore the conclusion is, that the magnitude of the large scalar and vector fields in matter persists in the chiral limit. In contrast to the case of a pion mass larger than the physical one binding energy and saturation density are decreased in the chiral limit but nuclear matter is still bound. Therefore the physics of infinite nuclear matter is similar to that of a non-vanishing pion mass.

6. Nucleon mass in nuclear matter

QCD in-medium sum rules establish the connection between the relativistic phenomenological description of nuclear matter, especially the appearance of large scalar and vector components to the fundamental theory of strong interactions, QCD. In Section 2.3 it has been shown that QCD in-medium sum rules relate the scalar and vector in-medium condensates $\langle \bar{q}q \rangle_{\rho_B}$ and $\langle q^\dagger q \rangle_{\rho_B}$ to the isoscalar scalar and vector self-energies of a nucleon in matter.

In order to derive expressions for the self-energies in the sum rule approach one needs to know the density dependence of the scalar condensate and the vector condensate, respectively. In contrast to the scalar condensate, to leading order the vector condensate is exactly known. It is given by the quark density in the nuclear matter rest-frame $\langle q^\dagger q \rangle_{\rho_B} = 3/2\rho_B$. The determination of the density behavior of the scalar condensate in matter is more evolved. It can be estimated with the help of the Hellmann-Feynman theorem in a model independent way to first order in density [51, 45] as shown in Section 6.2. In this estimation higher order corrections in the nucleon density coming from the nucleon kinetic energy and nucleon-nucleon interactions are neglected and the in-medium scalar condensate drops linearly with the nuclear density with the proportionality given by the pion-nucleon sigma term σ_N.

To determine corrections to this leading density dependence a large variety of models has been exploited. These were e.g. the Nambu-Jona-Lasinio (NJL) model [51, 52, 53, 54], various versions of the linear sigma model [55, 56], the Quark Meson Coupling model [57] or recently the Polyakov-NJL model [58]. The Hellmann-Feynman theorem relates the in-medium scalar quark condensate with the quark mass derivative of the total energy density. The latter quantity can also be calculated within hadron effective field theory [51], such as the DBHF approach (see Section 2.2). However, the unknown quark mass dependence of the mesonic couplings and meson masses of the OBE potentials used in the DBHF approach introduces large errors in the determination of the in-medium condensate [59, 60].

Most hadronic models do, however, not respect chiral symmetry. A more systematic and direct connection to QCD is provided by chiral EFT. Therefore in this work the in-medium scalar condensate has been determined by using the Hellmann-Feynman theorem upon application of the chiral EFT interaction where the explicit and implicit current quark mass dependence of the nuclear force is known up to NLO [20]. This chiral EFT interaction is also described in

Section 3.3.2. Later on this will be done is Hartree-Fock (HF) approximation and in order to estimate the influence of short-range correlations and quenching effects also a realistic Brueckner-Hartree-Fock (BHF) calculation has been performed.

In agreement with other estimations of the in-medium condensate, e.g. performed with more simple models [51] higher order corrections from the nucleon kinetic and interaction energy become significantly more important above saturation density and lead in general to a weaker reduction of the in-medium quark condensate in both cases when compared to the model independent calculation.

Moreover this procedure allows to identify how the different parts of the chiral interaction contribute to the change of the chiral condensate in matter.

The model independent leading order results, Eqs. (2.84) and (2.85) should be valid at low density. Thus the scalar self-energy Eq. (2.84) determines the density dependence of the effective nucleon mass $M^* = M + \Sigma_\mathrm{s}$ within the in-medium QCD sum rule approach

$$\frac{M^*}{M} = 1 - \frac{\sigma_N}{m_\pi^2 f_\pi^2}\rho_B. \tag{6.1}$$

Naturally, Eq. (6.1) represents the model independent leading order prediction for the in-medium scalar condensate $\langle\bar{q}q\rangle_{\rho_B}/\langle\bar{q}q\rangle_0$, i.e., the leading order term in Eq. (6.12) since it enters the expression for the scalar self-energy (2.84).

In the first part of this chapter a comparison of the leading order sum rule predictions Eqs. (2.84) and (2.85) to a many-body calculation of the scalar and vector self-energy components in Hartree-Fock approximation based on the chiral EFT interaction is presented. Only small deviations are observed at moderate densities.

However, concerning the in-medium condensate one has carefully to distinguish between contributions from the pion cloud and those of non-pionic origin [63, 64]. As demonstrated by Birse [63] a naive direct dependence of the nucleon mass on the quark condensate through Eq. (2.84) or Eq. (6.1), respectively, leads to contradictions with chiral power counting. The contributions from low momentum virtual pions which enter the in-medium condensate should not contribute by the same amount to the change of the nucleon properties in matter. They can therefore not as easily be associated with a partial restoration of chiral symmetry as the mean field field approximation, i.e. Eq. (6.4), would suggest. This problem has also been investigated by Chanfray et al. [64] in the framework of the linear sigma model. In their studies the authors were able to reconcile the phenomenology of Quantum Hadron Dynamics with chiral theory, in that case the linear sigma model. Their conclusion was that, in contrast to the scalar condensate $\langle\bar{q}q\rangle_{\rho_B}$ which is driven by the sigma field, i.e., the chiral partner of the pion, the lowering of the nucleon mass M^* is driven by a chiral invariant scalar field which corresponds to fluctuation along the chiral circle.

With other words, the condensate is to large extent reduced by the pion cloud surrounding the nucleons while the nucleon mass is not.

To set up the context for the following discussion, the argumentation of Birse is shortly sketched [63]: From Eq. (6.1) follows that the effective nucleon mass M^* is directly proportional to the nucleon sigma term σ_N. The chiral expansion of the sigma term leads to [84]

$$\sigma_N = Am_\pi^2 - \frac{9}{16\pi}\left(\frac{g_{\pi NN}}{2M}\right)^2 m_\pi^3 + \dots \ . \tag{6.2}$$

In the chiral limit the pion-nucleon coupling is connected to the axial vector coupling by the Goldberger-Treiman relation $g_{\pi NN} = g_A M/f_\pi$. The coefficient A involves counter terms related to short-distance physics whereas the non-analytic $\mathcal{O}(m_\pi^3)$ term arises purely from long-distance physics of the pion cloud. Inserting (6.2) into (6.1) implies a dependence of the effective nucleon mass M^* on the pion mass which is of order $\mathcal{O}(m_\pi)$.

At the mean field level, i.e., in $T-\rho$ approximation, the scalar self-energy (5.5) is on the other hand given by the scalar forward scattering amplitude $T_s(\mathbf{q}=0)$ ($T_s(\mathbf{q}=0)$ in (6.3) corresponds to the direct amplitudes F_S and g_S in (4.14) and (4.17), respectively.)

$$\Sigma_\mathrm{s}(k_\mathrm{F}) = T_s(\mathbf{q}=0)\,\rho_B \quad . \tag{6.3}$$

A comparison of Eq. (6.3) with Eqs. (6.1) and (6.2) would imply that the scalar part of the forward scattering amplitude contains a constant and a term of order m_π. Such a dependence contradicts, however, chiral power counting. In chiral EFT the leading term in the pion mass in the NN interaction originates from the low energy expansion of the OPE and is of order $\mathcal{O}(m_\pi^2)$ [18, 19, 17]. Hence the NN interaction cannot contain a term directly proportional to σ_N/m_π^2. Moreover, as stated in [63] the in-medium quark condensate $\langle\bar{q}q\rangle_{\rho_B}$ contains contributions from low-momentum virtual pions, which do not contribute to the properties of the nucleon in matter.

This is in agreement with the result shown in Section 5.2, namely that the dominant contributions to the scalar and vector self-energy are generated by NLO contact terms. This means that the reduction of the nucleon mass $M^* = M+\Sigma_\mathrm{s}$ is driven by short-distance physics. Pion dynamics is almost negligible for the generation of the self-energy and therefore has no impact on the properties of the in-medium nucleon mass (see Table 5.1)

With the present formalism at hand a consistent comparison of the in-medium scalar condensate, derived from the Hellmann-Feynman theorem, and the effective nucleon mass $M^* = M + \Sigma_\mathrm{s}$ where the scalar self-energy Σ_s enters can be performed. For the first time both quantities have been derived at the same order and from the same chiral EFT interaction. This is presented in the last part of this chapter.

6.1. HF self-energy vs. QCD in-medium sum rules

Applying Ioffe's formula Eq. (2.66) for the nucleon mass and the Gell-Mann, Oakes, Renner (GOR) relation to Eqs. (2.84) and (2.85) the QCD in-medium sum rules can be written as [46, 47]

$$\Sigma_{\rm s} = -\frac{\sigma_N M}{m_\pi^2 f_\pi^2}\rho_B \quad , \tag{6.4}$$

$$-\Sigma_0 = \frac{4(m_u+m_d)M}{m_\pi^2 f_\pi^2}\rho_B \quad , \tag{6.5}$$

where the difference between the scalar and vector density, ρ_S and ρ_B, can be neglected at low densities $k_F^2 \ll M^2$.

For the comparison of the sum rule predictions we turn to the density dependence of the self-energy. Fig. 6.1 contains the corresponding fields as predicted by leading order QCD sum rules, i.e., Eqs. (6.4) and (6.5). For the evaluation of Eqs. (6.4) the empirical value of $\sigma_N = 50$ MeV has been chosen for the nucleon sigma term, $f_\pi = 93$ MeV and $(m_u + m_d) = 12$ MeV. In Fig. 6.1 also the density dependence of the fields from the chiral EFT interaction are presented up to N^{3}LO. As in Fig. 5.3, the scalar $\Sigma_{\rm s}$, time-like vector Σ_0 and spatial vector $\Sigma_{\rm v}$ self-energies are determined at momentum $k = k_{\rm F}$. The density dependence is shown up to $k_{\rm F} = 1.8$ fm^{-1} which corresponds to about 2.5 times nuclear saturation density. As can be seen from Fig. 6.1 the relative contributions from the various orders remain the same over the entire density range considered.

Both, the QCD sum rule and the chiral EFT fields are well comparable in terms of a density expansion since both are obtained to leading order in density. In the case of the sum rules this corresponds to a Fermi gas of non-interacting nucleons. To go beyond the Fermi gas approximation would require to include higher order terms in the operator product expansion and the density expansion of the condensates [43, 44, 45, 145]. As explained in Section 2.3 contributions coming from the next order in the operator product expansion involve four-quark operators and combinations of quark and gluon fields. Attempts to fix the density dependence of higher order contributions in the operator product expansion have e.g. been performed in [146, 147].

In the EFT case higher orders in density can be introduced by a self-consistent dressing of the interaction (see discussion in Section 5.3) and of course by higher order terms in perturbation series which would finally end up in a full resummation of the Brueckner ladder diagrams.

At moderate nuclear densities the agreement between the QCD sum rules and N^{3}LO is quite remarkable. At higher densities the results from the sum rules tend to overshoot the N^{3}LO values which is, however, not too astonishing since the relations (6.4) are valid in the low density limit.

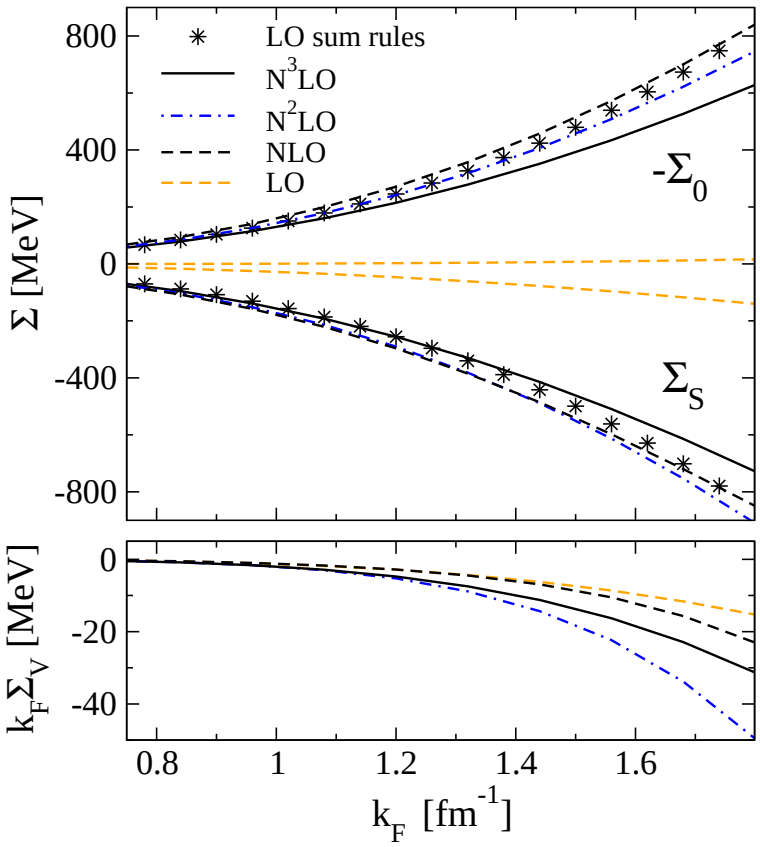

Figure 6.1: *Density dependence of the tree level scalar and vector self-energy components in nuclear matter obtained with the chiral EFT NN interaction [19]. The fields obtained in leading order (LO) up to next-to-next-to-next-to-leading order (N^3LO) are shown. The results from leading order QCD sum rules are shown as well.*

In view of the fact that in chiral NN dynamics the fields are dominantly generated by NLO contact terms, one could be tempted to interpret the present results in the way that the reduction of the quark condensates occurs at NLO in the chiral expansion. However, as discussed above such an interpretation is not straightforward. A closer inspection of the terms which drive the sum rule result reveals the following: the coefficient A in (6.2) is related to the unknown coupling C_1 in the effective ChPT pion-nucleon Lagrangian [148]. Becher and Leutwyler extracted a value of $A = 3.7$ GeV^{-1} fitting the elastic πN scattering amplitude at threshold [149]. Inserting this value into the sum rule expression (6.1) corresponds to a scalar self-energy (at $k_\mathrm{F} = 1,35$ fm^{-1}) of $\Sigma_\mathrm{s} = -513$ MeV at order m_π^0. At order m_π, i.e., when the $\mathcal{O}(m_\pi^3)$ term in the expansion (6.2) is included, the sigma term of 46.7 MeV is already close to its empirical value

and a self-energy of $\Sigma_s = -340$ MeV is obtained. Although this value for Σ_s is astonishingly close to the NLO result from chiral NN scattering, one has to keep in mind that already the LO result is of order m_π^2 in the pion mass. In contrast to the sum-rule approach there appears no significant repulsive contribution from pion dynamics which would correspond to the $\mathcal{O}(m_\pi^3)$ term in (6.2).

The present results are therefore in qualitative agreement with the findings of Refs. [63, 64], namely that long-distance physics related to pion dynamics plays only a minor role for the reduction of the nucleon mass in matter. Relating the in-medium nucleon mass to the in-medium scalar condensate through expression (6.1) one should be very careful. Although the sum rule mean fields, Eqs. (6.4) and (6.5), provide a reasonable approximation to the mean fields from chiral EFT, both approaches do not reflect the same physical concepts. The sum rule approach assumes that the nucleon properties are determined by the interaction with the in-medium condensates while conventional many-body approaches assume that the in-medium properties are determined by the interaction between the nucleons.

6.2. Chiral condensate in nuclear matter

The spontaneous breakdown of chiral symmetry involves a qualitative rearrangement of the QCD ground state, due to the appearance of scalar quark-antiquark pairs. The corresponding non-vanishing ground-state expectation value $\langle\bar{q}q\rangle$, denoted as the scalar quark condensate, is an order parameter of spontaneous chiral symmetry breaking. Any reduction of the scalar density of quarks in matter can therefore be interpreted as a signature of partial restoration of chiral symmetry.

The vacuum value of the lowest-dimensional quark condensate is about [84]

$$\langle\bar{q}q\rangle_0 \simeq -(225 \pm 25\,\mathrm{MeV})^3 \quad . \tag{6.6}$$

The density dependence of the chiral condensate $\langle\bar{q}q\rangle$ can be extracted exploiting the Hellmann-Feynman theorem with respect to the symmetry breaking current quark mass term of the QCD Hamiltonian. We consider isospin symmetric matter making thereby use of the isospin symmetry of the condensates ($\langle\bar{q}q\rangle \equiv \langle\bar{u}u\rangle \simeq \langle\bar{d}d\rangle$). Defining $\bar{q}q \equiv \frac{1}{2}(\bar{u}u + \bar{d}d)$ and $m_q \equiv \frac{1}{2}(m_u + m_d)$ the quark mass term is given by $2m_q\bar{q}q$. Isospin-breaking terms are neglected. With the help of the Hellmann-Feynman theorem one obtains the in-medium quark condensate by determining the energy density $\mathcal{E}$ of nuclear matter

$$2m_q(\langle\bar{q}q\rangle_{\rho_B} - \langle\bar{q}q\rangle_0) = m_q\frac{d\mathcal{E}}{dm_q}. \tag{6.7}$$

The derivative is taken at fixed density. The derivation of Eq. (6.7) is presented in detail in Appendix C. Note the short notation $\langle\Omega\rangle_{\rho_B} = \langle\rho_B|\Omega|\rho_B\rangle$ and

$\langle\Omega\rangle_0 = \langle 0|\Omega|0\rangle$ where Ω is an arbitrary operator. $|\rho_B\rangle$ represents the ground state of nuclear matter at rest with baryon density ρ_B and $|0\rangle$ the vacuum state. The energy density of nuclear matter is given by

$$\mathcal{E} = M\rho_B + \frac{E(\rho_B)}{A}\rho_B \tag{6.8}$$

where the second term of $\mathcal{E}$ is the energy per particle E/A (times the baryon density), i.e. the contributions from the nucleon kinetic energy and nucleon-nucleon interactions.

The nucleon sigma term σ_N can be written as [150]

$$\begin{aligned} \sigma_N &= 2m_q \int d^3x(\langle N|\bar{q}q|N\rangle - \langle 0|\bar{q}q|0\rangle) &(6.9)\\ &= m_q \frac{dM}{dm_q} &(6.10)\end{aligned}$$

where $|N\rangle$ is the state vector for a nucleon at rest and $|0\rangle$ is the vacuum state. Eq. (6.10) is obtained by a further application of the Hellman-Feynman theorem, i.e., Eq. (C.7), to Eq. (6.9) with $|\psi(m_q)\rangle = |N\rangle$ and $|\psi(m_q)\rangle = |0\rangle$, respectively.

Inserting Eq. (6.8) and Eq. (6.10) into Eq. (6.7) and using the Gell-Mann, Oakes, Renner relation

$$2m_q\langle\bar{q}q\rangle_0 = -m_\pi^2 f_\pi^2 \tag{6.11}$$

one obtains

$$\frac{\langle\bar{q}q\rangle_{\rho_B}}{\langle\bar{q}q\rangle_0} = 1 - \frac{\rho_B}{m_\pi^2 f_\pi^2}\left[\sigma_N + m_q\frac{d}{dm_q}\frac{E}{A}\right]. \tag{6.12}$$

The derivative of the energy per particle with respect to the quark mass can be re-expressed using the chain rule

$$\frac{\langle\bar{q}q\rangle_{\rho_B}}{\langle\bar{q}q\rangle_0} = 1 - \frac{\rho_B}{m_\pi^2 f_\pi^2}\left[\sigma_N + m_q\frac{\partial(E/A)}{\partial M}\frac{dM}{dm_q} + m_q\frac{\partial(E/A)}{\partial m_\pi}\frac{dm_\pi}{dm_q}\right]. \tag{6.13}$$

The derivative of the pion mass using Eq. (6.11) is given by

$$\frac{dm_\pi}{dm_q} = \frac{m_\pi}{2m_q} \tag{6.14}$$

valid to leading order in chiral perturbation theory. Introducing

$$\rho^\chi = \frac{m_\pi^2 f_\pi^2}{\sigma_N} \tag{6.15}$$

one finally obtains

$$\frac{\langle\bar{q}q\rangle_{\rho_B}}{\langle\bar{q}q\rangle_0} = 1 - \frac{\rho_B}{\rho^\chi}\left[1 + \frac{\partial(E/A)}{\partial M} + \frac{\partial(E/A)}{\partial m_\pi}\frac{m_\pi}{2\sigma_N}\right]. \tag{6.16}$$

The first term on the r.h.s. of Eq. (6.16) which reduces the condensate in matter is model independent and of first order in the nuclear density [51, 45]. Inserting the empirical value of $\sigma_N = (45 \pm 7)$ MeV for the sigma term [85] and taking $m_\pi = 138$ MeV and $f_\pi = 92.4$ MeV one finds in Table 6.1, that the in-medium scalar condensate is to leading order in density approximately $\frac{1}{3}$ smaller than its vacuum value at nuclear saturation density. In the following a value of $\rho_0 = 0.173$ fm^{-3}, corresponding to a Fermi momentum of $k_F = 1.37$ fm^{-1}, is chosen as the standard value for the nuclear saturation density.

From Fig. 6.2 one sees that to leading order a complete restoration of chiral symmetry would already occur at $\rho_B \approx 2.7\rho_0$. Such a scenario is unrealistic and contradictory to the knowledge from heavy ion reactions [73] and astrophysics, e.g. neutron stars [151]. Hence, one has to account for higher order corrections in density coming from the $d(E/A)/dm_q$ term in Eq. (6.12).

One might estimate this correction to be small due to the binding energy of $E/A \approx -16$ MeV, which is almost two orders of magnitude smaller than the nucleon mass contributing dominantly to the energy density in Eq. (6.8). Nevertheless, since the quark mass derivative of the interaction energy is the relevant quantity, it is by far not obvious that higher order corrections are negligible.

Thus, a reliable extraction of the density dependent scalar condensate $\langle\bar{q}q\rangle_{\rho_B}$ requires both, a sophisticated nuclear matter calculation *and* the exact knowledge of the current quark mass dependence of *all* model parameters entering into the energy density.

Previous estimates of the scalar condensate based on sophisticated ab-initio many-body approaches [59, 60] suffered from this problem. The relativistic Brueckner approach chosen in [59, 60] provides a reliable description of nuclear matter bulk properties. Such calculations are based on realistic NN potentials, e.g. one-boson-exchange (OBE) potentials [12]. However, the current quark mass dependences of the model parameters, i.e. meson masses and coupling constants, are unknown to large extent and have therefore either been roughly estimated or even been neglected [59, 60].

In [59] it was found that the largest uncertainty in the calculation of the in-medium quark condensate $\langle\bar{q}q\rangle_{\rho_B}$ arises due to the unknown quark mass dependence of the scalar isoscalar σ meson exchange which parameterizes effectively correlated two-pion exchange.

In the present work the energy per particle E/A is determined within Hartree-Fock approximation, Eq. (5.20). However, for a reliable estimate of the in-medium condensate the role of NN correlations, in particular short-range and tensor correlations, has to be considered. One might assume that NN correlations influence the result for the condensate, in particular at higher densities. In order to estimate their importance the self-consistent iteration scheme of non-relativistic BHF theory is applied in a second step. Chiral EFT in nuclear

matter has been studied at Hartree-Fock level and within the non-relativistic BHF approach in Section 5.4 where also BHF theory has been outlined.

Since the NN interaction is thereby based on chiral EFT, Eqs. (3.28)-(3.30) where the complete pion mass dependence is known up to NLO [20] we are free of uncertainties concerning unknown quark mass derivatives. Remaining ambiguities when applying the Hellman-Feynman theorem are only due to the not yet uniquely fixed LECs $\bar{D}_{S,T}$ in the NLO contact terms, see Eq. (3.30), and the LECs $\bar{d}_{16,18}$ showing up in the OPE exchange. The uncertainties coming from these LECs will be discussed.

As already mentioned we apply the non-relativistic BHF approach since the chiral EFT interaction is a non-relativistic potential and therefore can not be used within the relativistic DBHF approach (see Chapter 5.4). Nevertheless, differences between a relativistic and a non-relativistic treatment should be moderate concerning the derivative of the EOS with respect to the current quark mass.

6.2.1. Results: HF and BHF approximation

The prediction of the in-medium scalar condensate in both approaches, i.e., HF and BHF are shown in Fig. 6.2. As expected, deviations from the leading order result due to NN interactions and nucleon kinetic energy, Eq. (6.16), increase with density. For both approaches, HF and BHF, the additional contributions lead to a weaker reduction of the in-medium quark condensate. Especially in the case of the BHF calculation the leading order prediction provides a very good description of the quark condensate up to a density of $0.8\rho_B$.

At nuclear saturation density ρ_0 the reduction of the in-medium quark condensate is about 3% (BHF) and 12% (HF) smaller compared to leading order. Deviations are, however, growing with density, where at $\rho_B \approx 2 \div 3\rho_0$ the quark condensate is reduced to $\approx 35\%$ (HF) and $\approx 30\%$ (BHF). Naturally the BHF approach is more reliable in this density region. However, in summary effects from short-range NN correlations and the quenching of OPE and TPE due to Pauli blocking, both present in BHF, have only minor implications for the condensate as can be seen from the comparison to the HF result.

The uncertainty due to the not yet uniquely fixed LECs $\bar{d}_{16,18}$ in the renormalized OPE, Eq. (3.28) which was already mentioned in the context of the EOS in the chiral limit, enters also into the determination of the scalar condensate. However, now this uncertainty is much more severe. The light shaded bands in Fig. 6.2 indicate the range of possible variations: The LEC $\bar{d}_{18}$ is extracted from the Goldberger-Treiman discrepancy. In the present work the three empirically found values given in [20] are taken which have been extracted from three different πN phase shift analysis, $\bar{d}_{18} = -0.84$ GeV^{-2} [152], $\bar{d}_{18} = -0.97$ GeV^{-2} [153] and $\bar{d}_{18} = -1.54$ GeV^{-2} [154], respectively. Furthermore the LEC

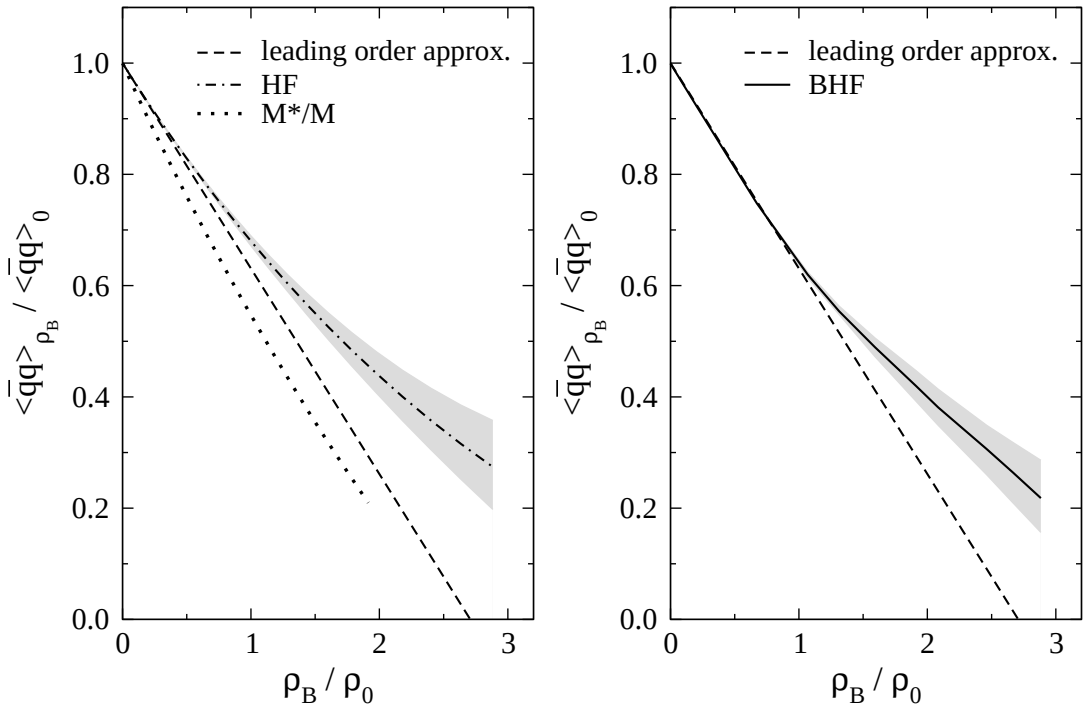

Figure 6.2: *In-medium scalar quark condensate as a function of density with $\sigma_N = 45$ MeV obtained in various approximations: A Hartree-Fock calculation of $\langle\bar{q}q\rangle_{\rho_B}/\langle\bar{q}q\rangle_0$ is shown compared to M^*/M where $M^* = M + \Sigma_s$ is evaluated at tree level in Hartree-Fock approximation (left). A full calculation based on the Brueckner-Hartree-Fock approach is shown on the right. The light shaded bands indicate the uncertainty of the corresponding result varying the LECs $\bar{d}_{16}$ from $\bar{d}_{16} = -0.91$ GeV^{-2} to $\bar{d}_{16} = -1.76$ GeV^{-2} and $\bar{d}_{18}$ from $\bar{d}_{18} = -0.84$ GeV^{-2} to $\bar{d}_{18} = -1.54$ GeV^{-2}. Dashed line: model-independent leading order result.*

$\bar{d}_{16}$ is varied in the range from $\bar{d}_{16} = -0.91$ to $\bar{d}_{16} = -1.76$ as done in [20]. The upper bound of the shaded band corresponds to $\bar{d}_{16} = -1.76$ and $\bar{d}_{18} = -0.84$ whereas the lower bound corresponds to $\bar{d}_{16} = -0.91$ and $\bar{d}_{18} = -1.54$. These uncertainties are also given in Table 6.1. The HF (dash-dotted line) and BHF (solid line) mean values are obtained with $\bar{d}_{16} = -1.23$ and $\bar{d}_{18} = -0.97$.

Comparing with previous approaches performed in a similar spirit [60] and [59] we find generally a stronger reduction of the scalar condensate. In [60] the calculations were done in the relativistic DBHF approach based on the OBE potential Bonn A. In this approach an unexpected increase of the in-medium scalar condensate at densities above $\rho < 2.5\rho_B$ has been found. The same tendency, i.e. an increasing quark condensate at high density has been observed in [59]. In [60] it was assumed that this increase is caused by a breakdown of

Table 6.1: *Predictions of $\langle\bar{q}q\rangle_{\rho_B}/\langle\bar{q}q\rangle_0$ obtained with the Hellmann-Feynman theorem in diverse approximations compared with M^*/M for three different values of the nucleon density ρ_B.*

	$\langle\bar{\mathbf{q}}\mathbf{q}\rangle_{\rho_\mathbf{B}}/\langle\bar{\mathbf{q}}\mathbf{q}\rangle_\mathbf{0}$		$\mathbf{M^*/M}$
ρ_B/ρ_0	Leading order	HF	BHF	in HF
0.5	0.815	0.828 ± 0.002	0.812 ± 0.001	0.759
1.0	0.630	0.677 ± 0.010	0.641 ± 0.004	0.546
1.5	0.445	0.550 ± 0.020	0.510 ± 0.014	0.354

the underlying assumptions related to the current quark mass dependences of the model parameters, i.e. meson masses and coupling constants. Moreover, the authors concluded that the use of not chirally invariant NN potentials may lead to wrong predictions in a density region where chiral restoration is expected to occur. As already mentioned in the present work such problems do not occur since the chirally invariant EFT interaction used here has a well defined quark mass dependence. The only source of uncertainty arises due to the LECs $\bar{d}_{16,18}$ from Eq. (3.28) which are not yet uniquely fixed and the unknown LECs $\bar{D}_{S,T}$, Eqs. (3.33) and (3.34), entering the short-range part, i.e., the contact force which could provide substantial corrections to the scalar quark condensate. Nevertheless, the same argument given in Section 5.5 is used to avoid a wide undefined variation. Therefore, the present calculation is restricted again to the case of $\alpha_{S,T} \approx 1$. However, as for the EOS calculated in Section 5.5, the prediction of the quark condensate is not considerably altered varying $\alpha_{S,T}$ for combinations of $\alpha_{S,T}$ where both parameters are close to each other. The contributions which change the condensate originate then mainly from TPE and renormalized contact forces. The LECs $C_{1\ldots7}$ in Eq. (3.30) do not depend on the pion mass after renormalization and the related contact terms do therefore not contribute to the change of the in-medium quark condensate.

Nevertheless, considering the possible band of variation due to the LECs $\bar{d}_{16,18}$, both, the HF and BHF calculations shown in Fig. 6.2 do not indicate a saturating behavior or even an increase of the condensate in the considered density range up to $3\rho_B$. Extrapolating the BHF prediction to high densities a complete restoration of chiral symmetry, i.e., a vanishing scalar quark condensate is not likely to happen below $4\rho_0$, even if one takes the range of uncertainty from not yet exactly known LECs into account.

The first determination of the in-medium quark condensate adopting the Hellmann-Feynman theorem has been carried out by Cohen et al. [51], based on the π-N Fock term. There the condensate was found to be reduced to a value of 0.694 at nuclear saturation density ρ_0 and 0.58 at about $1.5\rho_0$ which is in fair agreement with 0.677 ± 0.01 and 0.550 ± 0.020 obtained in the present HF calculation (third column of Table 6.1). This agreement, is, however, somewhat accidental since we find that TPE and contact interactions (which both have not been included in [51]) reduce the contribution from OPE by $\approx 50\%$. Moreover, in [51] the quark mass dependence of the pion-nucleon coupling $dg_{\pi N}/dm_q$ has been neglected and a different value for $g_{\pi N}$ has been used. Both calculations are, however, comparable in the sense that NN correlations are neglected and they are of the same order in the density. Moreover, short-range physics due to contact terms, which have been neglected in the simpler model used in [51] are found to provide only moderate corrections as can be seen from Fig. 6.3.

To study the different contributions in the calculation of the in-medium condensate in Fig. 6.2 (dash-dotted line) in Fig. 6.3 the derivatives $\partial(E/A)/\partial m_\pi$ from Eq. (6.16) are shown as a function of the density with respect to the different contributions coming from pion dynamics, Eqs. (3.28) and (3.29), and from the contact terms ($V^{\rm cont}$, Eq. (3.30)), respectively. The dashed-dotted line indicates the derivative $\partial(E/A)/\partial M$. The contribution coming from OPE is negative and considerably larger compared to those from TPE and contact interactions. In general the contributions from pion dynamics, i.e., OPE and TPE are smaller in BHF due to quenching effects. In the case of the contact interactions, Eq. (3.30), one has to keep in mind that the short-range terms $\tilde{m}_\pi^2 \ln \tilde{m}_\pi$ show up due to TPE and the renormalization of the leading order contact terms by pion loops. The contribution from nucleon interactions is getting substantially more important with increasing density compared to the contribution from the nucleon kinetic energy (dot-dashed line) which is of order $O(\rho^{5/3})$. *Thus the nuclear interaction provides important corrections to the Fermi gas approximation usually made in QCD sum rule approaches.*

It turns out that the calculation of the in-medium quark condensate is highly sensitive to the implicit pion mass dependence of the pion nucleon coupling constant $g_{\pi N}$ which has been often neglected in earlier works. This fact can also be seen from the relatively large bands of uncertainty in Fig. 6.2 since the corresponding LECs enter into the relative shift of g_A/F_π, Eq. (3.32), which is connected to $g_{\pi N}$ via the Goldberger-Treiman relation $g_{\pi N}/M = g_A/F_\pi$.

Lutz et al. [155] constructed a chiral power expansion scheme to calculate the nuclear EOS and to determine the in-medium condensate, respectively. Their approach is based on a chiral Lagrangian where the contributions to the EOS have been calculated from OPE iterated to second order. Additionally an attractive zero-range NN-contact interaction has been introduced where the coupling constants have to be adjusted to nuclear matter. The result for the in-

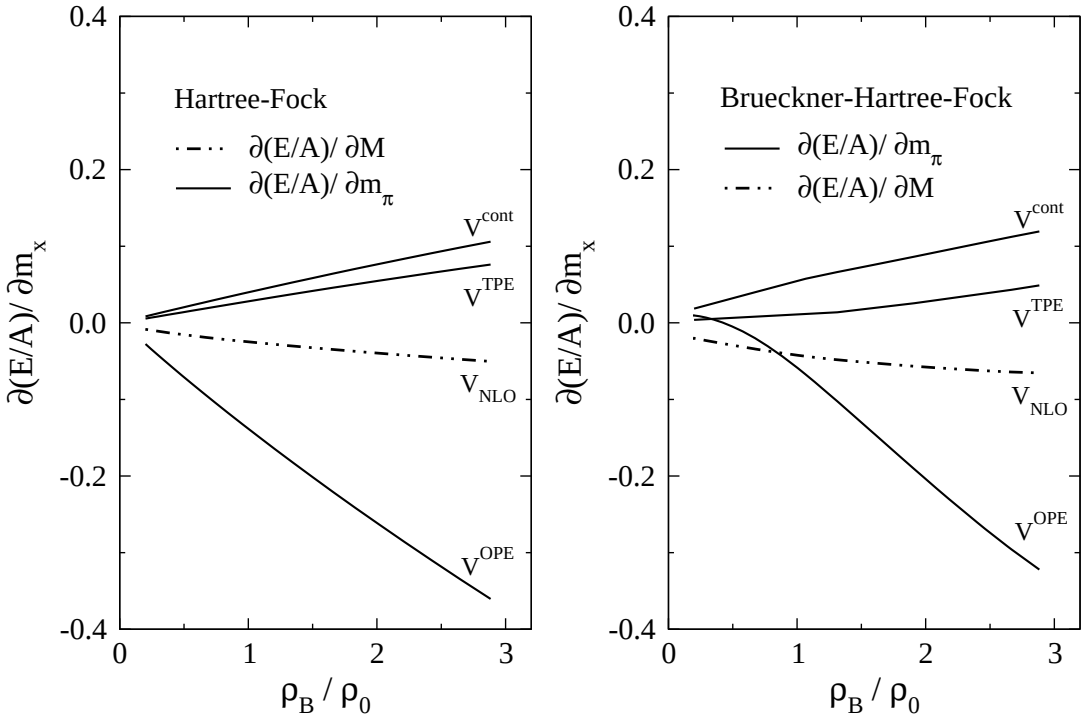

Figure 6.3: *The derivatives $\partial(E/A)/\partial m_\pi$ as a function of density with respect to the full NLO calculation as well as the separate contributions, i.e. OPE, TPE and contact interactions are shown. Additionally the dash-dotted line denotes $\partial(E/A)/\partial M$ for the full NLO calculation.*

medium quark condensate calculated within this chiral approach of is shown in Fig. 6.4(b).

Recently, the in-medium chiral condensate has been also calculated by Kaiser et al. [129] in the framework of in-medium chiral perturbation theory. Their chiral approach is an extended and improved version of their former approach [128], which has been already sketched in Section 5.4. Besides OPE and irreducible TPE effects from irreducible TPE together with intermediate $\Delta(1232)$-isobar excitations up to three-loop order in the energy density have been included in the calculation of the EOS and the in-medium chiral condensate. Instead of parameterizing the short-range physics (which cannot be resolved in an effective low-energy theory) by NN-contact terms as done by Lutz et al. [155], a momentum-space cut-off Λ is introduced which then encodes the dynamics at short distances [130].

As already mentioned the cut-off Λ is the result of a cut-off regularization of the chiral two-pion exchange. Nevertheless besides the fact that in [129] systematically effects from irreducible TPE processes have been included still

these two chiral approaches have been developed in the same spirit and are therefore well comparable. The result for the in-medium condensate calculated in the approach of Kaiser et al. [129] is presented in Fig. 6.4(c) on the right hand side. As one can see the in-medium quark condensate [129] exhibits a minimum at about 60% of its vacuum value at $\approx 1.8\rho_0$ and shows then a slight increase. The authors conclude in Ref. [129] that effects from TPE with virtual $\Delta(1232)$-isobar excitations are crucial to obtain such a behavior. This seems to be reasonable when comparing to the result of Lutz et al. or our calculation which is plotted once again in Fig. 6.4(a). Note that due to different choices of the pion mass m_π and the pion decay constant f_π additional deviations of the calculations presented in Fig. 6.4 are introduced, as can be seen in the case of the slopes of the linear density approximations. Kaiser et al., e.g., include already the kinetic energy contributions from a relativistic Fermi gas expanded up to order M^{-3} in the linear density approximation.

The agreement between our result and the result of Lutz et al. is actually good. In contrast to our calculation the contributions from irreducible TPE are not included in Ref. [155] which leads to a less deviating behavior from the linear density approximation since the derivative $\partial(E/A)/\partial m_\pi$ for the TPE is positive as shown in Fig. 6.3. However there is no one-to-one correspondence between the pion-exchange diagrams in the chiral NN potential used in our approach (see Fig.3.3) and those from in-medium chiral perturbation theory [155]. Additionally, the determination of the chiral condensate is extremely sensitive to the approach applied as well as to approximations, the parameters and their fixing, respectively. This can be seen from the fact that in Ref. [129] the contribution from irreducible TPE has the opposite sign compared to our calculation. Moreover the perturbative calculation by Kaiser et. al [129] including OPE, iterated OPE and irreducible TPE leads to an in-medium condensate below the linear density approximation (see Fig. 6 in Ref. [129]). This does not agree with our calculation (including OPE and irreducible TPE plus NLO NN-contacts) where in principle the same pion-dynamics is included. Keeping OPE and iterated OPE in the calculation of Kaiser et al. the reduction of the in-medium condensate is even larger. This completely disagrees with the calculation of Lutz et al. [155] which has been performed in the same spirit, in particular if one assumes that in [155] the contributions from the introduced phenomenological zero-range NN-contact interactions are small. The latter assumption is, however, confirmed by the present investigations and [129]. One has to keep in mind that in Ref. [155] any implicit dependence of the effective couplings parameterizing the short-distance physics is neglected. This is also the case for the momentum-space cut-off Λ in the approach of Kaiser et al. [129] which is adjusted to the empirical saturation properties of nuclear matter. Nevertheless Ref. [129] confirms an important result of this work namely that short-range NN-dynamics plays only a minor role for the change of the chiral condensate in

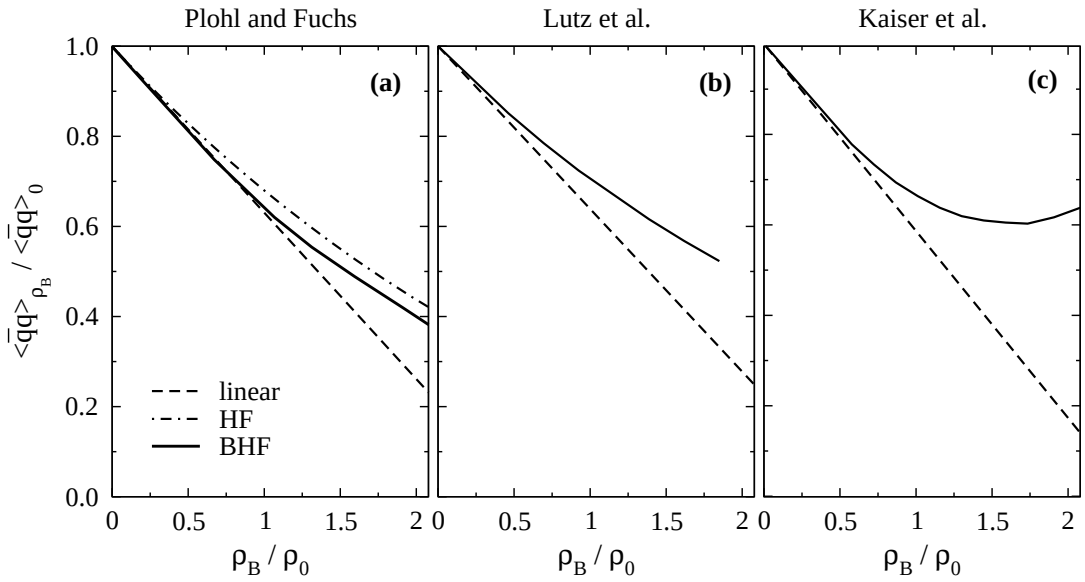

Figure 6.4: *Solid lines indicate the in-medium quark condensate* $\langle\bar{q}q\rangle_{\rho_B}/\langle\bar{q}q\rangle_0$ *as a function of density obtained within various approaches: (a) Hartree-Fock calculation and Brueckner-Hartree-Fock (see Fig. 6.2). Calculations performed within in-medium chiral perturbation theory: (b) OPE and NN-contact interaction iterated up to second order by Lutz et al. [155], (c) OPE, iterated OPE, irreducible TPE,* $\pi N\Delta$ *dynamics and* c_1*-contact vertex by Kaiser et al. [129]. Dashed line: model-independent leading order result. Note the slightly different slopes coming from different values of parameters. (*$\sigma_N = 45$ *MeV in all approaches.)*

matter. In order to improve our calculation one would have to include TPE with Δ-isobar excitations. To do so, one needs to know the pion mass dependence of the chiral NN interaction at NNLO. Since already at NLO significant uncertainties occur due to not known LECs it is likely to happen that this problem is amplified at NNLO due to even more unknown constants showing up in the chiral expansion of the NN potential.

Although deviations in the determination of the in-medium quark condensate occur when different approaches are compared we conclude that the contributions from nucleon interactions to the change of the scalar condensate in matter are mainly due to low-momentum virtual pions (also confirmed by Kaiser et al. [129]). In contrast to the generation of the scalar and vector fields Σ_s and Σ_0 which are generated by NLO contact interactions as shown in Section 5.2, contact terms and short-range correlations, i.e., short-distance physics, play only a minor role for the properties of the in-medium quark condensate. Nevertheless, for a fully reliable prediction of the in-medium quark condensate the little

known LECs $\bar{D}_{S,T}$ entering the NLO contact interactions, Eq. (3.30), have to be fixed with better precision.

6.3. The effective nucleon mass M^*

As discussed in the introduction of this chapter equalizing the scalar condensate and effective nucleon mass, is not as straightforward as relation (6.1) would suggest. This was also the conclusion from Section 6.1 and has been also discussed in the introduction to this chapter. It was shown that a direct dependence of the nucleon mass in nuclear matter on the in-medium quark condensate contradicts chiral power counting [63]. Now we are able to present finally a consistent comparison of the in-medium scalar condensate, derived from the Hellmann-Feynman theorem, and the effective nucleon mass in nuclear matter.

As one can see in Fig. 6.2 the ratio M^*/M is shown as a function of the density where the effective nucleon mass is given by $M^* = M + \Sigma_s$. The scalar field Σ_s is determined from the chiral EFT potential at NLO in HF approximation, making use of projection techniques on a relativistic operator basis as described in Chapter 4. As one can see also from Table 6.1, at saturation density the effective mass M^* or the ratio M^*/M, respectively, is reduced to a value of about 0.546 and is decreasing approximately linear up to $2\rho_0$. The reduction of the effective mass M^* is about $\approx 13\%$ larger at ρ_0 than that of the scalar condensate in the HF calculation, see also Table 6.1. At $1.5\,\rho_0$ the difference is about $20 \pm 2\%$. Thus the approximation of Eq. (6.4) does not hold. By a naive comparison of the two quantities the in-medium condensate may contribute at the utmost by about $\approx 80\%$ to the change of the the nucleon mass in matter at $1.5\,\rho_0$.

As already mentioned, the higher order contributions in Eq. (6.16) from the nucleon interaction are mainly due to OPE and TPE, i.e., low-momentum virtual pions give the main contribution to the change of the scalar quark condensate. The appearance of the large scalar field Σ_s which enters the effective nucleon mass $M^* = M + \Sigma_s$ originates on the other hand from NLO contact interactions (to be more precise from the part which is connected to the spin-orbit force), i.e., it is driven by short distance physics as shown in Section 5.2. Low-momentum pion dynamics is negligible concerning the appearance of the large scalar and vector fields Σ_s and Σ_0 at the considered order (NLO). The present investigations confirm thus the considerations of Ref. [63] which were based on a chiral expansion of the sigma term.

In summary, a direct dependence of the properties of the nucleon mass on the in-medium quark condensate as suggested by Eq. (6.1) can be ruled out.

7. Summary and conclusions

The investigation of nuclear matter as a strongly interacting Fermi system has a long history which goes back to the late forties/early fifties. One primary – and still not completely solved – goal is of course the exact determination of the nuclear equation of state over a wide range of nuclear densities. This question is of high relevance for the understanding of astrophysical phenomena such as neutron stars or supernovae explosions. There exist, however, a lot of other questions which are of fundamental interest and which are in some cases also tightly connected to the nuclear EOS: What are the relevant degrees of freedom to describe the interacting system at the particular scales? What is the role of relativity for nuclear dynamics? What is the origin of the reduction of the nucleon mass in matter and how is the relation to basic quantities in the language of QCD, i.e. the scalar quark condensate? How behaves the interacting system in the chiral limit?

The present thesis does not aim for a highly qualitative description of the nuclear many-body system but provides a systematic study of the questions addressed above where in the following the major results are summarized:

The appearance of large scalar and vector fields is a well established feature of relativistic nuclear dynamics. The saturation mechanism of nuclear matter or the single particle potential in finite nuclei are obtained by subtle cancellation effects between large attractive scalar and repulsive vector fields. These fields occur already at tree level and do not change too much when realistic many-body calculations are performed. Full self-consistent Brueckner calculations which account for short-range ladder correlations lead to mean fields of similar size, i.e., of several hundred MeV magnitude. The size of the scalar and vector fields coincides with the values derived from relativistic mean field phenomenology by fits to finite nuclei. Alternatively, QCD sum rules come to the same results.

The present thesis addresses the question about the origin of these fields. When the nucleon-nucleon interaction is described within the framework of a meson exchange picture, the situation is rather clear. The Lorentz character of the mesons determines automatically the Lorentz character of the interaction at the corresponding scale: the short-range repulsion is due to vector exchange (ω, ρ) while the intermediate range attraction originates from scalar exchange (σ). As a direct consequence large scalar and vector mean fields are generated in nuclear matter. However, since these fields are not observable, it is therefore a fundamental questions of nuclear physics whether the appearance of large

scalar/vector fields is intimately connected to the meson exchange picture or if it is a more general consequence of the vacuum NN interaction.

In order to address this question in a model independent way, the investigations presented in this work are based on a broad set of modern high precision NN potentials: Bonn, CD-Bonn, Nijmegen I/II, Nijmegen93, Argonne v_{18}, Reid93, Idaho N^{3}LO and $V_{\text{low k}}$. Except the fact that all these potentials fit NN scattering data with high accuracy they are based partially on quite different theoretical concepts. The one-boson-exchange potentials Bonn A, CD-Bonn, Nijmegen are developed in the framework of the traditional meson exchange picture, whereas the Argonne v_{18} and Reid93 potentials emanate from a purely phenomenological philosophy. Another class are effective low momentum interactions represented in this thesis by the Idaho N^{3}LO or $V_{\text{low k}}$ potentials which arise from QCD inspired effective field theory approaches. Though most of the various approaches are not restricted by the requirement of covariance symmetry arguments and NN scattering data enforce a certain spin-isospin operator structure on which the approaches rely.

Since the question whether the preconditions for the appearance of the large fields in matter is closely linked to a certain general relativistic structure of the NN interaction in a first step the symmetries of the Lorentz group are restored by mapping the various NN potentials on a covariant operator basis in Dirac space. The comparison of the various approaches to the NN interaction at the level of covariant amplitudes shows a remarkable agreement of the Lorentz structure between the meson exchange potentials, the non-relativistic phenomenological potentials and the EFT potentials. This could not have been expected a priori since in the case of not covariantly formulated NN interactions the relativistic structure imposed by the symmetries of the Lorentz group is hidden.

The projection procedure onto a covariant operator basis allows furthermore to calculate the relativistic self-energy operator at tree level in nuclear matter. This is a major result of the present thesis since this investigation shows that the vacuum structure of the NN interaction enforces the existence of large scalar and vector fields found to be a model independent fact, true for all types of interactions which have been considered[1]. The magnitude of the tree-level results for the self-energy fields is very similar to that predicted by relativistic mean field phenomenology and relativistic many body calculations and moreover we could show that the scale of these fields is set at tree level where higher-order correlations, although important for nuclear binding, change the size of the fields by less than 25%.

A certainly more direct connection to QCD is established by chiral EFT

[1]The accuracy of the applied projection technique has been tested by a comparison of the single particle potential determined from the relativistic self-energy at tree level to that obtained from a non-relativistic Hartree-Fock calculation where an excellent agreement was found.

where the NN interaction is derived from a systematic expansion of an effective Lagrangian which respects the basic symmetries of QCD. Therefore chiral EFT is considered as the exact mapping of QCD on effective hadronic degrees of freedom in the non-perturbative regime. Subjecting the chiral N^{3}LO Idaho potential to the present projection scheme allowed to investigate the structure of the self-energy. We found that scalar and vector mean fields of the same sign and magnitude are generated in nuclear matter as by the meson exchange or phenomenological potentials. These fields are generated by contact terms which occur at next-to-leading order in the chiral expansion. These are four-nucleon contact terms with two derivatives which generate the short-range spin-orbit interaction. The strength of the corresponding low energy constants, in particular those connected to the spin-orbit force, is dictated by P-wave NN scattering data. Pion dynamics as well as LO and N^{3}LO contacts provide only corrections to the fields generated by the NLO contact terms. EFT is therefore in perfect agreement with Dirac phenomenology where it is known since a long time that the large scalar/vector fields are generated by the short-range vector (ω) and scalar (σ) mesons which are connected intimately to the large spin-orbit interaction. The conclusion is that this is a direct consequence of P-wave NN scattering.

For future perspectives chiral EFT in combination with projection techniques may allow to determine the relativistic anti-proton potential in matter in a model independent way. Here the meson-exchange picture predicts a change in sign of the vector field due to g-parity and hence an extremely deep attractive potential. Such investigations in particular will be interesting in view of the forthcoming anti-proton facilities, e.g. Panda at FAIR [156].

In order to estimate the effect from short-range correlations the EOS has been determined for symmetric nuclear matter and for pure neutron matter, respectively, applying chiral EFT in a Brueckner-Hartree-Fock calculation in comparison to the tree level Hartree-Fock approximation. Though at NLO we observe a saturating behavior within the Brueckner-Hartree-Fock approach (in agreement with other chiral EFT approaches [126, 128]) the binding energy as well as the corresponding equilibrium density are overestimated in symmetric nuclear matter. At N^{3}LO strong over-binding due to the suppression of the hard core by high-momentum cut-offs is observed. Therefore the inclusion of higher order terms in density might open a promising perspective also for EFT potentials when applied to the nuclear many-body problem.

The EOS for neutron matter appears to be unbound at NLO and N^{3}LO where at the order N^{3}LO the EOS agrees qualitatively with most of the state-of-the-art many-body calculations.

The symmetry energy at NLO exhibits a down-bending behavior above the saturation density as observed within the chiral in-medium approach of Ref. [128] whereas at N^{3}LO a good agreement is found when compared to the Argonne v_{18}

interaction within the same approach as well as to variational calculations [117].

In this thesis also nuclear bulk properties have been studied in the chiral limit $m_\pi \to 0$ based on chiral effective field theory. This concerns both, the EOS (in Hartree-Fock and Brueckner-Hartree-Fock) as well as scalar and vector self-energy fields in matter. The essential ingredient in the present investigations is the chiral EFT nuclear force where the implicit and explicit pion mass dependence is known analytically up to NLO and allows a well defined extrapolation in the pion mass [20].

We found that nuclear bulk properties remain fairly stable in the chiral limit. The magnitude of the scalar and vector mean fields persists in the chiral limit as well as for larger pion masses than the physical one. In the chiral limit nuclear matter still appears to be bound at NLO though the binding energy and saturation density are decreased. This is also true in case of an extrapolation to larger pion masses than the physical where the binding energy and saturation density are increased. Uncertainties due to not completely constrained LECs have also been considered but a qualitative change concerning the properties of the EOS in the chiral limit has not been found.

Like in OBE models and RMF theory, in EFT the reduction of the nucleon mass $M^* = M + \Sigma_\mathrm{s}$ is driven by short-distance physics. Long-distance physics from virtual pions, i.e. the non-analytic term in the expansion of σ_N gives a sizable contribution to the modification of the in-medium quark condensate. Such contributions are, however, found to play only a minor role for the reduction of the nucleon mass. Nevertheless, at moderate nuclear densities the $\mathrm{N^3LO}$ scalar and vector fields agree almost perfectly with the prediction from leading order QCD sum rules.

Since this agreement is not understood in the present work the density dependence of the chiral order parameter or scalar quark condensate in nuclear matter has been calculated making use of the Hellmann-Feynman theorem which relates the scalar quark condensate with the current quark mass derivative of the nuclear energy density. In a first step the energy density was calculated in Hartree-Fock approximation. However, to be more realistic and to include also short range correlations also the Brueckner-Hartree-Fock approximation has been applied. Since the quark mass dependence of the chiral NN interaction is known up to NLO this approach is free from any ambiguities which arise concerning the analytic and chiral structure of the potential. The quark mass dependence of the pion-nucleon coupling constant $g_{\pi N}$ has thereby been taken into account and was found to be important. Uncertainties due to unknown low-energy constants entering the pion-nucleon coupling constant $g_{\pi N}$ do not change the results qualitatively.

Higher order corrections from the nucleon kinetic and interaction energy become significantly more important above saturation density when compared to the model independent leading order prediction for the scalar quark condensate.

They lead in general to a weaker reduction of the in-medium quark condensate and do not indicate a complete restoration of chiral symmetry in the density range where hadronic models are reliable. Since Hartree-Fock and Brueckner-Hartree-Fock provide quantitatively comparable results one can conclude that short-range correlations and quenching effects, both present in Brueckner theory, have only minor implications for the density dependence of the quark condensate. The substantial contributions from nucleon interactions are due to low-momentum virtual pions, i.e., OPE and TPE. Short-distance physics in terms of contact terms and short-range correlations have no important impact on the in-medium properties of the quark condensate.

The present formalism allows also to perform a consistent comparison of the in-medium scalar condensate, derived directly from the Hellmann-Feynman theorem, and the effective nucleon mass $M^* = M + \Sigma_s$ where the scalar self-energy Σ_s enters. For the first time both quantities were derived from the same chiral EFT interaction and at the same order. In general the effective nucleon mass calculated in the many-body approach is already smaller ($\approx 10\%$ at ρ_0) then the model independent leading order prediction which is used in the QCD sum rule approach.

Moreover, a *decoupling of the effective nucleon mass and the scalar condensate* is observed in the present investigations. It turns out, that the reduction of the two quantities, namely the in-medium condensate and the in-medium nucleon mass, are of different physical origin. While the latter is generated dominantly by short distance physics in terms of NLO contact interactions [62] virtual low-momentum pions provide the essential contributions responsible for the change of the in-medium scalar quark condensate.

A. Notation and conventions

The system of units used in this work are the natural units:

$$\hbar \ = c \ = \ 1 \ . \tag{A.1}$$

The metric $g^{\mu\nu}$ of Minkowski space is given by

$$g^{\mu\nu} = g_{\mu\nu} = diag(+1, -1, -1, -1) \ . \tag{A.2}$$

The covariant and contravariant vectors are then given as

$$x^{\mu} = (t, \mathbf{x}) \quad , \quad x_{\mu} = (t, -\mathbf{x}) \tag{A.3}$$

and the partial derivatives correspondingly

$$\partial^{\mu} = \frac{\partial}{\partial x_{\mu}} = (\partial_t, -\nabla) \quad , \quad \partial_{\mu} = \frac{\partial}{\partial x^{\mu}} = (\partial_t, +\nabla) \ . \tag{A.4}$$

For the Dirac matrices the representation

$$\gamma^0 \ = \ \begin{pmatrix} 1 & 0 \\ 0 & -1 \end{pmatrix} \ , \qquad \gamma^k \ = \ \begin{pmatrix} 0 & \sigma_k \\ -\sigma_k & 0 \end{pmatrix} \tag{A.5}$$

is used where the σ_k $(k = 1, 2, 3)$ are the conventional Pauli matrices

$$\sigma_1 \ = \ \begin{pmatrix} 0 & 1 \\ 1 & 0 \end{pmatrix} \ , \qquad \sigma_2 \ = \ \begin{pmatrix} 0 & -i \\ i & 0 \end{pmatrix} \ , \qquad \sigma_3 \ = \ \begin{pmatrix} 1 & 0 \\ 0 & -1 \end{pmatrix} \ . \tag{A.6}$$

The defining property for the γ-matrices to form a Clifford algebra is the anti-commutation relation

$$[\gamma_{\mu}, \gamma_{\nu}] = 2g_{\mu\nu} \ . \tag{A.7}$$

The free spinors for positive and negative energy states, u_{λ} and v_{λ}, forming a basis are defined as in Ref. [157] where λ is the helicity index. Conjugated spinors are defined as

$$\begin{aligned} \bar{u} \ &= \ u^{\dagger}\gamma_0 \\ \bar{v} \ &= \ v^{\dagger}\gamma_0 \ . \end{aligned} \tag{A.8}$$

The positive energy spinors are normalized to one and therefore one obtains

$$\sum_{\lambda,\lambda'} \bar{u}_\lambda u_{\lambda'} = \delta_{\lambda,\lambda'} \tag{A.9}$$

$$\sum_{\lambda,\lambda'} \bar{u}_\lambda \gamma^\mu u_{\lambda'} = \frac{k^\mu}{M} \delta_{\lambda,\lambda'} \quad . \tag{A.10}$$

Correspondingly one obtains expressions for the in-medium spinors u^*_λ

$$\sum_{\lambda,\lambda'} \bar{u}^*_\lambda u^*_{\lambda'} = \delta_{\lambda,\lambda'} \tag{A.11}$$

$$\sum_{\lambda,\lambda'} \bar{u}^*_\lambda \gamma^\mu u^*_{\lambda'} = \frac{k^{*\mu}}{M^*} \delta_{\lambda,\lambda'} \quad . \tag{A.12}$$

B. Momentum space OBEP

In this section the explicit expressions for the OBE potentials in the non-relativistic representation in momentum space are displayed.

Exemplary the derivation for the scalar meson (e.g. σ) exchange potential is shown. Starting from the Lagrangian Eq. (3.2)

$$\mathcal{L}_{\mathrm{NNs}} = -g_s\, \bar{\psi}\psi\varphi_{\mathrm{s}} \tag{B.1}$$

the Born term Feynman amplitude is given by

$$-i\mathcal{A}_s(q',q) = \bar{u}_1(\mathbf{q}')\kappa_s^{(1)}u_1(\mathbf{q})\; D_s(q'-q)\; \bar{u}_2(-\mathbf{q}')\kappa_s^{(2)}u_2(-\mathbf{q}). \tag{B.2}$$

where $\kappa_s = g_s\mathbf{1}$. The momentum transfer

$$\mathbf{k} = \mathbf{q}' - \mathbf{q}$$

and the centre-of-mass momentum is introduced

$$\mathbf{P} = \frac{1}{2}(\mathbf{q}+\mathbf{q}')\,.$$

Furthermore the momentum vector

$$\mathbf{n} = \mathbf{q}\times\mathbf{q}' \equiv \mathbf{P}\times\mathbf{k}$$

is defined.

The potential is then obtained by introducing the following approximations

- The meson propagators D_α, Eqs. (3.6, 3.7) are approximated by their static form $(-1)/(\mathbf{k}^2+m^2)$
- The energy E is expanded in $\mathbf{k}^2$ and $\mathbf{P}^2$

$$E(\mathbf{q}) = \sqrt{\frac{\mathbf{k}^2}{4}+\mathbf{P}^2+M^2} \simeq M + \frac{\mathbf{k}^2}{8M} + \frac{\mathbf{P}^2}{2M}. \tag{B.3}$$

- Terms to leading order in $\mathbf{k}^2/M^2$ and $\mathbf{P}^2/M^2$ are taken into account.

The scalar exchange potential $V^{\rm s}$ for σ and δ mesons is then obtained by evaluating i times the Feynman amplitude Eq. (B.2) where the vertex function for particle $i = 1$ is given by

$$\begin{aligned}
\bar{u}_1(\mathbf{q}\,')\kappa_s^{(1)}u_1(\mathbf{q}\,) &= -ig_s u_1^\dagger(\mathbf{q}\,')\,\gamma_0\,u_1(\mathbf{q}\,) \\
&= -ig_s\sqrt{\frac{(E'+M)\,(E+M)}{4M^2}}\left(1,\ \frac{-\boldsymbol{\sigma}\cdot\mathbf{q}\,'}{E'+M}\right)\begin{pmatrix} 1 \\ \frac{\boldsymbol{\sigma}\cdot\mathbf{q}}{E+M}\end{pmatrix} \\
&= -ig_s\frac{E+M}{2M}\left(1-\frac{\mathbf{q}\,'\cdot\mathbf{q}+i\,\boldsymbol{\sigma}_1\cdot(\mathbf{q}\,'\times\mathbf{q})}{(E+M)^2}\right) \qquad \text{(B.4)}
\end{aligned}$$

The following relation is used in the above derivation

$$(\boldsymbol{\sigma}\cdot\mathbf{a})(\boldsymbol{\sigma}\cdot\mathbf{b}) = \mathbf{a}\cdot\mathbf{b} + i\,\boldsymbol{\sigma}\cdot(\mathbf{a}\times\mathbf{b})\ .$$

Applying the approximation $E \approx M$ one obtains

$$\begin{aligned}
V^{\rm s}(\mathbf{k},\mathbf{P}) &= \frac{-g_{\rm s}^2}{\mathbf{k}^2+m_{\rm s}^2}\left(1-\frac{\mathbf{q}\,'\cdot\mathbf{q}+i\,\boldsymbol{\sigma}_1\cdot(\mathbf{q}\,'\times\mathbf{q})}{(E+M)^2}\right) \\
&\qquad\times\left(1-\frac{\mathbf{q}\,'\cdot\mathbf{q}+i\,\boldsymbol{\sigma}_2\cdot(\mathbf{q}\,'\times\mathbf{q})}{(E+M)^2}\right) \\
&= \frac{-g_{\rm s}^2}{\mathbf{k}^2+m_{\rm s}^2}\left(1-\frac{\mathbf{P}^2-\frac{1}{4}\mathbf{k}^2+i\,\boldsymbol{\sigma}_1\cdot(\mathbf{q}\,'\times\mathbf{q})}{4M^2}\right) \\
&\qquad\times\left(1-\frac{\mathbf{P}^2-\frac{1}{4}\mathbf{k}^2+i\,\boldsymbol{\sigma}_2\cdot(\mathbf{q}\,'\times\mathbf{q})}{4M^2}\right) \\
&= \frac{-g_{\rm s}^2}{\mathbf{k}^2+m_{\rm s}^2}\left(1-\frac{\mathbf{P}^2}{2M^2}+\frac{\mathbf{k}^2}{8M^2}-\frac{i\,(\boldsymbol{\sigma}_1+\boldsymbol{\sigma}_2)\cdot(\mathbf{q}\,'\times\mathbf{q})}{4M^2}+\ldots\right)
\end{aligned}$$

Keeping only the lowest order terms one arrives at

$$V^{\rm s}(\mathbf{k},\mathbf{P}) = \frac{-g_{\rm s}^2}{\mathbf{k}^{\,2}+m_{\rm s}^2}\left(1-\frac{\mathbf{P}^2}{2M^2}+\frac{\mathbf{k}^2}{8M^2}+\frac{\frac{i}{2}\,(\boldsymbol{\sigma}_1+\boldsymbol{\sigma}_2)\cdot\mathbf{n}}{2M^2}\right) \qquad \text{(B.5)}$$

As already described in chapter 3.2.1 the OBE potential can be written as

$$V = \sum_i [V_i + V_i'\,\boldsymbol{\tau}_1\cdot\boldsymbol{\tau}_2]\ O_i\ . \qquad \text{(B.6)}$$

The operators which are kept normally in this expansion are given by

$$\begin{aligned} O_1 &= \mathbf{1}\,, \\ O_2 &= \boldsymbol{\sigma}_1\cdot\boldsymbol{\sigma}_2\,, \\ O_3 &= (\boldsymbol{\sigma}_1\cdot\mathbf{k})(\boldsymbol{\sigma}_2\cdot\mathbf{k})\,, \\ O_4 &= \tfrac{i}{2}(\boldsymbol{\sigma}_1+\boldsymbol{\sigma}_2)\cdot\mathbf{n}\,, \\ O_5 &= (\boldsymbol{\sigma}_1\cdot\mathbf{n})(\boldsymbol{\sigma}_2\cdot\mathbf{n})\,. \end{aligned} \tag{B.7}$$

Thus for the scalar meson exchange, i.e., σ, δ mesons, the potential forms V_i are given by

$$\begin{aligned} V_1^{\rm s} &= -\frac{g_{\rm s}^2}{\mathbf{k}^{\,2}+m_{\rm s}^2}\left(1-\frac{\mathbf{P}^2}{2M^2}+\frac{\mathbf{k}^2}{8M^2}\right) \\ V_4^{\rm s} &= -\frac{g_{\rm s}^2}{2M^2}\frac{1}{\mathbf{k}^{\,2}+m_{\rm s}^2} \\ V_5^{\rm s} &= \frac{g_{\rm s}^2}{16M^4}\frac{1}{\mathbf{k}^{\,2}+m_{\rm s}^2}\,. \end{aligned} \tag{B.8}$$

The corresponding potential form for pseudo-scalar mesons π, η is

$$V_3^{\rm ps} = -\frac{g_{\rm ps}^2}{4M^2}\,\frac{1}{\mathbf{k}^2+m_{\rm ps}^2}\,, \tag{B.9}$$

and finally for the vector mesons ω, ρ

$$\begin{aligned} V_1^{\rm v} &= \frac{1}{\mathbf{k}^2+m_{\rm v}^2}\left\{g_{\rm v}^2\left(1+\frac{3\mathbf{P}^2}{2M^2}-\frac{\mathbf{k}^2}{8M^2}\right)-\frac{g_{\rm v}g_{\rm T}\mathbf{q}^2}{2M^2}+\frac{g_{\rm T}^2\mathbf{q}^4}{16M^2}\right\} \\ V_2^{\rm v} &= -\mathbf{q}^2\,V_3^{\rm v} \\ V_3^{\rm v} &= \frac{1}{4M^2}\frac{1}{\mathbf{k}^{\,2}+m_{\rm v}^2}\left[(g_{\rm v}+g_{\rm T})^2-\frac{g_{\rm v}\mathbf{q}^2}{8M^2}\right] \\ V_4^{\rm v} &= -\frac{1}{M^2}\frac{1}{\mathbf{k}^{\,2}+m_{\rm v}^2}\left[\frac{2}{3}g_{\rm v}^2+2g_{\rm v}g_{\rm T}-\frac{3g_{\rm T}^2\mathbf{q}^2}{8M^2}\right] \\ V_5^{\rm v} &= -\frac{1}{16M^2}\frac{1}{\mathbf{k}^{\,2}+m_{\rm v}^2}\left[g_{\rm v}^2+8g_{\rm v}g_{\rm T}+8g_{\rm T}^2\right]\,. \end{aligned} \tag{B.10}$$

In case of isovector meson exchange the potentials have to be multiplied by $\boldsymbol{\tau}_1\cdot\boldsymbol{\tau}_2$.

In case of the pseudo-scalar potential, e.g., one also finds, that on-shell, i.e., for $|\mathbf{q}|' = |\mathbf{q}|$, the field-theoretic potential amplitude $\mathcal{A}_{\rm ps}$ equals $V^{\rm ps}$. That means, that the nonlocality of the full field-theoretic Feynman amplitude influences the potential off-shell.

The resulting expressions for the OBE potentials, Eqs. (B.9-B.11), can now analytically be Fourier transformed to obtain the potential in coordinate space where the general form of the operators equivalent to the momentum operators, Eq. (B.8) is displayed in chapter 3.2.1.

C. Scalar quark condensate in matter

The in-medium quark condensate can be related to the energy density $\mathcal{E}$ in nuclear matter by applying the Hellmann-Feynman theorem. The Hellmann-Feynman theorem [158, 159] states that

$$\langle\psi(\lambda)|\frac{d}{d\lambda}H(\lambda)|\psi(\lambda)\rangle = \frac{d}{d\lambda}E(\lambda) \tag{C.1}$$

if $H(\lambda)$ is a Hermitian operator that depends on a real parameter λ and $\psi(\lambda)$ is a normalized eigenvector of $H(\lambda)$ with eigenvalue $E(\lambda)$

$$H(\lambda)|\psi(\lambda)\rangle = E(\lambda)|\psi(\lambda)\rangle, \qquad \langle\psi(\lambda)|\psi(\lambda)\rangle = 1. \tag{C.2}$$

Rewriting Eq. (C.1) one then obtains

$$\langle\psi(\lambda)|\frac{d}{d\lambda}H(\lambda)|\psi(\lambda)\rangle = \frac{d}{d\lambda}\langle\psi(\lambda)|H(\lambda)|\psi(\lambda)\rangle\,. \tag{C.3}$$

Explicit chiral symmetry breaking in the QCD Hamiltonian density

$$\mathcal{H}_{\rm QCD} = \mathcal{H}_0 + \mathcal{H}_{\rm m} \tag{C.4}$$

is induced by the current quark mass terms. $\mathcal{H}_0$ denotes the chirally invariant part and $\mathcal{H}_{\rm m}$ is given by

$$\mathcal{H}_{\rm m} = m_u\,\bar{u}u + m_d\,\bar{d}d + \cdots \tag{C.5}$$

where m_u and m_d denote the up-, and downquark current quark masses and u and d the corresponding fields, and $\cdots$ are contributions from heavier quarks which are neglected. Introducing $\bar{q}q \equiv \frac{1}{2}(\bar{u}u + \bar{d}d)$ and $m_q \equiv \frac{1}{2}(m_u + m_d)$ and $\delta m_q = m_d - m_u$ the current quark mass term $\mathcal{H}_{\rm m}$ can be rewritten

$$\mathcal{H}_{\rm m} = 2m_q\,\bar{q}q - \frac{1}{2}\delta m_q(\bar{u}u - \bar{d}d) + \cdots \tag{C.6}$$

where the isospin-breaking term is separated. Since good isospin is assumed the isospin-breaking terms are neglected. Identifying λ with the current quark mass

m_q and $H(\lambda)$ with $\int d^3x\, \mathcal{H}_{\mathrm{QCD}}$ in the Hellmann-Feynman theorem, Eq. (C.3), one obtains

$$2m_q\langle\psi(m_q)|\int d^3x\, \bar{q}q|\psi(m_q)\rangle = m_q\frac{d}{dm_q}\langle\psi(m_q)|\int d^3x\, \mathcal{H}_{\mathrm{QCD}}|\psi(m_q)\rangle\,. \quad \text{(C.7)}$$

Both side have been multiplied by m_q in order to make them renormalization-group invariant.

Now one considers two cases for which Eq. (C.7) can be evaluated, namely $|\psi(m_q)\rangle = |\rho_B\rangle$ and $|\psi(m_q)\rangle = |0\rangle$ in Eq. (C.7). $|0\rangle$ represents the vacuum state and $|\rho_B\rangle$ represents the ground state of nuclear matter with baryon density ρ_B. Taking the difference of these two cases one obtains

$$2m_q(\langle\bar{q}q\rangle_{\rho_B} - \langle\bar{q}q\rangle_0) = m_q\frac{d}{dm_q}\left(\mathcal{E}(\rho_N) - \mathcal{E}(0)\right)\,. \quad \text{(C.8)}$$

The derivate is taken at fixed density. The short notation $\langle\Omega\rangle_{\rho_B} = \langle\rho_B|\Omega|\rho_B\rangle$ and $\langle\Omega\rangle_0 = \langle 0|\Omega|0\rangle$ has been introduced, where Ω is an arbitrary operator.

Bibliography

[1] J.Chadwick, *The Existence of a Neutron*,
Proc. Roy. Soc. (London) A 136 (1932) 692.

[2] H. Yukawa, *On the Interaction of Elementary Particles. I.*,
Proc. Phys. Math. Soc. Japan 17 (1935) 48.

[3] A. Proca, *Sur la théorie ondulatoire des électrons positifs et négatifs*, J. Phys. Radium 7 (1936) 347.

[4] N. Kemmer, *Quantum Theory of Einstein-Bose Particles and Nuclear Interaction*, Proc. Roy. Soc. (London) A 166 (1938) 127.

[5] J. Schwinger, *On a field theory of nuclear forces*, Phys. Rev. 61 (1942) 387.

[6] W. Pauli, *Meson Theory of Nuclear Forces*, (Interscience, New York, 1946).

[7] M. Taketani, S. Nakamura, and M. Sasaki, *On the Method of the Theory of Nuclear Forces*, Prog. Theor. Phys. (Kyoto) 6 (1951) 581.

[8] J. L. Gammel and R. M. Thaler, *Spin-Orbit Coupling in the Proton-Proton Interaction*, Phys. Rev. 107 (1957) 291; *Spin-Orbit Coupling in the Neutron-Proton Interaction*, Phys. Rev. 107 (1957) 1337.

[9] G. Breit, *The Nucleon-Nucleon Spin-Orbit Potential*,
Proc. Natl. Acad. Sci. (U.S.) 46 (1960) 746.

[10] Y. Nambu, *Possible Existence of a Heavy Neutral Meson*,
Phys. Rev. 106 (1957) 1366.

[11] J. J. Sakurai, *Theory of strong interactions*, Ann. Phys. (N.Y.) 11 (1960) 1; *Spin-Orbit Force and a Neutral Vector Meson*, Phys. Rev. 119 (1960) 1784.

[12] R. Machleidt, K. Holinde and Ch. Elster, *The bonn meson-exchange model for the nucleon-nucleon interaction*, Phys. Rep. 149 (1987) 1.

[13] D.R. Entem, F. Fernandez, and A. Valcarce, *Chiral quark model of the NN system within a Lippmann-Schwinger resonating group method*,
Phys. Rev. C 62 (2000) 034002.

[14] G.H. Wu *et al.*, *Quark delocalization, color screening model and nucleon-baryon scattering*, Nucl. Phys. A 673 (2000) 279.

[15] S. Weinberg, *Phenomenological Lagrangians*, Physica 96 A (1979) 327.

[16] S. Weinberg, *Nuclear forces from chiral lagrangians* Phys. Lett. B 251 (1990) 288; *Effective chiral lagrangians for nucleon-pion interactions and nuclear forces*, Nucl. Phys. B 363 (1991) 3.

[17] E. Epelbaum, W. Glöckle, and U.-G. Meissner, *The two-nucleon system at next-to-next-to-next-to-leading order*, Nucl. Phys. A 747 (2005) 362.

[18] D.R. Entem and R. Machleidt, *Chiral 2 π exchange at fourth order and peripheral NN scattering*, Phys. Rev. C 66 (2002) 014002.

[19] D.R. Entem and R. Machleidt, *Accurate charge-dependent nucleon-nucleon potential at fourth order of chiral perturbation theory*,
Phys. Rev. C 68 (2003) 041001.

[20] E. Epelbaum, Ulf-G. Meissner and W. Gloeckle, *Nuclear forces in the chiral limit*, Nucl. Phys. A 714 (2003) 535.

[21] S. R. Beane and M. J. Savage, *The quark-mass dependence of two-nucleon systems*, Nucl. Phys. A 717 (2003) 91.

[22] E. Epelbaum, W. Glöckle, Ulf-G. Meissner, *Quark mass dependence of the nuclear force*, Eur. Phys. J. A 18 (2003) 499.

[23] S. Okubo and R. E. Marshak, *Velocity dependence of the two-nucleon interaction*, Ann. Phys. 4 (1958) 166.

[24] R.B. Wiringa, R.A. Smith, and T.L. Ainsworth *Nucleon-nucleon potentials with and without* $\Delta(1232)$ *degrees of freedom*, Phys. Rev. C 29 (1984) 1207.

[25] R.B. Wiringa, V.G.J. Stoks, and R. Schiavilla, *Accurate nucleon-nucleon potential with charge-independence breaking*, Phys. Rev. C 51 (1995) 38.

[26] S.K. Bogner, T.T.S. Kuo, and A. Schwenk, *Model-independent low momentum nucleon interaction from phase shift equivalence*,
Phys. Rep. 386 (2003) 1.

[27] B. D. Serot, J. D. Walecka, *Advances in Nuclear Physics, 16, 1,* eds. J. W. Negele, E. Vogt, (Plenum, N.Y., 1986).

[28] P. Ring, *Relativistic mean field theory in finite nuclei*,
Prog. Part. Nucl. Phys. 37 (1996) 193.

[29] A. Arima, M. Harvey, and K. Shimizu, *Pseudo LS coupling and pseudo SU_3 coupling schemes*, Phys. Lett. B 30 (1969) 517.

[30] J.N. Ginocchio, *Pseudospin as a Relativistic Symmetry*, Phys. Rev. Lett. 78 (1997) 436.

[31] A.V. Afanasjev, J. König, and P. Ring, *Cranked relativistic mean field description of superdeformed bands in ^{83}Sr*, Phys. Lett. B 367 (1996) 11.

[32] K.A. Brueckner, J.L. Gammel, *Properties of Nuclear Matter*, Phys. Rev. 109 (1958) 1023.

[33] M. R. Anastasio, L. S. Celenza, W. S. Pong and C. M. Shakin, *Relativistic nuclear structure physics*, Phys. Rep. 100 (1983) 327.

[34] B. ter Haar and R. Malfliet, *Nucleons, mesons and deltas in nuclear matter a relativistic Dirac-Brueckner approach*, Phys. Rep. 149 (1987) 207.

[35] R. Brockmann and R. Machleidt, *Relativistic nuclear structure. I. Nuclear matter*, Phys. Rev. C 42 (1990) 1965.

[36] T. Gross-Boelting, C. Fuchs, and Amand Faessler, *Covariant representations of the relativistic Brueckner T-matrix and the nuclear matter problem*, Nucl. Phys. A 648 (1999) 105.

[37] E. Schiller and H. Müther, *Correlations and the Dirac structure of the nucleon self-energy*, Eur. Phys. J. A 11 (2001) 15.

[38] E. N. E. van Dalen, C. Fuchs, and A. Faessler, *The relativistic Dirac-Brueckner approach to asymmetric nuclear matter*, Nucl. Phys. A 744 (2004) 227.

[39] E. N. E. van Dalen, C. Fuchs, and A. Faessler, *Momentum, density, and isospin dependence of symmetric and asymmetric, nuclear matter properties*, Phys. Rev. C 72 (2005) 065803.

[40] G.E. Brown, J.H. Gunn, and P. Gould, *Effective mass in nuclei*, Nucl. Phys. 46 (1963) 598.

[41] J. P. Jeukenne, A. Lejeune, and C. Mahaux, *Many-body theory of nuclear matter*, Phys. Rep. 25 (1976) 83.

[42] C. Mahaux, P.F. Bortignon, R.A. Broglia, and C.H. Dasso, *Dynamics of the shell model*, Phys. Rep. 120 (1985) 1.

[43] T.D. Cohen, R.J. Furnstahl and D.K. Griegel, *From QCD Sum Rules to Relativistic Nuclear Physics*, Phys. Rev. Lett. 67 (1991) 961.

[44] R.J. Furnstahl, D.K. Griegel and T.D. Cohen, *QCD sum rules for nucleons in nuclear matter*, Phys. Rev. C 46 (1992) 1507.

[45] E.G. Drukarev, and E.M. Levin, *Structure of nuclear matter and QCD sum rules*, Prog. Part. Nucl. Phys. 27 (1991) 77.

[46] P. Finelli, N. Kaiser, D. Vretenar and W. Weise, *Nuclear many-body dynamics constrained by QCD and chiral symmetry*,
Eur. Phys. J. A 17 (2003) 573.

[47] *Relativistic nuclear model with point-couplings constrained by QCD and chiral symmetry*, Nucl. Phys. A 735 (2004) 449.

[48] J. Kuckei, F. Montani, H. Müther, and A. Sedrakian, *The structure of nuclear systems derived from low momentum nucleon-nucleon potentials*, Nucl. Phys. A 723 (2003) 32.

[49] B.L. Ioffe, *Calculation of baryon masses in quantum chromodynamics*,
Nucl. Phys. B 188 (1981) 317.

[50] W. Weise, *Nucleons and nuclei in the context of low-energy QCD*,
Nucl. Phys. A 751 (2005) 565c.

[51] T.D. Cohen, R.J. Furnstahl and D.K. Griegel, *Quark and gluon condensates in nuclear matter*, Phys. Rev. C 45 (1992) 1881.

[52] S. Klimt, M. Lutz, and W. Weise, *Chiral phase transition in the SU(3) Nambu and Jona-Lasinio model*, Phys. Lett. B 249 (1990) 386.

[53] K. Tsushima, T. Maruyama, and A. Faessler, *Temperature and density dependence of quark dynamical properties: Application of"thermo field dynamics" to the SU(3) NJL model with instanton effects*,
Nucl. Phys. A 535 (1991) 497.

[54] T. Maruyama, K. Tsushima, and A. Faessler, *Chiral phase transition and dynamical properties of quarks at finite temperature and density: Application of the "thermo-field dynamics" to the SU(3) Nambu-Jona-Lasinio model with instanton effects*, Nucl. Phys. A 537 (1992) 303.

[55] G. Chanfray and M. Ericson, *QCD susceptibilities and nuclear-matter saturation in a relativistic chiral theory*, Eur. Phys. J. A 25 (2005) 151.

[56] G. Chanfray and M. Ericson, *QCD susceptibilities and nuclear matter saturation in a chiral theory: inclusion of pion loops*,
Phys. Rev. C 75 (2007) 015206.

[57] K. Saito, K. Tsushima, and A. W. Thomas, *Nucleon and hadron structure changes in the nuclear medium and impact on observables*, Prog. Part. Nucl. Phys. 58 (2007) 1.

[58] C. Ratti, M. A. Thaler, and W. Weise, *Phases of QCD: Lattice thermodynamics and a field theoretical model*, Phys. Rev. D 73 (2006) 014019.

[59] R. Brockmann and W. Weise, *The chiral condensate in nuclear matter*, Phys. Lett. B 367 (1996) 40.

[60] G.Q. Li and C.M. Ko, *Quark condensate in nuclear matter*, Phys. Lett. B 338 (1994) 118.

[61] C. Fuchs, *The high density equation of state: constraints from accelerators and astrophysics*, arXiv:0711.3367 [nucl-th].

[62] O. Plohl and C. Fuchs, *Relativistic self-energy in nuclear dynamics*, Phys. Rev. C 74 (2006) 034325.

[63] M. Birse, *What does a change in the quark condensate say about restoration of chiral symmetry in matter?*, Phys. Rev. C 53 (1996) R2048.

[64] G. Chanfray, M. Ericson, and P.A.M. Guichon, *Chiral symmetry and quantum hadrodynamics*, Phys. Rev. C 63 (2001) 055202.

[65] V.G.J. Stoks, R.A.M. Klomp, C.P.F. Terheggen, and J.J. de Swart, *Construction of high-quality NN potential models*, Phys. Rev. C 49 (1994) 2950.

[66] P. Ring, *Covariant Density Functional Theory and Applications to Finite Nuclei*, Lect. Notes Phys. 641 (2004) 175.

[67] W. Kohn, *Nobel Lecture: Electronic structure of matter - wave functions and density functionals*, Rev. Mod. Phys., Vol. 71, No. 5, 1253 (1999) and refs. therein.

[68] R. Dreizler, E. Gross, *Density Functional Theory*, Plenum Press, New York (1995).

[69] P. Hohenberg and W. Kohn, *Inhomogeneous Electron Gas*, Phys. Rev. B 136 (1964) 864.

[70] J. D. Walecka, *A theory of highly condensed matter*, Ann. Phys. 83 (1974) 497.

[71] H. P. Dürr, *Relativistic Effects in Nuclear Forces*, Phys. Rev. 103 (1956) 469.

[72] F. Coester, S. Cohen, B.D. Day, and C.M. Vincent, *Variation in Nuclear-Matter Binding Energies with Phase-Shift-Equivalent Two-Body Potentials*, Phys. Rev. C 1 (1970) 769.

[73] C. Fuchs and H.H. Wolter, *Modelization of the EOS*, Eur. Phys. J. A 30 (2006) 5.

[74] C. J. Horowitz and Brian D. Serot, *Properties of nuclear and neutron matter in a relativistic Hartree-Fock theory*, Nucl. Phys. A 399 (1983) 529.

[75] C. J. Horowitz and Brian D. Serot, *Two-nucleon correlations in a relativistic theory of nuclear matter*, Phys. Lett. B 137 (1984) 287.

[76] P. C. Martin and J. Schwinger, *Theory of Many-Particle Systems. I*, Phys. Rev. 115 (1959) 1342.

[77] W. Botermans and R. Malfliet, *Quantum transport theory of nuclear matter*, Phys. Rep. 198 (1990) 115.

[78] J. D. Bjorken, S. D. Drell, *Rel. Quantenmechanik*, (BI Taschenbuch Nr. 101, Mannheim, 1965).

[79] C. J. Horowitz and Brian D. Serot, *The relativistic two-nucleon problem in nuclear matter*, Nucl. Phys. A 464 (1987) 613.

[80] L. Sehn, C. Fuchs, and A. Faessler, *Nucleon self-energy in the relativistic Brueckner approach*, Phys. Rev. C 56 (1997) 216.

[81] M. A. Shifman, A. I. Vainshtein, and V. I. Zakharov, *QCD and resonance physics. theoretical foundations*, Nucl. Phys. B 147 (1979) 385.

[82] M. A. Shifman, A. I. Vainshtein, and V. I. Zakharov, *QCD and resonance physics. applications*, Nucl. Phys. B 147 (1979) 448.

[83] L. J. Reinders, H. Rubinstein, and S. Yazaki, *Hadron properties from QCD sum rules*, Phys. Rep. 127 (1985) 1.

[84] J. Gasser and H. Leutwyler, *Quark masses*, Phys. Rep. 87 (1982) 77.

[85] J. Gasser, H. Leutwyler, and M. E. Sainio, *Sigma-term update*, Phys. Lett. B 253 (1991) 252.

[86] R. Machleidt, *The Meson theory of nuclear forces and nuclear structure*, Adv. Nucl. Phys. 19 (1989) 189.

[87] R. Machleidt, *High-precision, charge-dependent Bonn nucleon-nucleon potential*, Phys. Rev. C 63 (2001) 024001.

[88] R. Machleidt and I. Slaus, *The nucleon-nucleon interaction*, J. Phys. G 27 (2001) R69.

[89] H. Müther and A. Polls, *Two-body correlations in nuclear systems*, Prog. Part. Nucl. Phys. 45 (2000) 243.

[90] R. Machleidt, *in: Computational Nuclear Physics 2 — Nuclear Reactions, edited by K. Langanke, J. A. Maruhn, and S. E. Koonin,* (Springer, New York, 1993), Chapter 1, p. 1.

[91] M.M. Nagels, T.A. Rijken, and J.J. de Swart, *Low-energy nucleon-nucleon potential from Regge-pole theory*, Phys. Rev. D 17 (1978) 768.

[92] E. Epelbaum, U. G. Meissner, W. Gloeckle, and C. Elster *Resonance saturation for four-nucleon operators*, Phys. Rev. C 65 (2002) 044001.

[93] R. Machleidt and D. R. Entem, *Recent advances in the theory of nuclear forces*, J. Phys. Conf. Ser. 20 (2005) 77; [arXiv:nucl-th/0608068].

[94] N. Kaiser, *Chiral 3π-exchange NN potentials: Results for representation-invariant classes of diagrams,* Phys. Rev. C 61 (1999) 014003.

[95] N. Kaiser, *Chiral 3π-exchange NN potentials: Results for diagrams proportional to gA^4 and gA^6,* Phys. Rev. C 62 (2000) 024001.

[96] N. Kaiser, *Chiral 3π-exchange NN potentials: Results for dominant next-to-leading-order contributions*, Phys. Rev. C 63 (2001) 044010.

[97] N. Kaiser, *Chiral 2π-exchange NN potentials: Two-loop contributions*, Phys. Rev. C 64 (2001) 057001.

[98] N. Kaiser, *Chiral 2π-exchange NN potentials: Relativistic $1/M^2$ corrections*, Phys. Rev. C 65 (2002) 017001.

[99] S. K. Bogner, T. T. S. Kuo, A. Schwenk, D. R. Entem and R. Machleidt, *Towards a unique low momentum nucleon nucleon interaction,* Phys. Lett. B 576 (2003) 265.

[100] S.K. Bogner, A. Schwenk, R.J. Furnstahl, and A. Nogga, *Is nuclear matter perturbative with low-momentum interactions?*, Nucl. Phys. A 763 (2005) 59.

[101] J. A. Tjon and S. J. Wallace, *Meson theoretical basis for Dirac impulse approximation*, Phys. Rev. C 32 (1985) 267.

[102] J.A. Tjon and S.J. Wallace, *General Lorentz-invariant representation of NN scattering amplitudes*, Phys. Rev. C 32 (1985) 1667.

[103] F. Gross, J.W. van Orden, K. Holinde, *Relativistic one-boson-exchange model for the nucleon-nucleon interaction*, Phys. Rev. C 45 (1992) 2094.

[104] F. Gross and A. Stadler, *High-precision covariant one-boson-exchange potentials for np scattering below 350 MeV*, arXiv:0704.1229 [nucl-th].

[105] B. C. Lehnhart, J. Gegelia, and S. Scherer, *Baryon masses and nucleon sigma terms in manifestly Lorentz-invariant baryon chiral perturbation theory*, J. Phys. G 31 (2005) 89; [arXiv:hep-ph/0412092].

[106] C. Fuchs, T. Waindzoch, A. Faessler, and D.S. Kosov, *Scalar and vector decomposition of the nucleon self-energy in the relativistic Brueckner approach*, Phys. Rev. C 58 (1998) 2022.

[107] K. Erkelenz, *Current status of the relativistic two-nucleon one boson exchange potential*, Phys. Rep. 13 (1974) 191.

[108] M. Rose, *Elementary Theory of Angular Momentum*, (Wiley, New York, 1957).

[109] V.G.J. Stoks, R.A.M. Klomp, M.C.M. Rentmeester, and J.J. de Swart, *Partial-wave analysis of all nucleon-nucleon scattering data below 350 MeV*, Phys. Rev. C 48 (1993) 792.

[110] R.A Arndt *et al.*, SAID, solution of summer 1999 (SM99).

[111] R. Machleidt, *Recent Advances in the Theory of Nuclear Forces and its Impact on Microscopic Nuclear Structure*, arXiv:0710.2940v1 [nucl-th].

[112] C. Fuchs, *The Relativistic Dirac-Brueckner Approach to Nuclear Matter*, Lect. Notes Phys. 641 (2004) 119.

[113] N. Kaiser, *Spin-orbit coupling in nuclei and realistic nucleon-nucleon potentials*, Phys. Rev. C 70 (2004) 034307.

[114] P.-G. Reinhard and M. Bender, *Mean Field: Relativistic versus Nonrelativistic*, Lect. Notes Phys. 641 (2004) 249.

[115] B. Cochet, K. Bennaceur, J. Meyer, P. Bonche, and T. Duguet, *Skyrme forces with extended density dependence*,
Int. J. Mod. Phys. E 13 (2004) 187.

[116] X.R. Zhou, G.F. Burgio, U. Lombardo, H.-J. Schulze, and W. Zuo, *Three-body forces and neutron star structure*, Phys. Rev. C 69 (2004) 018801.

[117] A. Akmal, V.R. Pandharipande, and D.G. Ravenhall, *Equation of state of nucleon matter and neutron star structure*, Phys. Rev. C 58 (1998) 1804.

[118] M.K. Banerjee, and J.A. Tjon, *Role of the tensor force in nuclear matter saturation*, Phys. Rev. C 58 (1998) 2120.

[119] M.K. Banerjee, and J.A. Tjon, *Relativistic and non-relativistic studies of nuclear matter*, Nucl. Phys. A 708 (2002) 303.

[120] B. Friedman and V. R. Pandharipande, *Hot and cold, nuclear and neutron matter*, Nucl. Phys. A 361 (1981) 502.

[121] R. B. Wiringa, V. Fiks, and A. Fabrocini, *Equation of state for dense nucleon matter*, Phys. Rev. C 38 (1988) 1010.

[122] E. Schiller, H. Müther, and P. Czerski, *Pauli exclusion operator and binding energy of nuclear matter*, Phys. Rev. C 59 (1999) 2934.

[123] T. Frick, Kh. Gad, H. Müther, and P. Czerski, *Nuclear self-energy and realistic interactions*, Phys. Rev. C 65 (2002) 034321; Kh.S.A. Hassaneen and H. Müther, *Correlations and spectral functions in asymmetric nuclear matter*, Phys. Rev. C 70 (2004) 054308.

[124] E. N. E. van Dalen, C. Fuchs, and A. Faessler, *Effective Nucleon Masses in Symmetric and Asymmetric Nuclear Matter*,
Phys. Rev. Lett. 95 (2005) 022302.

[125] M. Baldo and A.Fiasconaro, *Single particle spectrum and binding energy of nuclear matter*, Phys. Lett. B 491 (2000) 240.

[126] P. Saviankou, S. Krewald. E.Epelbaum, and Ulf-G. Meissner, *Saturation of nuclear matter in effective field theory*, arXiv:0802.3782v1 [nucl-th].

[127] N. Kaiser, M. Mühlbauer, and W. Weise, *Scales in nuclear matter: Chiral dynamics with pion nucleon form factors*, Eur. Phys. J. A 31 (2007) 53; [arXiv:nucl-th/0610060].

[128] N. Kaiser, S. Fritsch and W. Weise, *Chiral Dynamics and Nuclear Matter*, Nucl. Phys. A 697 (2002) 255.

[129] N. Kaiser, P. de Homont, and W. Weise, *In-medium chiral condensate beyond linear density approximation*, Phys. Rev. C 77, 025204 (2008); arXiv:0711.3154v1 [nucl-th].

[130] D. Vretenar and W. Weise, *Exploring the Nucleus in the Context of Low-Energy QCD,* Lect. Notes Phys. 641 (2004) 65.

[131] C. Ordez, L. Ray, and U. van Kolck, *Nucleon-nucleon potential from an effective chiral Lagrangian*, Phys. Rev. Lett. 72 (1994) 1982.

[132] D.B. Kaplan, M.J. Savage, and M.B. Wise, *Two nucleon systems from effective field theory*, Nucl. Phys. B 534 (1998) 329.

[133] E. Epelbaum, W. Glöckle, and U.-G. Meissner, *Nuclear forces from chiral Lagrangians using the method of unitary transformation. 2. The two nucleon system.* Nucl. Phys. A 671 (2000) 295.

[134] N. Kaiser, R. Brockmann, and W. Weise, *Peripheral nucleon-nucleon phase shifts and chiral symmetry*, Nucl. Phys. A 625 (1997) 758.

[135] W. Zhou, A. Lejeune, U. Lombardo, J. F. Mathiot, *Interplay of three-body interactions in the EOS of nuclear matter*, Nucl. Phys. A 706 (2002) 418.

[136] M. Procura, T. R. Hemmert, and W. Weise, *Nucleon mass, sigma term, and lattice QCD*, Phys. Rev. D 69 (2004) 034505.

[137] G.E. Brown and M. Rho, *Chiral restoration in hot and/or dense matter*, Phys. Rep. 269 (1996) 333.

[138] C. Fuchs, H. Lenske, and H. H. Wolter, *Density dependent hadron field theory*, Phys. Rev. C 52 (1995) 3043.

[139] F. Hofmann, C. M. Keil, and H. Lenske, *Density dependent hadron field theory for asymmetric nuclear matter and exotic nuclei*, Phys. Rev. C 64 (2001) 034314.

[140] E. N. E. van Dalen, C. Fuchs, and A. Faessler, *Dirac-Brueckner-Hartree-Fock calculations for isospin asymmetric nuclear matter based on improved approximation schemes*, Eur. Phys. J. A 31 (2007) 29.

[141] S. Typel and H. H. Wolter, *Relativistic mean field calculations with density-dependent meson-nucleon coupling*, Nucl. Phys. A 656 (1999) 331;

[142] T. Nikšić, D. Vretenar, P. Finelli, and P. Ring, *Relativistic Hartree-Bogoliubov model with density-dependent meson-nucleon couplings*, Phys. Rev. C 66 (2002) 024306.

[143] T. Nikšić, D. Vretenar, and P. Ring, *Relativistic random-phase approximation with density-dependent meson-nucleon couplings*, Phys. Rev. C 66 (2002) 064302.

[144] A. Bulgac, G. A. Miller, and M. Strikman, *Chiral limit of nuclear physics*, Phys. Rev. C 56 (1997) 3307.

[145] R. Thomas, S. Zschocke, and B. Kämpfer, *Evidence for In-Medium Changes of Four-Quark Condensates*, Phys. Rev. Lett. 95 (2005) 232301.

[146] R. Thomas, T. Hilger, and B. Kämpfer, *Four-Quark Condensates in Nucleon QCD Sum Rules*, Nucl. Phys. A 795 (2007) 19.

[147] R. Thomas, S. Zschocke, and B. Kämpfer, *Evidence for In-Medium Changes of Four-Quark Condensates*, Phys. Rev. Lett. 95 (2005) 232301.

[148] T. Becher and H. Leutwyler, *Baryon chiral perturbation theory in manifestly Lorentz invariant form*, Eur. Phys. J. C 9 (1999) 643.

[149] T. Becher and H. Leutwyler, *Low energy analysis of* $\pi N \to \pi N$, J. High Energy Phys. 06 (2001) 017.

[150] R. L. Jaffe and C. L. Korpa, *The pattern of chiral symmetry breaking and the strange quark content of the proton*, Comments Nucl. Part. Phys. 17 (1987) 163.

[151] T. Klähn *et al.*, *Constraints on the high-density nuclear equation of state from the phenomenology of compact stars and heavy-ion collisions*, Phys. Rev. C 74 (2006) 035802.

[152] SAID on-line program, R.A Arndt, R.L. Workman *et al.*, see website http://gwdac.phys.gwu.edu/.

[153] E. Matsinos, *The low-energy constants of the pion-nucleon system*, arXiv:hep-ph/9807395.

[154] R. Koch, *A calculation of low-energy* πN *partial waves based on fixed-t analyticity*, Nucl. Phys. A 448 (1986) 707.

[155] M. Lutz, B. Friman, and Ch. Appel, *Saturation from nuclear pion dynamics*, Phys. Lett. B 474 (2000) 7.

[156] K. Peters, *Hadron Physics at FAIR*, Nucl. Phys. B (Proc. Suppl.) 154 (2006) 35.

[157] C. Itzykson, J. B. Zuber, *Quantum field theory* (Mc Graw-Hill, New York, 1985).

[158] E. Merzbacher, *Quantum Mechanics* (Wiley, New York, 1970), 2nd ed.

[159] C. Cohen-Tannoudji, B. Diu, and F. Laloë, *Quantum Mechanics* (Wiley, New York, 1977), Vol. II.

List of Figures

List of Tables

Talks

1. *Comparison of realistic NN-Potentials on the level of covariant amplitudes*, talk given at "European Graduate School Workshop", October 4-7, 2004, Todtmoos, Germany.

2. *Model independent study of the Dirac structure of nucleon-nucleon interaction*, talk given at "22th Students' Workshop on Electromagnetic Interactions", September 4-9, 2005, Bosen (Saar), Germany.

3. *Model independent study of the Dirac structure of the nucleon-nucleon interaction*, talk given at "European Graduate School Workshop", October 4-7, 2005, Lauterbad, Germany.

4. *Model independent study of the nucleon self-energy in matter*, talk given at "XLIV International winter meeting on NUCLEAR PHYSICS ", January 29-February 05, 2006, Bormio, Italy.

5. *The relativistic self-energy in nuclear dynamics*, talk given at "Predeal International Summer School in Nuclear Physics 2006", August 28-September 09, 2006, Predeal, Romania.

6. *The relativistic self-energy in nuclear dynamics*, talk given at "Graduate School Workshop", September 6-9, 2006, Oberwölz, Austria.

7. *The relativistic self-energy in nuclear dynamics*, talk given at "III Workshop of the Virtual Institute (Dense Hadronic Matter and QCD Phase Transitions)", October 15-17, 2006, Rathen, Germany.

8. *The relativistic self-energy in nuclear dynamics*, talk given at "XXXVIII Arbeitstreffen Kernphysik in Schleching", February 22-March 01, 2007, Schleching, Germany.

9. *The relativistic self-energy in nuclear dynamics*, talk given at "European Graduate School Workshop", September 10-13, 2007, Todtmoos, Germany.

Publications

1. O. Plohl, C. Fuchs and E. N. E. van Dalen,
   Model-independent study of the Dirac structure of the nucleon-nucleon interaction
   Phys. Rev. C 73 (2006) 014003-1-4.

2. O. Plohl, C. Fuchs and A. Faessler,
   Model independent study of the nucleon self-energy in matter
   Presented at 44th International Winter Meeting on Nuclear Physics, Bormio, Italy, 29 Jan - 5 Feb 2006.
   arXiv:nucl-th/0603070.

3. O. Plohl and C. Fuchs,
   Relativistic self-energy in nuclear dynamics
   Phys. Rev. C 74 (2006) 034325-1-20.

4. O. Plohl and C. Fuchs,
   Nuclear matter in the chiral limit and the in-medium chiral condensate
   Nucl. Phys. A 798 (2008) 75-95.

5. O. Plohl and C. Fuchs,
   Nuclear symmetry energy in chiral EFT
   in Vorbereitung.

Lebenslauf

Kontakt

Institut für Theoretische Physik
Eberhard Karls Universität
Auf der Morgenstelle 14
72076 Tübingen
Phone: 07071/303157
E-mail: oliver.plohl@uni-tuebingen.de

Persönliche Daten

Am 22. März 1976 in 73760 Ostfildern-Ruit geboren. Slowenischer Staatsbürger.

Ausbildung

2004-2008: **Eberhard Karls Universität Tübingen**

Promotion **Feb 2004–Jul 2008**

- Institut: Institut für Theoretische Physik
- Thema der Dissertation: "General aspects of the nucleon-nucleon interaction and nuclear matter properties"
- Betreuer: Prof. Christian Fuchs

1997–2003: **Eberhard Karls Universität Tübingen**

Diplom in Physik, Dezember 2003

- Thema der Diplomarbeit: "Agent Based Market Models"
- Betreuer: PD Ralph Bilger

1987–1996: **Otto-Hahn-Gymnasium in Nellingen**

Schulabschluss allgemeinbildendes Abitur

Wissenschaftliche Tätigkeiten

Promotionsstipendiat im Graduiertenkolleg "Hadronen im Vakuum, in Kernen und Sternen" **Aug 2005–Jul 2008**

Wissenschaftlicher Angestellter 2II BAT/2 im Rahmen der Projektförderung für Nachwuchswissenschaftler der Uni Tübingen von Prof. Christian Fuchs **Feb 2004–Jul 2005**

Sonstige Tätigkeiten

Betreuung des Computer-Clusters des Instituts für Theoretische Physik als Systemadministrator **Jul 2004–Jul 2008**

Betreuung des CIP-Pools der Fakultät für Mathematik und Physik als Systemadministrator **Jul 2004–Aug 2007**

Assistent: physikalisches Praktikum für Naturwissenschaftler **Jan 2003–Jan 2004**

Akademische Lehrer

H. Müther, A. Fäßler, T. Gutsche, C. Fuchs, K. Langfeld, F. Gönnenwein, G. Staudt, O. Lutz, P. Grabmayr, R. Kleiner, W.-D. Hartmann, R. P. Hübener, H. Clement, C. Zimmermann, H. Reinhardt, H. Kaul, M. Wolff, O. Eibl, E. Plies, D. Kern, R. Bilger, F. Hasselbach, E. Lindner, F. Nüsslin, E. Schweda.

Danksagung

Vielen gebührt Dank, die mich während meiner Doktorarbeit unterstützt haben.

Mein besonderer Dank gilt meinem Betreuer Prof. Dr. Christian Fuchs, mir die Möglichkeit und Unterstützung auch in Form herausragender Ideen gegeben zu haben, an der in dieser Arbeit vorgestellten Thematik zu forschen. Zudem durfte ich auf zahlreichen internationalen Konferenzen unsere Ergebnisse vorzustellen. Ich danke auch für die finanzielle Unterstützung.
Ich danke Prof. Dr. Dr. h.c. mult. Amand Fäßler, mit dessen Unterstützung ich immer rechnen konnte und für die Motivation, diese Arbeit fertigzustellen.
Ich danke ihm und seinem Nachfolger Prof. Dr. Josef Jochum für die Organisation des internationalen Graduiertenkollegs "Hadrons in Vacuum in Nuclei and Stars", das diese Arbeit finanziell unterstützt hat und mir einen Aufenthalt an der Partneruniversität Basel ermöglichte, aber auch Einblicke in andere Forschungsgebiete der Physik in Form von interessanten Vorträgen und Seminaren anbot.
Prof. Dr. Thomas Gutsche möchte ich für seine außergewöhnliche Hilfsbereitschaft und Ratschläge danken, wie auch Prof. Dr. Herbert Müther für die Bereitstellung des BHF Programms und klärende Gespräche.
Ich danke zudem allen in meiner Arbeitsgruppe und Mitarbeitern des Institutes für das sehr angenehme Arbeitsklima und dem PTWAP Administrationsteam, in dem ich auch mitwirken durfte. Besonders dankbar bin ich Dominik Epple für die Einführung in die Welt der Computer Betreuung.

Allen, die mich unterstützt und mein Leben bisher so wundervoll bereichert haben...
...Tanja, Markus für die gemeinsame Bewältigung der Studien- und Freizeit, Birgit, Sebastian (...), Christoph, Simon, Tobias, Frank, Nils, Miriam ...
Elvira (still missing the espresso), Klemens, Diana (my best office mate ever), Vadim, Mohamed für die gemeinsame Zeit am Institut ...
...bin ich besonders dankbar.

Ich danke meinen Eltern, die immer für mich da waren, und mich mein Leben lang mit Liebe und Ermutigung unterstützt und begleitet haben, genauso wie meinem Bruder Marjan.